# Critical Properties of Dimers, Spin Chains and Interface Models

Nicolas Allegra

Université de Lorraine

# Thèse

pour obtenir le grade de :

Docteur de l'Université de Lorraine

dans la spécialité

Physique

par

Nicolas Allegra

## Propriétés critiques des modèles de dimères, de chaînes de spin et d'interfaces

---

## Critical Properties of Dimers, Spin chains and Interface Models

Thèse soutenue le 29 septembre 2015 devant le jury composé de :

| | | | |
|---|---|---|---|
| *M.* | Philippe Ruelle | Professeur, Université Catholique de Louvain | Président du jury |
| *M.* | Jesper Jacobsen | Professeur, Université Pierre et Marie Curie | Rapporteur |
| *M.* | Herbert Spohn | Professeur, Technical University Munich | Rapporteur |
| *M.* | Kay Wiese | Directeur de Recherche CNRS, LPTENS | Examinateur |
| *M.* | Gregory Schehr | Chargé de Recherche CNRS, LPTMS | Examinateur |
| *M.* | Malte Henkel | Professeur, Université de Lorraine | Directeur de Thèse |
| *M.* | Jean-Yves Fortin | Directeur de Recherche CNRS, IJL | Co-Directeur de Thèse |

**Institut Jean Lamour**
Faculté des Sciences et Technologies
F-54506 VANDOEUVRE les NANCY cedex France
Université de Lorraine

# Remerciements

Tout d'abord, je tiens à remercier Malte pour avoir accepté d'être mon directeur de thèse et de m'avoir tant appris durant ces trois années. Cette thèse témoigne de sa double compétence en physique statistique à l'équilibre et hors de l'équilibre. Je le remercie de m'avoir permis de travailler sur divers sujets et ainsi de m'écarter du sujet initial tout en gardant un oeil bienveillant sur moi. Je le remercie aussi pour toutes ces discussions quotidiennes de physique et autres et de m'avoir soutenu quotidiennement. Mes seconds remerciements vont naturellement envers Jean-Yves qui est rapidement devenu mon second directeur de thèse et avant tout mon ami, malgré notre fondamentale divergence VTT / Vélo de route. Je le remercie d'avoir supporté ma présence journalière dans son bureau, de m'avoir permis d'aller à Séoul, de m'avoir appris tant de choses et surtout d'avoir été présent durant ces trois années.

Je tiens ensuite à remercier mes deux rapporteurs Herbert Spohn et Jesper Jacobsen d'avoir accepté de lire ma thèse et d'assister à la soutenance. Je les remercie aussi pour les discussions que j'ai pu avoir avec eux à Paris, aux Houches, à Florence et ailleurs. J'en profite pour remercier Jesper pour son cours de M2 à Paris que j'ai particulièrement apprécié et qui m'a tant servi pendant ces années de thèse. Je remercie également Kay Wiese et Grégory Schehr pour avoir été examinateurs de cette thèse, ce fut un grand plaisir de les avoir dans mon jury. Je remercie aussi ce dernier pour la parfaite organisation de l?école des Houches l'été dernier où j'ai pu écrire une bonne partie de cette thèse dans un cadre exceptionnel. Un grand merci à Philippe Ruelle de m'avoir fait l'honneur de présider ce jury et de m'avoir invité à Louvain où j'ai pu apprécier la fameuse hospitalité belge. Finalement, un mot de remerciements aux excellents professeurs que j'ai eu la chance d'avoir tout au long de ces années et je suis particulièrement reconnaissant envers Jérôme Léon qui a su me donner le goût de la recherche en physique.

Ces trois années à Nancy n'auraient pas été les mêmes sans la présence de tous les membres du groupe. Je pense en premier à Christophe avec qui j'ai tant discuté, appris et même couru. Si c'était à refaire, je ferais volontiers une thèse avec toi. Merci à Bertrand pour m'avoir permis de voyager plus que je ne l'aurai rêvé et de s'être toujours intéressé à mes recherches. Je n'ai ni la place, ni la patience de remercier les membres du groupe un à un mais je tiens à remercier Loïc pour m'avoir beaucoup aidé et de m'avoir toujours donné les bonnes références. Rapidement, mes remerciements vont aussi envers Alexandre, Dragi, Olivier, Thierry, Gunnar et bien-sûr Jérôme avec qui j'ai pu travailler dans ma dernière année. Je le remercie pour ses explications claires et précises, ainsi que pour ses nombreux conseils. J'en profite pour remercier les deux autres membres de la communauté du cercle arctique, Jean- Marie et Jacopo pour cette collaboration incroyablement intéressante. Je remercie aussi Laurent Chaput et Jérémie Unterberger pour diverses discussions et conseils ainsi que toutes les personnes avec qui j'ai pu échanger au cours de mes voyages, je pense notamment à Masayuki Hase et Segun Goh.

Une thèse n'en serait pas vraiment une sans la présence d'autres thésards. Je pense tout d'abord à Sophie avec qui j'ai tant partagé et qui a réussi à venir à ma soutenance malgré un emploi du temps chargé. Merci aussi à Pierre, Dimitri, Hugo, Mariana, Nelson, Emilio, Sasha et Xavier pour la bonne ambiance dans notre bureau. Je remercie aussi Thimothée d'être venu de Paris pour ma soutenance et Thomas et mes autres camarades de classe pour tous ces moments avant la thèse. Evidemment, tous mes amis hors de la physique sont aussi remerciés et ils se reconnaitront si jamais ils tombent sur ces lignes. Pour finir, mes remerciements les plus profonds vont vers ma famille et surtout mes parents qui m'ont toujours soutenu et qui m'ont permis d'être là où je suis aujourd'hui.

# Contents

# PART I

# Critical properties of $2d$ dimer models and related $c = 1$ CFT's

CHAPTER 1

# Some properties of 2$d$ critical systems and dimer models

## Contents

This chapter is mainly a review of basic knowledge and personal views about the classical dimer model in the framework of 2$d$ classical phenomena. The field of lattice statistical physics is exemplified by the so-called high-temperature expansion of the square lattice Ising model leading to a pure combinatorial problem very similar to the one we will be interested in. Then, by introducing Grassmann algebra we shall see how to define and express the partition function of the dimer model in a fermionic framework. After a rapid survey of the standard Kasteleyn solution and its main applications, some of the most interesting relations to other combinatorial problems are presented in a quite pedestrian way. The third part of this chapter is dedicated to the so-called monomer-dimer model, which turns out to be more complicated to study. We will see how to extract some informations about the phases using in one hand a mean-field method and in another hand a sophisticated transfer matrix approach which leads to the famous result about the absence of phase transition, and which can be proved rigorously as we shall see at the end of the chapter.

## 1.1 Introduction to lattice models and dimers

Lattice models has always played a great role in the history of physics when it comes to the description of the phases of matter, mainly because of the intrinsic nature of the microscopic world. Following Onsager's solution of the 2$d$ Ising model in the forties [165, 122, 123], the introduction of the Bethe ansatz [20] and the discovery of the machinery of transfer matrices, the field of exact solutions of lattice statistical physics models has exploded leading to the birth of a new field of theoretical and mathematical physics known as *exactly solved models* [17]. The confluence of this new field with 2$d$ conformal field theory [18] discovered by Belavin, Polyakov and Zamolodchikov (see [56] for an extensive monography) had a huge impact in theoretical physics, from high energy to condensed matter, leading to a whole new level of understanding of classical and quantum integrable systems [141]. In the next few pages, we will explore a few properties of different lattice models that I find relevant for the discussion to come.

### 1.1.1 Ising model and graph expansion

We shall start our discussion about statistical lattice models and relation to some combinatorial problems, examining a particular combinatorial solution of the ferromagnetic Ising model introduced by Lenz and Ising, with the following hamiltonian

$$H = -J \sum_{\langle ij \rangle} s_i s_j. \tag{1.1}$$

The exact computation of the partition function of this model in 2$d$ was started by Onsager [165, 122, 123] in the forties and led to a rather good understanding of the phase diagram of the model (see Fig. 1.2). Another approach to compute, in an exact way, the partition function is to write down explicitly how the latter can be expand around some specific temperature values, *i.e.* in the limit of low or high temperature. Kramers and Wannier were able to show that the high temperature expansion and the low temperature expansion of the model are equivalent up to an overall rescaling of the free energy, under the restricted assumption that there is only one critical point in between. In the following we will briefly explain how this expansion can be performed

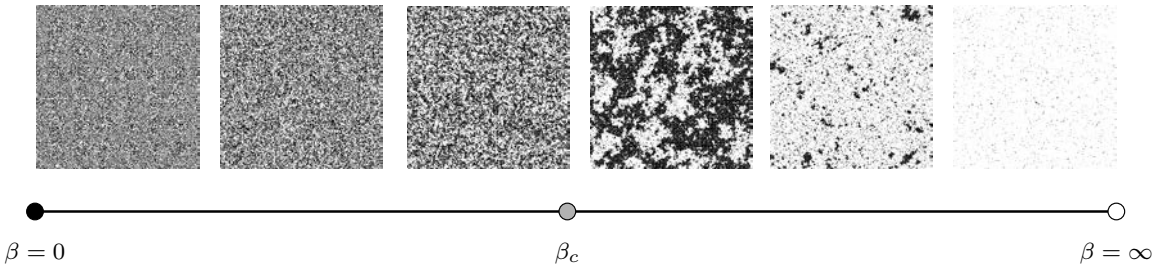


Figure 1.1: ($a$) Phase diagram of the 2$d$ ferromagnetic Ising model with free boundary conditions. The point $\beta = \infty$ correspond to the ferromagnetic phase and the point $\beta = 0$ correspond to the disordered phase around our high-temperature expansion is performed separated by a critical point at $\beta_c = \ln(1+\sqrt{2})/2$, which can be found exactly using the Kramers-Wannier duality.

in the high temperature limit, for the case of the 2$d$ Ising model on the square lattice[1]. Here we expect the partition function to be dominated by the completely random, disordered configurations of maximum entropy. Our goal is to find a way to expand the partition function in $\beta J \ll 1$.

$$Z = \sum_{\{s\}} \exp\left(\beta J \sum_{\langle ij \rangle} s_i s_j\right) = \sum_{\{s\}} \prod_{\langle ij \rangle} \exp\left(\beta J s_i s_j\right). \tag{1.2}$$

There is a useful way to rewrite $\exp(\beta J s_i s_j)$ which relies on the fact that the product $s_i s_j$ only takes value $\pm 1$. It does not take long to check the following identity

$$\exp(\beta J s_i s_j) = a(1 + b s_i s_j), \tag{1.3}$$

with $a = \cosh \beta J$ and $b = \tanh \beta J$. Using this graph expansion, we can write the partition function as the sum over all the configurations of polygons. A graphical representation can be associated with the expansion of the product as follows. We color any given edge if the term $b s_i s_j$

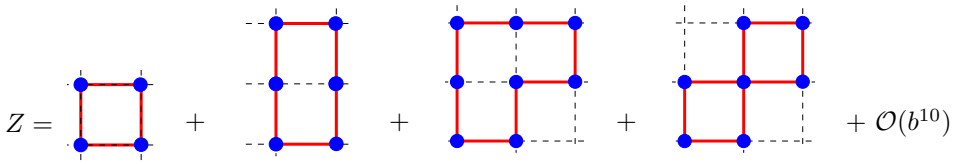


is taken, and leave the edge empty if we take the term 1. The contribution of graphs in which any vertex is incident on an odd number of colored edges then vanishes upon taking the sum over spin configurations. In other words, non-zero contributions correspond to graphs consisting of closed polygons and the partition function reads

$$Z = \sum_{\{s\}} \prod_{\langle ij \rangle} \exp(\beta J s_i s_j) = a^{2V} \sum_{\{s\}} \prod_{\langle ij \rangle} (1 + b s_i s_j)). \tag{1.4}$$

This is often referred to as a high-temperature expansion, since $\tanh \beta J \ll 1$ when $\beta J \ll 1$, but

[1] This method is quite generic and can be extended for a lot of models in any dimensions

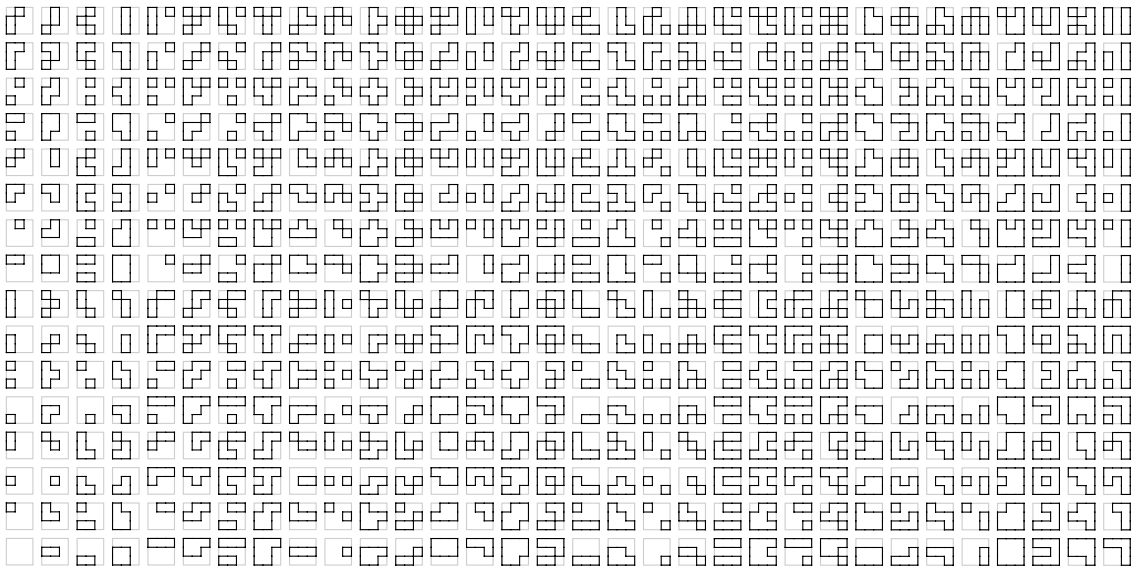

Figure 1.2: The list of all 512 loop configurations for the $4 \times 4$ Ising partition function Eq. (1.4) without periodic boundary conditions. I thank Pr Werner Krauth for sharing his code with me.

we stress that this is an exact rewriting of $Z$ that holds for any $\beta$. With a lot of hard work one can estimate behavior of thermodynamic functions from these series. In particular one can see singularities in the free energy, indicative of a phase transition, and even estimate the behavior near the singularities. A similar high temperature expansion can also be done for spin correlations.

### 1.1.2 From Grassmann algebra to dimer models

Grassmann variables [19], thanks to their nilpotent properties, are very suitable to tackle combinatorial lattice models, and many of this models has been partially or entirely solved in the frame of fermionic field theory and the dimer model was one of them [184, 185]. In this context, we should mention the study of spanning trees and spanning forests [36, 35] as well as the edge-coloring problem [74, 75] which is a special case of a more general loop model [110, 135]. A $n$-dimensional Grassmann algebra [2] is the algebra generated by a set of variables $\{a_i\}$, with $i = 1...n$ satisfying

$$\{a_i, a_j\} = 0, \tag{1.5}$$

*i.e.* they anti-commute, which implies in particular that $a_i^2 = 0$. The algebra generated by these quantities contains all expressions of the form

$$\begin{aligned} f(a) &= f^{(0)} + \sum_i f^i a_i + \sum_{i<j} f^{ij} a_i a_j + .. \\ &= \sum_{0 \leqslant p \leqslant n} \sum_i \frac{1}{p!} f^{i_1 ... i_p} a_{i_1} a_{i_2} ... a_{i_p}, \end{aligned} \tag{1.6}$$

[2] The presentation closely follows [98].

where the coefficients are antisymmetric tensors with $p$ indices, each ranging from 1 to $n$. Since there are $\binom{n}{p}$ such linearly independent tensors, summing over $p$ from 0 to $n$ produces a $2n$-dimensional algebra. The anticommuting rule allows us to define an associative product

$$f_1(a)f_2(a) = f_1^0 f_1^0 + \sum_i (f_1^0 f_2^i + f_1^i f_2^0)a_i + \frac{1}{2}\sum_{ij}(f_1^{ij} f_2^0 + f_1^i f_2^j - f_1^j f_2^i + f_1^0 f_2^{ij})a_i a_j + .. \quad (1.7)$$

Please note that in general $fg$ is not equal to $\pm gf$. Nevertheless the subalgebra containing terms with an even number (possibly zero) of $a$ variables commutes with any element $f$. Having defined sum and products in the Grassmann algebra we now define a left derivative $\partial_i := \partial_{a_i}$. The derivative gives zero on a monomial which does not contain the variable $a_i$. If the monomial does contain $a_i$, it is moved to the left (with the appropriate sign due to the exchanges) and then suppressed. The operation is extended by linearity to any element of the algebra. A right derivative can be defined similarly. From this definition the following rules can be obtained

$$\begin{aligned} \{\partial_i, \partial_j\} &= 0 \\ \{\partial_i, a_j\} &= \delta_{ij}. \end{aligned} \quad (1.8)$$

Integrals are defined as linear operations over the functions $f$ with the property that they can be identified with the (left) derivatives [19]. Correspondingly

$$\begin{aligned} \int \mathrm{d}a_i \ f(a) &= \partial_i f(a), \\ \int \mathrm{d}a_i \, \mathrm{d}a_j \ f(a) &= \partial_i \partial_j f(a), \end{aligned} \quad (1.9)$$

which leads to the generalization

$$\int \mathrm{d}a_{i_k} \, \mathrm{d}a_{i_{k-1}} ... \, \mathrm{d}a_{i_1} \ f(a) = \partial_{i_k} \partial_{i_{k-1}} ... \partial_{i_1} f. \quad (1.10)$$

It is obvious that this definition fulfills the constraint of translational invariance ($C$,$D$ constant)

$$\int \mathrm{d}a_1 (C + D a_1) = \int \mathrm{d}a_1 [C + D(a_1 + a_2)], \quad (1.11)$$

which requires

$$\int \mathrm{d}a_i \ a_j = \delta_{ij}. \quad (1.12)$$

**Quadratic and quartic form**

Changes of coordinates are required to preserve the anti-commuting structure of the Grassmann algebra, this allows non-singular linear transformations of the form $b_i = \sum_j A_{ij} a_i$. One then can verify that by setting $f(a) = F(b)$ one can obtain the following relation

$$\int \prod_i \mathrm{d}a_n ... \, \mathrm{d}a_1 f(a) = \det A \int \prod_i \mathrm{d}b_n ... \, \mathrm{d}b_1 F(b), \quad (1.13)$$

at variance with the commuting case in which the factor on the right hand side would have been $\det^{-1} A$. We note $\int \mathcal{D}[a,\bar{a}] = \int \prod_i \mathrm{d}a_i \, \mathrm{d}\bar{a}_i$ the Grassmann measure. In the multidimensional integral, the symbols $\mathrm{d}a_1, ..., \mathrm{d}a_N$ are again anticommuting with each other. The basic expression of the Grassmann analysis concern the Gaussian fermionic integrals [184] which is related to the determinant

$$\det A = \int \mathcal{D}[a,\bar{a}] \exp\Big( \sum_{i,j=1}^{N} a_i A_{ij} \bar{a}_j \Big), \tag{1.14}$$

where $\{a_i, \bar{a}_i\}$ is a set of completely anticommuting Grassmann variables, the matrix in the exponential is arbitrary. The two Grassmann variables $a_i$ and $\bar{a}_i$ are independent and not conjugate to each other, they can been seen as composante of a complex Grassmann variables. The Gaussian integral of the second kind is related to the Pfaffian of the associated skew-symmetric matrix

$$\mathrm{pf} A = \int \mathcal{D}[a] \exp\Big( \frac{1}{2} \sum_{i,j=1}^{N} a_i A_{ij} a_j \Big). \tag{1.15}$$

The pfaffian form is a combinatorial polynomial in $A_{ij}$, known in mathematics for a long time. The pfaffian and determinant of the associated skew-symmetric matrix are algebraically related by $\det A = (\mathrm{pf} A)^2$. This relation can be most easily proved in terms of the fermionic integrals. The linear superpositions of Grassmann variables are still Grassmann variables and it is possible to make a linear change of variables in the integrals. The only difference with the rules of the common analysis, is that the Jacobian will now appear in the inverse power. New variables of integration can be introduced, in particular, by means of the transformation to the momentum space. The permanent of $A$ and the so-called haffnian can be written with Grassmann variables as well

$$\begin{aligned} \mathrm{perm} A &= \int \mathcal{D}[b,\bar{b}] \int \mathcal{D}[a,\bar{a}] \exp\Big( \sum_{i,j=1}^{N} a_i \bar{a}_i A_{ij} b_j \bar{b}_j \Big), \\ \mathrm{hf} A &= \int \mathcal{D}[a,\bar{a}] \exp\Big( \frac{1}{2} \sum_{i,j=1}^{N} a_i \bar{a}_i A_{ij} a_j \bar{a}_j \Big), \end{aligned} \tag{1.16}$$

which are related by the formula $\mathrm{perm} A = (\mathrm{hf} A)^2$. We recall that the definition of the permanent differs from that of the determinant in that the signatures of the permutations are not taken into account.

**Box 1** (Proof of $\det A = (\mathrm{pf}A)^2$ by a Grassmann analysis)**.**

The Pfaffian of an anti-symmetric $2n \times 2n$ matrix $A$ is defined as

$$\mathrm{pf}A := \frac{1}{2^n n!} \sum_{\{i_1,i_2,\ldots,i_n\}} \epsilon_{i_1 i_2 \ldots i_{2n}} A_{i_1 i_2} \ldots A_{i_{2n-1} i_{2n}}, \tag{1.17}$$

where $\epsilon_{i_1 i_2 \ldots i_{2n}}$ is the anti-symmetric tensor and the sum is over all permutations of the indices. The Pfaffian can be proven to obey the Pfaffian identity $\det A = (\mathrm{pf}A)^2$. A short, elegant proof of this Pfaffian identity can be constructed using the Grassmann integral. Consider the Grassmann integral

$$I(A) := \int \mathcal{D}[\psi] \exp\Big(\frac{1}{2} \sum_{i,j} \psi_i A_{ij} \psi_j\Big) \tag{1.18}$$

where we note $\int \mathcal{D}[\psi] = \int \prod_i \mathrm{d}\psi_i$ the Grassmann measure and $I(A) = \mathrm{pf}A$. Now consider $I(A)^2$. This can be written as a product of Grassmann integrals over two independant sets of Grassmann variables $\psi$ and $\phi$. Change Grassmann integration variables to

$$\varphi_i := \psi_i + \phi_i$$
$$\bar{\varphi}_i := \bar{\psi}_i - \bar{\phi}_i$$

and then it is easy to show that the resulting Grassmann integral is then equal to

$$\int \mathcal{D}[\varphi, \bar{\varphi}] \exp\Big(\sum_{i,j} \varphi_i A_{ij} \bar{\varphi}_j\Big) = \det A \tag{1.19}$$

and thus complete the proof. The proof of the other identity $\mathrm{perm}A = (\mathrm{hf}A)^2$ follows exactly the same strategy with commuting nilpotent variables instead of Grassmann variables.

### Definition of a dimer covering

A graph $\mathcal{G}$ is a pair of sets $(V, E)$, where $V$ is a finite set of vertices, and $E$ is a finite set of non-oriented edges. We define the adjacent matrix (also called connectivity matrix) $A = (A_{ij})$, where the $ij$-entry is associated with the ordered pair of vertices $(v_i, v_i)$, then $A_{ij} = 1$ if $v_i$ and $v_j$ are joined by an edge, and 0 otherwise (*cf.* Fig. 5.1 for the square lattice). The perfect matching number is the number of configuration with the property that each site of the lattice is paired with exactly one of its linked neighbors [151]. In the language of theoretical physics, the enumeration of perfect matching of a planar graph $\mathcal{G}$ is equivalent to compute the partition function of the dimer model on the given lattice. In the simplest form, the number of dimers is the same in all the configurations, and the partition function is given by the equally-weighted

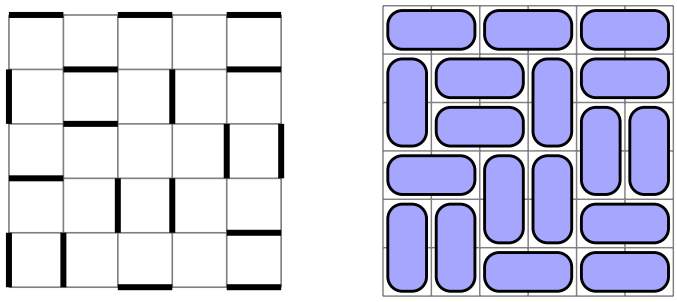

($a$) ($b$)

Figure 1.3: ($a$) Perfect matching of the square lattice, and ($b$) its "domino" representation. This combinatorial problem reduces to the calculation of the partition function Eq. (1.20) with $t = 1$.

average over all possible dimer configurations [3]. For example, in the case of the $2 \times 2$ square lattice where the weight of dimers are choose to be equal to one, the partition function is just a sum of two terms 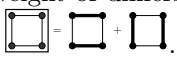 . Initially, the dimer model (see Fig. 5.1) has been introduced by physicists to describe absorption of diatomic molecules on a $2d$ subtrate [78], yet it became quickly a general problem studied in various scientific communities. From the mathematical point of view, this problem known as perfect matching problem [151]– is a famous and active problem of combinatorics and graph theory [76] with a large spectrum of applications. The enumeration of so-called Kekule structures of molecular graphs in quantum chemistry are equivalent to the problem of enumeration of perfect matchings [205, 206]. Besides, a recent connection between dimer models and $D$-brane gauge theories has been discovered [87, 81], providing a very powerful computational tool.

### Haffnian formulation

In the following, we will include equal fugacities $t$ for dimers, so that the average to be taken then includes weighting factors for dimers and we write the partition function as

$$Q_0[t] = \int \mathcal{D}[\eta] \exp(-\beta \mathcal{H}), \tag{1.20}$$

where the Hamiltonian for the dimer written using commuting nilpotent variables (see Appendix 1.1) can be written as a sum over every vertices (see Fig. 1.4), preventing two dimers to occupy the same site

$$\mathcal{H} = -\frac{t}{2} \sum_{ij} \eta_i A_{ij} \eta_j, \tag{1.21}$$

where $A_{ij}$ is the adjacent matrix of the lattice considered. Let us put $\beta = 1$ in the folllowing. The nilpotent variables can be seen as commuting Grassmann variables, or simply a product of two sets of standard Grassmann variables where $\eta_i = \theta_i \bar{\theta}_i$. The perfect matching number of the graph

[3] Throughout this work, we will use the physics terminology and use the expression *perfect matching* in some specific cases.

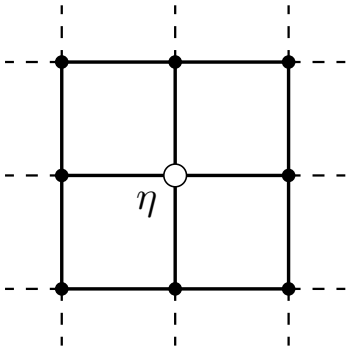


Figure 1.4: At every vertices, we put a nilpotent variable $\eta$, such that $\eta^2 = 0$ forbidden two dimers to occupy the same site.

$\mathcal{G}$ is equal to the partition function in the case $t = 1$

$$\begin{aligned} Q_0[1] &= \int \mathcal{D}[\eta] \exp\Big(\frac{1}{2}\sum_{ij} \eta_i A_{ij} \eta_j\Big) \\ &= \int \mathcal{D}[\theta, \bar{\theta}] \exp\Big(\frac{1}{2}\sum_{ij} \theta_i \bar{\theta}_i A_{ij} \theta_j \bar{\theta}_j\Big) \\ &= \mathrm{hf} A. \end{aligned} \tag{1.22}$$

In the second line we decomposed the nilpotent variables using two sets of Grassmann variables, and we finally find the well known graph theory result

$$\text{perfect } \mathcal{G} = \mathrm{hf} A. \tag{1.23}$$

Considering holes in the perfect matching problem (monomers in the dimer model) is equivalent to remove rows and columns at the positions of the holes in the adjacent matrix (see Fig. 1.5). The resulting combinatorial problem is called the near-perfect matching problem. The partition function of the dimer model with a fixed number of holes (monomers) can be written as

$$\begin{aligned} Q_n[1] &= \int \mathcal{D}[\theta, \bar{\theta}] \prod_{p=1}^{n} \theta_{q_p} \bar{\theta}_{q_p} \exp\Big(\frac{1}{2}\sum_{ij} \theta_i \bar{\theta}_i A_{ij} \theta_j \bar{\theta}_j\Big) \\ &= \int \mathcal{D}[\theta, \bar{\theta}] \exp\Big(\frac{1}{2}\sum_{ij} \theta_i \bar{\theta}_i A^{\setminus\{q_p\}}_{ij} \theta_j \bar{\theta}_j\Big) \\ &= \mathrm{hf} A^{\setminus\{q_p\}}, \end{aligned} \tag{1.24}$$

where the index $n$ stands for the number of monomers in $Q_n[t]$. Finally, the result is the same but now the matrix $A^{\setminus\{q_p\}}$ is the adjacent matrix of the original graph with positions of the $n$ monomers removed. Suppose we remove two sites $q_1$ and $q_2$ on the graph $\mathcal{G}$, then it is similar to

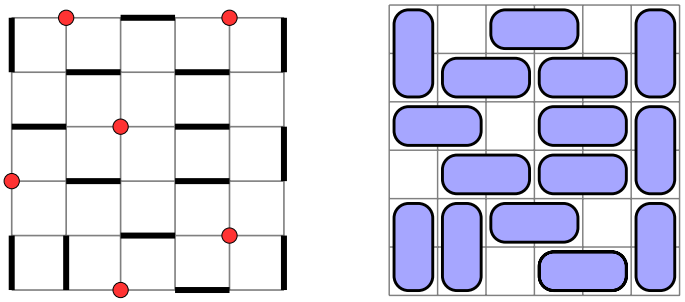

($a$) ($b$)

Figure 1.5: ($a$) Dimer model with 6 monomers, and ($b$) its "domino" representation.

introduce two nilpotent variables $\eta_{q_1}$ and $\eta_{q_2}$ on the lattice, the correlation function between these two monomers is then $\mathrm{hf}A^{\setminus(q_1,q_2)}\mathrm{hf}^{-1}A$ and more generally the $n$-point correlation function reads

$$\left\langle \prod_{p=1}^{n} \eta_{q_p} \right\rangle = \left\langle \prod_{p=1}^{n} \theta_{q_p}\bar{\theta}_{q_p} \right\rangle = \frac{\mathrm{hf}A^{\setminus\{q_p\}}}{\mathrm{hf}A}. \tag{1.25}$$

The partition function and correlations can be studied in the case $t \neq 1$ as well, in that case, the matrix elements of $A$ are $A_{ij} = \pm t$ and the generalization is straightforward. Generally speaking, correlations between monomers are equal to correlations between nilpotent variables in this framework, which can be written in terms of a ratio between two haffnian. Unlike the determinant which can be computed by a $\mathcal{O}(L^3)$ time algorithm by Gauss elimination, there is no polynomial-time algorithm for computing permanent. The problem of converting a permanent problem into a determinant problem is a long standing problem in pure mathematics, the simplest version of this problem, is called the Pólya permanent problem [176]. Given a $(0,1)$-matrix $A := (A_{ij})_{L\times L}$, can we find a matrix $B := (B_{ij})_{L\times L}$ such that $\mathrm{perm}A = \det B$ (or equivalently $\mathrm{hf}A = \mathrm{pf}B$) where $B_{ij} = \pm A_{ij}$.

### Kasteleyn orientation and Pfaffian formulation

The partition function of the 2$d$ dimer model on the square lattice was solved independently using pfaffian methods [120, 71, 201] for several boundary conditions. Other lattice geometries have been studied as well, *e.g.* the triangular lattice [68], the Kagomé lattice [208, 209, 214], the triangular Kagomé lattice [149], the hexagonal lattice [66], the star lattice [73], or more complicated geometries [215] (see [212] for a review). The Kasteleyn theorem is a recipe to find a matrix[4] $K$ in such way that $\mathrm{hf}A = \mathrm{pf}K$, where the elements of the matrix are $K_{ij} = \pm 1$. Kasteleyn theorem is based on a special disposition of arrows on the edges of a planar graph[5]. The product of arrows around any even cycle whose interior contains an even (respectively odd) number of vertices is odd (respectively even). Such a disposition is given in Fig. 1.7($b$) for the square lattice. We define an antisymmetric matrix $K$, where $K_{ij} = 1$ if an arrow points from the site $i$ to the site $j$, $K_{ij} = -1$

[4] We will call this matrix the Kasteleyn matrix in the following.
[5] This is a *condicio sine qua non* and the theorem is no longer valid for non-planar graph.

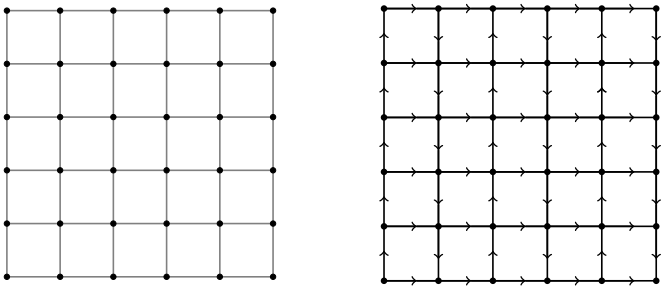

($a$) ($b$)

Figure 1.6: ($a$) Square lattice and ($b$) the orientation prescription of the Kasteleyn matrix.

if the arrow points from $j$ to $i$, and $K_{ij} = 0$ otherwise. Let us notice that in general the entries $K_{ij}$, if they exist, are not necessarily real (see [68] for the triangular lattice). Kasteleyn theorem states that the perfect matching number of a given planar graph $\mathcal{G}$ is given by

$$\text{perfect } \mathcal{G} = \text{hf}A = \text{pf}K, \tag{1.26}$$

which is equal to $\pm\sqrt{\det K}$. The $\pm$ sign is chosen to make the partition function positive, henceforth we will omit this sign in the rest of the article. Differently, this pfaffian can be express in terms of Grassmann variables $a$

$$\text{pf}K = \int \mathcal{D}[a] \exp\Big(\frac{1}{2}\sum_{i,j=1}^{N} a_i K_{ij} a_j\Big). \tag{1.27}$$

Let us mention that this Kasteleyn orientation can be recover with a Grassmann analysis. The question is how to go from the Grassmann haffnian form Eq. (1.22) (with $A_{ij} = 1$ if the edge $i-j$ and 0 else) to the Grassmann pfaffian form Eq. (1.15) (with $K_{ij}$ unknown). Using straightforward Berezin manipulations on the haffnian we can check that it is equal to a pfaffian with the proper Kasteleyn entries $K_{ij}$. This can be easily generalized for any graph as long as it can be represented with an adjacent matrix. For the square lattice, we can choose Boltzmann weights $t_x$ and $t_y$ for horizontal and vertical dimers, then the pfaffian can be computed by Fourier transform and Kasteleyn found for free boundary conditions (*cf.* [120] for details on calculations)

$$Q_0[t_x, t_y] = \prod_{p=1}^{M/2}\prod_{q=1}^{N/2}\left[4t_x^2\cos^2\frac{\pi p}{M+1} + 4t_y^2\cos^2\frac{\pi q}{N+1}\right]. \tag{1.28}$$

In table 1.1, we compute $Q_0[1,1]$ using MATHEMATICA®, for different $M$ and $N$ with $t_x = t_y = 1$ (perfect matching number). All these values can be numerically checked using diverse algorithms which enumerate all the possible configurations on the square lattice (see [144] for details). In the rest of the paper we will omit the labels $t_x$ and $t_y$ in the partition function and just keep $Q_0$. While the approach detailed here only works for planar graphs, it is possible to extend beyond that. For instance, for any graph that can be embedded on a toroid, the number of dimer distributions can be expressed as a combination of four pfaffians, as shown by Kasteleyn. The case of surface of high genius have been studied as well in [53].

| $M \setminus N$ | 2 | 4 | 6 | 8 | 10 | 12 |
|---|---|---|---|---|---|---|
| 2 | 2 | 5 | 13 | 34 | 89 | 233 |
| 4 | 5 | 36 | 281 | 2245 | 18061 | 145601 |
| 6 | 13 | 281 | 6728 | 167089 | 4213133 | 106912793 |
| 8 | 34 | 2245 | 167089 | 12988816 | 1031151241 | 82741005829 |
| 10 | 89 | 18061 | 4213133 | 1031151241 | 258584046368 | 65743732590821 |
| 12 | 233 | 145601 | 106912793 | 82741005829 | 65743732590821 | 53060477521960000 |

Table 1.1: Perfect matching number $Q_0[1,1]$ of the square lattice, for different $M$ and $N$.

#### Entropy in the thermodynamic limit

The asymptotic form $L \to \infty$ of the partition function (for $M = N = L$) can be easily found from Eq. (5.2)

$$Q_0 \sim \exp \frac{GL^2}{\pi}, \tag{1.29}$$

where is the $G$ is Catalan constant[6]. The factor $G/\pi$ is the entropy per site of the dimer model on the square lattice. This entropy can also be calculated for other bipartite lattices like the honeycomb lattice, and for non-bipartite lattices like triangular, Kagomé lattice and triangular Kagomé lattice. The pfaffian method can be used to compute the partition function of the dimer model on various geometries and boundary conditions leading to different values of the entropy (*cf.* [212] for review), as long as the lattice has a Kasteleyn orientation (*i.e.* planar according to the Kasteleyn theorem) and as long as $N \times M$ is even. Obviously it is impossible to fill an odd size lattice with dimers, without leaving one site empty. We shall take notice later that the form of the free energy is strongly dependent of the parity of the lattice.

### 1.1.3 Local statistics and non-local properties

This theory was used to compute the partition functions, as well as dimer and monomer correlation functions in a perturbative way, leading to exact correlation exponents in the thermodynamic limit [71, 72]. In the case of dimer correlations, we will see that, the knowledge of the Kasteleyn matrix is enough to get access to any type of probabilities of configurations while for monomers, things are much more complicated and a perturbative modification of the Kasteleyn matrix can be performed to extrapolate the scaling limit of the behavior of monomer correlations.

#### Dimer correlations

The Kasteleyn matrix is a very powerful objet, which gives us all the details about probabilities of presence of dimers [72]. For example the occupation probability of a dimer on the link $ij$ is $\text{Proba}[i \to j] = K_{ij} \times K_{ij}^{-1}$ can be computed and we found

[6] $G = 1^{-2} - 3^{-2} + 5^{-2} - 7^{-2} + ... = 0.915965594...$

$$\text{Proba}[(x,y)(x+1,y)] = \frac{4\left[(-1)^x-(-1)^{x+1}\right]}{(L+1)^2}\sum_{p,q=1}^{L/2}\frac{\cos\frac{\pi q}{L+1}\sin^2\frac{\pi py}{L+1}}{\cos^2\frac{\pi p}{L+1}+\cos^2\frac{\pi q}{L+1}}\sin\frac{\pi qx}{L+1}\sin\frac{\pi q(x+1)}{L+1}$$

.

This quantity $\text{Proba}[(x,y),(x+1,y)]$ is always a rational number in finite size, but can tend to an irrational number when $L\to\infty$. A famous case is the probability of a dimer on the middle of the surface, in this case on can show that $\text{Proba}[(L/2,0),(L/2+1,0)]\to 1/\pi$ (see Fig. 1.7). The probability of two dimers on the links $ij$ and $mn$ is

$$\text{Proba}[i\to j|m\to n] = \det\begin{pmatrix} K^{-1}_{ij} & K^{-1}_{im} \\ K^{-1}_{mj} & K^{-1}_{mn}\end{pmatrix}. \tag{1.30}$$

In the rest of the thesis, we shall use the term *correlation* even though this quantity is a normalized probability. Correlations between more than two dimers are available using the Kasteleyn matrix

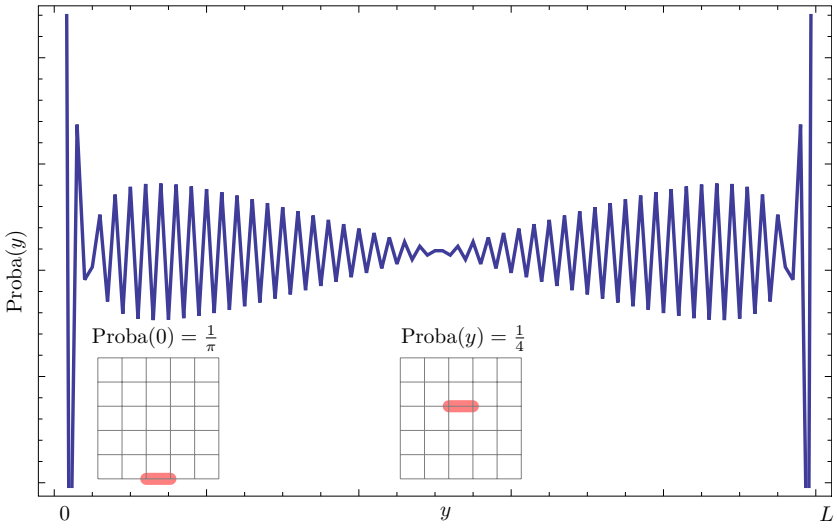


Figure 1.7: Dimer occupation probability $\text{Proba}[(x,y),(x+1,y)]$ as a function of $y$

as well. It can be shown [71, 72] that dimer-dimer correlations on the square lattice decrease as the inverse square of the distance between the two dimers in the thermodynamic limit

$$\text{P}(r)\sim r^{-2}. \tag{1.31}$$

This is always true for of two horizontal dimers on the same row. For the so-called ÒtransverseÓ correlation function of two dimers separated by a distance $r$ on the same column, the exponent depends on the parity of $r$ *i.e.* $\text{P}(r)\sim r^{-2}$ for $r$ odd and $\text{P}(r)\sim r^{-4}$ for $r$ even (see [3] for details). Furthermore it has been also shown that correlations are always critical [121] for bipartite lattices and *a contrario* exponential for non-bipartite lattices as the triangular lattice for example, where the underlying fermionic theory is a massive theory [68]. More generally we can note $\{b_i\}$ (and $\{w_i\}$) the set of vertices belonging to the odd (and even) sublattice, in such way that the

probability of a configuration of dimer covering Proba$[b_1 \to w_1|b_2 \to w_2|b_3 \to w_3|b_4 \to w_4]$ can be written in a determinant form. This kind of process is obviously called (by mathematician) a determinantal process, meaning that any $n$-point correlation function can be written in terms of the determinant of some kernel.

**Monomer correlations**

Throughout this thesis the monomer-monomer correlation function $C$ will be defined as the ratio of the number of configurations with monomers at fixed positions to the number of configurations without monomer. Thus computing a monomer-monomer correlation is *stricto sensu* equivalent to compute the partition function with two sites (and all the links connected to these sites) deleted. Since such a graph is still planar, KasteleynÕs construction is still applicable. The one complication is that we must ensure that on the new lattice with deleted sites, the product of arrows around the holes is still odd. If all the monomers are located on the boundary of the lattice at ordinate $\{x_i\}$, there is no non-local defect lines between monomers (see Fig. 1.8), and the modified matrix $K^{\setminus\{x_i\}}$ defined from $K$ by removing all the rows and columns corresponding to the monomers positions has still the proper Kasteleyn orientation. Then the pfaffian of this modified Kasteleyn matrix $K^{\setminus\{x_i\}}$ gives us the partition function of the dimer model with fixed monomer positions. It follows that the correlation function between two monomers on the boundary is

$$C(x_1, x_2) := \frac{Q_2(x_1, x_2)}{Q_0} = \mathrm{pf}\big(K^{-1} K^{\setminus(x_1,x_2)}\big) = \big\langle a_i a_j \big\rangle, \tag{1.32}$$

where $x_1$ and $x_2$ are the positions of the two monomers. This pfaffian has been computed by Priezzhev and Ruelle (*cf.* [178] for details) in the thermodynamic limit for a arbitrary number of monomers at positions $\{x_i\}$, using a perturbative analysis of the matrix $K^{\setminus\{x_i\}}$ around the original Kasteleyn matrix $K$. The result for the $2n$-point correlation is given by

$$C(x_1, x_2 ... x_{2n}) = \mathrm{pf}\ C, \tag{1.33}$$

where the matrix element $C_{ij} := C(x_i, x_j)$ is the 2-point function of a $1d$ complex free-fermion, equal to

$$C_{ij} = -\frac{2}{\pi |x_i - x_j|}, \tag{1.34}$$

if $x_i$ and $x_j$ are on opposite sublattices and $C_{ij} = 0$ otherwise. For monomers in the bulk, the things are much more complicated. One sees that the product of arrows around a deleted site is now equal to $+1$ (see Fig. 1.8). We thus must construct a string of reversed arrows from one monomer to the second (see Fig. 1.8($b$)). As long as the arrows are chosen to make all plaquettes clockwise odd, the correlation is independent of the choice of the path. In the general case of bulk monomers, the relation Eq. (1.32) is no longer correct, because the matrix $K^{\setminus(x_i,x_j)}$ is no more a Kasteleyn matrix. Then correlations betweens two monomers defined by $Q_2(x_i, x_j)/Q_0$ is not equal to correlations between two Grassmann variables $\langle a_i a_j \rangle$, but disorder operators must be add

$$\frac{Q_2(x_i, x_j)}{Q_0} = \Big\langle a_i \exp\Big(2 \sum_{p,q} K_{pq} a_p a_q\Big) a_j \Big\rangle, \tag{1.35}$$

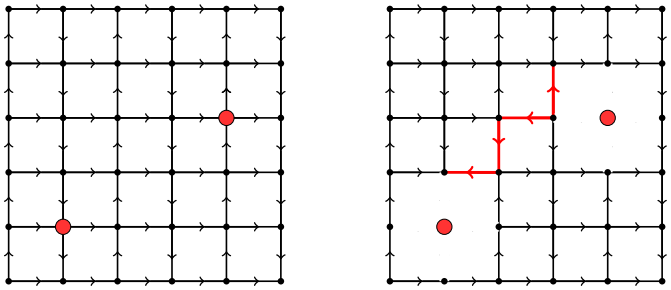

$(a)$ $(b)$

Figure 1.8: Modification of the Kasteleyn matrix in the presence of two monomers. The monomers (red dots) destroy the corresponding links and the orientation $(a)$ has to be changed to respect the proper orientation $(b)$.

where the sum is over all the links connecting sites $i$ and $j$, to take account of the reversing line between the two monomers. Using a pfaffian perturbative analysis it was shown that monomer correlations decrease at the thermodynamic limit as [71, 72]

$$C(r) \sim r^{-1/2}. \tag{1.36}$$

This result is very similar to the construction of the spin correlation functions in the Ising model in terms of fermionic variables [118, 177]. In fact, on the square lattice, the monomer-monomer correlations was shown to have the same long-distance behavior as the spin-spin correlations in two decoupled Ising models, explained by the deep relation between the two correlation functions for the square lattice given by Perk and Au-Yang [13]. These disorder operators are absent in the haffnian theory Eq. (1.25), and are the price to pay to solve the problem analytically.

## 1.2 Relation to other statistical models

The prominence of the dimer model in theoretical physics and combinatorics also comes from the direct mapping between the square lattice Ising model without magnetic field and the dimer model on a decorated lattice [154, 120, 71, 201] and conversely from the mapping of the square lattice dimer model to a eight-vertex model [16, 211]. Furthermore the magnetic field Ising model can be mapped onto the general monomer-dimer model [90].

### 1.2.1 Back to Ising

The formulation of the Ising model in term of graph-expansion (as we saw in the beginning of the chapter) can be related to dimer configurations on a decorated square lattice [121] (as shown Fig. 1.9). Every graph of the partition function of the Ising model can be written using this mapping, but the mapping is not so explicit because of several serious issues.

- Since a vertex with no polygons corresponds to three dimer configurations on the internal

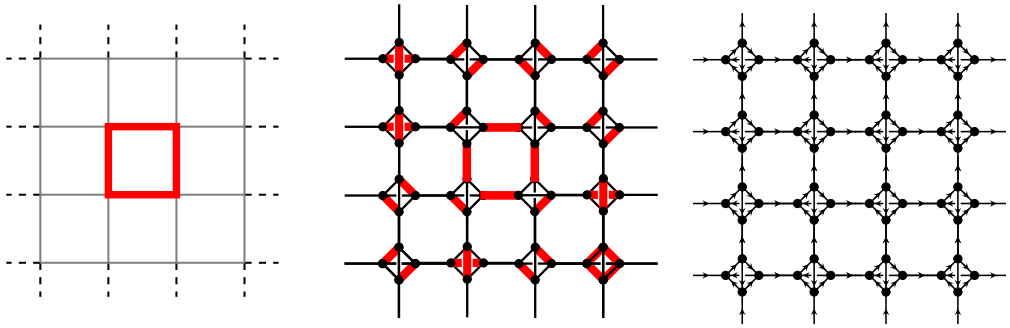

Figure 1.9: Left: a graph of order $b^4$ in the high temperature expansion of the Ising model on the square lattice and (center) its corresponding dimer covering in a decorated Fisher lattice. Right: Kasteleyn orientation of the decorated graph.

decoration  , the mapping is not "one-to-one" but "one-to-three".

- Second, the decorated lattice is a non-planar graph and as we saw earlier, the Kasteleyn theorem breaks down in that case, and it is not obvious that a proper Kasteleyn orientation does exist.

Actually, if one considers the orientation of the decorated lattice shown in Fig. 1.9, one can verify that the oriented graph is actually properly Kasteleyn oriented and that the pfaffian of this matrix is the perfect matching of the lattice. This seems to be a coincidence since the two complications cancel each other exactly (see [121] for details).

### 1.2.2 Temperley bijection and spanning trees

Another problem which is of great interest in lattice statistical physics is the computation of the number of spanning trees covering a given graph $\mathcal{G}$. The resolution of this problem comes to the use of another "graph-theory" matrix know as the Laplacian matrix. This problem is described by a free fermionic field theory via the matrix-tree theorem, stating that the number of spanning trees on a graph $\mathcal{G}$ is given by the determinant of a minor of the Laplacian matrix $\Delta$ of $\mathcal{G}$ (*cf.* [155]). Using that, the partition function of spanning trees on the square lattice can be computed and the result looks very similar to the dimer model. Indeed, Temperley [200] found a bijection between spanning trees on the $m \times n$ square lattice and dimer covering of the $(2m+1) \times (2n+1)$ square lattice with a boundary site removed.

- The mapping is a bijection, to each configuration of dimer on the $(2m+1) \times (2n+1)$ lattice corresponds to a unique spanning tree on the $2m \times 2n$.
- The position of the monomer does not matter, as long as it is on the boundary and on the proper sublattice[7]. This observation tells us that the partition function of dimer with one

[7] To convince ourselves we need at least a $5 \times 5$ lattice, because on the $3 \times 3$ lattice shown Fig. 1.2.2, the only possibility is to put the monomer on one of the four corners.

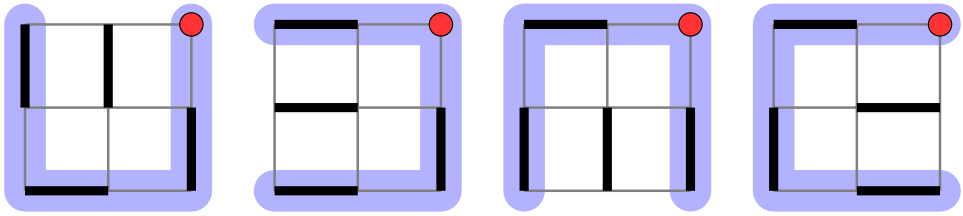

Figure 1.10: Temperley bijection between the four configurations of dimer coverings of the $3 \times 3$ lattice with one monomer on the corner and the four spanning tree coverings of the $2 \times 2$ lattice.

boundary monomer does not depend of its exact location.

- Then the partition function of dimer with one boundary site removed can be written in term of the Laplacian matrix and the final result is (for $m = n = L$ odd)

$$Q_1 = \prod_{p,q=1}^{\frac{1}{2}(L-1)} \left[ 4t_x^2 \cos^2 \frac{\pi p}{L+1} + 4t_y^2 \cos^2 \frac{\pi q}{L+1} \right] \times (t_x t_y)^{\frac{1}{2}(L-1)},$$

as shown in [202]. We shall see in the next chapter, that this solution can be recover with a grassmann analysis of the partition function of the dimer model with an arbitrary number of monomers. This bijection actually holds for a large class of graph [213], and can also be generalized for non-boundary monomers [27, 111, 175]. One thing to already notice about the spanning trees associated to dimer on the square lattice is that the boundary conditions for the tree are closed on the four side of the square, which will be crucial for the conformal field theory interpretation. Finally, let us mention that the continuum field theory describing spanning trees is the logarithmic $c = -2$ CFT of symplectic fermions which is deeply connected to the $c = 1$ Dirac fermion theory. We will get back to this in chapter III.

### 1.2.3 From dimer covering to edge coloring

In this section we present a very recent formulation of the 4-edge coloring problem on the square lattice based on a modification of the partition function of the dimer model on the same lattice [75]. From a statistical physics point of view, this problem can be seen as the ground state of the $q = 4$ anti-ferromagnetic Potts model with spin variables living on the edges of the lattice [134].

#### General statement

$\mathcal{G}$ a simple regular graph of degree $q$. Labeling the edges as $\alpha = 1, 2..., E$ where $E$ is the total number of edges, a dimer covering $n$ of $\mathcal{G}$ can be represented as $n = (n_1, n_2...n_E)$ where $n_\alpha = 0, 1$ is the number of dimers on edge $\alpha$, subject to the constraint that exactly one of the edges connected to each vertex hosts a dimer. The procedure is quite general to any graph of degree $q$ but we expose the case $q = 4$ to make link to the square lattice dimer model. Now we consider that each

edge $\alpha$ has a Boltzmann weight $w_\alpha$ and we formally write the the dimer partition function as

$$Q_0 = \sum_n \prod_\alpha w_\alpha^{n_\alpha}. \tag{1.37}$$

Next, we introduce colored dimers and define a 4-colored dimer covering which consists of dimers

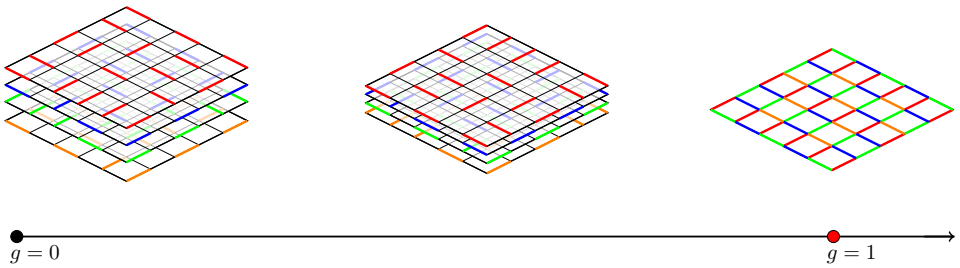


Figure 1.11: The four coloring problem seen as interacting layers of dimers. On the left one have four independent dimer coverings ($g = 0$) and on the right the 4-egde coloring problem ($g = 1$)

that all have the same color, which may take one out of 4 values: $\mu = 1, 2, 3, 4$. Because all vertices have degree 4, any 4-edge-coloring of $\mathcal{G}$ is also a 4-dimer-covering, but unlike generic 4-dimer-coverings it satisfies the additional Òcoloring constraintÓ that no edge should have more than one dimer. We therefore want to extract the former from the latter. To this end, consider the partition function for 4-dimer-coverings, $i.e$ four independent layers of colored dimer covering, which is given by

$$Q_0^4 = \sum_{n^{(1)}\dots n^{(4)}} \prod_\alpha w_\alpha^{n_\alpha^{(1)}+n_\alpha^{(2)}+n_\alpha^{(3)}+n_\alpha^{(4)}}, \tag{1.38}$$

where $n^\mu$ denotes a $\mu$-colored dimer covering of the lattice. This corresponds to the point $g = 0$ in Fig. 1.11. Each term in the sum corresponds to a 4-dimer-covering. A term that also corresponds to a 4-edge-coloring will contain exactly one factor of $w_\alpha$ for each edge $\alpha$. Conversely, for a term that does not correspond to a 4-edge-coloring, at least one edge $\alpha$ will contain more than one dimer and thus comes with a factor $w_\alpha^p$ with $p \geqslant 2$, and, equivalently, at least one edge $\beta$ will not have a dimer and thus comes with a factor $w_\beta^0 = 1$. The latter property implies that if we successively


differentiate a term in the last equation with respect to each dimer weight $w_\gamma$ , the final result will be 1 for any term representing a 4-edge-coloring and 0 for all other terms, which corresponds to the point $g = 1$ in Fig. 1.11. Therefore the number of 4-edge-colorings $Z_{\text{color}}$ is given by

$$Z_{\text{color}} = \Big(\prod_\alpha \partial_{w_\alpha}\Big) Q_0^4. \tag{1.39}$$

We have thus shown that the number of 4-edge-coloring $Z$ can be obtained from the partition function $Q_0$ of the dimer model with edge-dependent dimer weights $w$ on the same graph. This

formulation of the generating function of the coloring problem in terms of dimer coverings holds for any regular graph $\mathcal{G}$.

**Grassmann formulation**

Now we can express the partition function of the dimer model using Grassmann variables as we did before, we have now to introduce 4 types of colored Grassmann variables $a^{(\mu)}$

$$Q_0^4 = \int \prod_{\mu=1}^{4} \mathcal{D}[a^{(\mu)}] \exp\Big(\frac{1}{2}\sum_{\mu}\sum_{i,j=1}^{N} a_i^{(\mu)} \widehat{K}_{ij} a_j^{(\mu)}\Big), \tag{1.40}$$

where the $\mu$ stands for the four differents set of Grassmann variables and where the Kasteleyn matrix $\widehat{K}_{ij}$ stands here for $w_{ij}K_{ij}$. Here we do not expose the demonstration in great details and we send the reader back to the original paper [75]. By adding a pair of Grassmann variables $\xi_{ij}$ and $\bar{\xi}_{ij}$ for each link $K_{ij}$, we ensure that it can be used only by one of the color for each distribution, if it was used by two or more we would get at least a double instance of that Grassmann variable, and hence get 0. However, as we are dealing with Grassmann variables, this leads to sign problems. We can avoid that by observing that a pair of Grassmann variables always commutes, and thus does not give us any additional sign trouble. Thus we now have the following formula for the number of 4-coloring of the square lattice

$$Z_{\text{color}} = \int \prod_{\mu=1}^{4} \mathcal{D}[a^{(\mu)}] \exp\Big(\frac{1}{2}\sum_{\mu}\sum_{i,j=1}^{N} a_i^{(\mu)} \bar{\xi}_{ij} \widehat{K}_{ij} \xi_{ij} a_j^{(\mu)}\Big). \tag{1.41}$$

We end up with a quartic fermionic which is of course non-solvable by pfaffian methods. Another approach based on a height mapping can also be followed, leading to several theoretical predictions about the critical behavior of this model and support the conjecture that the scaling limit[8] is well described by a Wess-Zumino-Witten SU(4)$_{k=1}$ conformal field theory [134][9]. This particular problem can be shown to be a special point in the parameter space of compact polymers model called FPL$_2$ [110, 108].

## 1.3 About the full monomer-dimer model

The general monomer-dimer problem is a much more complex and challenging problem in statistical physics and combinatorics, it is defined as the dimer model with a finite density of monomers (see Fig. 1.12). The challenge is to compute the partition function for any density. For the general monomer-dimer problem there is no exact solution except in 1$d$, on the complete and locally tree-like graphs [2] or scale free networks [216]. Furthermore the behavior of monomer-monomer correlations for finite density has been studied numerically [145], and strong evidences for exponential correlations has been established, in accordance with mean-field calculations using Grassmann variables [167]. From a computational point of view, this lack of exact solution has been formalized [112] and the problem has been shown to belong to the $\#P$-complete enumeration class [112].

[8] The two points $g = 0$ and $g = 1$ of Fig. 1.11 seem to be very well understood but we can ask ourselves what about in between ?

[9] Which was apparently conjectured by N.Read in a private communication

### 1.3.1 Mean-field approximation

In the beginning of this chapter, we saw that we can express the hamiltonian of the dimer model Eq. (5.4) using commuting nilpotent variables $\eta_i$ which can be written as a couple of non-commuting Grassmann variables $\eta_i = \theta_i\theta_i^\dagger$ and on gets, for a general lattice with adjacent matrix $A$

$$\mathcal{H} = -\frac{t}{2}\sum_{i,j}\theta_i\theta_i^\dagger A_{ij}\theta_j\theta_j^\dagger, \tag{1.42}$$

where the partition function is the sum over all the configurations of the grassmann variables $Z = \int \mathcal{D}[\theta,\theta_i^\dagger]\mathrm{e}^H$, using the expression $\mathcal{J}[\theta,\theta^\dagger] = \sum_i J_i\theta_i\theta_i^\dagger$ for the monomer current, one can write explicitly the generator of correlation functions as

$$Z[J] = \int \mathcal{D}[\theta,\theta_i^\dagger]\mathrm{e}^{-\mathcal{H}-\mathcal{J}}. \tag{1.43}$$

Using the following bosonic Hubbard-Stratanovich transformation

$$\exp\frac{t}{2}\sum_{i,j}\theta_i\theta_i^\dagger A_{ij}\theta_j\theta_j^\dagger = \int \mathcal{D}[\varphi]\exp\Big[-\frac{1}{2t}\sum_{i,j}\varphi_i A_{ij}^{-1}\varphi_j + \sum_i \varphi_i\theta_i\theta_i^\dagger\Big], \tag{1.44}$$

where $\varphi_i$ are bosonic variables, the generator of correlation functions can be written as

$$Z[J] = \int \mathcal{D}[\varphi,\zeta,\zeta^\dagger]\exp\Big[-\frac{1}{2t}\varphi_i A_{ij}^{-1}\varphi_j + (1+J_i+\varphi_i)\zeta_i\zeta_i^\dagger\Big]. \tag{1.45}$$

Now the integration over grassmann variables can be performed and finally we found $Z[J] =$

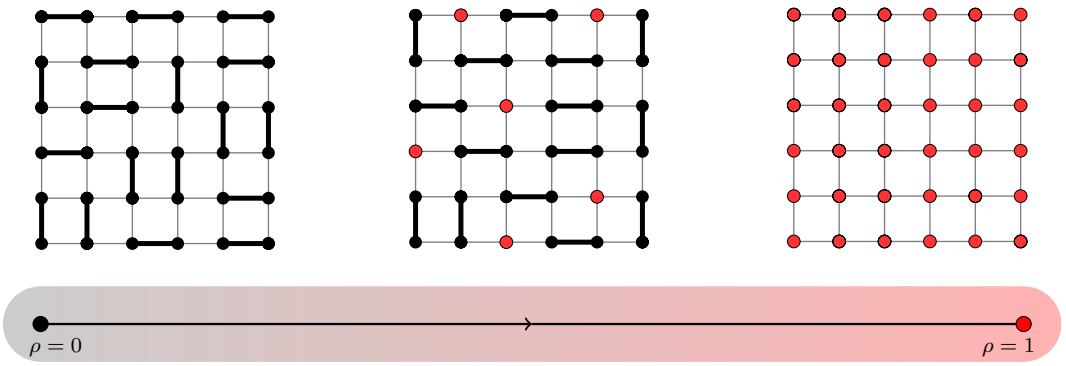


Figure 1.12: Phase diagram of the monomer-dimer model

$\int \mathcal{D}[\varphi]\exp -\frac{\mathcal{S}[\varphi,J]}{t}$, where the action is

$$\mathcal{S}[\varphi,J] = \frac{1}{2}\sum_{ij}(\varphi_i - J_i)A_{ij}^{-1}(\varphi_j - J_j) - t\sum_i \ln\big(1+\varphi_i\big). \tag{1.46}$$

In order to extract information about this system, we shall use a saddle point approximation

$$Z[J] = \int \mathcal{D}[\varphi] \exp\Big[ - \frac{\mathcal{S}[\varphi, J]}{t} \Big] = \exp\Big[ - \frac{\mathcal{S}[\hat{\varphi}, J]}{t} \Big] \Big( 1 + \mathcal{O}(t) \Big), \tag{1.47}$$

where $\hat{\varphi}$ is solutions of $\delta S / \delta \varphi_i = 0$.

$$\frac{\delta \mathcal{S}}{\delta \varphi_i} = 0 \to \rho_i = \frac{1}{t} \sum_j A^{-1}_{ij} \hat{\varphi}_j = \frac{1}{1 + \hat{\varphi}_i}, \tag{1.48}$$

hence

$$J_i = \rho_i^{-1} - 1 - t \sum_j A_{ij} \rho_j. \tag{1.49}$$

and the correlation function is

$$C_{ki} = \frac{\partial \rho_k}{\partial J_i} = \Big( - t A_{ki} - \frac{\delta_{ki}}{\rho_k^2} \Big)^{-1}. \tag{1.50}$$

Now we can write the effective action in the saddle point approximation by using the above expression of $\rho_k$ in function of the field in the saddle point $\hat{\varphi}_k$, and we get

$$\mathcal{S}[J] = \frac{1}{2} \sum_{ij} \rho_i A_{ij} \rho_j + \sum_i \ln \rho_i. \tag{1.51}$$

Using this effective action in presence of a current of monomers, we can use standard field theory methods to compute the density $\rho_i = \langle \theta_i \theta_i^\dagger \rangle$, and correlation function of monomers like $\langle \rho_i \rho_j \rangle = \langle \theta_i \theta_i^\dagger \theta_j \theta_j^\dagger \rangle$ or more complicated object using functional derivatives of the generator of correlation functions $\mathcal{Z}[J]$

$$\langle \rho_{i_1} ... \rho_{i_N} \rangle = \lim_{J \to 0} \frac{1}{\mathcal{Z}[0]} \frac{\delta^N \mathcal{Z}[J]}{\delta J_{i_1} ... \delta J_{i_N}}. \tag{1.52}$$

If we want to look at connected correlation functions, we shall introduce $\mathcal{W}[J] = \ln \mathcal{Z}[J]$ such that

$$\frac{\delta \mathcal{W}[J]}{\delta J_i} = \sum_{kl} \Big[ \frac{\rho_0 - 1}{\rho_k^2} \delta_{kl} + p A_{kl} (\rho_0 - \rho_k) \Big] \frac{\delta \rho_l}{\delta J_i} + \rho_0 = \rho_i.$$

Correlation functions can be obtained by taking derivatives as follow

$$\mathcal{C}_{ij} = \langle \rho_i \rho_j \rangle_c = \lim_{j \to 0} \frac{\delta^2 \mathcal{W}[J]}{\delta J_i \delta J_j} = \frac{\partial \rho_i}{\partial J_k}.$$

The effective action is then

$$\begin{aligned} \Gamma[\rho] &= \mathcal{W}[J] + \sum_i J_i \rho_i \\ &= - \frac{p}{2} \sum_{ij} \rho_i A_{ij} \rho_j + \sum_i \ln \rho_i + \sum_i (1 - \rho_i). \end{aligned} \tag{1.53}$$

We specialize now to the case of uniform hole density $\rho_i = \rho$ and also for the case of the square lattice where the number of nearest neighbors is four and assuming that the number of sites on the lattice is $N$. Then,

$$\Gamma[\rho] = \frac{-4zN\rho^2}{2} + N\log N + N(1-\rho), \tag{1.54}$$

and the current can be written as $J = -4t\rho + \rho^{-1} - 1$, sending the current to zero give the density in terms of $t$

$$\rho = \frac{2}{1+\sqrt{1+16t}}. \tag{1.55}$$

So in the region $t \to 0$, $t = 1 - 4\rho$. Now we compute the propagator $C_{ij}$, $\delta_{ij}$ become $A(\mathbf{q}) = 2a\sum_{k=x,y}\cos q_k a$, such that

$$C(\mathbf{q}) = \left(\rho^{-2} - 2ta\sum_{k=x,y}\cos q_k a\right)^{-1}. \tag{1.56}$$

The conclusion of this mean-field calculation is that for any non-zero monomer density, the system is non-critical (with a finite correlation length). This mean-field analysis gives a rather good approximation of the behavior of the system, but more involved technics have to be implemented to get access to non mean-field results, as the exact value of the correlation length.

### 1.3.2 Baxter approach and matrix product state

One cannot conclude this chapter on the monomer-dimer model without mentioning one of the most impressive advance, which the *numerical* solution of the model by Baxter [15], with a method which is sometimes referred as variational transfer matrix approach, but which is nothing but the *matrix product state method* that we know today. This method is very efficient to compute precise approximations of thermodynamic quantities of the model.

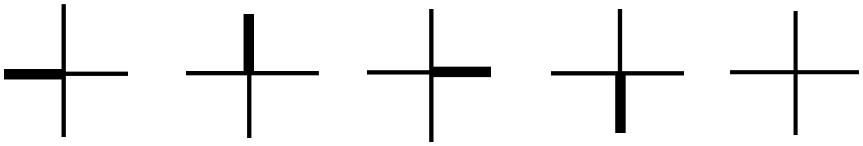

Figure 1.13: Vertex representation of the monomer-dimer model. The extreme-right vertex corresponds to a monomer with weight 1, and the others correspond to vertical and horizontal dimers with weights $s^2$

#### Transfert matrix formulation

Let us consider a square lattice of size $m \times n$ with periodic boundary conditions. For any site $(i,j)$, the occupation of horizontal edges is given by the binary variables $\beta_{i,j}$ and $\beta_{i+1,j}$ and the

occupation of vertical edges is given by $\alpha_{i,j}$ and $\alpha_{i,j+1}$ such that a vertex has a Boltzmann weight $\omega(\alpha_{i,j}, \alpha_{i,j+1}|\beta_{i,j}, \beta_{i+1,j})$ which is equal to zero when there is more than one dimer on every vertex, *i.e.* $\alpha_{i,j} + \alpha_{i,j+1} + \beta_{i,j} + \beta_{i+1,j} > 1$. Then the partition function can be written as

$$Z = \sum_{\{\alpha,\beta\}} \prod_{(i,j)} \omega(\alpha_{i,j}, \alpha_{i,j+1}|\beta_{i,j}, \beta_{i+1,j}). \tag{1.57}$$

This expression is the usual form of the partition function of a vertex model with vertex weight $\omega$. In this fashion the monomer-dimer model is mapped onto a 5-vertex model as show on Fig. 1.14. The partition function can be written in another form

$$Z = \sum_{\{\beta\}} \prod_{i=1}^{m} \overbrace{\Big( \sum_{\{\alpha\}} \prod_{j=1}^{n} \omega(\alpha_{i,j}, \alpha_{i,j+1}|\beta_{i,j}, \beta_{i+1,j}) \Big)}^{T(\beta_{i+1,1}, ..., \beta_{i+1,n}|\beta_{i,1}, ..., \beta_{i,n})}, \tag{1.58}$$

in such way that the partition function reduces to a trace over the vectorial space $V \otimes V^*$[10]

$$\begin{aligned} Z &= \sum_{\{\beta\}} \prod_{i=1}^{m} T(\beta_{i+1,1}, ..., \beta_{i+1,n}|\beta_{i,1}, ..., \beta_{i,n}) \\ &= \sum_{\substack{\beta_{1,1}...\beta_{1,n}, \\ \beta_{m,1}...\beta_{m,n}}} T(\beta_{1,1}, ...|\beta_{m,1}, ...)...T(\beta_{3,1}, ...|\beta_{2,1}, ...)...T(\beta_{2,1}, ...|\beta_{1,1}, ...) \\ &= \mathrm{Tr}\ \hat{T}^m, \end{aligned} \tag{1.59}$$

where $T$ is the vertical transfer matrix with matrix element $T(\beta_{i+1,1}, ..., \beta_{i+1,n}|\beta_{i,1}, ..., \beta_{i,n})$. As usual, in the limit $m \to \infty$, the trace is dominated by the largest eigenvalue $\Lambda$ of $T$ and

$$Z \sim \Lambda^m. \tag{1.60}$$

**Product matrix state formulation**

Let us define $|\Lambda\rangle$ the eigenvector corresponding to the largest eigenvalue $\Lambda$ of the transfer matrix $T$. For any vector $|\psi_0\rangle \in V$, we have

$$T^m|\psi_0\rangle \sim T^m|\Lambda\rangle\langle\Lambda|\psi_0\rangle. \tag{1.61}$$

Now let us choose $\langle\beta_1, \beta_2, ..., \beta_n|T|\psi_0\rangle = 1$ such that

$$\langle\beta'_1, \beta'_2, ..., \beta'_n|T|\psi_0\rangle = \sum_{\beta_1,...,\beta_n} T(\beta'_1, \beta'_2, ..., \beta'_n|\beta_1, \beta_2, ..., \beta_n)\langle\beta_1, \beta_2, ..., \beta_n|\psi_0\rangle, \tag{1.62}$$

$$= \sum_{\beta_1,...,\beta_n} \sum_{\alpha_1,...,\alpha_n} \prod_{j=1}^{n} \omega(\alpha_j, \alpha_{j+1}|\beta_j, \beta'_{j+1}). \tag{1.63}$$

[10] $V = \mathbb{Z}_2^{\otimes n}$

The same calculation can be repeated for $T^m$, after a few lines of calculation we end up with

$$\langle \beta_{m+1,1}, ..., \beta_{m+1,n} | T^m | \psi_0 \rangle = \sum_{\alpha_{1,1},...,\alpha_{1,n}} \prod_{j=1}^{n} \sum_{\beta_{1,j},...,\beta_{m,j}} \prod_{i=1}^{m} \omega(\alpha_{i,j}, \alpha_{i,j+1} | \beta_{i,j}, \beta_{i+1,j}). \quad (1.64)$$

The transfer matrix $T$ correspond to the partition function of a system with a single column with weights $\alpha_{i,j}$ $(j = 1...n)$ and fixed horizontal weights $\beta_{ij}$ and $\beta_{i+1,j}$. This partition function

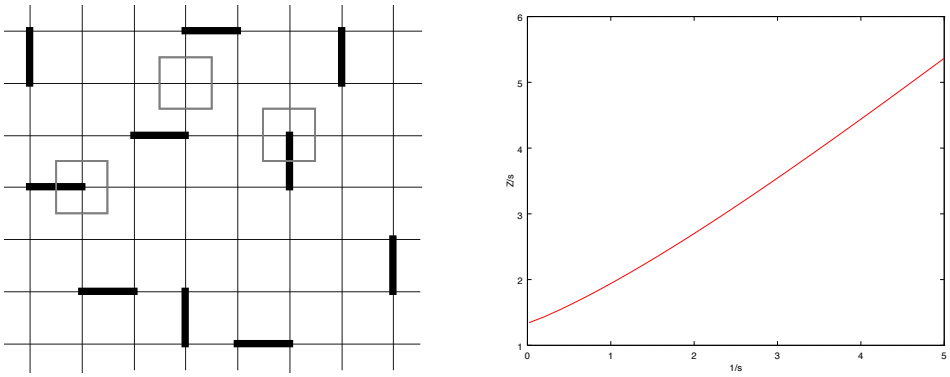


Figure 1.14: Left: Vertex representation of the monomer-dimer model. Partition Function of the system can be represented as a sum of product of local Boltzmann weights. Right: Numerical results from Baxter's method. The partition function increases smoothly with $s^{-1}$ indicating no phase transition in this model. The point $s^{-1} = 0$ is the exact solution saw in the beginning of the chapter and equal to $\exp(G/\pi) \approx 1.338..$, with $G$ is the Catalan constant.

can computed introducing another transfer matrix for which $\beta_{ij}$ and $\beta_{i+1,j}$ are parameters. The elements of this transfer matrix are

$$\begin{aligned} G_{\beta_{m+1,j}}(\alpha'_1, ..., \alpha'_n | \alpha_1, ..., \alpha_n) &= \langle \alpha'_1 ... \alpha'_n | \hat{G}_{m+1,j} | \alpha_1 ... \alpha_n \rangle \\ &= \sum_{\beta_{1,j},...,\beta_{m,j}} \prod_{i=1}^{m} \omega(\alpha_{i,j}, \alpha_{i,j+1} | \beta_{i,j}, \beta_{i+1,j}), \end{aligned} \quad (1.65)$$

such that

$$\begin{aligned} \langle \beta_{m+1,1}, ..., \beta_{m+1,n} | T^m | \psi_0 \rangle &= \sum_{\substack{\alpha_{1,1}...\alpha_{1,n}, \\ \alpha_{m,1}...\alpha_{m,n}}} \prod_{j=1}^{n} G_{\beta_{m+1,j}}(\alpha_{1,j+1}, ..., \alpha_{n,j+1} | \alpha_{1,j}, ..., \alpha_{n,j}) \\ &= \mathrm{Tr}_H \left[ \hat{G}_{m+1,n} \hat{G}_{m+1,n-1} ... \hat{G}_{m+1,1} \right], \end{aligned} \quad (1.66)$$

where we choose periodic boundary conditions $\alpha_{m+1,j} = \alpha_{1,j}$ and $H = \mathbb{Z}_2^{\otimes m}$ is a vectorial space encoding the configurations of links $\alpha$ on a row. Finally

$$|\Lambda\rangle \sim \langle \beta_{m+1,1}, ..., \beta_{m+1,n} | T^m | \psi_0 \rangle = \mathrm{Tr}_H \left[ \hat{G}_{m+1,n} \hat{G}_{m+1,n-1} ... \hat{G}_{m+1,1} \right], \quad (1.67)$$

we have expressed the vector $|\Lambda\rangle$ as a matrix product state, and starting from the expression Eq. (1.67), the next will be to use a variational principle to optimize the matrices $\hat{G}$, some details can be found in the original paper [15], and we show on figure 1.14 numerical results of this method[11]. It is quite clear that the numerical calculations do not show any divergences of the thermodynamic quantities then no phase transition for any non-zero densities. This numerical method can be applied to any model with local Boltzmann weights defined on the vertices of a lattice and future challenge emerging out of this present work is the study of other two dimensional dimer related models as the trimer model [83] or the four-color model [134, 75] which can be seen as an interacting colored dimer model.

### 1.3.3 Heilmann-Lieb theorem and Ising model in a magnetic field

From a computational point of view, the problem has been shown to belong to the $\#P$-complete enumeration class [112] and all the methods available are either efficient but approximative [15, 125] or exact but desperately slow [1]. Let us start by counting the number of ways $N_{2p}(M,N)$ of choosing the positions of $2p$ monomers on a $M\times N$ lattice, the result is a simple binomial expression $N_{2p}(M,N)=\binom{M^2/2}{p}\binom{N^2/2}{p}$. Using this formula we can sum up over the number of monomers $2p$ to obtain the number of ways to choose the positions of the monomers. Finally the number of terms in the full partition function is one (the pure dimer model) plus all the terms with an even number of monomers (one choose $M=N=L$ for simplicity)

$$N(L)=1+\sum_{p=1}^{L^2/2}N_{2p}(L)=\frac{2^{L^2}\Gamma\left(\frac{L^2+1}{2}\right)}{\sqrt{\pi}\Gamma\left(\frac{L^2+2}{2}\right)}. \tag{1.68}$$

This number grows as $2^{L^2}$ when the size of the lattice goes to infinity, making the problem impossible to solve analytically. We can formally write down the full monomer-dimer partition function as a sum over the number and the positions of monomers

$$Z_{M\times N}=Q_0+\sum_{\{r_i\}}Q_2+\sum_{\{r_i\}}Q_4+...+\sum_{\{r_i\}}Q_{M\times N}, \tag{1.69}$$

where $Q_0$ is the dimer partition function, and $Q_2,Q_4...Q_{M\times N}$ are the partition functions with two, four...$M\times N$ monomers with fixed positions. For concreteness[12], we consider the partition function

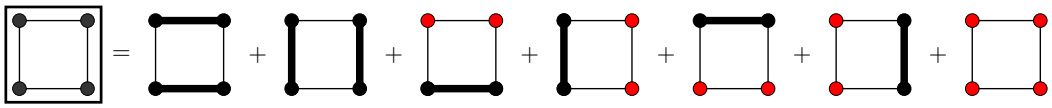

Figure 1.15: Diagrammatic representation of Eq. (1.69), the first two diagrams are $Q_0$, the four next are $Q_2$ and the last is $Q_4$. The coefficient here are different $Z_{2\times 2}(x)=x^4+4x^2+2$, because the condition are free on the figure and periodic in Eq. (1.69).

[11] Thanks to Christophe Chatelain for the simulations and for discussions on this problem

[12] The presentation and the enumerative results come again from the book of W.Krauth [144].

$Z_{L\times L}(\beta)$ for an $L\times L$ square lattice with periodic boundary conditions and we follow closely [144]. $Z_{L\times L}(\beta)$ is a polynomial in $x=\mathrm{e}^{-\beta\epsilon}$ with positive coefficients which, for small lattices, are given by

$$\begin{aligned} Z_{2\times 2}(x) &= x^4+8x^2+8, \\ Z_{4\times 4}(x) &= x^{16}+32x^{14}+400x^{12}+...+3712x^2+272, \\ Z_{6\times 6}(x) &= x^{36}+72x^{34}+...+5409088488x^{12}+...+90176. \end{aligned} \tag{1.70}$$

The coefficients of $Z_{2\times 2}(x)$ correspond to the fact that in the $2\times 2$ lattice without periodic boundary conditions, we can build one configuration with zero dimers and eight configurations each with one and with two dimers (see Fig. 1.3.3). Generally for a $L\times L$ lattice

$$Z_{L\times L}=\sum_{k=0}^{L^2/2}\alpha_{2k}x^{2k}, \tag{1.71}$$

where the $\alpha_k$ are the number of configurations of dimers with $k$ monomers. The way a phase transition can nevertheless take place in the limit of an infinite system limit involves considering the partition function as a function of $x$, taken as a complex variable, and study the repartition of the positions of the zeros on the complex plane. For the monomer-dimer model, Heilmann and Lieb

**Box 2** (Sketch of the proof)**.**

Standard algorithms allow us to compute the (complex-valued) zeros of these polynomials, that is, the values of x for which $Z_{L\times L}(x)=0$, etc. For all three lattices, the zeros remain on the imaginary axis, and the partition function can be written as

$$\begin{aligned} Z_{2\times 2}(x) &= (x^2+1.1716)(x^2+6.828), \\ Z_{4\times 4}(x) &= (x^2+0.102)(x^2+0.506)...(x^2+10.343), \\ Z_{6\times 6}(x) &= (x^2+0.024)(x^2+0.121)...(x^2+10.901). \end{aligned} \tag{1.72}$$

Generally we can write the partition function as a product

$$\boxed{Z_{L\times L}=\prod_{k=1}^{L^2}(x+iz_k),} \tag{1.73}$$

where $\{z_k\}$ are the zeros of the function $Z_{L\times L}$. It is shown that, for given non-negative weight , $Z_{L\times L}$ cannot be zero if $\Re(x_i)>0\ \forall i=1,2...L\times L$ or if $\Re(x_i)<0\ \forall i=1,2...L\times L$. In particular, if $x_i\ \forall i=1,2...L\times L$ , this leads to the conclusion that the zeros of $Z_{L\times L}$ appear on the imaginary-$x$ axis (or at $x=0$), a result that holds also in the appropriate thermodynamic limit. Now in order to complete the proof, one must show that the zeros stay on the imaginary axis and never cross the real one at the thermodynamic limit. More generally, it can be showed by recursion that the zeros of the partition function for any lattice are sandwiched in by the zeros of partition functions for lattices with one more site (see [125] for details), concluding the proof of absence of phase transition in any dimensions and for any lattices.

shown in a famous work [89, 90] that the zeros stay on the imaginary axis. This corresponds to the absence of a phase transition in the monomer-dimer system in any dimension, except, eventually, at $x = 0$ which correspond to the pure dimer case, confirming the results of Baxter presented in the past section. A partial proof of this result is shown in the **box 2** above. A natural extension of this model, is to add interactions between dimers on the same plaquette for instance. It has been shown that for a range of values of the interaction, the system can be critical even with a non-zero monomer density [4, 3, 167]. A short introduction of this model will be discussed in the end of the third chapter.

## 1.4 Conclusions

In this chapter, we gave a rather personal overview of the field of combinatorial statistical models and specially systems which are related to dimer models. We have voluntary chosen very few simple examples that are relevant for this study and omit a lot of technicalities. In particular we have mentioned a couples of times relations to conformal field theory that we have not defined in much details, for sake of clarity. Nevertheless, in the third chapter of this thesis, a more detailed comparison to conformal field theory will be examined, and some of the most familiar applications will be treated. We have seen that non-commuting variables are very useful to describe the partition function of this kind of models. In the next chapter, this approach will used in a rather different way to compute exactly the partition function of the simple dimer model. We shall focus in the computation of the extension of the dimer model when one allows for the presence of a finite number of fixed monomers. While this problem is very difficult to handle with the Kasteleyn theory, leading only to results in a perturbative way, the alternative approach will give us the exact expression on a discrete level.

CHAPTER 2

# Dimer model: Plechko solution and generalization

## Contents

In this chapter, the fully-detailed Grassmann solution of the dimer model originally found by Plechko is presented, as well as informations you can get for the Ising model. Then the solution is extended for the case with an arbitrary number of monomers, which will lead to the exact form of correlation functions in a pfaffian formulation. In particular, we show that the problem become simpler when we consider boundary monomers, and a closed expression for correlations can be found. After that, the simple application of the case of one boundary monomer is shown to be exactly the known result confirming the exactness of our solution. We shall finish by noticing some purely combinatorial properties of the partition function with boundary monomers.

## 2.1 Plechko solution

The approach introduce presently has been developed by Plechko in a series of papers [171, 172] and allows for the exact partition function for the $2d$ Ising model. In this chapter we briefly recall the method of resolution of the $2d$ dimer model based on the integration over Grassmann variables and factorization principles for the partition function. The hamiltonian of the dimer model on a general graph can be written as we saw before as

$$Q_0 = \int \mathcal{D}[\eta] \exp\Big( -\frac{t}{2} \sum_{ij} \eta_i A_{ij} \eta_j \Big), \tag{2.1}$$

which in the particular case of a square lattice of size $L \times L$ with $L$ even takes the following form

$$Q_0 = \int \mathcal{D}[\eta] \prod_{m,n}^{L} (1 + t_x \eta_{mn}\eta_{m+1n})(1 + t_y \eta_{mn}\eta_{mn+1}), \tag{2.2}$$

where $\eta_{mn}$ are nilpotent and commuting variables on every vertices of the square lattice.

### 2.1.1 Fermionization and mirror symmetry

The integrals can be computed introducing a set of Grassmann variables $(a_{mn}, \bar{a}_{mn}, b_{mn}, \bar{b}_{mn})$, (*cf.* Fig. 2.1(*a*)), such that

$$\begin{aligned}
(1 + t_x \eta_{mn}\eta_{m+1n}) &= \int \mathcal{D}[\bar{a}]\, \mathcal{D}[a] e^{a_{mn}\bar{a}_{mn}} (1 + a_{mn}\eta_{mn})(1 + t_x \bar{a}_{mn}\eta_{m+1n}), \\
(1 + t_y \eta_{mn}\eta_{mn+1}) &= \int \mathcal{D}[\bar{b}]\, \mathcal{D}[b] e^{b_{mn}\bar{b}_{mn}} (1 + b_{mn}\eta_{mn})(1 + t_y \bar{b}_{mn}\eta_{mn+1}).
\end{aligned} \tag{2.3}$$

This decomposition allows for an integration over variables $\eta_{mn}$, after rearranging the different link variables $A_{mn} := 1 + a_{mn}\eta_{mn}$, $\bar{A}_{m+1n} := 1 + t_x \bar{a}_{mn}\eta_{m+1n}$, $B_{mn} := 1 + b_{mn}\eta_{mn}$ and $\bar{B}_{mn+1} := 1 + t_y \bar{b}_{mn}\eta_{mn+1}$. Then the partition function becomes

$$Q_0 = \mathrm{Tr}_{\{a,\bar{a},b,\bar{b},\eta\}} \prod_{m,n}^{L} (A_{mn}\bar{A}_{m+1n})(B_{mn}\bar{B}_{mn+1}), \tag{2.4}$$

where we use the notation for the measure of integration

$$\mathrm{Tr}_{\{a,\bar{a},b,\bar{b},\eta\}} X(a,\bar{a},b,\bar{b},\eta) = \int \mathcal{D}[\bar{a}]\,\mathcal{D}[a]\,\mathcal{D}[\bar{b}]\,\mathcal{D}[b]\,\mathcal{D}[\eta] \prod_{mn} e^{a_{mn}\bar{a}_{mn}+b_{mn}\bar{b}_{mn}} X(a,\bar{a},b,\bar{b},\eta). \quad (2.5)$$

We finally obtain the following exact expression

$$Q_0 = \mathrm{Tr}_{\{a,\bar{a},b,\bar{b},\eta\}} \prod_{n=1}^{\overrightarrow{L}} \Big( \prod_{m=1}^{\overleftarrow{L}} \bar{B}_{mn} \prod_{m=1}^{\overrightarrow{L}} \bar{A}_{mn} B_{mn} A_{mn} \Big). \quad (2.6)$$

**Box 2** (Mirror symmetry)**.**

Then, the non-commuting link variables are moved in such a way that each $\eta_{mn}$ is isolated and can be integrated directly. This rearrangement is possible in two dimensions thanks to the mirror ordering introduced by Plechko for the Ising model. The ordering process can be detailed as follow

$$\begin{aligned}
\prod_{m,n}^{L} (A_{mn}\bar{A}_{m+1n})(B_{mn}\bar{B}_{mn+1}) &= \prod_{n=1}^{\overrightarrow{L}} (A_{1n}\bar{A}_{2n})(B_{1n}\bar{B}_{1n+1})(A_{2n}\bar{A}_{3n})(B_{2n}\bar{B}_{2n+1})\cdots \\
&= \prod_{n=1}^{\overrightarrow{L}} (A_{1n}\bar{A}_{2n})(A_{2n}\bar{A}_{3n})\cdots(B_{1n}B_{2n}\cdots\bar{B}_{2n+1}\bar{B}_{1n+1}) \\
&= \prod_{n=1}^{\overrightarrow{L}} (B_{1n}(A_{1n}\bar{A}_{2n})B_{2n}(A_{2n}\bar{A}_{3n})\cdots\bar{B}_{2n+1}\bar{B}_{1n+1}) \\
&= \prod_{n=1}^{\overrightarrow{L}} (\bar{B}_{Ln}..\bar{B}_{2n}\bar{B}_{1n})(B_{1n}A_{1n}\bar{A}_{2n}B_{2n}A_{2n}\bar{A}_{3n}..\bar{A}_{Ln}B_{Ln}A_{Ln})
\end{aligned}$$

where the products are ordered according to the orientation of the arrows. The Grassmann terms in brackets $(\cdots)$ on the first line of the previous equation are commuting objects, since they are integral representations of commuting scalars. This also imposes the boundary conditions $\bar{A}_{1n} = 1$, $\bar{A}_{L+1n} = 1$, $\bar{B}_{m1} = 1$, and $\bar{B}_{mL+1} = 1$, or $\bar{a}_{0n} = \bar{a}_{Ln} = \bar{b}_{m0} = \bar{b}_{mL} = 0$ (for open boundary conditions only).

### 2.1.2 Pfaffian solution without monomer

The integration over the $\eta_{mn}$ variables is performed exactly, recursively from $m = 1$ to $m = L$ for each $n$. Each integration leads to a quantity $L_{mn} = a_{mn} + b_{mn} + t_x\bar{a}_{m-1n} + (-1)^{m+1}t_y\bar{b}_{mn-1}$ which is moved to the left of the products over $m$, hence a minus sign is needed in front of $\bar{b}$ each

time a $L_{mn}$ crosses the product of $\bar{B}$ terms on the left. Finally

$$Q_0 = \mathrm{Tr}_{\{a,\bar{a},b,\bar{b}\}} \overrightarrow{\prod_{m,n}^{L}} L_{mn}, \tag{2.7}$$

becomes an integration over products of linear Grassmann terms. This can be further simplified by introducing additional Grassmann variables $c_{mn}$ such that

$$L_{mn} = \int \mathrm{d}c_{mn} \exp(c_{mn} L_{mn}). \tag{2.8}$$

This expresses $Q_0$ as a Gaussian integral over variables $(a, \bar{a}, b, \bar{b}, c)$, and therefore $Q_0$ is a simple determinant of a quadratic form. Indeed, after partially integrating over variables $(a, \bar{a}, b, \bar{b})$ and symmetrization of the expressions, one obtains

$$\begin{aligned} Q_0 &= \mathrm{Tr}_{\{a,\bar{a},b,\bar{b},c\}} \exp\left(\sum_{mn} c_{mn} L_{mn}\right) \\ &= \int \mathcal{D}[c] \exp \sum_{mn} \left[\frac{1}{2} t_x (c_{m+1n} c_{mn} - c_{m-1n} c_{mn}) + \frac{1}{2} t_y (-1)^{m+1} (c_{mn+1} c_{mn} - c_{mn-1} c_{mn})\right]. \end{aligned} \tag{2.9}$$

**Box 3** (Symmetrization)**.**

We use the following definition for the Fourier transform

$$c_{mn} = \frac{2 i^{m+n}}{L+1} \sum_{p,q=1}^{L} c_{pq} \sin\left(\frac{\pi p m}{L+1}\right) \sin\left(\frac{\pi q n}{L+1}\right), \tag{2.10}$$

with $c_{0n} = c_{L+1n} = c_{m0} = c_{mL+1} = 0$. Inserting Eq. (2.10) into Eq. (2.9), and using two following sum identities

$$\frac{2}{L+1} \sum_{m=1}^{L} \sin\left(\frac{\pi p m}{L+1}\right) \sin\left(\frac{\pi q m}{L+1}\right) = \delta_{p,q}, \tag{2.11}$$

$$\frac{2}{L+1} \sum_{m=1}^{L} (-1)^{m+1} \sin\left(\frac{\pi p m}{L+1}\right) \sin\left(\frac{\pi q m}{L+1}\right) = \delta_{p+q,L+1}. \tag{2.12}$$

The summation is performed only for 1/4 of the Fourier modes, (see Fig. 2.1($b$)), since the other are related by the symmetry $p \to L+1-p$ and $q \to L+1-q$. This block representation is convenient for computing the remaining integrals over the momenta. This leads to a block representation of the action in the momentum space, for momenta inside the reduced sector $1 \leq p, q \leq L/2$. The four components of these vectors will be written $c^{\mu}_{\alpha}$ with $\mu = 1 \cdots 4$, leading to

$$Q_0 = \int \mathcal{D}[c] \exp S_0[c], \tag{2.13}$$

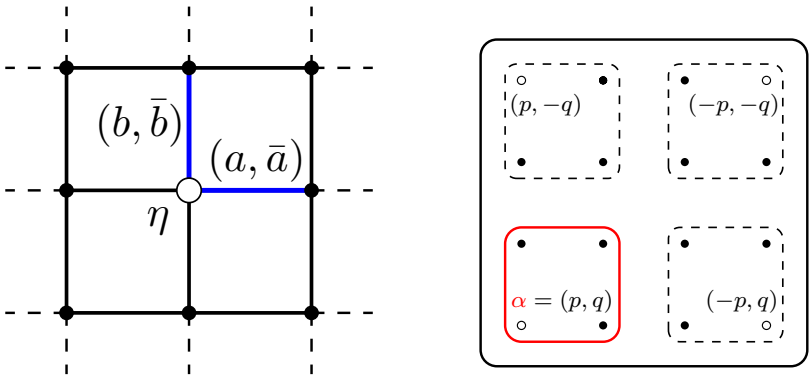


Figure 2.1: $(a)$ Grassmann representation for each dimer, with one nilpotent variable $\eta$ per site, and two pairs of Grassmann variables for the two directions along the links connecting two neighboring sites. $(b)$ Block partition of the Fourier modes. The modes considered in the summation Eq. (**??**) belongs to the sector inside the reduce domain (red delimitation) $1 \leq p, q \leq L/2$. For one point labeled $\alpha = (p, q)$ inside this domain correspond 3 others points related by symmetry $p \to L+1-p$ and $q \to L+1-q$ (open circles).

with $S_0[c] = \frac{i}{2} c_\alpha^\mu M_\alpha^{\mu\nu} c_\alpha^\nu$ [1], where the antisymmetric matrix $M$ is defined by

$$M_\alpha = \begin{pmatrix} 0 & 0 & a_y(q) & a_x(p) \\ 0 & 0 & -a_x(p) & a_y(q) \\ -a_y(q) & a_x(p) & 0 & 0 \\ -a_x(p) & -a_y(q) & 0 & 0 \end{pmatrix} \tag{2.14}$$

with

$$\begin{aligned} a_x(p) &= 2t_x \cos \frac{\pi p}{L+1}, \\ a_y(q) &= 2t_y \cos \frac{\pi q}{L+1}. \end{aligned} \tag{2.15}$$

This matrix can be written as

$$M_\alpha = a_x(p)\Gamma_x + a_y(q)\Gamma_y, \tag{2.16}$$

where the matrices $\Gamma_x$ and $\Gamma_y$ are

$$\Gamma_x = \begin{pmatrix} 0 & 0 & 0 & 1 \\ 0 & 0 & -1 & 0 \\ 0 & 1 & 0 & 0 \\ -1 & 0 & 0 & 0 \end{pmatrix}, \; \Gamma_y = \begin{pmatrix} 0 & 0 & 1 & 0 \\ 0 & 0 & 0 & 1 \\ -1 & 0 & 0 & 0 \\ 0 & -1 & 0 & 0 \end{pmatrix}, \tag{2.17}$$

[1] Einstein notations are used

with $\Gamma_x^2 = \Gamma_y^2 = -1$. Hence the expression Eq. (2.9) is directly related to the pfaffian of the matrix $M$ (*cf.* 1.1 for details) and is simply equal to

$$\begin{aligned} Q_0 &= \prod_{\alpha} \mathrm{pf} M_\alpha \\ &= \prod_{p,q}^{L/2} [a_x(p)^2 + a_y(q)^2]. \end{aligned} \tag{2.18}$$

Finally one simply obtains the following well known result

$$Q_0 = \prod_{p,q=1}^{L/2} \left[ 4t_x^2 \cos^2 \frac{\pi p}{L+1} + 4t_y^2 \cos^2 \frac{\pi q}{L+1} \right]. \tag{2.19}$$

The fermionization can also be performed for toroidal boundary conditions. We refer here to the experience with the $2d$ Ising model on a torus [171]. The final result can be written in terms of a combination of the periodic-antiperiodic boundary conditions for fermions $c_{M+1n=\pm c_{1n}}$ and $c_{mN+1=\pm c_{m1}}$. The main ingredient of this recipe is the mirror factorization Eq. (5.7) of the partition function, which allows a direct integration over nilpotent variables. This mirror factorization is then the major obstacle to the generalization of this formalism in $d > 2$. Indeed, for the $3d$ case, a generalization of this factorization is far from obvious and remains to find.

### 2.1.3 Majorana fermions lattice theory

In this section, we derive the continuum limit of the dimer action Eq. (2.9) and reformulate in terms of two copies of Ising models. By an adequate change of variables [88] $c_{mn} \to i^{3/2+m^2} c_{mn}$, the action $\mathcal{S}_0$ can be written as a complex fermion field theory

$$\mathcal{S}_0 = \sum_{m,n} \left[ \frac{1}{2} t_x (c_{m+1n} c_{mn} - c_{m-1n} c_{mn}) + \frac{i}{2} t_y (c_{mn+1} c_{mn} - c_{mn-1} c_{mn}) \right].$$

We can introduce the formal derivative using series expansions $c_{m+1n} = c_{mn} + \partial_x c_{mn}$ and $c_{mn+1} = c_{mn} + \partial_y c_{mn}$, up to first order in lattice elementary step, so that the action can be recognized as a purely kinetic form with no mass contribution:

$$\mathcal{S}_0 = \sum_{m,n} \left[ t_x \partial_x c_{mn} c_{mn} + i t_y \partial_y c_{mn} c_{mn} \right]. \tag{2.20}$$

It is convenient to define the following fields:

$$\begin{aligned} &c_-(m,n) = c_{2m2n},\ c_+(m,n) = c_{2m2n+1}, \\ &\bar{c}_-(m,n) = c_{2m+12n+1},\ \bar{c}_+(m,n) = c_{2m+12n}, \end{aligned} \tag{2.21}$$

and express the previous action in terms of these fields only:

$$\begin{aligned} \mathcal{S}_0 = &- \sum_{m,n=1}^{L/2} \sum_{\sigma=\pm} \left[ t_x (c_\sigma \partial_x \bar{c}_{-\sigma} + \bar{c}_\sigma \partial_x c_{-\sigma}) \right. \\ &+ \left. i t_y (c_\sigma \partial_y c_{-\sigma} + \bar{c}_\sigma \partial_y \bar{c}_{-\sigma}) \right]. \end{aligned} \tag{2.22}$$

Site variables $(m,n)$ now designate the locations of reduced cells containing four sites and take values between 0 and $L/2$. Field vectors $(c_\sigma, \bar{c}_\sigma)$ are composed of two independent components and describe two coupled Ising models labeled by index $\sigma = \pm$. This action can be diagonalized with a linear transformation, and new set of Grassmann variables:

$$\begin{aligned}
\varphi_- &= \frac{1}{2}\left(c_- + c_+ + \bar{c}_- + \bar{c}_+\right), \\
\bar{\varphi}_- &= \frac{1}{2}\left(c_- + c_+ - \bar{c}_- - \bar{c}_+\right), \\
i\varphi_+ &= \frac{1}{2}\left(c_- - c_+ + \bar{c}_- - \bar{c}_+\right), \\
i\bar{\varphi}_+ &= \frac{1}{2}\left(c_- - c_+ - \bar{c}_- + \bar{c}_+\right).
\end{aligned} \tag{2.23}$$

We obtain finally a diagonalized form for the action, defining the complex derivative in two-dimensions, $\partial = t_x\partial_x + it_y\partial_y$ and $\bar{\partial} = t_x\partial_x - it_y\partial_y$:

$$\mathcal{S}_0 = -\sum_{m,n=0}^{L/2}\left(\bar{\varphi}_+\bar{\partial}\bar{\varphi}_+ - \varphi_+\partial\varphi_+ - \bar{\varphi}_-\bar{\partial}\bar{\varphi}_- + \varphi_-\partial\varphi_-\right).$$

Following Plechko [173], it is useful to introduce Dirac matrices

$$\sigma_1 = \begin{pmatrix} 0 & 1 \\ 1 & 0 \end{pmatrix}, \sigma_2 = \begin{pmatrix} 0 & -i \\ i & 0 \end{pmatrix}, \sigma_3 = \begin{pmatrix} 1 & 0 \\ 0 & -1 \end{pmatrix},$$

and define spinor $\Psi_\sigma = \begin{pmatrix} \varphi_\sigma \\ \bar{\varphi}_\sigma \end{pmatrix}$. It has to be noted that $\varphi_\sigma$ and $\bar{\varphi}_\sigma$ are not conjugated but independent Grassmann variables. The action can then be put into a compact expression,

$$\mathcal{S}_0 = \sum_{m,n=0}^{L/2}\sum_{\sigma=\pm} {}^t\bar{\Psi}_\sigma\left(\sigma_1\partial_1 + \sigma_2\partial_2\right)\Psi_\sigma, \tag{2.24}$$

where $\bar{\Psi}_\sigma = i\sigma_2\Psi_\sigma$ and $\partial_1 = t_x\partial_x$, $\partial_2 = t_y\partial_y$. Here the resulting action is of Majorana form [173], equivalent to two independent Ising models at criticality, since no mass term is present.

### The Ising model *via* the Plechko method

Originally [171, 172] this method was used to construct a fermionic field theoretical derivation of the Ising model on a general $2d$ lattice. The exact same method shown above can be extend for the Ising model replacing the nilpotent variables $\eta$ by spins $\sigma$ variables

$$Z = \int \mathcal{D}[\sigma]\exp\Big(-\frac{J}{2}\sum_{ij}\sigma_i A_{ij}\sigma_j\Big). \tag{2.25}$$

This method is particularly useful to express the partition function of a general Ising model as shown in Fig. 2.2. For example we can write the partition function for the two first case of the figure (*i.e.* square and triangular) as

$$Z = \mathrm{Tr}_{\{\sigma\}}\prod_{mn}(\alpha_1\sigma_{mn}\sigma_{m+1n} + \alpha_2\sigma_{m+1n}\sigma_{m+1n+1} + \alpha_3\sigma_{mn}\sigma_{m+1n+1} + \alpha_0), \tag{2.26}$$

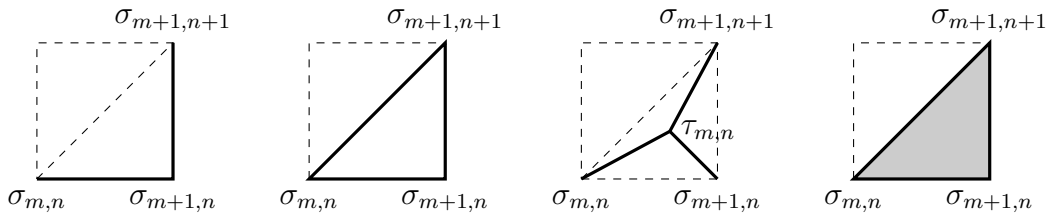


Figure 2.2: Square, triangular and hexagonal lattices. On the right, we can imagine arbitrary interactions between spins. Figures from [107]

and $\{\alpha_0, \alpha_1, \alpha_2, \alpha_3\}$ is a set of four coefficients which can easily be determined for any given lattice. Starting from here and following the same strategy can lead in a simple way to exact information about the critical point.

- Determination of the value of the critical temperature as a consequence of the Krammers Wannier duality in terms of the $\alpha$'s
- Computation of the critical exponents *e.g* $M = \left(1 - \frac{\alpha_0^* \alpha_1^* \alpha_2^* \alpha_3^*}{\alpha_0 \alpha_1 \alpha_2 \alpha_3}\right)^{1/8}$ for $T \leqslant T_c$, leading to the famous Onsager result $M \sim t^{1/8}$ at criticality (The $\alpha_i^*$ are rescaled functions of the $\alpha$, see [173] for details and $t = 1 - T_c/T$.)
- Spin correlation functions can be obtained as well via Toeplitz determinant.
- The fermionic action in the continuum limit is also easy to derive

$$S_{\text{Ising}} = \int \mathrm{d}^2 x \Big( \psi(x) \partial \psi(x) + \bar{\psi}(x) \bar{\partial} \bar{\psi}(x) + m \psi(x) \bar{\psi}(x) \Big) \tag{2.27}$$

  where $m$ is a mass term depending of the parameters $\alpha_i$ and vanishing at criticality. We can therefore conclude that the critical Ising model corresponds, in the continuum limit, to two massless Majorana fermions, *i.e.* a $c = 1/2$ unitary CFT.

This method of grassmann variables has been widely used to solve in a very simple and elegant fashion many problems, *e.g.* the $2d$ Ising model [171, 172], boundary-field Ising model [42], the Blume-Capel model [170, 44] or more general spin models [77, 43].

## 2.2 Pfaffian solution with $2n$ monomers

Let us now consider the case where an even number of monomers are present on the lattice at different positions $\mathbf{r}_i = (m_i, n_i)$ with $i = 1, \cdots, 2n$. The partition function $Q_{2n}(\{\mathbf{r}_i\})$ is the number of all possible configurations with the constraint imposed by the fixed monomers as we have defined in the first chapter.

### 2.2.1 General solution of the problem

This quantity can be evaluated by inserting nilpotent variables $\eta_{m_i n_i}$ in the partition function, which prevents possible dimers to occupy sites $\mathbf{r}_i$. It can be useful to introduce an additional Grassmann variable $h_i$ such that $\eta_{m_i n_i} = \int \mathrm{d}h_i \exp(h_i \eta_{m_i n_i})$. These insertions are performed at point $\mathbf{r}_i$ in $Q_0$, and the integration over $\eta_{m_i n_i}$ modifies $L_{m_i n_i} \to L_{m_i n_i} + h_i$. However, by moving the $\mathrm{d}h_i$ variable to the left of the remaining ordered product, a minus sign is introduced in front of each $\bar{b}_{mn_i-1}$ in $\bar{B}_{mn_i}$ for all $m > m_i$. We can replace $\bar{b}_{mn-1}$ by $\epsilon_{mn}\bar{b}_{mn-1}$ such that $\epsilon_{mn_i} = -1$ for $m > m_i$, and $\epsilon_{mn} = 1$ otherwise. The integration is then performed on the remaining variables $(a, \bar{a}, b, \bar{b})$ as usual, so that $Q_{2n}(\{\mathbf{r}_i\})$ can be expressed as a Gaussian form, with a sum of terms corresponding to the monomer insertion, resulting to the following form for the the partition function

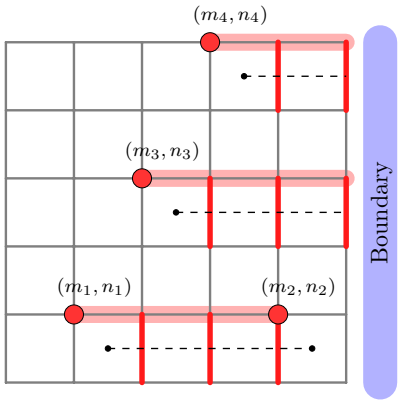


Figure 2.3: Typical dimer configuration for a $6 \times 6$ square lattice. The dashed line is the extra term that arises from moving towards the border the Grassmann field conjugated to the monomer. This is equivalent to change the sign of the $t_y$ couplings (red links) from the monomers to the boundary. When two monomers are located on the same horizontal line, the change of sign concerns only the couplings between the two monomers.

$$Q_{2n}(\{\mathbf{r}_i\}) = \int \mathcal{D}[c]\,\mathcal{D}[h] \exp\left[ S_0 + \sum_{\mathbf{r}_i} c_{m_i n_i} h_i + 2t_y \sum_{\mathbf{r}_i, m=m_i+1}^{L} (-1)^{m+1} c_{mn_i-1} c_{mn_i} \right]. \quad (2.28)$$

The inclusion or monomers is equivalent to inserting a magnetic field $h_i$ at points $\mathbf{r}_i$, as well as a sum of quadratic terms $c_{mn_i-1}c_{mn_i}$ running from the hole position to the boundary on the right (see Fig. 2.3). Another possibility would be to join two monomers by a line of terms by moving $\mathrm{d}h_{m_i n_i}$ until $\mathrm{d}h_{m_j n_j}$ as in the Kasteleyn theory. In this case, the additional quadratic terms in the action starting from $\mathbf{r}_i$ and ending on the boundary have to be treated in the computation of the fermionic integral. We first rewrite $S_0$ in the Fourier space using the block partition label $\alpha = (p, q)$ for momenta $p$ and $q$ inside the reduced sector $1 \cdots L/2$, and vectors $\mathbf{c}_\alpha =^t (c_{pq}, c_{-pq}, c_{p-q}, c_{-p-q})$. Also the 4 components of vector $\mathbf{c}_\alpha$ will be written $c_\alpha^\mu$ where $\mu = 1 \cdots 4$. Then $S_0 = \frac{i}{2} c_\alpha^\mu M_\alpha^{\mu\nu} c_\alpha^\nu$, where the antisymmetric quadratic form $M_\alpha$ is defined by Eq. (2.14). The part of the field interaction can be Fourier transform as before with a linear field $H_{pq}$ depending on $h_i$s and we

obtain

$$\sum_{\mathbf{r}_i} c_{m_i,n_i} h_i = \sum_{p,q=1}^{L} c_{pq} H_{pq} = \sum_{\alpha,\mu} c_\alpha^\mu H_\alpha^\mu. \tag{2.29}$$

The last contribution connecting the monomers to the boundary can be written as $\frac{i}{2} c_\alpha^\mu V_{\alpha\beta}^{\mu\nu} c_\beta^\nu$, with matrix $V_{\alpha\beta} = V_{pq,p'q'}$ given by

$$V_{pq,p'q'} = \sum_{\mathbf{r}_i} \frac{8 t_y (-1)^{n_i}}{(L+1)^2} \left\{ \sum_{m=m_i+1}^{L} \sin\frac{\pi p m}{L+1} \sin\frac{\pi p' m}{L+1} \right\} \left[ \sin\frac{\pi q (n_i-1)}{L+1} \sin\frac{\pi q' n_i}{L+1} - (q \leftrightarrow q') \right].$$

The different components $V_{\alpha\beta}^{\mu\nu}$ are given implicitly, for the first elements, by $V_{\alpha\beta}^{11} = V_{pq,p'q'}$, $V_{\alpha\beta}^{12} = V_{pq,-p'q'}$, $V_{\alpha\beta}^{21} = V_{-pq,p'q'}$, and so on. Then the total fermionic action contains three terms

$$S = \frac{i}{2} c_\alpha^\mu M_\alpha^{\mu\nu} c_\alpha^\nu + \frac{i}{2} c_\alpha^\mu V_{\alpha\beta}^{\mu\nu} c_\beta^\nu + c_\alpha^\mu H_\alpha^\mu. \tag{2.30}$$

The first two terms contain only modes of the same sector $\alpha$, and the last connects modes from different sectors $\alpha$ and $\beta$. Matrices $M_\alpha^{\mu\nu}$ and $V_{\alpha\beta}^{\mu\nu}$ are antisymmetric: $M_\alpha^{\mu\nu} = -M_\alpha^{\nu\mu}$ and $V_{\alpha\beta}^{\mu\nu} = -V_{\beta\alpha}^{\nu\mu}$. Also $V_{\alpha\alpha} = 0$. Then the quantity $Q_{2n}(\{\mathbf{r}_i\})$ can be formally written as

$$\begin{aligned} Q_{2n}(\{\mathbf{r}_i\}) &= \int \mathcal{D}[c]\, \mathcal{D}[h] \exp\left( \frac{i}{2} c_\alpha^\mu [M_\alpha^{\mu\nu} \delta_{\alpha\beta} + V_{\alpha\beta}^{\mu\nu}] c_\beta^\nu + c_\alpha^\mu H_\alpha^\mu \right) \\ &= \int \mathcal{D}[c]\, \mathcal{D}[h] \exp\left( \frac{i}{2} c_\alpha^\mu W_{\alpha\beta}^{\mu\nu} c_\beta^\nu + c_\alpha^\mu H_\alpha^\mu \right), \end{aligned} \tag{2.31}$$

with $W_{\alpha\beta}^{\mu\nu} = \delta_{\alpha\beta} M_\alpha^{\mu\nu} + V_{\alpha\beta}^{\mu\nu}$ (*cf.* Fig. 2.4(*a*)). By construction, $W$ is antisymmetric and satisfies $W_{\alpha\beta}^{\mu\nu} = -W_{\beta\alpha}^{\nu\mu}$. This matrix can be represented as a block matrix of global size $L^2 \times L^2$

$$W = \left( \begin{array}{cccc} \underbrace{M_{\alpha=(1,1)}}_{4\times 4 \text{ matrix}} & V_{(1,1),(1,2)} & V_{(1,1),(1,3)} & \cdots \\ -V_{(1,1),(1,2)} & M_{(1,2)} & V_{(1,2),(1,3)} & \cdots \\ -V_{(1,1),(1,3)} & -V_{(1,2),(1,3)} & M_{(1,3)} & \cdots \\ \vdots & & & \end{array} \right)_{L^2/4 \text{ blocks}} \tag{2.32}$$

where each of the $(L^2/4) \times (L^2/4)$ blocks is a $4 \times 4$ matrix. Labels $\alpha$ are ordered with increasing momentum $(1,1), (1,2) \cdots (1, L/2), (2,1) \cdots$ In the action the linear terms in $c_\alpha^\mu$ can be removed using a linear change of variables $c_\alpha^\mu \to c_\alpha^\mu + g_\alpha^\mu$, where $g_\alpha^\mu$ are Grassmann constants. After some algebra, we find the correct values for the constants that eliminate the linear contribution are given by $g_\alpha^\mu = i (W^{-1})_{\alpha\beta}^{\mu\nu} H_\beta^\nu$. After substitution of these values in the overall integral, and a rescaling of variables $c_\alpha \to c_\alpha / \sqrt{i}$, the action becomes a product over variables $c$ and $h_i$

$$\begin{aligned} Q_{2n}(\{\mathbf{r}_i\}) &= \int \mathcal{D}[c]\, \mathcal{D}[h] \exp\left[ \frac{1}{2} c_\alpha^\mu W_{\alpha\beta}^{\mu\nu} c_\beta^\nu - \frac{i}{2} (W^{-1})_{\alpha\beta}^{\mu\nu} H_\alpha^\mu H_\beta^\nu \right] \\ &= \mathrm{pf}(W) \int \mathcal{D}[h] \exp\left[ -\frac{i}{2} (W^{-1})_{\alpha\beta}^{\mu\nu} H_\alpha^\mu H_\beta^\nu \right]. \end{aligned}$$

The fields $H^{\mu}_{\alpha}$ can be expressed with $h_i$ as $H^{\mu}_{\alpha} = \sum_{i=1}^{2n} \Lambda^{\mu}_{i,\alpha} h_i$, where coefficients $\Lambda^{\mu}_{i,\alpha}$ can be rewritten using a 4-dimensional vector, such as

$$\mathbf{\Lambda}_{\mathbf{i},\alpha} = \frac{2}{L+1} \sin \frac{\pi p m_i}{L+1} \sin \frac{\pi q n_i}{L+1} \mathbf{\Lambda}_{\mathbf{i}} =: r_i(\alpha) \mathbf{\Lambda}_{\mathbf{i}}, \tag{2.33}$$

where the vector

$$\mathbf{\Lambda}_{\mathbf{i}} = \begin{pmatrix} i^{m_i+n_i} \\ -i^{-m_i+n_i} \\ -i^{m_i-n_i} \\ i^{-m_i-n_i} \end{pmatrix}, \tag{2.34}$$

depends only on the location parity of the monomer $\mathbf{r}_i$ in the bulk. Functions $r_i(\alpha)$ are normalized $\sum_{\alpha} r_i(\alpha) r_j(\alpha) = \delta_{ij}$. Then we obtain the following formal and compact expression for $Q_{2n}(\{\mathbf{r}_i\})$

$$\begin{aligned} Q_{2n}(\{\mathbf{r}_i\}) &= \mathrm{pf}(W) \int \mathcal{D}[h] \exp\left( \frac{1}{2} \sum_{i,j} h_i h_j \Lambda^{\mu}_{i,\alpha} (W^{-1})^{\mu\nu}_{\alpha\beta} \Lambda^{\nu}_{j,\beta} \right) \\ &=: \mathrm{pf}(W) \int \mathcal{D}[h] \exp\left( \frac{1}{2} \sum_{i,j} h_i h_j C_{ij} \right). \end{aligned} \tag{2.35}$$

Finally, we found a pfaffian expression of the partition function

$$Q_{2n}(\{\mathbf{r}_i\}) = \mathrm{pf}(W)\mathrm{pf}(C), \tag{2.36}$$

where $C$ is a real $(2n \times 2n)$ antisymmetric matrix with elements $C_{ij} = \Lambda^{\mu}_{i,\alpha} (W^{-1})^{\mu\nu}_{\alpha\beta} \Lambda^{\nu}_{j,\beta}$. It is also worth noting that we have a similar structure in the real space, where the total action Eq. (5.9) is expressed by $\mathcal{S} = \frac{1}{2} c_{mn} W_{mn,m'n'} c_{m'n'} + \sum_{\mathbf{r}_i} c_{m_i n_i} h_i$, with $W$ containing both the connectivity matrix $M$ and the contribution of the line of defects $V$. A direct computation also leads to the factorization $Q_n(\{\mathbf{r}_i\}) = \mathrm{pf}(W)\mathrm{pf}(C)$, where $C_{ij} = (W^{-1})_{m_i n_i, m_j n_j}$ is a $(n \times n)$ antisymmetric matrix.

**Box 4** (Properties of the matrix $C$)**.**

- The size of the matrix grow linearly with the number of monomers $\dim C = 2n \times 2n$ and $C_{ij} = 0$ if $n_i$ and $n_j$ have the same parity.
- We verify easily that the matrix $C_{ij}$ is antisymmetric by using the antisymmetry property of $W$

$$\begin{aligned} C_{ji} &= \Lambda^{\mu}_{j,\alpha}(W^{-1})^{\mu\nu}_{\alpha\beta}\Lambda^{\nu}_{i,\beta} \\ &= \Lambda^{\nu}_{j,\beta}(W^{-1})^{\nu\mu}_{\beta\alpha}\Lambda^{\mu}_{i,\alpha} \\ &= -\Lambda^{\nu}_{j,\beta}(W^{-1})^{\mu\nu}_{\alpha\beta}\Lambda^{\mu}_{i,\alpha} \\ &= -C_{ij}. \end{aligned}$$

  Then, $C_{ij}$ can be formally expressed as a scalar product

$$C_{ij} = \sum_{\alpha,\beta} \left\langle \mathbf{\Lambda_{i},}_{\alpha} | W^{-1}_{\alpha,\beta} | \mathbf{\Lambda_{j},}_{\beta} \right\rangle .$$

$Q_{2n}$ is therefore a product of two pfaffians where the monomer locations are specified in matrix $W$. The matrix $V$ can be rewritten using additional matrices after considering the different components

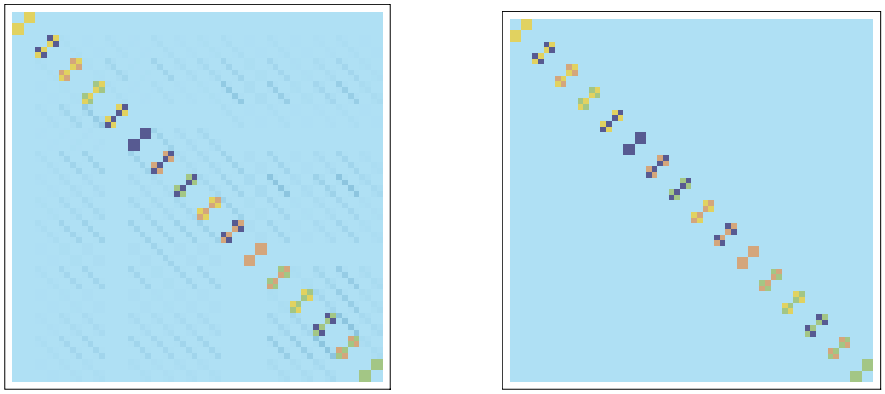

$(a)$ $(b)$

Figure 2.4: $(a)$ Graphical representation of the matrix $W = M + V$. $(b)$ When the monomers are on the boundaries of the domain, the off diagonal term $V$ vanishes and the matrix $W$ reduces to the matrix $M$.

$(\mu, \nu)$. We can indeed express $V$ using four functions $u^{a,s}_k(\alpha,\beta)$, and $v^{a,s}_k(\alpha,\beta)$, for each monomer at location $\mathbf{r}_k = (m_k, n_k)$, with $m_k < L$, and such that

$$V_{\alpha\beta} = -2t_y \sum_{\mathbf{r}_k} \sum_{c,c'} u^{c}_k(\alpha,\beta)\Gamma_{cc'}v^{c'}_k(\alpha,\beta), \tag{2.37}$$

where the $\Gamma_{cc'}$ are defined as

$$\Gamma_{sa} = \begin{pmatrix} 1 & 0 & 0 & 0 \\ 0 & 1 & 0 & 0 \\ 0 & 0 & -1 & 0 \\ 0 & 0 & 0 & -1 \end{pmatrix}, \Gamma_{aa} = \begin{pmatrix} 0 & 1 & 0 & 0 \\ 1 & 0 & 0 & 0 \\ 0 & 0 & 0 & -1 \\ 0 & 0 & -1 & 0 \end{pmatrix}, \Gamma_{ss} = \begin{pmatrix} 0 & 0 & 1 & 0 \\ 0 & 0 & 0 & 1 \\ -1 & 0 & 0 & 0 \\ 0 & -1 & 0 & 0 \end{pmatrix}, \Gamma_{as} = \begin{pmatrix} 0 & 0 & 0 & 1 \\ 0 & 0 & 1 & 0 \\ 0 & -1 & 0 & 0 \\ -1 & 0 & 0 & 0 \end{pmatrix}.$$

Functions $u$ and $v$ are given by

$$\begin{aligned} u_k^s(\alpha,\beta) &= \frac{2}{L+1} \sum_{m=m_k+1}^{L} \sin\frac{\pi p m}{L+1} \sin\frac{\pi p' m}{L+1}, \\ u_k^a(\alpha,\beta) &= \frac{2}{L+1} \sum_{m=m_k+1}^{L} (-1)^{m+1} \sin\frac{\pi p m}{L+1} \sin\frac{\pi p' m}{L+1}, \\ v_k^s(\alpha,\beta) &= \frac{2}{L+1} \left[ \sin\frac{\pi q n_k}{L+1} \sin\frac{\pi q'(n_k-1)}{L+1} + \sin\frac{\pi q' n_k}{L+1} \sin\frac{\pi q(n_k-1)}{L+1} \right], \\ v_k^a(\alpha,\beta) &= \frac{2(-1)^{n_k}}{L+1} \left[ \sin\frac{\pi q n_k}{L+1} \sin\frac{\pi q'(n_k-1)}{L+1} - \sin\frac{\pi q' n_k}{L+1} \sin\frac{\pi q(n_k-1)}{L+1} \right]. \end{aligned} \tag{2.38}$$

The first two sums can be written explicitly, and the result can be found in [5]. This close solution to the dimer model with an arbitrary number of monomers at fixed location can be formally used to compute correlations between monomers, dimers as we shall see in the next chapter.

**Fermion correlations and disorder operators**

The addition of monomers in the dimer model is therefore equivalent to inserting a magnetic field $h_i$ at points $\mathbf{r}_i$, as well as a line of defect running from the monomer position to the right boundary $m = L$. If two monomers have the same ordinate $n_i = n_j$, the line of defects will only run between the two monomers and will not reach the boundary. This can be viewed as an operator acting on the links crossed by the line and running from a point on the dual lattice to the boundary on the right-hand side. More specifically, we can express the correlation functions, after integration over the fermionic magnetic fields $h_i$, as an average over composite fields

$$\begin{aligned} \frac{Q_{2n}(\{\mathbf{r}_i\})}{Q_0} &= \Big\langle \prod_{\{\mathbf{r}_i\}} c_{m_i n_i} \exp\Big(2t_y \sum_{m=m_i+1}^{L} (-1)^{m+1} c_{m n_{i-1}} c_{m n_i}\Big) \Big\rangle_0 \\ &= \Big\langle \prod_{\{\mathbf{r}_i\}} c_{m_i n_i} \mu(\mathbf{r}_i + \mathbf{e_4}) \Big\rangle_0 \\ &= \Big\langle \prod_{\{\mathbf{r}_i\}} \Psi_4(\mathbf{r}_i) \Big\rangle_0, \end{aligned} \tag{2.39}$$

where $\mu(\mathbf{r}+\mathbf{e_4})$ is a fermionic disorder operator, whose role is to change the sign of the vertical links across its path starting from vector $\mathbf{r}+\mathbf{e_4}$ on the dual lattice. The integration $\langle\cdots\rangle_0$ is performed relatively to the action $S_0$. Elementary vectors $\mathbf{e_i}$ define a four-component fermionic field $\Psi_\mu(\mathbf{r}) = c_{mn}\mu(\mathbf{r}+\mathbf{e}_\mu)$, which is the fermionic counterpart of the scalar field introduced for the Ising-spin

model [118, 177]. In the latter case, a linear differential equation can be simply found for $\Psi_\mu(\mathbf{r}) = \sigma(\mathbf{r})\mu(\mathbf{r}+\mathbf{e}_\mu)$, with $\sigma(\mathbf{r}) = \pm 1$, leading to a Dirac equation. Here the general correlator between monomers is directly mapped onto the correlator between these fermionic composite fields. Likewise the Kasteleyn theory, where disorder lines are absent on the boundary and where correlations between monomers correspond to correlations between Grassmann variables Eq. (1.32), here the correlation between monomers on the boundaries are exactly correlation functions between the fermionic fields

$$\frac{Q_{2n}(\{\mathbf{r}_i\})}{Q_0} = \Big\langle \prod_{\{\mathbf{r}_i\}} c_{m_i n_i} \Big\rangle_0. \tag{2.40}$$

This result about monomer correlations written in terms of disorder operators is the fermionized version of the Coulomb gas framework, where monomers act like dual magnetic charges which create a dislocation of the height field and correspond to the vertex operator of the corresponding bosonic field theory which will be detailed in the next chapter about the bosonic formulation of the model.

### Enumerative check

Now that we pretend to have an exact solution for the partition function of the dimer model on a square lattice of size $L \times L$ valid for any number of monomers, we would like to insure that everything is correct, and in order to do this, we need an enumerative algorithm to compare with our solution. Here, as an example we take the $4 \times 4$ lattice with two monomers. The number

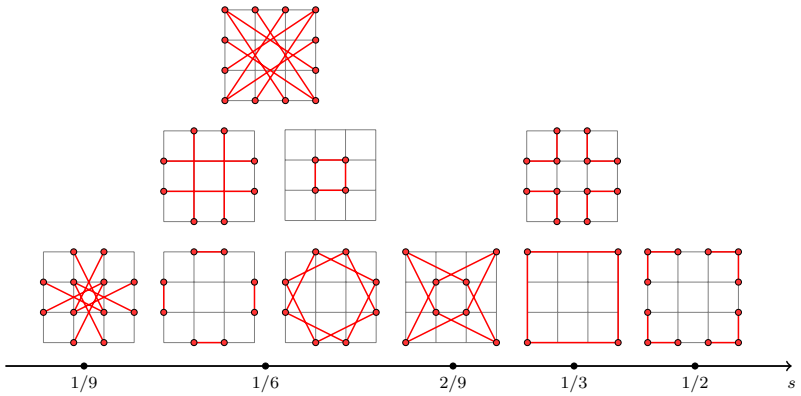


Figure 2.5: This figure represents all the choices of the location of two monomers on a $4 \times 4$ lattice. Let us detail explicitly the example of the right diagram with $s = 1/2$. If we choose to impose a monomer on a corner and its direct adjacent neighbor, there is 8 way to do this, each of these 8 ways are represented by two red dots linked together by a red line. The value of $s$ is explain in the main text. In that case $s = 1/2$ meaning that the two monomers at these positions cut exactly in half the number of configurations.

of way to choose the positions of the two monomers is $N_{2p}(M,N) = \binom{M^2/2}{p}\binom{N^2/2}{p}$ with $2p = 2$

and $M = N = 2$ then $N_2(4,4) = 64$. We can define a number $s$ which will be the ratio of the partition function $Q_0$ without monomers (36 in that case) by the partition function $Q_2$ with two monomers at fixed positions. This quantity will be a rational number $\in [1/2, 0[$ for any size lattice and is completely defined by the matrices $W$ and $C$ written above. The results shown in Fig. 2.5 completely agree with enumeration algorithms[2], confirming the exactness of our solution. We saw in the previous paragraph that this quantity is simply the correlation function $C_{ij}$ between the two monomers which becomes a lot simpler in the case where there are on the boundaries of the domain.

### 2.2.2 Boundary monomers and $1d$ complex fermion chain

As we have seen before, the correlation between monomers become much more simpler in the case where there are restricted to live on the boundaries of the lattice. In this section we shall study these correlations and try to extract a closed expression starting to the case where the monomers are on the same boundary (Fig. 2.10($a$)). The generalization of different boundaries (Fig. 2.10($b$,$c$)) is much more tricky but we will see that a compact closed formula is also available.

#### Monomers on the same boundary

Although the general problem remains in principle tractable, we can simplify it further by considering monomers on the boundary $m_i = L$ of the rectangle only, with the convention $n_i > n_j$ if $i > j$. When the monomers are on the boundaries of the domain, the off diagonal term $V$ vanishes and the matrix $W$ reduces to the matrix $M$ (*cf.* Fig. 2.4($b$)). In that case, the previous action contains

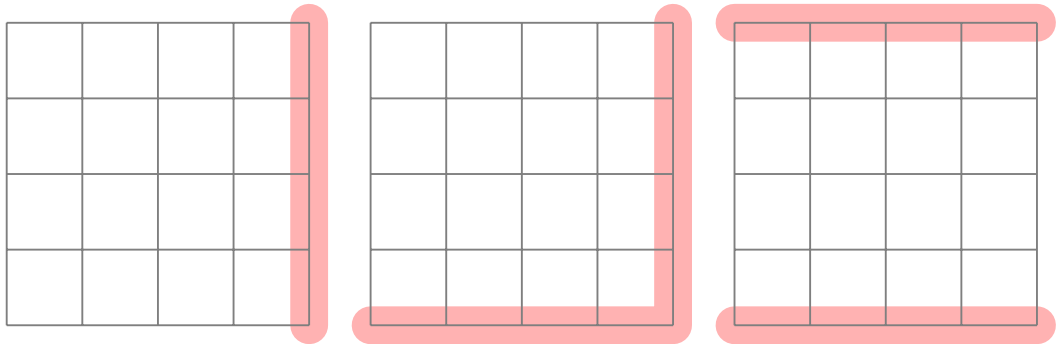


Figure 2.6: The three different possibilities of two monomer's location. ($a$) on a same boundary ($b$) on adjacent boundaries or ($c$) on opposite boundaries.

no defect line term, only the couplings with fields remain and the problem can be transformed into a $1d$ system of particles on a chain (see Fig. 2.7). Using the previous Fourier transform for the $c$'s

[2]For this small size, it can be check by hands

variables, the magnetic field term becomes

$$\sum_{\mathbf{r}_i} c_{m_i,n_i} h_i = \sum_{p,q=1}^{L} c_{pq} H_{pq},$$
$$H_{pq} = \sum_{\mathbf{r}_i} \frac{2 i^{m_i+n_i}}{L+1} \sin\frac{\pi p m_i}{L+1} \sin\frac{\pi q n_i}{L+1} h_i. \tag{2.41}$$

Then the partition function can be integrated on the $c_{mn}$'s using the block partition $(p,q)$ and we find that

$$Q_{2n}(\{\mathbf{r}_i\}) = Q_0 \int \mathrm{d}h_1 \cdots \mathrm{d}h_{2n} \exp S_H, \tag{2.42}$$

where

$$S_H = \sum_{p,q=1}^{L/2} \frac{i t_x \cos\frac{\pi p}{L+1} \left(H_{p-q}H_{-pq} + H_{pq}H_{-p-q}\right) + i t_y \cos\frac{\pi q}{L+1} \left(H_{-pq}H_{-p-q} + H_{pq}H_{p-q}\right)}{2t_x^2 \cos^2\frac{\pi p}{L+1} + 2t_y^2 \cos^2\frac{\pi q}{L+1}}.$$

Grassmann fields $H_{pq}$ has the following properties: $H_{-pq} = -H_{pq}$ and $H_{-p-q} = -H_{p-q}$. In

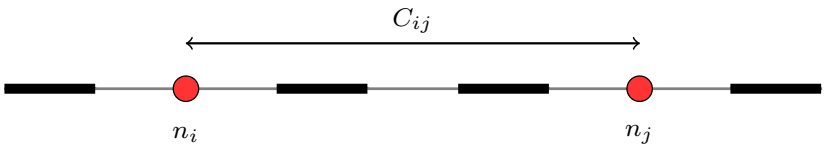


Figure 2.7: Configuration of 2 monomers on the boundary at the position $n_i$ and $n_j$ correlated by $C_{ij}$. This correlation decreases as the inverse of the distance and vanishes if $n_i$ and $n_j$ have the same parity.

that case, the first sum on the right hand side of the previous equation vanishes due to the anti-commuting property, and we can reduce the field-dependent action to one single sum

$$S_H = {\sum_{p,q=1}}' \frac{i t_y \cos\frac{\pi q}{L+1}}{t_x^2 \cos^2\frac{\pi p}{L+1} + t_y^2 \cos^2\frac{\pi q}{L+1}} H_{pq} H_{p-q}, \tag{2.43}$$

where the prime symbol is meant for summation over half of the modes $p, q = 1 \cdots L/2$. This action would vanish if all the $n_i$ were for example even, since the Grassmann fields satisfy in this case $H_{pq}H_{p-q} = -H_{pq}^2 = 0$. In general, the field action can be rewritten as a quadratic form over the real-space fields $h_i$: $S_H = \sum_{i<j} C_{ij} h_i h_j$, where the elements of the matrix $\hat{C}$ are antisymmetric $C_{ij} = -C_{ji}$, and equal to

$$C_{ij}(L) = \frac{4\left[(-1)^{n_i} - (-1)^{n_j}\right]}{(L+1)^2} \sum_{p,q=1}^{L/2} \frac{i^{1+n_i+n_j} t_y \cos\frac{\pi q}{L+1} \sin^2\frac{\pi p}{L+1}}{t_x^2 \cos^2\frac{\pi p}{L+1} + t_y^2 \cos^2\frac{\pi q}{L+1}} \sin\frac{\pi q n_i}{L+1} \sin\frac{\pi q n_j}{L+1} \tag{2.44}$$

These elements are zero if $n_i$ and $n_j$ have the same parity and in general the integration over the field variables $h_i$ leads directly to a pfaffian form for the partition function $Q_{2n}(\{\mathbf{r}_i\}) = Q_0(-1)^n \mathrm{pf}(C)$. The $(-1)^n$ factor comes from the rearrangement of the measure $\mathrm{d}h_1 \cdots \mathrm{d}h_{2n} = (-1)^n \, \mathrm{d}h_{2n} \cdots \mathrm{d}h_1$, so that the $2n$-function reads

$$\int \prod_{i=1}^{2n} \mathrm{d}h_i \exp\left( -\sum_{i<j} C_{ij} h_i h_j \right) = \mathrm{pf}(C). \tag{2.45}$$

This sign could also be absorbed in the definition of matrix elements $C_{ij} \to -C_{ij}$. The resulting partition function is always positive with this definition. For example, if there are 2 monomers at the boundary, $\mathrm{pf}(\hat{C}) = -C_{12}$, and 4 monomers[3] leads to $\mathrm{pf}(\hat{C}) = C_{12}C_{34} - C_{13}C_{24} + C_{14}C_{23}$ (*cf.* Fig. 2.8). $C_{ij}$ are zero if $n_i$ and $n_j > n_i$ have the same parity. In the case $n_1 = L/2 - k$ and

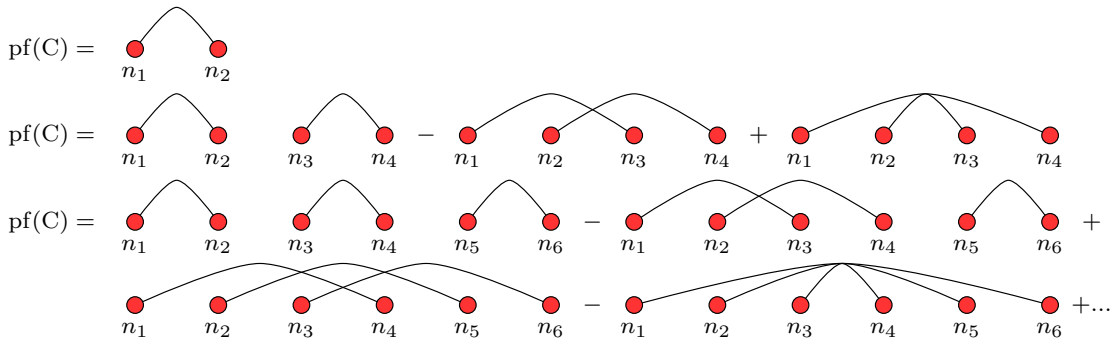


Figure 2.8: Diagrammatical representation of the pfaffian of $C$ for 2, 4 and 6 monomers

$n_2 = L/2 + k + 1$, $C_{12} \simeq \frac{2}{\pi} r^{-1} - \frac{2}{\pi} r^{-3}$ instead, with $r = 2k + 1$ and amplitude $2/\pi$. This result is in agreement with the work of Priezzhev and Ruelle [178] on the scaling limit of the correlation functions of boundary monomers in a system of closely packed dimers in terms of a $1d$ chiral free fermion theory. We should notice that the expression Eq. (2.44) is an exact closed expression for the 2-point correlation between monomers on the boundary $m_i = m_j = L$, leading to an explicit result for the partition function with $2, 4 ... 2n$ monomers. We will show in a next section how to find the correlation between monomers on different (opposite or adjacent) boundaries of the lattice.

### General case

In the case where the monomers are on the boundaries, we were able to compute exactly the 2-point correlation function Eq. (2.44) in the discrete case. In the bulk case, the things are much more complicated and an exact closed-form expression on the discrete level seems hard. Nevertheless, a perturbative expansion can be performed to evaluate the pfaffian expression of the correlation

[3] As a straightforward application, the number of perfect matching with a monomer on each corner can be computed and the result is $Q_4^{\mathrm{corner}} = \{1, 8, 784, 913952, 1211936774...\}$

function. We start from the exact pfaffian expression of matrix $C$

$$C_{ij} = \Lambda^{\mu}_{i,\alpha}(W^{-1})^{\mu\nu}_{\alpha\beta}\Lambda^{\nu}_{j,\beta}. \tag{2.46}$$

The inverse matrix $W^{-1}$ can be computed using formally the expansion

$$W^{-1} = (M+V)^{-1} = M^{-1} - M^{-1}VM^{-1} + \mathcal{O}(V^2). \tag{2.47}$$

In particular it is convenient to write the inverse matrix $M^{-1}$ as

$$M^{-1}_{\alpha} = \bar{a}_x(p)\Gamma_x + \bar{a}_y(q)\Gamma_y, \tag{2.48}$$

with

$$\begin{aligned}\bar{a}_x(p) &= -\frac{a_x(p)}{a_x(p)^2 + a_y(q)^2}\\ \bar{a}_y(q) &= -\frac{a_y(q)}{[a_x(p)^2 + a_y(q)^2}.\end{aligned} \tag{2.49}$$

In the following we will consider only the first of this expansion

$$\begin{aligned}C_{ij} &= \sum_{\alpha,\beta}\left\langle \mathbf{\Lambda_{i},}_{\alpha}|W^{-1}_{\alpha\beta}|\mathbf{\Lambda_{j},}_{\beta}\right\rangle = \sum_{\alpha}\sum_{\mu} r_i(\alpha)\bar{a}_\mu(\alpha)r_j(\alpha)\left\langle \mathbf{\Lambda_i}|\Gamma_\mu|\mathbf{\Lambda_j}\right\rangle\\ &- \sum_{\alpha,\beta}\sum_{\mu,\nu}\sum_{\mathbf{r}_k}\sum_{c,c'=\{a,s\}} r_i(\alpha)\bar{a}_\mu(\alpha)u^c_k(\alpha,\beta)v^{c'}_k(\alpha,\beta)\bar{a}_\nu(\beta)r_j(\beta)\left\langle \mathbf{\Lambda_i}|\Gamma_\mu\Gamma_{cc'}\Gamma_\nu|\mathbf{\Lambda_j}\right\rangle + ...\\ &= C^{(0)}_{ij} + C^{(1)}_{ij} + ...\end{aligned} \tag{2.50}$$

The structure of this expansion make possible a further diagrammatic expansion of the quantities $C_{ij}$ as a series of term $C^{(k)}_{ij}$, with $k \geq 0$. The first term $C^{(0)}_{ij}$ has symmetry factors

$$\begin{aligned}\left\langle \mathbf{\Lambda_i}|\Gamma_x|\mathbf{\Lambda_j}\right\rangle &= \overbrace{i^{m_i+n_i+m_j+n_j}}^{c_{ij}}\overbrace{\left[(-1)^{m_i}-(-1)^{m_j}\right]\left[(-1)^{n_i}+(-1)^{n_j}\right]}^{\gamma^{(1)}_{ij}} := c_{ij}\gamma^{(1)}_{ij},\\ \left\langle \mathbf{\Lambda_i}|\Gamma_y|\mathbf{\Lambda_j}\right\rangle &= \underbrace{i^{m_i+n_i+m_j+n_j}}_{c_{ij}}\underbrace{\left[1+(-1)^{m_i+m_j}\right]\left[(-1)^{n_j}-(-1)^{n_i}\right]}_{\gamma^{(2)}_{ij}} := c_{ij}\gamma^{(2)}_{ij}.\end{aligned} \tag{2.51}$$

It is easy to see that $\left\langle \mathbf{\Lambda_i}|\Gamma_x|\mathbf{\Lambda_j}\right\rangle = 0$ for monomers on the boundary or on the same column, when $m_i = m_j$. *A contrario*, for pairs of monomers on the same line $n_i = n_j$, we have $\left\langle \mathbf{\Lambda_i}|\Gamma_y|\mathbf{\Lambda_j}\right\rangle = 0$. The first term $C^{(0)}_{ij}$ can be expressed in the discrete case as

$$\boxed{C^{(0)}_{ij}(L) = \frac{2c_{ij}}{(L+1)^2}\sum_{p,q=1}^{L/2}\left\{\frac{\gamma^{(1)}_{ij}t_x\cos\frac{\pi p}{L+1} + \gamma^{(2)}_{ij}t_y\cos\frac{\pi q}{L+1}}{t_x^2\cos^2\frac{\pi p}{L+1} + t_y^2\cos^2\frac{\pi q}{L+1}}\right\}\sin\frac{\pi p m_i}{L+1}\sin\frac{\pi p m_j}{L+1}\sin\frac{\pi q n_i}{L+1}\sin\frac{\pi q n_j}{L+1}}$$

where $\gamma^{(1)}_{ij}, \gamma^{(2)}_{ij}$ and $c_{ij}$ are defined in Eq. (2.51). This expression is valid for 2 monomers on any of the four boundaries of the lattice, and is identical, when $m_i = m_j = L$, to expression obtained

for the same ($m_i = n_i = L$) boundary case Eq. (2.44). Indeed the first order of the expansion Eq. (2.47) is valid only on the boundaries where the matrix $W$ is actually equal to the matrix $M$. One could demonstrate that this 2-point correlation is actually exact $C_{ij}^{(0)} = C_{ij}$ for boundary monomers because of the cancelation of higher terms in the perturbative expansion, accordingly the expression Eq. (2.52) is a general exact result for any positions anywhere on the four boundaries. Therefore, it will be very efficient to use this exact closed-form to evaluate scaling behaviors of correlation functions between monomers on the surface and at the corners.

### 2.2.3 Single monomer on the boundary and localization phenomena

We can recover the partition function for one monomer on the boundary using the previous analysis. In this case the size $L$ has to be odd in order to accommodate for the presence of one single monomer. The action Eq. (2.9) is still valid, but the Fourier transform leads to a different block arrangement for the bulk terms which are represented by the red zones in Fig. 2.9

$$S_0 = 2it_x \sum_{p,q\geq 1}^{\frac{1}{2}(L-1)} \cos\frac{\pi p}{L+1}\left(c_{pq}c_{-p-q} + c_{p-q}c_{-pq}\right) + 2it_x \sum_{p\geq 1}^{\frac{1}{2}(L-1)} \cos\frac{\pi p}{L+1} c_{p\frac{1}{2}(L+1)}c_{-p\frac{1}{2}(L+1)}$$
$$+ 2it_y \sum_{p,q\geq 1}^{\frac{1}{2}(L-1)} \cos\frac{\pi q}{L+1}\left(c_{pq}c_{p-q} + c_{-pq}c_{-p-q}\right) + 2it_y \sum_{q\geq 1}^{\frac{1}{2}(L-1)} \cos\frac{\pi q}{L+1} c_{\frac{1}{2}(L+1)q}c_{\frac{1}{2}(L+1)-q}.$$

$S_0$ contains Fourier modes that cover the Brillouin zone (see Fig. 2.9) except for term $c_{\frac{1}{2}(L+1)\frac{1}{2}(L+1)}$

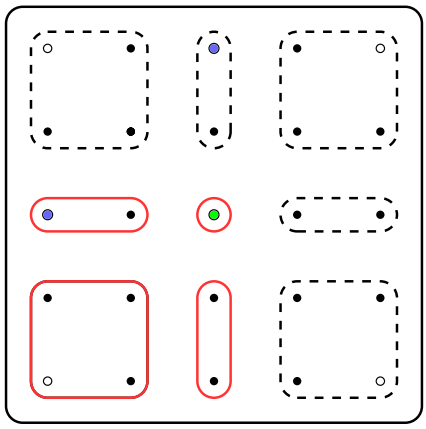

Figure 2.9: Block partition of the Fourier modes for $L$ odd (here $L = 5$). There are 3 blocks of momenta $(p, q)$ taken into account into the integration, plus one point (green dot) at location $(\frac{1}{2}(L+1), \frac{1}{2}(L+1))$. The first block of momenta $(p, q)$ is represented in the red square for values $1 \leq p, q \leq \frac{1}{2}(L-1)$, with corresponding momenta $(\pm p, \pm q)$ (open dots). Then there are 2 additional lines of values $p = \frac{1}{2}(L-1)$ with $1 \leq q \leq \frac{1}{2}(L-1)/2$, and corresponding momentum $(\frac{1}{2}(L-1), -q)$, and $q = \frac{1}{2}(L-1)$ with $1 \leq p \leq \frac{1}{2}(L-1)/2$, and corresponding momentum $(-p, \frac{1}{2}(L-1))$, blue dots.

which is located in the middle of the zone and not present in the sums Eq. (2.52). The integration over Grassmann variables $c_{pq}$ is therefore zero in absence of coupling with this mode. Inserting a single monomer on the boundary at location $\mathbf{r} = (L, n)$ is equivalent, as previously demonstrated, to inserting a Grassmann field $h$ and a field contribution $S_H = c_{Ln}h$ in the action, which can be expanded using Fourier transformation

$$\begin{aligned} S_H &= \frac{2i^{L+n}}{L+1}\sum_{p,q}(-1)^{p+1}\sin\frac{\pi p}{L+1}\sin\frac{\pi qn}{L+1}c_{pq}h \\ &= \sum_{p,q} c_{pq}H_{pq}. \end{aligned} \tag{2.52}$$

Since there is only one Grassmann field, all terms $H_{pq}$ are only proportional to $h$, and therefore the quadratic form in Eq. (2.43) is zero. However one term contributes to the integration over $c_{\frac{1}{2}(L+1)\frac{1}{2}(L+1)}$, and corresponds to $c_{\frac{1}{2}(L+1)\frac{1}{2}(L+1)}H_{\frac{1}{2}(L+1)\frac{1}{2}(L+1)}$. After integration over the remaining $c_{pq}$ and $h$ variables, the partition function can then be factorized as

$$Q_1 = \frac{-2i^{n+1}\sin(\pi n/2)}{L+1}\prod_{p,q=1}^{\frac{1}{2}(L-1)}\left[4t_x^2\cos^2\frac{\pi p}{L+1}+4t_y^2\cos^2\frac{\pi q}{L+1}\right]\prod_{p=1}^{\frac{1}{2}(L-1)}2t_x\cos\frac{\pi p}{L+1}\prod_{q=1}^{\frac{1}{2}(L-1)}2t_y\cos\frac{\pi q}{L+1}.$$

This result is consistent to the fact that a monomer can be put only at odd site locations. We can use the formula $\prod_{p=1}^{\frac{1}{2}(L-1)}2\cos(\frac{\pi p}{L+1}) = \sqrt{\frac{L+1}{2}}$, to simplify the previous expression and recover the Tzeng-Wu [202] solution that we have showed in the first chapter

$$\boxed{Q_1 = \prod_{p,q=1}^{\frac{1}{2}(L-1)}\left[4t_x^2\cos^2\frac{\pi p}{L+1}+4t_y^2\cos^2\frac{\pi q}{L+1}\right]\times(t_xt_y)^{\frac{1}{2}(L-1)}\times[-i^{n+1}\sin(\pi n/2)].} \tag{2.53}$$

This solution will be used in the next chapter to extract finite-size scaling behavior of the free energy in a CFT framework, where *boundary changing conditions* operators has to be carefully study to infer the central charge of the model in the context of the height mapping formulation.

### Localization phenomena

We can notice that the partition function with one monomer in a system of size $L \times L$ ($L$ odd) is equal to the partition function without monomers on a lattice of size $L-1\times L-1$. The probability is therefore constant for all location of the monomer, at even sites only, the last term in bracket being equal to zero ($n$ odd) or unity ($n$ even), proving that the monomer is fully delocalized on the boundary, unlike the bulk case where monomers are actually localized in a finite region of the domain [27, 174]. Actually it has been shown that the delocalization probability, *i.e.* the probability that the vacancy can reach the boundary of the square lattice, decay with the system size as $L^{-1/4}$ and moreover the analyze of the distribution $p(s)$ for the size $s$ of the domain accessible to the monomer in an infinite system has been studied in the context of spanning webs and has been shown to decrease a $p(s) \sim s^{-9/8}$. The same kind of analysis has been done for the triangular lattice [111].

## 2.3 Fun with dimers

In this section, one shows a curious combinatorial analogy between the partition function of the close packing dimer model on a $L \times L$ square lattice with open boundary conditions, and the same partition function with boundary monomers. One start reminding some properties of the pure dimer model partition function, and we show, thanks to our exact calculation of the partition function with $2n$ monomers, that this analogy can be understood and demonstrated. Hereinafter, the Boltzmann weights $t_x$ and $t_y$ are taken to be the unity in such way that the partition function is exactly equal to the perfect matching number. All the results presented in this section has been checked with depth-first [144] algorithms up to size $L = 10$. For bigger sizes, Monte-Carlo or transfer matrix simulations [145] has to be implement.

### 2.3.1 Partition function without monomers

The partition function of the pure dimer model on a $M \times N$ lattice with open boundary conditions is

$$Q_0(M,N) = \prod_{p=1}^{M/2}\prod_{q=1}^{N/2}\left[4\cos^2\frac{\pi p}{M+1} + 4\cos^2\frac{\pi q}{N+1}\right], \tag{2.54}$$

which can be written for the special case of the square geometry $M = N = L$

$$\boxed{Q_0(L) = 2^{L/2}.g_{L/2}^2} \tag{2.55}$$

where $g_{L/2}$ is a number sequence (OEIS A065072) [4] equal, for $L = 2, 4, 6, 8, 10, 12, 14...$, to

$$g_{L/2} = \{1, 3, 29, 901, 89893, 28793575, 29607089625...\}.$$

The resulting sequence for the partition function is then (OEIS A004003) for $L = 2, 4, 6, 8, 10, 12, 14$

$$Q_0 = \{2, 36, 6728, 12988816, 258584046368, 53060477521960000, 11220220877603617800000 0...\}.$$

For example, the number of configurations of dimers on the chessboard ($L = 8$) is $Q_0(8) = 2^4 g_4^2 = 2^4 \times 901^2 = 12988816$ as previously noticed by Fisher [71]. Another observation is that the number of configuration on the square $L \times L$ is always even.

**Box 5** (Number theory curiosity)**.**

It is less trivial to notice that $\{g_p\}$ is a sequence of odd number satisfying the relation

$$\begin{aligned} g_p &= p + 1 (\text{mod } 32) \quad \text{if} \quad p \quad \text{even} \\ &= (-1)^{(p-1)/2} \times p (\text{mod } 32) \quad \text{if} \quad p \quad \text{odd}. \end{aligned} \tag{2.56}$$

The proof of this statement can be found in the original paper [117]. The exact solution of the dimer model with one boundary monomer allows for the same kind of number theory analysis (*cf.* [138] for details).

[4] The On-Line Encyclopedia of Integer Sequences https://oeis.org/

The aim of the following sections is to look in more details at the form of the partition function of a dimer model of on a $L \times L$ square ($L$ even) lattice with $2n$ monomers. One allows the $2n$ monomers to be anywhere on the four boundaries of the square (see Fig. 2.10).

### 2.3.2 Partition function with two boundary monomers

We saw previously that the expression of this partition function $Q_{2n}$ is related to the pure dimer model $Q_0$ by the formula

$$Q_{2n} = Q_0.\mathrm{pf}(C), \tag{2.57}$$

where the size of the matrix $C$ depends on the number of monomers. Previously, the partition $Q_0$ has been shown to possess a remarkable expression Eq. (2.55) and we would like to determine whether or not, the partition function $Q_{2n}$ admits the same kind of properties. In the case of two

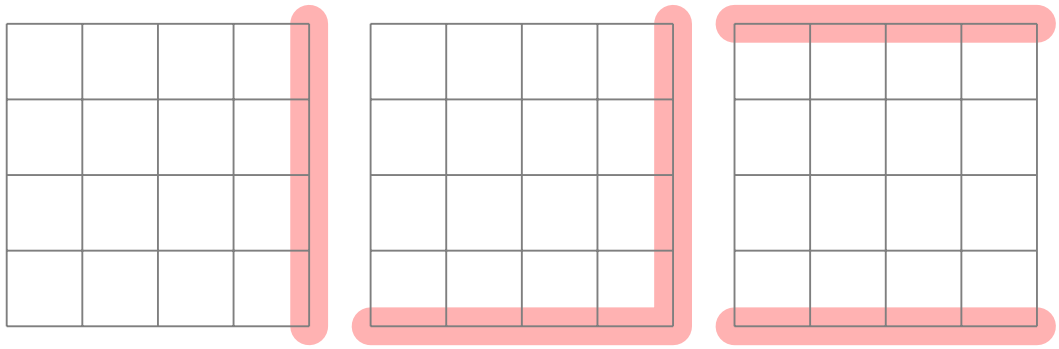


Figure 2.10: The three different possibilities of two monomer's location. ($a$) on a same boundary ($b$) on adjacent boundaries or ($c$) on opposite boundaries.

monomers anywhere on the boundaries, we saw that $W = M$ and then the expression Eq. (2.57) reduces to

$$Q_2 = Q_0.C_{ij}. \tag{2.58}$$

#### Inline boundary monomers

Initially, we choose to restrict the monomers to live on the same boundary $m_i = m_j = L$ with $n_i, n_j \in [1, L]$ (*cf.* Fig. 2.10(a)). In that particular situation the matrix elements $C_{ij}$ take the following form Eq. (2.44)

$$C_{ij} = R_{ij}\sqrt{\frac{2}{L+1}}\sum_{p,q=1}^{L/2} \frac{i^{1+n_i+n_j}\cos\frac{\pi q}{L+1}\sin^2\frac{\pi p}{L+1}}{\cos^2\frac{\pi p}{L+1}+\cos^2\frac{\pi q}{L+1}}\sin\frac{\pi q n_i}{L+1}\sin\frac{\pi q n_j}{L+1}, \tag{2.59}$$

where

$$\begin{aligned} R_{ij} &= \pm 2 \ \text{ if } n_i \in \mathbb{Z}_{2p}(\mathbb{Z}_{2p+1}) \text{ and } n_j \in \mathbb{Z}_{2p}(\mathbb{Z}_{2p+1}) \\ &= 0 \ \text{ if } \ n_i \in \mathbb{Z}_{2p} \text{ and } n_j \in \mathbb{Z}_{2p+1} \text{ or converserly.} \end{aligned} \tag{2.60}$$

In table 2.1, we evaluate this expression using MATHEMATICA®, restricting one monomer to be in $n_j = 1$ and the second to be between 1 to $L$ for several system sizes. One can observe that there

| $C_{ij}(L)$ | 4 | 6 | 8 | 10 | 12 | 14 |
|---|---|---|---|---|---|---|
| $(1,1),(2,1)$ | 1/2 | 1/2 | 1/2 | 1/2 | 1/2 | 1/2 |
| $(1,1),(4,1)$ | 1/3 | 9/29 | 275/901 | 27293/89893 | 8724245/28793575 | 8962349805/29607089625 |
| $(1,1),(6,1)$ | . | 7/29 | 199/901 | 19279/89893 | 6103405/28793575 | 6242309595/29607089625 |
| $(1,1),(8,1)$ | . | . | 169/901 | 15395/89893 | 4750015/28793575 | 4800013155/29607089625 |
| $(1,1),(10,1)$ | . | . | . | 13761/89893 | 4036195/28793575 | 3979640565/29607089625 |
| $(1,1),(12,1)$ | . | . | . | . | 3721985/28793575 | 3520442385/29607089625 |
| $(1,1),(14,1)$ | . | . | . | . | . | 3311911215/29607089625 |
| $g_{L/2}$ | 3 | 29 | 901 | 89893 | 28793575 | 29607089625 |

Table 2.1: Correlation function $C_{ij}$ for a boundary monomer ($m_i = m_j = L$) fixed on the first site $n_j = 1$ as function of the ordinate $n_i$ for several system sizes $L$ (see Fig. 2.10($a$)). The value of $C_{ij}$ where the two monomers are on the corner $(1,1),(2,1)$ is always equal to 1/2, because it is equivalent to force a dimer to be on the corner and then split the number of configuration by two. Bottom line: Values of the sequence $g_L$ for $L = 4..14$.

is a curious relation between the expression $C_{ij}$ and the sequence $g_{L/2}$ present in the partition function $Q_0$, more precisely one can deduce a proportionality relation

$$C_{ij}(L) \propto g_{L/2}^{-1}, \tag{2.61}$$

which appears to be valid for all system sizes $L$ in the case of inline monomers.

### General case

The general expression of the matrix elements of the correlations between boundary monomers Eq. (2.52), valid in all the geometries of Fig. 2.10 can be written as

$$\begin{aligned} C_{ij} = \frac{2c_{ij}}{(L+1)^2} \sum_{p,q=1}^{L/2} \Big\{ & \frac{\gamma_{ij}^{(1)} \cos\frac{\pi p}{L+1}}{t_x^2 \cos^2\frac{\pi p}{L+1} + t_y^2 \cos^2\frac{\pi q}{L+1}} + \frac{\gamma_{ij}^{(2)} \cos\frac{\pi q}{L+1}}{t_x^2 \cos^2\frac{\pi p}{L+1} + t_y^2 \cos^2\frac{\pi q}{L+1}} \Big\} \\ & \times \sin\frac{\pi p m_i}{L+1} \sin\frac{\pi p m_j}{L+1} \sin\frac{\pi q n_i}{L+1} \sin\frac{\pi q n_j}{L+1}, \end{aligned} \tag{2.62}$$

where $\gamma_{ij}^{(1)}, \gamma_{ij}^{(2)}$ and $c_{ij}$ are defined in Eq. (2.51). In table 2.2 , we evaluate this expression for the two other geometries. The same relation holds in this case as well, and we conjecture that the expression of the 2-point correlation takes the following form

$$C_{ij}(L) = \alpha_{ij}^{(2)}(L) g_{L/2}^{-1}, \tag{2.63}$$

| $C_{ij}(L)$ | 4 | 6 | 8 | 10 | 12 |
|---|---|---|---|---|---|
| $(1,1),(L,1)$ | $1/3$ | $7/29$ | $169/901$ | $13761/89893$ | $3721985/28793575$ |
| $(1,1),(L,3)$ | $1/(2\times 3)$ | $5/29$ | $138/901$ | $12127/89893$ | $3407775/28793575$ |
| $(1,1),(L,5)$ | . | $5/(2\times 29)$ | $95/901$ | $9475/89893$ | $2864755/28793575$ |
| $(1,1),(L,7)$ | . | . | $95/(2\times 901)$ | $6389/89893$ | $2194565/28793575$ |
| $(1,1),(L,9)$ | . | . | . | $6389/(2\times 89893)$ | $1471805/28793575$ |
| $(1,1),(L,11)$ | . | . | . | . | $1471805/(2\times 28793575)$ |
| $C_{ij}(L)$ | 4 | 6 | 8 | 10 | 12 |
| $(1,1),(L,1)$ | $1/3$ | $7/29$ | $169/901$ | $13761/89893$ | $3721985/28793575$ |
| $(1,2),(L,2)$ | $1/6$ | $2/29$ | $30/901$ | $1634/89893$ | $314210/28793575$ |
| $(1,3),(L,3)$ | $1/6$ | $9/29$ | $125/901$ | $11109/89893$ | $3178965/28793575$ |
| $(1,4),(L,4)$ | $1/3$ | $9/29$ | $155/901$ | $4720/89893$ | $984400/28793575$ |
| $g_{L/2}$ | 3 | 29 | 901 | 89893 | 28793575 |

Table 2.2: Top: Correlation function $C_{ij}$ between a monomer at position $(m_i = n_i = 1)$ and another at position $(m_j = L, n_j)$ for several system sizes $L$ and for $n_j = 1, 3, 5, 7, 9, 11$ (*cf.* Fig. 2.10($b$)). We note that the expression of the last line in each row is the half of the expression of the penultimate line. Bottom: Correlation function $C_{ij}$ between opposite side monomers for several system sizes $L$ and for $n_i = n_j = 1, 2, 3, 4$ (see Fig. 2.10($c$)).

no matter the positions of the two monomers on the boundaries, where $\alpha_{ij}^{(2)}$ depends only of the positions of the two monomers and of the system size $L$. We did not succeed to prove this equality between a double product ($g_{L/2}$ define by Eq. (2.55) ) and a double sum ($C_{ij}(L)$ defined by Eq. (2.62)), but there is, numerically speaking, absolutely no-doubt that is true. Considering that relation valid, the partition function of the dimer model with two boundary monomers reads

$$\boxed{Q_2(L) = \alpha_{ij}^{(2)}(L).g_{L/2}} \tag{2.64}$$

### 2.3.3 Partition function with $2n$ boundary monomers

It is worth looking at higher number of monomers to conjecture a more general form of the partition function. We have conjectured that the matrix elements of the correlation matrix are proportional to the sequence $g_{L/2}$, thus thanks to the general pfaffian solution with $2n$ monomers Eq. (2.57), we obtains the formulas

$$\begin{aligned} Q_2 &= Q_0.C_{ij}, \\ Q_4 &= Q_0.\big(C_{ij}C_{kl} - C_{ik}C_{jl} + C_{il}C_{jk}\big), \\ Q_6 &= Q_0.\big(C_{ij}C_{kl}C_{mn} - C_{il}C_{jl}C_{mn} + C_{il}C_{jm}C_{kn} - ...\big), \\ &\vdots \end{aligned} \tag{2.65}$$

where the pure partition function takes the form Eq. (2.55), therefore the partition functions are proportional to power of $g_{L/2}$

$$\begin{aligned} Q_0(L) &= 2^{L/2}.g_{L/2}^2, \\ Q_2(L) &= \alpha_{ij}^{(2)}(L).g_{L/2}, \\ Q_4(L) &= \alpha_{ijkl}^{(4)}(L).g_{L/2}^0, \\ Q_6(L) &= \alpha_{ijklmn}^{(6)}(L).g_{L/2}^{-1}, \\ &\vdots \end{aligned} \tag{2.66}$$

which can be generalized for $2n$ monomers at positions $i_1, i_2, ..., i_{2n}$

$$Q_{2n}(L) = \alpha_{i_1 i_2 ... i_{2n}}^{(2n)}(L).g_{L/2}^{2-n}, \tag{2.67}$$

in such way that a relation between $Q_{2p}$ et $Q_{2q}$ can be founded ($p, q \geqslant 1$), dropping all the indices but $p$ and $q$ for simplicity, we found

$$\boxed{\frac{Q_{2p}}{Q_{2q}} = \frac{\alpha^{(2p)}}{\alpha^{(2q)}} g^{q-p},} \tag{2.68}$$

valid for $2p$ and $2q$ monomers anywhere on the boundaries of the square lattice. Finally all these numerical relations between dimer partition functions with and without boundary monomers are the consequence of Eq. (2.57) and Eq. (2.63), which are unfortunately no longer valid for bulk monomers. The all purpose of this chapter was mainly to extend the result of Fisher about the relation between the partition function of dimers and the integer sequence $g_{L/2}$ in the case of boundary monomers which of course is nothing more than a purely mathematical curiosity.

## 2.4 Conclusions of the chapter

In this work the classical dimer model was discussed in great details in a fermionic formulation. Then we presented a practical and complete fermionic solution of the $2d$ dimer model on the square lattice with an arbitrary number of monomers. Furthermore, the Tzeng-Wu solution of the dimer model with a boundary monomer was found to be included in our theory. The exact expression of correlation functions between monomers has been written in terms of the product of two pfaffians, and we gave an explicit formula for boundary correlations valid for the four boundaries of the rectangle. In the following chapter, interpretations of finite size effects of the Tzeng-Wu solution in a CFT/Coulomb gas framework will been performed, and we will show that a careful examination of boundary conditions in the model allowed us to recover the central charge of the free fermion/free boson field theory. Extensions of the CFT interpretation of the free energy will be analyzed for correlation functions.

CHAPTER 3

# CFT analysis of the 2$d$ dimer model

## Contents

In this chapter, the bosonic formulation of the dimer model is presented *via* the so-called height mapping. The model will be then interpreted as a Coulomb gas theory of electric and magnetic charges. This theory will be very useful in order to compare with exact results about dimer and monomer correlations performed in the section 4. Special attention will be paid to boundary conditions and corner effects in a CFT framework, which will be crucial in order to interpret finite-size effects to the free energy. Correlation functions will be analyzed as well using our pfaffian solution and compared to height mapping/CFT predictions.

## 3.1 Bosonic theory and boundary conditions

In the previous chapters, we introduced the dimer model in terms of grassmann/fermionic variables and we saw that partition functions as well as correlation functions can be computed exactly in the discrete level leading to simple pfaffian expressions. Here another strategy is pursued, in order to make predictions not on a discrete level but on the scaling limit.

### 3.1.1 Height mapping and Coulomb gas formalism

To any dimer covering we can associate a height on the dual lattice (on the plaquette) which is defined as follows [217, 148, 97, 95]. When encircling an even vertex in the positive (counterclockwise) direction, the height $h$ increases by $+1$ upon crossing an empty edge and decreases by $-3$ upon crossing an edge that is covered by a dimer (*cf.* Fig. 5.3). It is easy to notice that for the allowed configuration the average values $h_{\text{vertex}}$ that the height variables can take at a given site of the direct lattice (a vertex) are $h_{\text{vertex}} = \pm 3/2$ or $h_{\text{vertex}} = \pm 1/2$. This mapping works *stricto sensu* for the close packed case. We will find it simpler to work with the rescaled height field $\phi = \frac{\pi}{2} h$. By fixing the rescaled height at an arbitrary point, *e.g.* $\phi(0) = 0$, these rules define

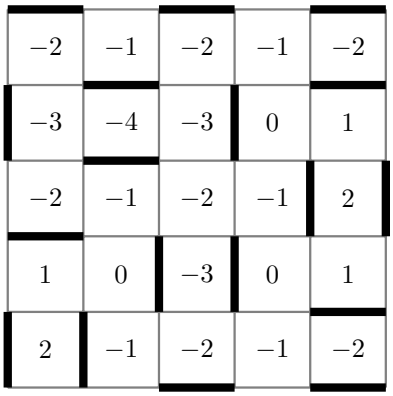


Figure 3.1: Height mapping of the dimer model with free boundary conditions. For pedagogical purposes we will keep the field $h$ on the figures.

the entire height function $\phi(\vec{r})$ uniquely. By integrating out the short distance fluctuations, one obtains an effective quadratic action $\mathcal{S}$ for the bulk height field $\phi(\vec{r})$, defined in the continuum,

which corresponds to the long-wavelength modes

$$\boxed{\mathcal{S}[\phi] = \frac{g}{2}\int \mathrm{d}x\,\mathrm{d}y\ \left(\nabla\phi\right)^2.} \tag{3.1}$$

Here $g$ is a constant which control the stiffness of the height model. It is *a priori* unknown. The field has to be invariant under the transformation $\phi = \phi + 2\pi n$ to respect lattice symmetries. The derivation of this gaussian field has been actually proved rigorously by mathematicians [126, 127]. Electric charges $e$ correspond to vertex operators appearing in the Fourier expansion of any operator periodic in the height field. Dual magnetic charges $m$ correspond to a dislocation in the height field and correspond to the dual vertex operator

$$\begin{aligned} V_e(z) &= :\mathrm{e}^{ie\phi}: \\ V_m(z) &= :\mathrm{e}^{im\psi}: \end{aligned} \tag{3.2}$$

where $\psi$ is the dual field of $\phi$ and defined as

$$\partial_i\psi = \epsilon_{ij}\partial_j\phi. \tag{3.3}$$

These operators are primary operators of the $c = 1$ CFT. The scaling dimension associated to the insertion of a particle with electromagnetic charge $(e, m)$ is given by

$$x_g(e,m) = \frac{e^2}{4\pi g} + \pi g m^2. \tag{3.4}$$

For example, two monomers on opposite sublattices correspond to two charges $m = 1$ and $m = -1$. It is known from exact results [71, 72] that, the exponent for bulk monomer-monomer correlations is $1/2$, it fixes $g_{\text{free}} = 1/4\pi$ for the stiffness constant of the gaussian field theory describing the free dimer model. We saw previously that bulk dimer-dimer exponent is 2. Hence the bulk monomer and dimer scaling dimensions defined by $x_b^{(m)} := x_{\frac{1}{4\pi}}(0,1)$ and $x_b^{(d)} := x_{\frac{1}{4\pi}}(1,0)$ are

$$\text{free dimer}: \quad g_{\text{free}} = \frac{1}{4\pi} \to \begin{cases} x_b^{(d)} := x_{\frac{1}{4\pi}}(1,0) = 1 \\ x_b^{(m)} := x_{\frac{1}{4\pi}}(1,0) = 1/4. \end{cases} \tag{3.5}$$

In this theory the conformal spin of an operator is defined by $s(e,m) = em$, then monomers and dimers are spinless particles but fermions which are order-disorder composite operators [118] have magnetic and electric charges and carry spins $1/2$. The fermion operator has then scaling dimension $x_{\frac{1}{4\pi}}(1/2,1) = 1/2$. It is also possible to define parafermion operators which obey fractional statistics [80] for particular values of the stiffness $g$. The use of such a mapping to study correlation functions dates back to Blöte, Hilhorst, and Nienhuis [160, 22]. The neutral 2-point correlation functions for vertex operators are then given by the standard formula [159]

$$\begin{aligned} \Big\langle V_{m=+1}(z)V_{m=-1}(0)\Big\rangle &\sim z^{-2x_{\frac{1}{4\pi}}(0,1)} = z^{-1/2} \\ \Big\langle V_{e=+1}(z)V_{e=-1}(0)\Big\rangle &\sim z^{-2x_{\frac{1}{4\pi}}(1,0)} = z^{-2}. \end{aligned} \tag{3.6}$$

The general $2n$-point function is given by the product

$$\Big\langle V_{m_1=\pm1}(z_1)...V_{m_{2n}=\pm1}(z_{2n})\Big\rangle \sim \frac{\prod_{i<j}(b_i-b_j)^{1/2}\prod_{k<l}(w_k-w_l)^{1/2}}{\prod_{p<q}(b_p-w_q)^{1/2}}, \tag{3.7}$$

where $\{b_k\}$ and $\{w_k\}$ are the sets of the even/odd sublattice coordinates. In this Coulomb gas interpretation of the dimer model, monomers located on the same sublattice are seen as repealing equal charges, and monomers on opposite sublattice are seen as attractive opposite charges. It is known from exact results [178, 7] that, the exponent for monomer correlations is 1 in the case (see Eq. (1.33)) where the monomers are restricted to live the same boundary. Hence the surface monomer scaling dimension is $x_s^{(m)} := 1/2$.

### 3.1.2 A few word about conformal field theory in the plane

In this section we give some basic notions of conformal field theory, we will need in the remaining of the work. A conformal field theory (CFT) is a quantum field theory endowed of an additional symmetry, the one under conformal transformations, whose effect is to modify the background metrics just with a local scale factor, the conformal group always contains the PoincareÓ group as a subgroup. The special case of dimension $d = 2$ is of special interest because the dimension of the conformal group becomes infinite, and this fact allows for the complete solvability of the theory. More specifically, if one writes the coordinates of the background, that we take now to be the full plane $\mathbb{R}^2$, as complex coordinates $z$, $\bar{z}$, the conformal group is exactly the group of holomorphic (and antiholomorphic) functions, suggesting the power of the complex formalism in CFT. From a statistical physics point of view, a critical system is described by a field theory which is invariant under scaling transformation, plus rotation and translation invariance. If one makes the addition postulate of short range interaction, it seems natural to assume the invariance of the conformal transformation as well (transformation which preserves angles). The conformal invariance can be seen as a scaling transformation which act locally on the system. Then finally a $2d$ critical systems which fulfilled these conditions will be described by a CFT. The continuum limit of a relevant physical quantity, as the magnetization in the Ising model, or the height field in the bosonic theory, will be encoded in a field $\phi(z, \bar{z})$ which will transform under a scaling transformation as

$$\phi(\lambda z, \lambda \bar{z}) = \lambda^{-\Delta} \bar{\lambda}^{-\bar{\Delta}} \phi(z, \bar{z}). \tag{3.8}$$

We can define the scaling dimension of the field $\phi$ as $x = \Delta + \bar{\Delta}$ and the spin as $s = \Delta - \bar{\Delta}$. In the case of the free boson description of the dimer model we introduced earlier, there are two different fields which describe dimer and monomer with respective scaling dimension $x_b^{(d)} = 1$ and $x_b^{(m)} = 1/4$. In dimension $d = 2$, conformal transformations are given by holomorphic and anti-holomorphic transformation

$$z \to z'(z), \tag{3.9}$$
$$\bar{z} \to \bar{z}'(z). \tag{3.10}$$

Of course, it is not the purpose of this thesis to detailed properly this theory, but just to give a little intuition of the phenomenology and send the reader to the yellow book [56] or the orange book [93] for a complete discussion.

### 3.1.3 Rectangular geometry and boundary conditions

On Fig. 3.2, we show a configuration of dimers on the square lattice with free boundary conditions. The choice of these conditions impose very specific boundary conditions for the height variable.

Indeed, we observe that the value of the height $h$ is (..101..) along the boundary until the corner and (..$-10-1$..) along the next boundary [192] (a similar analysis has been done for the strip geometry [196, 197]). Then we have, from the point a view of the field theory two different averaged boundary

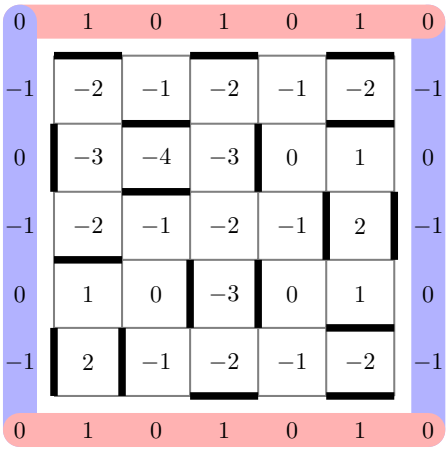


Figure 3.2: Height mapping of the dimer model with free boundary conditions. The different values of the height $h$ on each sides of each corner are induced by a *bcc* operator of scaling dimension 1/32. The dimension does not change if one chooses a rectangle $M \neq N$.

conditions either sides of the corner, let us call the boundary fields $h_b = 1/2$ and $\bar{h}_b = -1/2$. The proper way to understand how corners change the behavior of the height field is through boundary CFT (*cf.* [92] for introduction).

**Box 6** (Derivation the *bcc* operator dimension)**.**

Let us consider the same geometry as Fig. 3.2 with only one change of boundary conditions on the left bottom corner defined by the position $(x, y) = (0, 0)$. The difference of value between each sides of the corner is denoted $\Delta\phi$. Now we compute the difference of free energy between this configuration with a discontinuity of the field in the origin and the same configuration with usual Dirichlet conditions. This is done by the calculation of the partition function $Z(\Delta\phi)$ by path integration over all the configurations compatible with the boundary conditions. We decompose the field $\phi$ into an harmonic function $\phi_{\text{cl}}(\Delta\phi)$ which satisfies the boundary conditions, and a ÒfluctuatingÓ part $\phi_{\text{fl}}$ satisfying Dirichlet boundary conditions. Because of the gaussian action, we have the factorization $Z(\delta h) = Z_{\text{cl}}(\Delta\phi) + Z_{\text{fl}}$. By subtracting an harmonic function to the classical part $(2\Delta\phi/\pi)\arg(x + y)$ (see [196]), equal to 0 on the horizontal boundary $y = 0$ and $\Delta\phi$ on the vertical boundary at $x = 0$ the Dirichlet conditions is restored. The resulting contribution to the free energy is $\frac{g}{2\pi}\Delta\phi^2 \ln L$. In a CFT context, this change of boundary conditions is interpreted as a operator which lies in $(0, 0)$ and has dimension $\frac{g}{2\pi}\Delta\phi^2$. A more rigorous derivation of this formula, for general domain can be found here [188].

Hence it is natural to introduce local operators [37] acting on the corners of the domain, these objets called *boundary condition changing* operators (*bcc*) can be showed to be primary operators of the CFT [38] . A careful analysis shows that the difference of boundary conditions has non negligible consequences in the thermodynamic limit and the precise procedure based on the contribution of theses operators on the free energy can be found in [196]. It has been shown that the dimension of the *bcc* operator which creates a field shift of value $\Delta\phi_b = \frac{\pi}{2}(h_b - \bar{h}_b) = \phi_b - \bar{\phi}_b$ on the corner is

$$h_{bcc} = \frac{g}{2\pi}\Delta\phi_b^2, \tag{3.11}$$

with $g_{\text{free}} = 1/4\pi$ here. More details of the derivation of this formula will be given in **Box 6**. In the previous situation without any monomer, the corner shift in the height $h$ is equal to $\Delta h_b = 1$ then $\Delta\phi_b = \pi/2$, hence the dimension of the corner *bcc* operator is $h_{bcc} = 1/32$. Furthermore, the addition of a monomer on the boundary or at the corner will change the value of the field, and we will behold further that it will be relevant in order to study quantities as the free energy and correlation functions. A general framework to study partition functions and conformal boundary states on the rectangular geometry with different boundary conditions in a boundary CFT framework has been developed recently [24, 25]. In the section 4, finite size effects to the free energy for the free and interacting cases will be study in this CFT framework, and the influence of these *bcc* operators will be crucial to identify the correct underlying central charge of the theory. Furthermore the presence of monomers on the boundaries or at the corners will change again the values of the *bcc* operators which will be important for the study of surface and corner correlation functions.

## 3.2 Dimer models in various geometries

The study of finite size effects in statistical physics is a long standing and still active field of research [179]. *A fortiori* the possibility to solve a model in a non homogeneous geometry [96] is of prime interest for the understanding of behavior of physical systems in real situations. In the case of the dimer model on the rectangle with free boundary conditions, the system admits surfaces and corners, both of them play an important role in the behavior of the free energy in the thermodynamic limit. The exact solution of the close packing dimer model Eq. (5.2) on a even lattice ($M \times N = 2p$) allows for the study of the finite size effect of the free energy which has already been performed in the early time of the dimer model history [69], and has continued in a long series of articles using analytical [106, 104, 105, 102, 161] and numerical methods [137, 138, 136, 213] for various geometries and boundary conditions. Some of these results have been motivated by the conformal interpretation of finite size effects [21, 39, 38] and leading to a somehow controversial result [136, 182] about the central charge of the underlying field theory.

### 3.2.1 Boundary CFT and conformal mapping

In the previous page, we analyze a dimer configuration on a finite rectangle domain using this height mapping formulation. In this context, we saw that boundary conditions are not the same on the four edges of the rectangle and we have interpreted that phenomena as conformal boundary conditions separated by *bcc* operators. In the context of boundary CFT, the value of the dimension of these operators can be found to be proportional to the square of the difference of height. Let us

say a few words about what do we mean by boundary CFT. Conformal invariance allows for the choice of a reference domain trough conformal mapping (see Eq. (3.3) for an example). One has to introduce the stress-energy tensor $T_{\mu\nu}$ to explore the constraint given by conformal invariance. The stress-energy tensor is defined by the variation at the action $\mathcal{S}$ under an infinitesimal transformation $x_\mu \to x_\mu + a_\mu(x)$

$$\delta\mathcal{S} = \frac{1}{2\pi}\int \mathrm{d}^2 x T_{\mu\nu}\nabla^\mu a^\nu. \tag{3.12}$$

One of the consequences of the translation, rotation and dilation invariance are that we have the following conservation laws which can be written in complex coordinates

$$\nabla_{\bar{z}} T = 0, \tag{3.13}$$
$$\nabla_z \bar{T} = 0, \tag{3.14}$$
$$\mathrm{Tr}T = 0. \tag{3.15}$$

The tensor $T_{\mu\nu}$ has two independent coordinates, one is holomorphic $T(z)$ and the other is anti-holomorphic $\bar{T}(\bar{z})$. Until now, we have defined our theory on the plane $\mathbb{R}^2$ but one may want to choose to define the theory on the half-plane. The consequence of that is the translation symmetry breaking in one direction. The conservation of the current $j^\mu$ along the boundary implies that

$$\bar{T}(\bar{z}) = T(z), \tag{3.16}$$

on the boundary. This condition means that no energy will cross the boundary or in another word, that the system is decoupled from the rest of the world. We can show that the boundary conditions

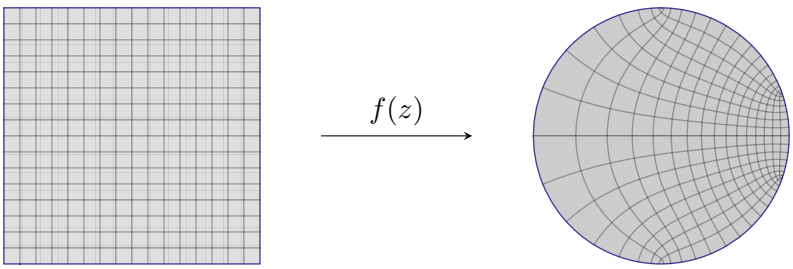


Figure 3.3: $f(z)$ is a conformal transformation which will map the square domain into a disk domain. The tensor $T_{\mu\nu}$ on the boundaries have to respect $\bar{T}(\bar{z}) = T(z)$

on the four edges of the rectangle in the dimer model are actually conformal boundary conditions in the sense that we can check that the formula Eq. (3.16) is correct for any point on the boundary of the domain.

### 3.2.2 CFT on a rectangle and corner free energy

Furthermore the exact solution Eq. (2.53) of the dimer model on a odd lattice ($M \times N = 2p+1$) with a monomer on a boundary allows for the study of the free energy in that case as well. Adding

a finite number of monomers in the dimer model is equivalent to a zero density of monomers in the continuum limit. Hence the presence of monomers does not give any contribution in the expression of the free energy, the only feature which plays a crucial role is the parity of the size of the lattice (even or odd). Because they are the simplest expressions of a even (odd) lattice with an even (odd) number of monomers, these two partition functions are sufficient to study all the details of the asymptotic limit of the free energy. In the following let us choose the square geometry $M = N = L$ for simplicity[1]. The free energy on a finite lattice of typical length $L$ at criticality has the generic following form [2]

$$\mathcal{F} = L^2 f_{\text{bulk}} + L f_{\text{surface}} + a \log L + f_0 + o\Big(\frac{\log L}{L}\Big). \tag{3.17}$$

The first term is the extensive contribution of the free energy, whereas the second one represents contribution from the lattice surface. In general, the coefficients $f_{\text{bulk}}$ and $f_{\text{surface}}$ are non-universal, but the next order coefficient is assumed to be universal, depending only on the shape and boundary conditions of the system. Universal properties of critical models, as the central charge $c$ of the underlying conformal field theory appear in the subleading corrections. The study of statistical systems and their field theory representation in the presence of corners has been covered extensively, *e.g.* Ising and Potts model, loop model and percolation [109, 203, 143, 142], using various theoretical and numerical machinery. In two dimensions, as pointed out by Cardy and Peschel [39], the universal contribution to the free energy of a critical system in a domain with a corner with angle $\theta$ has been determined using the complex transformation

$$z \to z^{\theta/\pi}, \tag{3.18}$$

which maps the upper half-plane onto the corner and looking at the holomorphic component of the stress-energy tensor in the corner. This mapping gives us the explicit form of the logarithmic contribution $\mathcal{F}_{\text{corner}} = a \log L$ in Eq. (3.17) and the result is $\frac{c}{24}\big(\frac{\theta}{\pi} - \frac{\pi}{\theta}\big) \log L$. It turns out that a additional complication arises because of the *bcc* operators [38] acting in the corners (*cf.* Fig. 3.4) as we saw in the section before. In that particular case, the Cardy-Peschel contribution is slightly modified to taking into account this change of boundary conditions [133], and the logarithmic corner contribution becomes (see **Box 7** for details)

$$\boxed{\mathcal{F}_{\text{corner}} = \Big[\frac{\pi}{\theta} h_{bcc} + \frac{c}{24}\Big(\frac{\theta}{\pi} - \frac{\pi}{\theta}\Big)\Big] \log L} \tag{3.19}$$

where $h_{bcc}$ is the scaling dimension of the *bcc* operator. This *bcc* operator changes the boundary condition either sides of the corner in the height field representation.

[1] The entire procedure can be extended to the case $M \neq N$ where the aspect ratio has to be taken into account, and no significant change appears [132].

[2] The presentation here closely follows [194].

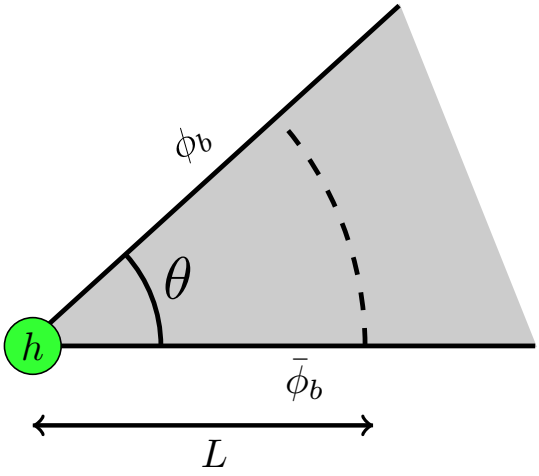


Figure 3.4: Corner of angle $\theta$ in a system of typical length $L$, in our situation $\theta = \pi/2$. The green dot symbolize a *bcc* operator of scaling dimension $h_{bcc}$ which changes the value of the field either sides of the corner.

**Box 7** (Derivation of the Cardy-Peschel formula)**.**

The Cardy-Peschel term can be computed as follows. The mapping $w = z^{\theta/\pi}$ maps the upper half-plane onto the corner (see Fig. 3.4). The holomorphic component of the stress-tensor in the corner $T(w)$ will transform according to the usual transformation

$$T(w) = \left(\frac{\mathrm{d}w}{\mathrm{d}z}\right)^{-2}\Big[T(z) - \frac{c}{12}\{w,z\}\Big], \tag{3.20}$$

where $\{w,z\}$ is the Schwarzian derivative $\{w,z\} = \frac{w'''}{w'} - \frac{3}{2}\left(\frac{w''}{w'}\right)^2$. Then the strategy consists to analyze how look the generators of translation in the corner, using the definition $\hat{D} = \frac{1}{2\pi i}\int \mathrm{d}w T(w) w + \text{h.c}$ where the integration is over the dashed line in Fig. 3.4 and the conformal mapping, and the fact that we work with a chiral theory $T(z) = \bar{T}(\bar{z})$

$$\hat{D} = \frac{\pi}{\theta}\hat{L}_0 + \frac{c}{24}\Big(\frac{\theta}{\pi} - \frac{\pi}{\theta}\Big). \tag{3.21}$$

The final step is to use the definition $F_{\text{corner}} = -\log\langle L^{-\hat{D}}\rangle$. When there is a *bcc* operator at the corner, $\langle\hat{L}_0\rangle = h_{bcc}$ and the formula Eq. (3.19) is found. Without any *bcc* operator $\langle\hat{L}_0\rangle = 0$ and only the second term in Eq. (3.19) remains.

**Extrapolation of the central charge**

In their recent paper about corner free energy contribution in the free boundary conditions dimer model with one monomer at the boundary [103], the authors analyzed the asymptotic contributions of the four corners of the rectangular system and found that the contribution of the four corners of the $L \times L$ ($L$ odd) lattice is [3]

$$\mathcal{F}_{\text{corner}} = \frac{1}{2} \log L. \tag{3.22}$$

The CFT formula Eq. (3.19) gives in the square geometry case ($\theta = \pi/2$)

$$\mathcal{F}_{\text{corner}} = \left[ \frac{-c}{4} + 2\left(h_{bcc}^{(1)} + h_{bcc}^{(2)} + h_{bcc}^{(3)} + h_{bcc}^{(4)}\right) \right] \log L, \tag{3.23}$$

where $h_{bcc}^{(\nu=1..4)}$ are the dimensions of the four *bcc* operators living on the corners. We know that the partition function with one monomer on the boundary does not depend of the location of the monomer, then let us choose to put it on the corner for simplicity. In this following case, the

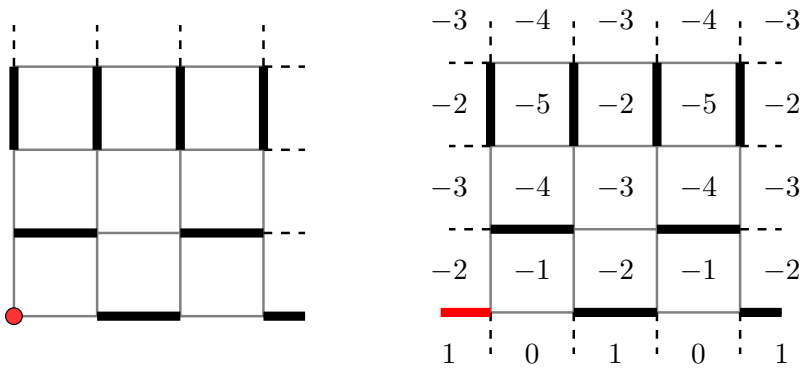


($a$) ($b$)

Figure 3.5: ($a$) Representation of the corner region of a lattice with one monomer at the corner. ($b$) The monomer can be represented by a virtual red dimer which gives the same configurations. The different values of the height field either sides of the corner are induced by a *bcc* operator of scaling dimension 9/32.

height field is shifted either sides of the corner, precisely we obtain the value $h = (..0101..)$ in one side and $h = (.. - 2 - 3 - 2 - 3..)$ on the other side (see Fig. 3.5), making a height shift of $\Delta\phi_b = 3\pi/2$, therefore using Eq. (3.11), the dimension of the *bcc* operator on the corner is 9/32 (which is actually the dimension of the original *bcc* plus the dimension of the corner monomer operator as we will see in the next section). The three other corners induce a height shift of $\pi/2$, thus the dimension of the *bcc* operators is 1/32 as in the case where monomer are absent. Finally we find

$$\mathcal{F}_{\text{corner}} = \left[ \frac{-c}{4} + 2\left(\frac{9}{32} + \frac{1}{32} + \frac{1}{32} + \frac{1}{32}\right) \right] \log L. \tag{3.24}$$

[3] *cf.* [103] for details of the asymptotic calculation.

The comparison with the asymptotic result Eq. (3.22) gives us the value of the central charge of the free bosonic field theory, *i.e.* $c = 1$. One can notice that the same result holds if the monomer is somewhere on the boundary but not at the corner, in that case, there is five *bcc* operrtors, four on each corners of dimension $1/32$ and another responsible for the shift at the surface with dimension $1/2$ then using Eq. (3.19)

$$\mathcal{F}_{\text{corner}} = \Big[\frac{-c}{4} + \frac{1}{2} + 2\Big(\frac{1}{32} + \frac{1}{32} + \frac{1}{32} + \frac{1}{32}\Big)\Big] \log L = \frac{1}{2} \log L, \tag{3.25}$$

in accordance with the fact that the partition function with one boundary monomer does not depend of its location. Obviously this result seems completely natural in the height mapping framework or in the free complex fermion representation of the dimer model Eq. (5.9), nonetheless the presence of *bcc* operators acting on the corners has never been extensively studied in this context, leading to misinterpretation of asymptotic results and thus to a different value of the central charge of the theory. In the pure dimer situation Eq. (5.2), the four *bcc* operators has dimension $1/32$, we claim that the corner free energy should be equal to

$$\mathcal{F}_{\text{corner}} = \Big[\frac{-1}{4} + 2\big(4h_{bcc}\big)\Big] \log L = 0. \tag{3.26}$$

This result nicely agrees with the literature, where no corner free energy term has never been found in the free boundary conditions close packed dimer model, neither theoretically [29] nor numerically [136], strengthening our analysis. Obviously the number of monomers does not play any role at the thermodynamic limit because the density is always zero. The result depends only on the parity of the lattice and the analysis of the model with zero and one monomer are just the simplest cases that we can study leading to the general statement

- $\mathcal{F}_{\text{corner}} = 0$ for an even lattice.
- $\mathcal{F}_{\text{corner}} = 1/2 \log L$ for an odd lattice.

We claim here that the analysis of the free energy in the height mapping formulation of boundary conditions, leads again to $c = 1$. In the following section, we shall compute analytically correlation functions between monomers where boundary fields has to be properly interpreted and we will show that the exact solution fully agrees with this theory, reinforcing the present result about the significance of these *bcc* operators. Finally we conclude, that the free bosonic formulation of the dimer model allows for the complete study and interpretation of finite size effects in a CFT context, and unified all the results known about this very simple but non-trivial model.

### A word about the $c = -2$ CFT

It is beyond the scope of this thesis to enter into the wide area of conformal analysis of finite size effects (see [194] for more details), nor all the literature of $c = -2$ models, but just to pointing out the difference of result when one looks carefully at the *bcc* operator contribution in the corner free energy. This statement is also based on the mapping of the dimer model to the spanning tree model [200] and, equivalently, to the Abelian sandpile model [152] which both belong to a $c = -2$ symplectic fermion theory. Taking $h_{bcc} = 0$ leads *de facto* to $c = -2$, suggesting that the dimer model may be a logarithmic CFT (LCFT) [106, 178, 182]. This argument turns out to be valid in

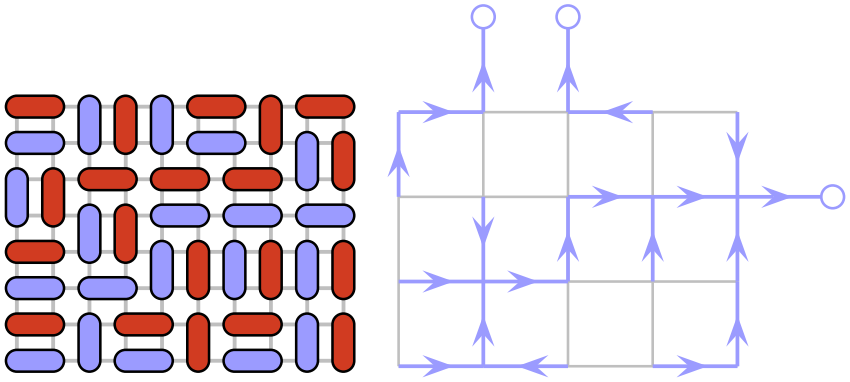

Figure 3.6: A dimer configuration on the square lattice with open boundary condition on the left and its equivalent spanning tree representation as explained in the first chapter. Here there is two kind of boundary conditions for the tree, open on the top and right and closed on the left and bottom, which can be tacking into account using two *bcc* operators of dimension -1/8. Figures from [106]

the spanning trees formulation because in the odd case, there is no change of boundary conditions at the corners while in the even geometry, there is two *bcc* of dimensions -1/8 on opposite corners (see Fig. 3.6). It will be very interesting to understand in details how to reconcile the two CFT descriptions of the dimer model, and we let this problem for futur work.

### 3.2.3 Transfer matrix formulation and CFT on a infinite strip

Previously another type of finite size effect analysis [106] has been performed for the close packing dimer model on a strip with periodic and free boundary conditions, and it has been shown that the result depends strongly on the parity of the length of the strip as it should be, and the notion of effective central charge has to be introduce [99]. We consider a square lattice with periodic boundary conditions and an even number of columns $N$ and consider a staggered configuration. Consider now superposing a generic dimer configuration with the staggered configuration, the resulting superposition is shown in fig and consists in a certain number $s$ of strings (see Fig. 3.7). The dynamics under which these strings propagate in the vertical direction has the following properties [4]

- The configurations of dimer fully determine by the configurations of strings.
- The number of strings is conserved *i.e.* the number of fermions is conserved, so that the transfer matrix is block-diagonal.
- When moving from a horizontal row to the next, a string can either go straight or jump exactly one site to the left or to the right.

[4] More details about the transfer matrix can be found in the next chapter

These properties follow directly from the definition of the superposition and from the definition of a valid dimer covering. The properties of strings suggest to view dimer configurations as a discrete time evolution process, where the time increases along the vertical direction. In what follows it is convenient to refer to the horizontal direction as space and vertical direction as time. The time evolution is then accomplished by the row-to-row transfer matrix $T$ which will be detailed below. We view the system as a set of fermionic particles on the lattice $\mathbb{Z} + 1/2$ that evolve in the $y$-direction, which is imaginary time. We do not write down explicitly the actual form of the

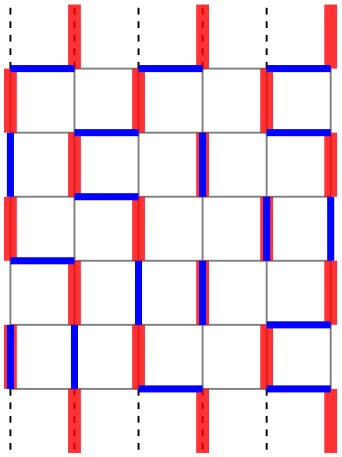

Figure 3.7: We choose a staggered dimer configuration which we call a reference configuration (red). Any other dimer configuration (blue) will be compared to the reference by superposition of the two. We define the particle locations as the vertical edges that are not occupied by a real dimer only a reference one. Particles can jump from a vertical edge to another only if a real horizontal dimer connects the two. Here, a fermion will be defined as an even vertical edge occupied only by a reference dimer or an odd vertical edge occupied only by a real dimer.

transfer matrix here, since we dot not need its expression for the purpose of the discussion and will be fully detailed in the next chapter about the arctic circle phenomenon. The partition function for periodic boundary conditions in the imaginary-time direction is

$$Q_0 = \mathrm{Tr} T^N. \tag{3.27}$$

Through this expression, the analogy between a quantum $1d$ model and a $2d$ statistical system is obvious and will be useful to characterize the conformal spectrum of a classical or quantum theory on a strip or cylinder. In all cases, the free energy per site can be related to the leading eigenvalue of the transfer matrix [5], and critical exponents can be inferred from various subleading eigenvalues. A powerful tool that we will use for analyzing critical properties of a model is various geometries in the conformal mapping. Here on may ask about the form of the free energy when one choose to consider the dimer model on a infinite long strip of width $L$. One obvious consequence is that the value of the height field on both sides of the strip will depend of the parity of $L$. For $L$ even the two boundary values are the same while there are not for odd $L$ (see Fig. 3.9). The half-plane

[5] or the exponential of the hamiltonian

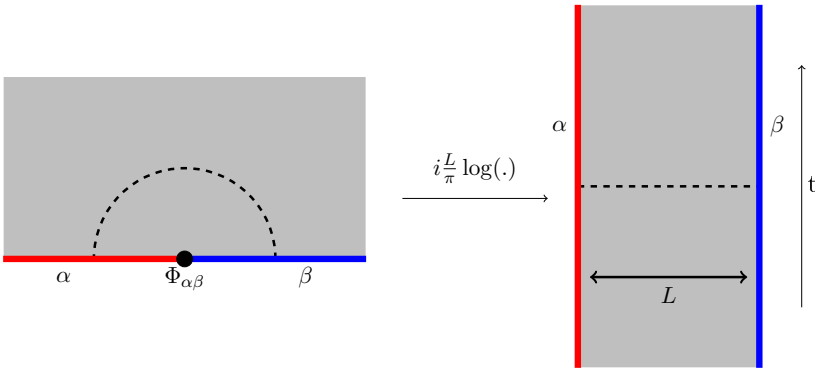


Figure 3.8: Conformal mapping between the half-plane with a *bcc* operator $\Phi_{\alpha\beta}$ in 0 and the stripe with different boundary conditions on the left and right of the strip. Figure from [58]

can be mapped into a infinite stripe of width $L$ using the following conformal mapping

$$w = \frac{iL}{\pi} \log z, \tag{3.28}$$

which can be used to compute correlation functions in this geometry starting from correlation on the half-plane. The general form of the free energy per unit length of an infinitely long strip of finite width $L$ at criticality is

$$\mathcal{F}_L = f_{\text{bulk}} L + f_{\text{surf}} + \frac{A}{L} + ..., \tag{3.29}$$

where $f_{\text{bulk}}$ is the free energy per bulk site, and $f_{\text{bulk}}$ is the free energy per boundary site assuming identical boundary conditions on the two sides of the strip, and $A$ is a constant. Unlike the free energy densities $f_{\text{bulk}}$ and $f_{\text{surf}}$, the constant $A$ is universal. The value of $A$ is related to the central charge $c$ of the underlying CFT, and depends on the boundary conditions in the transversal direction. This last point will be crucial here, indeed in the case or dimer model on a strip the boundary conditions on both side of the strip will depend on the parity of the width $L$. These different boundary conditions in the strip geometry will lead to a change of boundary condition in the point $x = 0$ of the real line in the half space geometry (see Fig. 3.8). This change of boundary condition will be interpreted, just like in the case of the corner we saw before, as the presence of a *bcc* operator acting on the boundary. This *bcc* has to be carefully analyzed and its conformal dimension will appear in the expression of the universal part of the free energy. The details of the calculation are not presenting here since there are quite standard and we send the curious reader to [21, 39, 38] for details.

### Cylinder geometry

In the cylinder geometry the actual expression for the constant term $A^{(\text{cyl})}$ is

$$A^{(\text{cyl})} = -\frac{\pi}{24} c_{\text{eff}} = 4\pi \Big( h_{\text{bcc}} - \frac{c}{24} \Big), \tag{3.30}$$

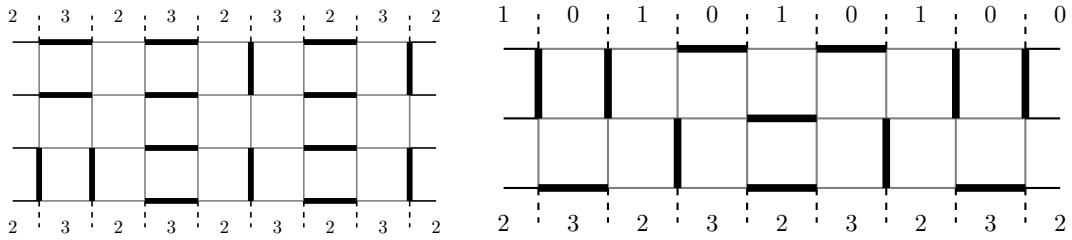


Figure 3.9: Strip/cylinder geometry with even width (left) and odd width (right). For the cylinder geometry, there is periodic boundary conditions in the longitudinal direction while there is open boundary conditions in the strip case. For an even width $L$ the boundary conditions are the same, but for odd $L$ there are different. This can be seen as the insertion of a *bcc* operator acting at infinity. Using the mapping $w = \frac{iL}{\pi}\log z$, the strip is mapped to to the half-plane with the *bcc* operator at the origin. The dimension of the *bcc* operator can be computed using Eq. (3.11).

where $c_{\text{eff}}$ is called the effective central charge. We have now to distinguish between the cases $L$ even and $L$ odd

- $L$ even (Fig. 3.9($a$)), $\Delta\phi = 0$ then by Eq. (3.11)$\rightarrow h_{bcc} = 0$ and by Eq. (3.30) $\rightarrow A^{(\text{cyl})}_{\text{even}} = -\frac{\pi}{6}$.
- $L$ odd (Fig. 3.9($b$)), $\Delta\phi = 2$ then by Eq. (3.11)$\rightarrow h_{bcc} = 1/8$ and by Eq. (3.30) $\rightarrow A^{(\text{cyl})}_{\text{odd}} = \frac{\pi}{3}$.

**Strip geometry**

In the strip geometry the actual expression for the constant term $A^{(\text{strip})}$ is

$$A^{(\text{strip})} = -\frac{\pi}{24}c_{\text{eff}} = \pi\Big(h_{\text{bcc}} - \frac{c}{24}\Big). \tag{3.31}$$

We have to distinguish between the cases $L$ even and $L$ odd as well

- $L$ even (Fig. 3.9($a$)), $\Delta\phi = 0$ then by Eq. (3.11)$\rightarrow h_{bcc} = 0$ and by Eq. (3.31) $\rightarrow A^{(\text{str})}_{\text{even}} = -\frac{\pi}{24}$ .
- $L$ odd (Fig. 3.9($b$)), $\Delta\phi = 2$ then by Eq. (3.11)$\rightarrow h_{bcc} = 1/8$ and by Eq. (3.31) $\rightarrow A^{(\text{str})}_{\text{odd}} = \frac{\pi}{12}$.

Finally let us mention that in this bosonic theory, the "real" central charge is found to be $c = 1$ and the effective central charge is found to be $c_{\text{eff}}$, while in the spanning tree interpretation it would be the other way around where $c = -2$ is the real central charge and $c = 1$ is the effective central charge. We do not fully understand how to reconcile the two CFT and we hope that a better understanding of this two theories will come from future work. However, this might not be so surprising considering the strong relations between the partition functions (which are both determinantal). This connection has been first noticed here [61] and applied for the rectangular geometry here [24] and there [25].

## 3.3 Scaling behavior of monomer and dimer correlation functions

### 3.3.1 Boundary conformal dimensions

After the study in full details of the expression of the free energy in the rectangular and strip (and cylinder) geometries, the next step will be to determined all the correlations in the model, albeit their scaling dimension and amplitudes. If we take, for a moment, the example of the Ising model from a CFT point a view. We know that the conformal content is fairly simple, *i.e.* that only two operators are primary (actually three with the unity operator), which are the spin operator $\sigma$ and the energy density operator $\epsilon$. In this unitary CFT, we know from the Kac table that $\bar{h}_\sigma = h_\sigma := x_b^{(\sigma)} = 1/16$ and $\bar{h}_\epsilon = h_\epsilon = x_b^{(\epsilon)} = 1/2$. These scaling dimensions are valid in the bulk, specified by the index $b$. In $2d$ any analytical function $w(z)$ on the complex plane provides a conformal mapping with a local dilation factor $b(z) = |\,\mathrm{d}z/\,\mathrm{d}w|$. Such mapping can be used to deduce surface exponents starting from the half-space geometry. The same conformal mapping approach can be used to extract exponents close to a wedge of angle $\theta$, is that case the surface exponent is recover in the limit $\theta \to \pi$. The corner and surface exponents are not independent and and relation can be found between them using conformal invariance (see **box 8** below)

**Box 8** (Corner dimension)**.**

In two dimensions the critical behavior near a wedge can be related to that of a half-plane if the system shows conformal invariance. Consider the conformal transformation $w = z^{\theta/\pi}$, which maps the surface geometry of the $z$-plane into a wedge of opening angle $\theta$ in the $w$-plane. If one knows the dimension of an operator on the surface $x_s$, it is possible to compute the scaling dimension of the same close to a wedge of internal angle $\theta$ using this transformation, and the result is

$$x_c = \frac{\pi}{\theta} x_s, \tag{3.32}$$

which for $\theta = \pi/2$ give $x_c = 2x_s$. The details of this calculation can be found in the nice review [96] where all kinds of geometries are studied thoroughly.

Conformal invariance predicts more than just exponents of correlation functions, but also predicts the complete form of the correlation functions, and how the correlators scale with the distance to the surface of corner. In the following, we will be interesting only on the exponents for dimer and monomer correlations and the full analysis of the correlations are not presented here.

### 3.3.2 Monomer correlations

Here, we shall analyze monomer-monomer correlation functions using our pfaffian solution detailed previously and compared to the Coulomb gas interpretation of the dimer model. As we saw in the previous section, the dimer model on a rectangular geometry admits *bcc* operators on every

of the four corners, and it has to be taken into account for the analysis of the scaling dimension operators, in particular for corner correlations. Indeed in the case of monomers deep in the bulk[6] or deep in the surface[7], the scaling dimensions are respectively $x_b^{(m)} = 1/4$ and $x_s^{(m)} = 1/2$, leading to the following scaling of correlation functions (see Fig. 3.11($a$))

$$\text{monomer correlations} \rightarrow \begin{cases} \text{bulk-bulk behavior} \rightarrow C(L) \sim L^{-2x_b^{(m)}} \sim L^{-1/2} \\ \text{surface-surface behavior} \rightarrow C(L) \sim L^{-2x_s^{(m)}} \sim L^{-1} \\ \text{bulk-surface behavior} \rightarrow C(L) \sim L^{-x_s^{(m)}-x_b^{(m)}} \sim L^{-3/4}. \end{cases} \tag{3.33}$$

These known results are in perfect agreement with our exact solution (*cf.* Fig. 3.10) where we fixed the positions of two monomers for increasing system size $L$ (all the correlations are measured for $t_x = t_y = 1$).

**Box 9** (Amplitudes of the monomer correlations)**.**

The amplitude $B$ of the asymptotic two-point correlation function, which behaves like $Bd^{-1/2}$, has been determined explicitly in the thermodynamic limit [13], $B = 2^{-3/4}A^2 \approx 0.247...$ with $A = 2^{1/12}\mathrm{e}^{3\zeta'(-1)}$ and where $\zeta(s)$ is the Riemann zeta function. This value appears to be in perfect agreement with our numerical fit. Our exact solution allows for numerical extrapolation of amplitudes for any monomer (and also dimer) correlations with a very high precision.

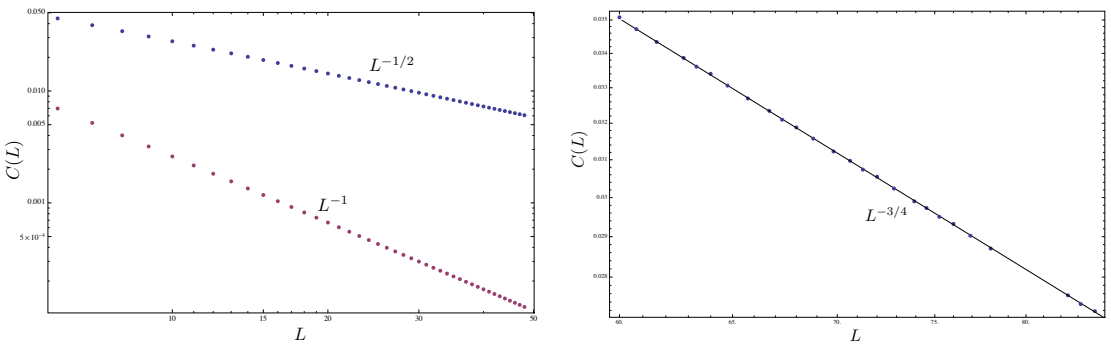


($a$) ($b$)

Figure 3.10: ($a$) Bulk-bulk and surface-surface correlation functions. ($b$) Bulk-surface monomer correlation functions

The behaviors of bulk and surface monomer correlation functions had already been studied in several papers, and the scaling dimensions are related to the scaling dimensions of operators of the 2$d$ Ising model *via* the expression of monomer-monomer correlations as spin-spin correlations [13].

[6] far from surfaces and corners.
[7] far from corners.

### Corner critical behavior

Now we consider the effects of corners in our system, which seems to be more difficult to consider as we have seen for the corner contribution to the free energy. Fortunately conformal invariance predicts a relation for the scaling dimension of an operator in the vicinity of a corner of an angle $\theta$ in terms of the scaling dimension of the same operator on the surface [39]

$$x_c = \frac{\pi}{\theta} x_s. \tag{3.34}$$

If we believe in this formula, we should obtain the value $x_c^{(m)} = 1$ for $\theta = \pi/2$, which leads to the behavior $C(L) \sim L^{-2}$ for corner-corner correlation functions. This result contradicts our exact evaluation, where the exponent seems to change according to the exact location of the monomers (see Fig. 3.11($b$) and Fig. 3.13), and where three different cases arise. Unlike the surface and bulk cases where the scaling dimensions are uniquely defined, the corner scaling dimension appears to be less trivial to analyze, and the influence of the *bcc* operators has to be carefully taking into account. We should mention that the same kind of analysis has been done for the Ising model, where the magnetization was measured for various spins close to a corner [169]. We saw previously

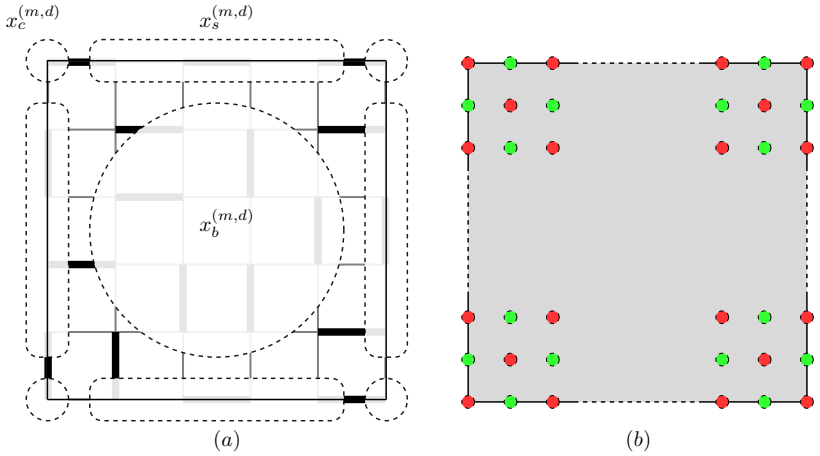


Figure 3.11: ($a$) Bulk, surface and corner decomposition of the square. ($b$) Representation of the values of the scaling dimensions of monomer operators close to the corners. Monomers on red sites have dimension $x_{c_+}^{(m)} = 1/2$ while monomers on green sites have dimension $x_{c_-}^{(m)} = 3/2$. Let us notice that this distinction is different from the even/odd sublattice distinction because opposite sublattice sites may have the same dimension and *vice verca*.

Eq. (3.23), that *bcc* operators add a logarithm term in the expression of the free energy $\mathcal{F}$ of a rectangular system, then this contribution to the partition function scale as

$$Q(L) \sim L^{-2\left(h_{bcc}^{(1)}+h_{bcc}^{(2)}+h_{bcc}^{(3)}+h_{bcc}^{(4)}\right)} = L^{-2(1/32+1/32+1/32+1/32)}. \tag{3.35}$$

Indeed putting two monomers exactly on the corner of the same boundary (see Fig. 3.13($a$)) is equivalent to a height shift of value $3\pi/2$ in each corner. This height shift is induced by an

operator of dimension 9/32, leading to the following behavior of the partition function with the two monomers

$$Q_2(L) \sim L^{-2\left(1/32+1/32+9/32+9/32\right)}. \tag{3.36}$$

Here the correlation function scale then as $C(L) = Q_2 Q_0^{-1} \sim L^{-1}$ leading to the value $x_c^{(m)} = 1/2$ of the monomer corner scaling dimension. Nevertheless, if one choose the diagonal corners (see Fig. 3.13($b$)), we place a monomer on the first corner which is again equivalent to the insertion of a *bcc* operator of dimension 9/32 (see Fig. 3.5) and the other one on a neighboring site of the other corner which is equivalent to the insertion of a *bcc* operator of dimension 25/32 (see Fig. 3.12), we found the behavior $C(L) \sim L^{-2}$. Finally, if both of the two monomers are on a

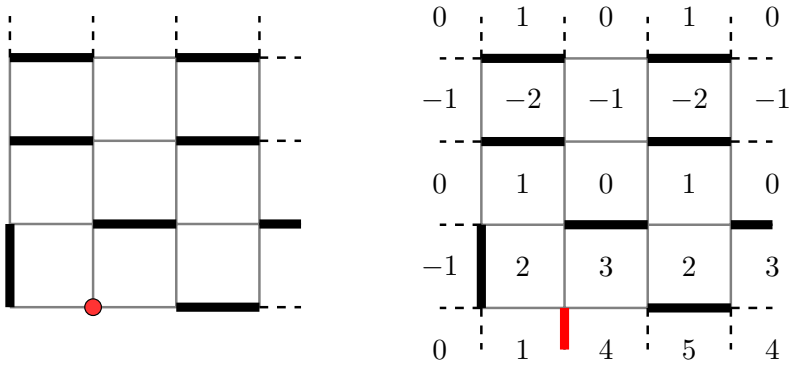


($a$) ($b$)

Figure 3.12: ($a$) Representation of the corner region of a lattice with one monomer at the corner. ($b$) The monomer can be represented by a virtual red dimer which gives the same configurations. The different values of the height field either sides of the corner are induced by a *bcc* operator of scaling dimension 25/32.

neighboring site of a corner (see Fig. 3.13($c$)), then the correlation function is $C(L) \sim L^{-3}$. This three different situations are summarized in Fig. 3.13, showing that our exact computations are in perfect agreements with Coulomb gas predictions for the behavior of correlation functions in the vicinity of a corner. A more general statement is that the monomer scaling dimension near a corner depends crucially of the sublattice considered as explained in Fig. 3.11($b$). This phenomena leads to two different values of the scaling dimensions of corner monomers $x_{c_+}^{(m)} = 1/2$ and $x_{c_-}^{(m)} = 3/2$ which is in agreement with the CFT formula Eq. (3.34) in average $x_c^{(m)} = (x_{c_+}^{(m)} + x_{c_-}^{(m)})/2 = 2x_s^{(m)} = 1$ when lattice effects are forgotten.

### Finite size scaling

A general study of the finite size behavior of correlation functions can be performed as well, leading to the following scaling ansatz

$$C(r_1, r_2, L) = |r_1 - r_2|^{-x_1-x_2} \Phi(|r_1 - r_2|^{-1} L), \tag{3.37}$$

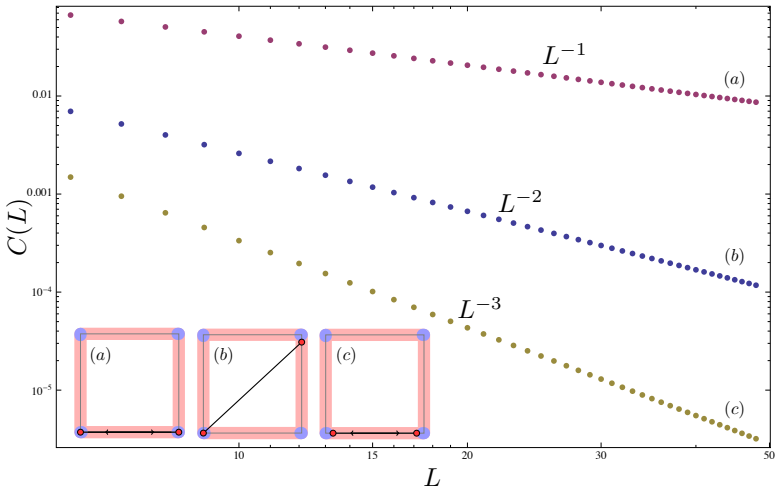


Figure 3.13: Corner-Corner in the three different situations pictured on the graphical representation: $(a)$ the two monomers exactly on the corners. $(b)$ One monomer on one corner and the other one on a adjacent site of another corner. $(c)$ Two monomers on adjacent sites of opposite corners.

where $r_1$ and $r_2$ are the positions of the two monomers, with respective scaling dimensions $x_1$ and $x_2$. The scaling function $\Phi(u)$ depends on the position of the operators and goes to a constant in the scaling limit $u \to \infty$ (see Fig. 3.14). The translation and rotational invariance has been checked analytically and numerically, and in the following we will use $|r_1 - r_2| = r$

$$C(r) \sim r^{-x_1 - x_2}. \tag{3.38}$$

This scaling behavior is shown for bulk-bulk and surface-surface correlations in Fig. 3.14. The exact form of the scaling function $\Phi$ seems hard to obtain explicitly, but at least for boundary and corner cases it should be possible to extract the scaling behaviors using the expression Eq. (2.52) of exact correlation functions. We let this question for a future work and we hope that comparisons with CFT predictions can be made.

### 3.3.3 Dimer correlations and composite particles

As we have shown in the first chapter of this thesis, the bulk correlation between a dimer covering the two neighboring sites $i$ and $j$ and another dimer covering the two neighboring sites $m$ and $n$ can be computed in the Kasteleyn-Fisher-Temperley pfaffian formalism leading to a behavior in $L^{-2}$ in the thermodynamic limit. Let us note $D(L)$ this quantity. In the Coulomb gas approach, dimers are interpreted as electric charges with scaling dimensions $x_b^{(d)} := x_{\frac{1}{4\pi}}(1,0)$, the result for dimer-dimer correlations gives us the value $x_b^{(d)} = 1$.

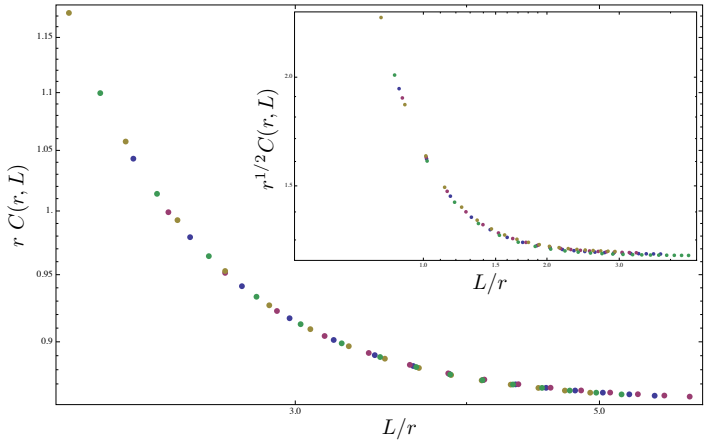


Figure 3.14: Finite size scaling of monomer surface-surface and bulk-bulk (inset) correlation functions in log-log scale for $L = 100, 200, 300, 400$. The surface correlations are measured far from the corners and the bulk correlations are measured far from boundaries and corners.

### Dimer correlations

Actually it is straightforward to study dimer correlations here. Indeed a dimer can be seen as two neighboring monomers, thus a dimer-dimer correlation is simply a 4-point monomer-monomer correlation, which can be evaluated with our solution. In the following, one shows how to construct the dimer-dimer correlation in the boundary case, for the bulk case the situation is essentially the same but expressions are less convenient. Explicitly the correlation between two dimers at position $(r_i, r_j)$ and $(r_m, r_n)$ is

$$Q_4(r_i, r_j, r_m, r_n)Q_0^{-1} = C_{ij}C_{mn} - C_{im}C_{jn} + C_{in}C_{jm}. \tag{3.39}$$

If we choose that $r_i$ and $r_m$ are on the same sublattice (then $r_j$ and $r_n$ are on the other one), a straightforward consequence is that the second term $C_{im}C_{jn}$ vanishes, moreover the first term $C_{ij}C_{mn}$ tends to a constant in the thermodynamic limit in such way that we can define the dimer-dimer correlation function as

$$Q_4(r_i, r_j, r_m, r_n)Q_0^{-1} - C_{ij}C_{mn} = C_{in}C_{jm} \sim D(L). \tag{3.40}$$

In this way, all the configurations of dimer correlations are available, and all the scaling dimensions of electric charges (bulk, surface, corner) may be analyzed *stricto sensu* and compared with the Coulomb gas theory. We can show that the well known bulk behavior is recovered very precisely, furthermore, surface and corner correlations may be examined as well leading to the following behaviors

$$\text{dimer correlations} \rightarrow \begin{cases} \text{bulk-bulk behavior} \rightarrow D(L) \sim L^{-2x_b^{(d)}} \sim L^{-2}, \\ \text{surface-surface behavior} \rightarrow D(L) \sim L^{-2x_s^{(d)}} \sim L^{-2}, \\ \text{corner-corner behavior} \rightarrow D(L) \sim L^{-2x_c^{(d)}} \sim L^{-4}. \end{cases} \tag{3.41}$$

Unlike monomer correlations, dimer correlations are much easier to interpret in the Coulomb gas framework. Indeed, the absence of additional change of boundary conditions[8] in the partition function allows for a direct determination of dimer scaling dimensions. The particular form of

| scaling dimension ($g_{\text{free}} = 1/4\pi$) | bulk | surface | corner |
|---|---|---|---|
| $x^{(d)}$ | 1 | 1 | 2 |
| $x^{(m)}$ | 1/4 | 1/2 | 1/2 or 3/2 |

Table 3.1: Bulk, surface and corner values of dimer and monomer scaling dimensions for the free ($g_{\text{free}} = 1/4\pi$) fixed point. The corner monomer scaling dimension depends of its exact location.

dimer correlations Eq. (3.40) predicts that $x_s^{(d)} = 2x_s^{(m)} = 1$[9] and $x_c^{(d)} = x_{c_+}^{(m)} + x_{c_-}^{(m)} = 2$[10]. We notice here that the formula Eq. (3.34) checked out in that case. A careful and detailed study of surface and corner operators has to be performed to unravel this point. The scaling form of correlation functions Eq. (3.37) holds in the dimer case as well, using the dimer scaling dimensions (see Table 3.1). The solution presented here can be also used to calculate more complex correlation functions, combining dimer and monomer scaling dimensions. *A posteriori*, more complicated object like trimers with dimension $x_{\bullet\bullet\bullet}$, quadrimers with dimension $x_{\bullet\bullet\bullet\bullet}$ or more generally, string of $k$ neighboring monomers ($k$-mer) with dimension $x_{\bullet\ldots\bullet}$, can be studied as well, which correspond to various charged particles in the Coulomb gas formalism.

### Quantum dimer model and classical limit

Dimer models have regained interest because of its quantum version, the so-called quantum dimer model, originally introduced by Rokhsar and Kivelson [183] in a condensed matter context. This model was introduced to give a description of the phenomena of resonating valence bond states by Anderson. Consider all dimer coverings of the square lattice. To each configuration assign a vector. Assume these vectors form an orthogonal basis for the Hilbert space. Notice that if we rotate a plaquette with two parallel dimers we get an allowed configuration. These special plaquettes are called flippable. Let us write the Hamiltonian by introducing local kinetic and potential terms. where a dimer represent a singlet of two spins. One of the nice feature of the quantum dimer

$$\widehat{H} = \sum \left[ \frac{v}{t} \left( |\square\!\!\square\rangle\langle\square\!\!\square| + |\square\!\!\square\rangle\langle\square\!\!\square| \right) - \left( |\square\!\!\square\rangle\langle\square\!\!\square| + |\square\!\!\square\rangle\langle\square\!\!\square| \right) \right]$$

model is its relation to the classical model at the point $v/t = 1$ of the parameter space, namely the so-called Rokhsar-Kivelson (RK) point. Specifically, the ground state of the wave-function at this RK point can be written as the partition function of the classical model

$$|\Psi_0\rangle_{\text{RK}} = \frac{1}{\sqrt{Q_0}} \sum_{\mathcal{C}} |\mathcal{C}\rangle, \tag{3.42}$$

[8] Of course the four corner *bcc*'s with dimension 1/32 are still present but do not play any role in dimer-dimer correlation functions.

[9] Let us notice that the fact that $x_b^{(d)} = x_s^{(d)}$ is a pure coincidence.

[10] A dimer in the corner is formed by two neighboring monomers with dimension $x_{c_+}^{(m)}$ and $x_{c_-}^{(m)}$.

where $\sum_{\mathcal{C}} |\mathcal{C}\rangle = Q_0$ the number of classical dimer covering of the lattice. Thus all informations about the ground state at the RK point comes directly from the knowledge of the partition function of the classical model, indeed all our analysis of the dimer model holds for the RK wave function as well. Let us mention that the full phase diagram outside the RK point is very rich and beyond the scope of the present discussion (see [156, 79] for reviews). As a step towards the understanding of the finite-temperature phase diagram of the quantum dimer model, we can mention the particular limit when kinetic terms goes to zero, which is a classical dimer model with an interaction that tends to align dimers on the same plaquette. In figure Fig. 3.15, we show a particular dimer

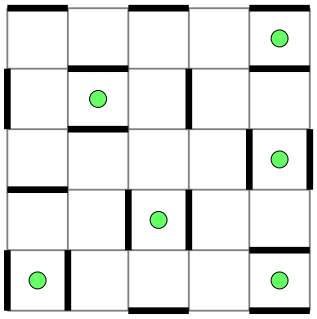

Figure 3.15: Dimer model with plaquette interaction

configuration with 6 aligning plaquettes, representing by the green dots. If we define the number of green dots by $\mathcal{N}$, then the partition function of this model can be written as a sum of dimer configurations $\mathcal{C}$ weighted by $\mathcal{N}$ *i.e.*

$$Z = \sum_{\mathcal{C}} \exp(-\beta\nu\mathcal{N}), \tag{3.43}$$

where $\nu > 0$ is the strength of the interaction. Other kind of interactions can be cooked up, for example on can create an anti-ferromagnet order choosing $\nu < 0$ or adding interaction that tends to align dimers along the same line in order to create a nematic order [167]. The dimer-dimer correlations which are critical in the non-interacting case are found to remain critical, but with continuously varying exponents, down to a finite temperature where the dimers order through a Kosterlitz-Thouless (KT) transition, we do not enter into all this details here and report the interested reader to [4, 3, 55]. We mention here that the height mapping remains valid for the interacting dimer model and it can be showed that, at the critical point, the interactions renormalize the free theory to another value of the stiffness constant $g$[11]. It has been shown that the renormalized value of the stiffness becomes $g_{\mathrm{KT}} = 2/\pi$ instead of $g_{\mathrm{free}} = 1/4\pi$ for the free case. The same analysis of corner contribution to free energy as well as scaling dimensions (bulk, surface, corner) can be studied in the interacting dimer model using the height mapping. For the corner contribution to the free energy term, just like the free case, the result depends only on the parity of the lattice and the analysis of the model with zero and one monomer can be studied. As an example, the corner free energy for the even-case lead, using Eq. (3.23) and Eq. (3.19) to $\mathcal{F}_{\mathrm{corner}} = 7/4 \log L$.

[11] In a more fancy language, we often read that the interaction deforms the compactification radius of the free boson.

## 3.4 Conclusions and perspectives

In this work the classical dimer model was discussed in great details both in a fermionic and bosonic field theory formulation. The bosonic formulation of the model is based on the so-called height mapping and it is well suited for phenomenological predictions about correlations between dimers and monomers in a Coulomb gas context. Then we presented a practical and complete fermionic solution of the $2d$ dimer model on the square lattice with an arbitrary number of monomers. Furthermore, the Tzeng-Wu solution of the dimer model with a boundary monomer was found to be included in our theory. Interpretations of finite size effects of the Tzeng-Wu solution in a CFT/Coulomb gas framework has been performed, and we showed that a careful examination of boundary conditions in the model allowed us to recover the central charge of the free fermion/free boson field theory. The exact expression of correlation functions between monomers has been written in terms of the product of two pfaffians, and we gave an explicit formula for boundary correlations valid for the four boundaries of the rectangle. This solution has been used to compute correlations for several configurations in order to extract bulk, surface and corner scaling dimensions for dimer and monomer operators. All these results were interpreted in the Coulomb gas formalism, and we showed that all the predictions of the CFT were in accordance with a $c = 1$ theory.

CHAPTER 4

# Field theory formulation of the arctic circle

## Contents

## 4.1 The Aztec diamond dimer model

### 4.1.1 Introduction and generalities

The *arctic circle* is the name given by Jockush, Propp & Shor to a phenomenon they discovered in 1995 [113] while studying dimer coverings of the Aztec diamond [63, 65]. The phenomenon consists in the appearance, in the thermodynamic limit, of a curve that separates two macroscopic domains, one in which the dimers appear to be frozen, meaning that one knows their exact position with a probability that goes quickly to one in the thermodynamic limit, and another domain where the dimers fluctuate. The same phenomenon was observed in other models [47], in particular in the six-vertex model with domain-wall boundary conditions [139, 166, 49, 50], a system that already possessed a long history connected to integrability and to the evaluation of the norm of Bethe states [140, 100, 101]. In fact, the phenomenon itself appears to have been known as early as 1977, in a different context though: the statistics of large Young tableaux [204]. Since the late 1990s, there has been an intense activity in this area, which lies at the frontier between physics, mathematics and computer science. Among the many results that were collected are the limiting distribution of dimers around the origin in the thermodynamic limit [46, 114], the fluctuations of the boundary described by the Airy process [114], a general theory for dimer models [128] and the calculation of the corresponding arctic curves in connection with algebraic geometry [129], calculations of various correlation functions [23, 162, 164], steps towards extension to interacting models [139, 50, 48] (*i.e.* models that cannot be mapped to free fermions; for example: the six-vertex model at $\Delta \neq 0$, or dimers with aligning interactions [4]), and numerical investigations (see [54] for example). This chapter is partially based on the following paper [6].

#### Aztec diamond

The Aztec diamond is defined as follows. Let us consider the diamond shaped subset containing $2n^2$ squares. This geometry is called the Aztec diamond and can be seen as a regular square lattice where the four corners are removed. Then one considers the set of random tilings with dominos of the Aztec diamond with uniform weight. Using a connection between domino tilings and the alternating-sign matrices, the number of dominos tilling $\mathrm{AD}(n)$ of the Aztec diamond of size $n$ has been computed [64, 65] and a surprising result appears

$$\boxed{\mathrm{AD}(n) = 2^{\frac{n(n+1)}{2}}.} \tag{4.1}$$

For large $n$ the Aztec diamond divides into five regions delimited by the arctic circle found originally by Cohn, Elkies, Noam and Propp [45]. Inside the arctic circle there is a disordered region of the tiling. Outside this boundary the tilings forms a completely regular brick wall pattern (*e.g.* Fig. 5.4). From a physics point of view, the bulk phase is a massless [1] phase and the four boundary phases are massive (with infinite mass) phases. Let us mention that generalization of the Aztec diamond to more complicated graph can be studied as well (see [28, 26] for example), the shape of the arctic curve, the partition function and some others correlation functions has been computed using a transfer matrix formalism very similar to the one we will use in the following sections.

[1] "Massless" is the field theory terminology, which is synonym to "gapless" in the condensed matter terminology, which is synonym to "disordered" in the statistical physics terminology...

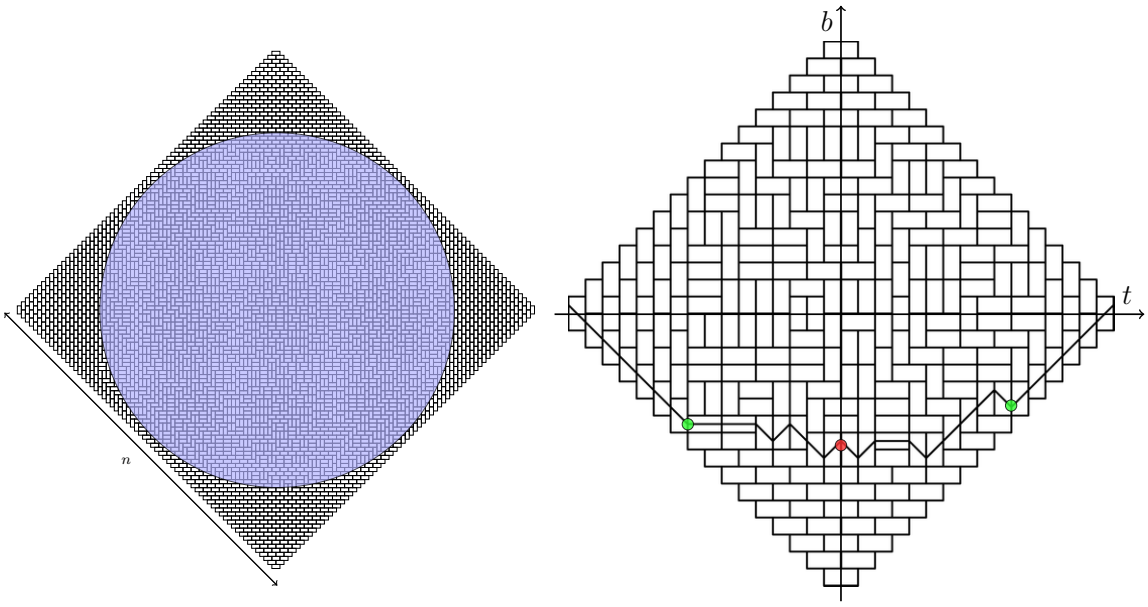


Figure 4.1: Left: Aztec diamond dimer covering. For sufficiently large sizes, a particular curve seems to separate a disordered (the temperate region) region from a frozen region (the arctic region). In this case, the curve can be showed to be a circle. Right: Every dimer configurations of the Aztec diamond can be mapped to configurations of non-intersecting paths, fluctuations of the central point (red dot). The south path (the one shown on the figure) is related to the GUE Tracy-Widom distribution [115]. In the case of fluctuations near the tangency points (green dots), another process arises: the GUE minor process [116]. See also **box 10**

**Box 10** (Relation to random matrix ensembles)**.**

It is possible to draw continuous lines in the Aztec diamond of order $n$ by adding in each domino a line pattern depending on its type as shown in Fig. 5.4. Let $t$ be the horizontal coordinate with $t = 0$ in the middle of the diamond and denote $b_{l,n}(t), l = 0, ..., n-1$ be the position of the $l^{th}$ line at time $t$. Then it is proven (see [115]) that, under proper rescaling the first line (see Fig. 5.4) of the set of non-intersecting $b_{0,n}(0)/n^{1/3} \to \zeta_2$ as $n \to \infty$ with $\zeta_2$ a random variable in the gaussian unitary ensemble (GUE) distribution. This model is closely related to the corner growth process for which fluctuations can be also computed and showed to be GUE as well. When the disordered region touches the boundaries (the tangency points) we expect that the GUE minor process should be the universal limit [116]. Random matrix connection has been found to appear in other limit shape phenomena, like in the 6-vertex model [51] or plane partitions [163, 164]. We will get back to boundary fluctuations later on in the fermionic transfer matrix formulation of the problem where the Airy kernel will show up using the exact expressions of correlators of fermions near the boundaries. We send the reader to one of the appendix of [6] for more details.

### 4.1.2 Height mapping and scalar field theory

In this paragraph, we shall use the same formulation of the dimer covering we have done before for the square geometry but for the Aztec diamond. Previously we claimed that the perfect matching of a graph $\mathcal{G}$ can be computed as the pfaffian of a matrix as long as the graph is planar. In the present case, we are dealing with the so-called Aztec diamond which can be think as a regular square lattice with some vertices removed. The Kasteleyn theorem can be applied for this lattice, exactly on the same way as for the usual square lattice and the Kasteleyn matrix can be written down explicitly without too much trouble. The main feature we want to explore in this chapter is the behavior of correlation in the scaling limit where the lattice spacing goes to zero. From a purely technical point a view, this task is rather complicated and the explicit form of the inverse Kasteleyn matrix was computed by Helfgott [91]. The formula is expressed in terms of Krawtchouk polynomials and a asymptotic analysis seems quite non-trivial.

#### Height field and main hypothesis

For this particular lattice, we can perform the same height mapping (see Fig. 4.2) as for the regular square lattice on the rectangle as we did in the previous chapter. By fixing the rescaled height

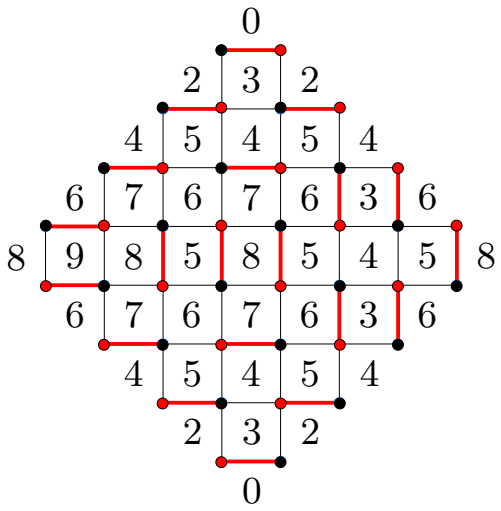


Figure 4.2: Aztec diamond dimer covering. Conversely to the rectangle geometry of the previous chapter, the boundary value of the height field is no more asymptotically flat but linear on each edge of the diamond. The machinery of boundary CFT fails to give any information about critical properties of the renormalized field theory.

at an arbitrary point, *e.g.* $h(0) = 0$ on the bottom plaquette, these rules define the entire height function $h(\vec{r})$ uniquely, exactly in the same way that for the regular square lattice we saw in the past chapter. The next step is the assumption that the fluctuation of the height field can still be described by a gaussian free field in the asymptotic limit. It has been conjectured by Propp, (see [180]), that in the limit $n \to \infty$, a random dimer tiling of the Aztec diamond looks like a

random dimer configuration of the usual plane under a certain measure. By integrating out the short distance fluctuations, one obtains an effective quadratic action $\mathcal{S}_0$ for the bulk height field $\phi(\vec{r}) = \frac{\pi}{2}h(\vec{r})$, defined in the continuum, which corresponds to the long-wavelength modes

$$\mathcal{S}_0[\phi] \propto \int \mathrm{d}^2x \; \eta^{\mu\nu}(\partial_\mu\phi)(\partial_\nu\phi), \tag{4.2}$$

where $\eta_{\mu\nu}$ is the flat metric. In the later case, we focused on the value of the height function at the boundaries and found out that the asymptotic value of the field $\phi_b$ tends to a constant that we can associate to a conformal boundary field.

**Box 11** (Conformal transformation of the metric in $d = 2$)**.**

For any metric on a two dimensional manifold, a particular coordinate system exists where the metric is conformally flat, *i.e.* the metric is the product of a scalar field (the conformal factor $\xi$ below), with a flat metric. The components of the metric in one coordinate system $(x, y)$ is related to metric in a second coordinate system $(w, z)$ by

$$\begin{aligned} g_{\mu\nu}\,\mathrm{d}x^\mu\,\mathrm{d}x^\nu &= g_{xx}\,\mathrm{d}x^2 + 2g_{xy}\,\mathrm{d}x\,\mathrm{d}y + g_{yy}\,\mathrm{d}y^2 \\ &= \xi(\mathrm{d}w^2 \pm \mathrm{d}z^2). \end{aligned}$$

Thus, we look for $w(x, y)$ and $z(x, y)$ such that $g^{wz} = 0$ and $g^{zz} \pm g^{ww} = 0$. After a tedious calculation one shows that the first equality is satisfied if

$$\begin{aligned} \partial_x w &= p\big(g^{xy}\partial_x z + g^{yy}\partial_y z\big) \\ \partial_y w &= -p\big(g^{xx}\partial_x z + g^{xy}\partial_y z\big), \end{aligned}$$

and to satisfy $g^{zz} \pm g^{ww} = 0$ we require that

$$\pm p^2 = \big(g^{xx}g^{yy} - (g^{xy})^2\big)^{-1} = \det g,$$

which gives $\partial_x w = \sqrt{g}g^{y\alpha}\partial_\alpha z$ and $\partial_y w = -\sqrt{g}g^{x\alpha}\partial_\alpha z$ which imply

$$\partial_y(\sqrt{g}g^{y\alpha}\partial_\alpha z) = -\partial_x(\sqrt{g}g^{x\alpha}\partial_\alpha z), \tag{4.3}$$

or $\nabla^\alpha\nabla_\alpha z = 0$. Thus any solution of the Laplace equation on the surface, in the original coordinates, provides a coordinate transformation to a metric of the form $g_{\mu\nu} = \xi(\mathrm{d}w^2 \pm \mathrm{d}z^2)$ with the conformal factor $\xi$ given $\xi^{-1} = \nabla^\alpha z\nabla_\alpha z$.

The hypothesis that the bulk field can be described by a free field plus the knowledge of boundary states allowed us to use the machinery of boundary CFT to get informations about the scaling limit of the field $\phi_b$. Here the things are rather different, indeed the bulk field can be shown to converge also towards a free field but the boundary value of the height field is no more asymptotically flat but linear on each edge. This boundary field does not map directly to a conformal boundary field because it is straightforward to show that the stress-energy tensor does not vanish on the boundaries. The simplest scenario would be that the action still describe the low energy fluctuating

degrees of freedom can be seen as a field-theory in a curved space-time where the flat metric is replace by a conformal metric $\eta_{\mu\nu} \to g_{\mu\nu} = \mathrm{e}^{2\sigma}\eta_{\mu\nu}$ (some basic notions of curved field theory in $2d$ are recall in the **box 11**). In this next few lines, one recall some simple notion of $2d$ geometry and quantum field theory that will be useful in the context of our theory. Let us consider a $2d$ manifold with a Riemann metric described by the metric tensor $g_{\mu\nu}(x)$ which is supposed positive[2] definite so that in any coordinate system $x = x^\mu$ the interval

$$\mathrm{d}x^2 = g_{\mu\nu}(x)\,\mathrm{d}x^\mu\,\mathrm{d}x^\nu, \tag{4.4}$$

is positive. The field theory is required to be generally covariant, *i.e.*, the action functional, which involves the metric $g$ as the functional parameter. Let us consider the scalar free case (with no gauge field) where the action $\mathcal{S}_0[\phi(x), g(x)]$ must be invariant in any coordinate systems and can be written in the following form

$$\boxed{\mathcal{S}_0[\phi(x), g(x)] = \frac{\kappa}{2}\int \mathrm{d}^2x\sqrt{g}(g^{\mu\nu}\partial_\mu\phi\partial_\nu\phi)} \tag{4.5}$$

where we have changed the notation for the stiffness constant from $g$ to $\kappa$ to avoid confusion with the metric. The stress-energy tensor can be defined as before as the variation of the action $\delta\mathcal{S}_0[\phi(x), g(x)]$ under a variation of the metric $\delta g_{\mu\nu}(x) \to g_{\mu\nu}(x) + \delta g_{\mu\nu}(x)$. In $2d$, things are considerably simpler, indeed any surface in two-dimension is conformally flat (see [60] for a survey and the **box 11** above for a short demonstration), it means that any $2d$ metric can be put in the form

$$g_{\mu\nu}(x) = \mathrm{e}^{2\sigma(x)}\eta_{\mu\nu}, \tag{4.6}$$

where $\eta_{\mu\nu}$ is the flat metric and $\sigma(x)$ is related to the scalar curvature as

$$\mathcal{R}(x) = -\mathrm{e}^{-2\sigma}\partial_\mu^2\sigma. \tag{4.7}$$

The consequence of this result is that, in $2d$ the curved metric can be, up to a local rescaling, turn to the flat metric. Let us notice that another parameter can vary in this theory, the gauge field $A_\mu$ associate with the $U(1)$ gauge invariance of Eq. (4.8). In that case the derivative will be replace by a covariant derivative $\partial_\mu \to \mathcal{D}_\mu = \partial_\mu - iA_\mu$. The scalar lagrangian we are looking for is then fully determined by two functions

- the conformal factor $\sigma(x)$ such that $g_{\mu\nu} = \mathrm{e}^{2\sigma}\eta_{\mu\nu}$,
- the gauge field $A_\mu$ such that $\to \mathcal{D}_\mu = \partial_\mu - iA_\mu$,

and the action describing the fluctuating field inside the arctic circle may be written in a fully covariant form as

$$\mathcal{S}_0[\phi] \propto \int \sqrt{g}\,\mathrm{d}^2x\; g^{\mu\nu}(\mathcal{D}_\mu\phi)(\mathcal{D}_\nu\phi). \tag{4.8}$$

A more thorough discussion of the bosonic field theory inside the arctic circle will be exposed elsewhere [6]. A possible way to check if that theory describes the large scale fluctuations inside

[2] and non-degenerate

the arctic circle would be to exploit some exact results for the inverse Kasteleyn on the Aztec diamond, and determine the asymptotic behavior of correlations anywhere inside the diamond. But as we said earlier, this task seems quite non-trivial and another approach will be used in the following. Although in the next chapter we will follow another strategy and sick for the fermionized theory describing this $c = 1$ field theory, *i.e.* the Dirac field in curved space. For the fermionic case (the Dirac action), it is a little bit more complicated because of the Dirac matrices which satisfy $\{\gamma_\mu, \gamma_\nu\} = 2g_{\mu\nu} = 2\mathrm{e}^{2\sigma(x)}\eta_{\mu\nu}$, which is no more conventional Clifford algebra. We shall see later that this complication can be dealt with using tetrads defined as $g^{\mu\nu} = e^\mu_a e^\nu_b \eta^{ab}$ will help express everything in the euclidian metric $\eta_{ab}$.

### 4.1.3 Transfer matrix formulation

In this section, the method introduced in chapter III is applied to the dimer model on the square lattice, where the arctic circle phenomenon has been originally discovered. We will consider the simplest version of the dimer model where the vertical and horizontal dimers have the same Boltzmann weight choose to unity. In that way, the computation of the partition function is nothing but counting the perfect matching number of the square graph. The fermionic transfer matrix is formulated and diagonalized. We consider a square lattice with periodic boundary conditions and an even number of columns $N$ and consider a staggered configuration. Consider now superposing a generic dimer configuration with the staggered configuration, the resulting superposition is shown in Fig. 4.3 and consists in a certain number of strings propagating in the vertical direction. The dynamic of these lines has the following properties

- The configurations of dimer fully determine by the configurations of strings.
- The number of strings is conserved *i.e.* the number of fermions is conserved, so that the transfer matrix is block-diagonal.
- When moving from one horizontal row to the next, a string can either go straight or jump exactly one site to the left or to the right.

These properties follow directly from the definition of the superposition and from the definition of a valid dimer covering. The properties of strings suggest to view dimer configurations as a discrete time evolution process, where the time increases along the vertical direction. In what follows it is convenient to refer to the horizontal (resp. vertical) direction as space (resp. time). The time evolution is then accomplished by the row-to-row transfer matrix $T$ which will be detailed below. We view the system as a set of fermionic particles on the lattice $\mathbb{Z} + 1/2$ that evolve in the $y$-direction, which is imaginary time. Here we write the transfer matrix for the dimer model on the square lattice. First, we are still dealing with fermionic particles on the lattice $\mathbb{Z} + \frac{1}{2}$, and with the initial and final states $|\psi_0\rangle$. The transfer matrix, however, is not invariant under translations of *one site*, but only of *two sites*. It is convenient to distinguish the two species of fermions associated to each sublattice

$$a_j^\dagger \equiv c^\dagger_{2j+\frac{1}{2}} \qquad\qquad b_j^\dagger \equiv c^\dagger_{2j-\frac{1}{2}}\,, \qquad j \in \mathbb{Z}\,. \tag{4.9}$$

and define the even $T_{\text{even}}$ transfer matrix as operators which act on the two fermions $a_j^\dagger$ and $b_j^\dagger$ as

$$\begin{aligned} T_{\text{even}}\; a_j^\dagger\; T_{\text{even}}^{-1} &= a_j^\dagger, \\ T_{\text{even}}\; b_j^\dagger\; T_{\text{even}}^{-1} &= a_{j-1}^\dagger + b_j^\dagger + a_j^\dagger. \end{aligned} \tag{4.10}$$

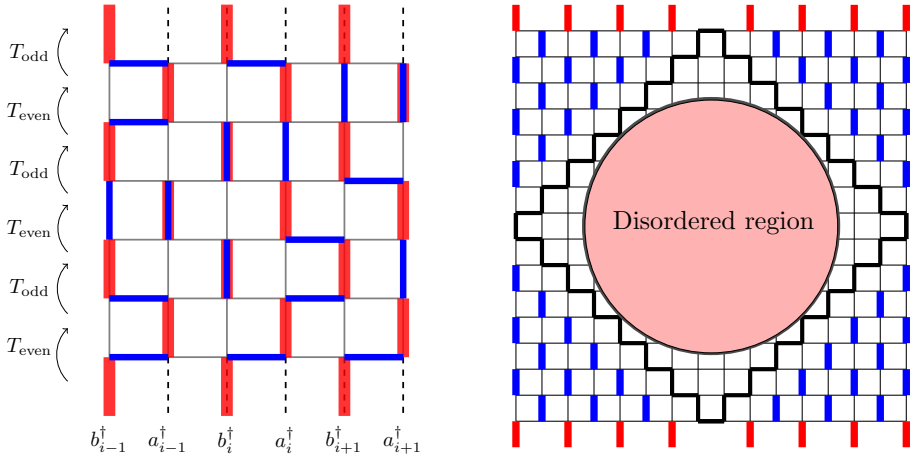


Figure 4.3: Left: We define the particle locations as the vertical edges that are not occupied by a real dimer only a reference one. Particles can jump from a vertical edge to another only if a real horizontal dimer connects the two. This superposition consists in a certain number of strings. It can go to the left, straight ahead, or to the right. In this setup. Right: The Aztec diamond can easily be generated by imposing a particular configuration of dimer at the bottom and bottom of the lattice (red dimers), in such way that this condition freezes every dimers in a certain region (blue dimers). In terms of fermion, the initial and final states $|\Psi_0\rangle$ are the so-called domain wall initial states that we will define precisely in the main text.

and the odd transfer matrix and odd $T_{\text{odd}}$ which act as

$$\begin{aligned} T_{\text{odd}}\; a_j^\dagger\; T_{\text{odd}}^{-1} &= b_{j+1}^\dagger + a_j^\dagger + b_j^\dagger, \\ T_{\text{odd}}\; b_j^\dagger\; T_{\text{odd}}^{-1} &= b_j^\dagger. \end{aligned} \tag{4.11}$$

The Fourier modes are defined as

$$a^\dagger(k) \;=\; \sum_{j\in\mathbb{Z}} e^{ikj}\, a^\dagger(j) \qquad b^\dagger(k) \;=\; \sum_{j\in\mathbb{Z}} e^{ikj}\, b^\dagger(j)\,, \qquad k\in[-\pi,\pi]\,, \tag{4.12}$$

in such way that the even and odd transfer matrices read in Fourier space

$$\begin{cases} T_{\text{even}} \begin{pmatrix} a^\dagger(k) \\ b^\dagger(k) \end{pmatrix} T_{\text{even}}^{-1} &= \begin{pmatrix} 1 & 0 \\ 1+e^{ik} & 1 \end{pmatrix} \begin{pmatrix} a^\dagger(k) \\ b^\dagger(k) \end{pmatrix} \\ T_{\text{odd}} \begin{pmatrix} a^\dagger(k) \\ b^\dagger(k) \end{pmatrix} T_{\text{odd}}^{-1} &= \begin{pmatrix} 1 & 1+e^{-ik} \\ 0 & 1 \end{pmatrix} \begin{pmatrix} a^\dagger(k) \\ b^\dagger(k) \end{pmatrix} \end{cases} \tag{4.13}$$

In terms of the fermions $a$ and $b$ the initial state $|\Psi_0\rangle$ can be defined as a state filled (empty) of fermions $b$ (of fermions $a$) on one side and empty (filled) on the right. Now, let us consider the

double-row transfer matrix $T^2 = T_{\text{even}} T_{\text{odd}}$,

$$T^2 \begin{pmatrix} a^\dagger(k) \\ b^\dagger(k) \end{pmatrix} T^{-2} = \begin{pmatrix} 1 & 2\mathrm{e}^{-ik/2}\cos\frac{k}{2} \\ 2\mathrm{e}^{ik/2}\cos\frac{k}{2} & 1+4\cos^2\frac{k}{2} \end{pmatrix} \begin{pmatrix} a^\dagger(k) \\ b^\dagger(k) \end{pmatrix}. \tag{4.14}$$

$T^2$ is hermitian, and it is easily diagonalized

$$\boxed{T^2 = \exp\left[-\int \frac{\mathrm{d}k}{2\pi} 2\varepsilon(k)\left(c_+^\dagger(k)c_+(k) - c_-^\dagger(k)c_-(k)\right)\right]} \tag{4.15}$$

with

$$\begin{pmatrix} c_+^\dagger(k) \\ c_-^\dagger(k) \end{pmatrix} = U(k) \begin{pmatrix} a^\dagger(k) \\ b^\dagger(k) \end{pmatrix} = \begin{pmatrix} \sin\alpha(k) & \mathrm{e}^{-ik/2}\cos\alpha(k) \\ \cos\alpha(k) & -\mathrm{e}^{-ik/2}\sin\alpha(k) \end{pmatrix} \begin{pmatrix} a^\dagger(k) \\ b^\dagger(k) \end{pmatrix} \tag{4.16}$$

and

$$\varepsilon(k) = -\log\lambda = -\mathrm{arcsinh}\left(\cos\frac{k}{2}\right) \tag{4.17}$$

$$\lambda(k) = \tan\alpha(k) = \sqrt{1+\cos^2\frac{k}{2}} - \cos\frac{k}{2}. \tag{4.18}$$

From this point of view, the analogy with $1d$ quantum spin chain is obvious. The double-row transfer matrix $T^2$ can be seen as the exponential of a quantum hamiltonian for the two kind of fermions $c_+$ and $c_-$. The two crucial ingredients (see Fig. 4.3) are now the free-fermion hamiltonian $H = -\log T^2$ and the DWIS $|\psi_0\rangle$ which can be defined in the basis $\{c_+, c_-\}$. In the next section, we shall see that the exact same analogy can be done for the 6-vertex model that we will interpreted as a $1d$ quantum problem with particular initial and final state.

## 4.2 Classical $2d$ systems and $1d$ quantum interpretation

In the past section we have seen how one can interpreted the arctic circle phenomenon in the dimer model in terms of the evolution of a $1d$ fermionic hamiltonian with particular initial and final states. The problem of computation of local observables in the arctic circle is equivalent to the computation of observables in the quantum quench protocol. Another typical model for which the phenomenon of arctic curve is very much studied is the 6-vertex model with domain wall boundary conditions (DWBC) [218], where some features has been computed exactly (see [9, 49, 50, 51] for details and references) for any value $\Delta$ of the model.

### 4.2.1 6-vertex model and DWBC

The 6-vertex model is defined in terms of local Boltzmann weights which live on the vertices of a general graph and is the prototypal model of an exactly solved model in statistical mechanics. For

a general introduction and solution of this solved model one can not avoid Baxter's book [17]. It is conventional to draw the vertices of the six-vertex model as


(4.19)

with weights $a, b, c \in \mathbb{R}$. The configurations of the six-vertex model are in one-to-one correspondence with (directed) self-avoiding trajectories on the square lattice as illustrated in Fig. 4.4.(c). The trajectories can touch—a situation that corresponds to the first vertex with weight $a$—, but they cannot overlap along an edge. By convention, we decide that the trajectories never cross. This is convenient, because then we do not have to be too careful about the statistics of the particles whose trajectories we are describing. We view the system as a set of fermionic particles on the lattice $\mathbb{Z} + \frac{1}{2}$ that evolve in the $y$-direction, which is imaginary time. The six vertices drawn above are then operators acting on two neighboring sites $x$ and $x+1$. They can be written respectively as

$$\begin{aligned}
\text{weight } a: &\quad \begin{cases} c_x^\dagger c_x \, c_{x+1}^\dagger c_{x+1} \\ (1 - c_x^\dagger c_x)\,(1 - c_{x+1}^\dagger c_{x+1}) \end{cases} \\
\text{weight } b: &\quad \begin{cases} c_x^\dagger c_{x+1} \\ c_{x+1}^\dagger c_x \end{cases} \\
\text{weight } c: &\quad \begin{cases} (1 - c_x^\dagger c_x) c_{x+1}^\dagger c_{x+1} \\ c_x^\dagger c_x (1 - c_{x+1}^\dagger c_{x+1})\,. \end{cases}
\end{aligned} \tag{4.20}$$

Summing these six terms, we build the $\mathcal{R}$-matrix of the six-vertex model,

$$\begin{aligned}
\mathcal{R}_{x,x+1} = {} & a \left[ c_x^\dagger c_x \, c_{x+1}^\dagger c_{x+1} + (1 - c_x^\dagger c_x)\,(1 - c_{x+1}^\dagger c_{x+1}) \right] \\
& + b \left[ c_x^\dagger c_{x+1} + c_{x+1}^\dagger c_x \right] \\
& + c \left[ c_x^\dagger c_x (1 - c_{x+1}^\dagger c_{x+1}) + (1 - c_x^\dagger c_x) c_{x+1}^\dagger c_{x+1} \right],
\end{aligned} \tag{4.21}$$

which can be written as

$$\mathcal{R}_{x,x+1} = a \exp\left[ \log\left( \frac{b+c}{a} \right) \left( c_x^\dagger c_{x+1} \, + \, c_{x+1}^\dagger c_x \right) \right],$$

provided that

$$\Delta \, = \, \frac{a^2 + b^2 - c^2}{2ab} \, = \, 0\,, \tag{4.22}$$

and this is what we assume from now on. Since the $\mathcal{R}$-matrix is gaussian at $\Delta = 0$, the model is free, the transfer matrix is gaussian as well, and all observables can be obtained from the propagator

using Wick's theorem. The techniques developed in previous parts apply, as we explain below. We focus once again on the DWIS $|\Psi_0\rangle$, which is completely filled with particles on the left, and completely empty on the right. The evolution of the system is generated by iterations the transfer matrix. After a number of iterations, we project the one-dimensional system of particles back to the DWIS (Fig. 4.4.(a)). Because of the initial and final states, most vertices on the left and right of the system are forced to be in the configurations with weight $a$ in (4.19), as illustrated in Fig. 4.4.(b). Only a central region, which turns out to be a square, is not determined *a priori* by those initial and final states. The square in the middle hosts configurations of the six-vertex model with boundary conditions (Fig. 4.4.(b)) that are known traditionally as "domain-wall boundary conditions". Therefore, our setup, which combines the DWIS with the transfer matrix, is well suited to revisit this popular problem.

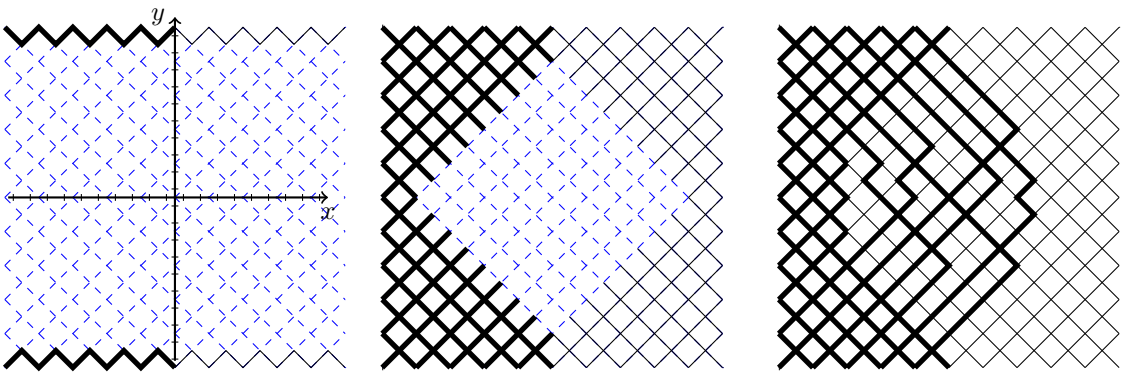


(a) (b) (c)

Figure 4.4: Six-vertex model on the square lattice. We regard the horizontal axis as space, and the vertical axis as imaginary time. (a) One starts form the domain-wall initial state (DWIS) at the bottom, then we apply the transfer matrix several times, and finally, we project back to the DWIS at the top. (b) Because of the DWIS, a large number of edges are constrained to be either empty or filled; the only vertices that are not fixed by the choice of boundary conditions are the ones inside the square region in the middle of the figure. This central square is what is known in the literature as the six-vertex model with domain-wall boundary conditions. (c) A configuration of vertices compatible with the boundary conditions: note that one can interpret the filled edges as trajectories in space-time. This is the idea of the mapping to a fermion model.

### 4.2.2 The transfer matrix

We need to define two transfer matrices, one for the even rows and another for the odd rows. Using the notations of the previous chapter, we call $a^\dagger, a$ the fermion creation/annihilation modes that

live on the the sublattice $2\mathbb{Z}+\frac{1}{2}$, and $b^\dagger, b$ the ones that live on $2\mathbb{Z}-\frac{1}{2}$. Then we write

$$\begin{cases} T_{ab} & \equiv & \displaystyle\prod_{x\in 2\mathbb{Z}+\frac{1}{2}} \mathcal{R}_{x,x+1} \\ T_{ba} & \equiv & \displaystyle\prod_{x\in 2\mathbb{Z}-\frac{1}{2}} \mathcal{R}_{x,x+1}\,. \end{cases} \tag{4.23}$$

Notice that the terms commute within each product; but, of course, $T_{ab}T_{ba} \neq T_{ba}T_{ab}$. The weighted configurations of the model are obtained by applying iteratively these two operators one after the other. One could then focus on one of the double-row transfer matrices $T_{ab}T_{ba}$ or $T_{ba}T_{ab}$, which

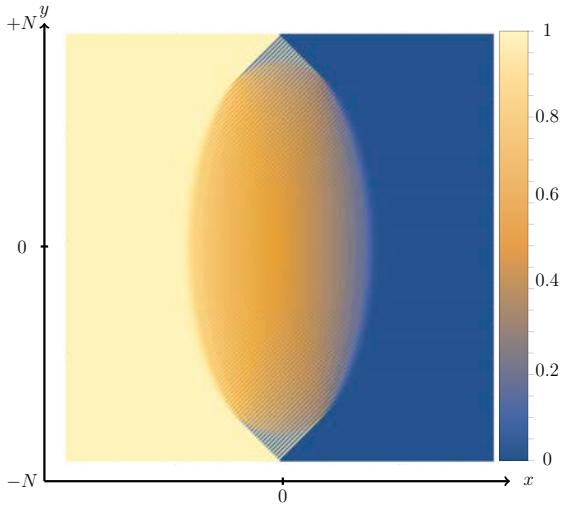


Figure 4.5: Numerical density snapshot for a system of size $2N = 400$, and for $b/a = 1/2$, $c/a = \sqrt{1+b^2}$, for general parameters satisfying the free fermion condition $a^2 + b^2 = c^2$ the arctic curve is an ellipse. The shape of the arctic curve as well as the partition function has been computed out of the free-fermion point in [139, 218]

generate the imaginary time evolution. However the drawback of both those operators is that they are not hermitian, it is more convenient for the following, to deal with a hermitian generator of translations in imaginary time. Thus, we define our (double-row) transfer matrix as the operator

$$T^2 \;=\; T_{ab}^{\frac{1}{2}}\, T_{ba}\, T_{ab}^{\frac{1}{2}} \tag{4.24}$$

whose hermiticity follows from $T_{ab}^\dagger = T_{ab}$ and $T_{ba}^\dagger = T_{ba}$. Again, the upper script/exponent in $T^2$ is there to remind us that it is an operator that adds *two rows* to the system, instead of one. We will always deal with $T^2$, there will be no object $T$. Now let's diagonalize $T^2$. In $k$-space, using the definition (4.12), the Fourier modes are

$$\begin{cases} T_{ab} & = & \exp\left[\log\left(\dfrac{b+c}{a}\right)\displaystyle\int\frac{\mathrm{d}k}{2\pi}\left(\mathrm{e}^{i\frac{k}{2}}\,a^\dagger(k)b(k) \;+\; \mathrm{e}^{-i\frac{k}{2}}\,b^\dagger(k)a(k)\right)\right] \\ T_{ba} & = & \exp\left[\log\left(\dfrac{b+c}{a}\right)\displaystyle\int\frac{\mathrm{d}k}{2\pi}\left(\mathrm{e}^{-i\frac{k}{2}}\,a^\dagger(k)b(k) \;+\; \mathrm{e}^{i\frac{k}{2}}\,b^\dagger(k)a(k)\right)\right]. \end{cases} \tag{4.25}$$

Then the problem boils down to the diagonalization[3] of a $2 \times 2$ matrix

$$T^2 = \exp\left[-\int_{-\pi}^{\pi} \frac{\mathrm{d}k}{2\pi}\, 2\varepsilon(k)\, \left(c_+^\dagger(k)c_+(k) - c_-^\dagger(k)c_-(k)\right)\right], \tag{4.26}$$

Once again, the transfer matrix $T^2$ Eq. (4.26) can be seen as the exponential of a $1d$ fermionic hamiltonian, and the arctic curve can be generate (see Fig. 4.5) using the initial and final states $|\Psi_0\rangle$. Having this in mind one wants now to generalize this quench protocol for a larger class of fermionic hamiltonian.

### 4.2.3 Fermionic chain with a generic dispersion relation

#### Single band models and quantum quench protocol

One may want to actually use a simpler model. Indeed both of these models are written of on hamiltonian with two bands in the dispersion relation (two kind of fermions), and the phenomenon of arctic curve can occurred in model with one band. For example, if one considers dimer model on the hexagonal lattice Fig. 4.6, the actual "hamiltonian" can be written (see [195]) as

$$H = \int_{\mathrm{BZ}} \frac{\mathrm{d}k}{2\pi}\, \epsilon(k)\, c^\dagger(k)c(k), \tag{4.27}$$

where the dispersion relation is $\epsilon(k) = -\log\left(1 + u^2 + 2u\cos k\right)$, where $u$ is the fugacity of the non-vertical dimers. This model will be related to a simple generalization of the XX chain that we will discussed in details in the next section. In that case, the arctic curve can be showed to be a ellipse shifted from the origin. The details of the study of this model is not presented here, and we send the reader to the incoming paper [6]. Our motivation for revisiting this ancient problem comes from the physics of quantum quenches in spin chains, and in particular their description by $2d$ CFT. This topic, launched by Calabrese & Cardy in 2006 [30], received a lot of attention in recent years [32, 31, 190, 189, 191, 82, 59, 193, 11, 12, 124, 147]. The usual quantum/classical correspondence tells us that, modulo Wick rotation, the real-time evolution of a one-dimensional quantum model is equivalent to a two-dimensional classical statistical model. In that setup, the initial state of the quantum system becomes a boundary condition in the classical model. Then the game is to chose the quantum system and the initial state such

- the bulk of the slab is described by a massless quantum field theory
- the boundary state $|\Psi_0\rangle$ renormalizes to a conformal boundary.

The second property is crucial and underlies most of the published works in that area. Fortunately, conformal boundary conditions are the rule rather than the exception: it is usually argued that, as soon as the correlations in the initial state are short range, the initial state corresponds to a conformal boundary condition in the thermodynamic limit. There, we introduce a quantum quench model which, we argue, may be regarded as a toy-model for arctic circle problems. The crucial ingredients are the $U(1)$-symmetry, or conservation of the number of particles, together with the

[3] Here and in what follows, we drop the unimportant normalization constant $a^{\text{number of sites}}$ that comes from the factor $a$ in the r.h.s of (4.21).

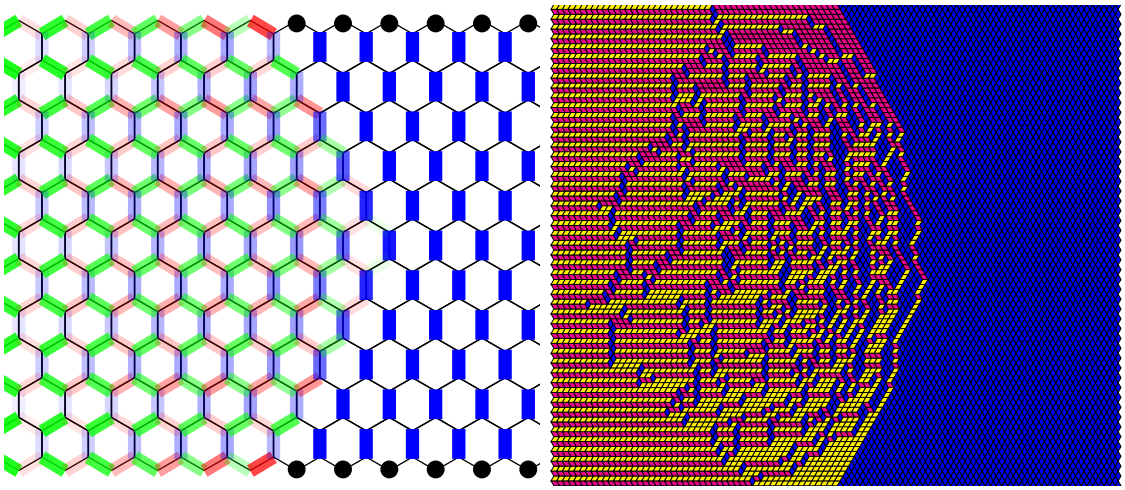

Figure 4.6: Left: slab geometry for dimers on the honeycomb lattice. The initial state $|\psi_0\rangle = \prod_{x<0} c_x^\dagger |0\rangle$ with fermions on the left corresponds in dimer language to the insertion of monomers (black dots) on the right ($x > 0$). The mean dimer occupancies are shown on all links, with the following color convention. Vertical dimers are in blue, and dimers on the left (right) side of each hexagon are shown in green (red). The shading is darker for larger probabilities, lighter for smaller ones, in such a way that zero densities do not appear. We are interested in the critical region in the middle, where all colors appear simultaneously. In the present picture the fugacity $u$ corresponding to the red links, is $u = 1/2$. Right: A dimer configuration drawn with lozenge, which may help visualize the height configuration. The arctic curve in that case in a shifted ellipse of equation $\left(\frac{1-u^2}{u}x + Ru\right)^2 + y^2 = R^2$.

*domain-wall initial state* (DWIS), see below and Fig. 5.5. Because of particle conservation, the standard argument about the initial state renormalizing to a conformal boundary condition *does not apply* (see also the discussion in [192]). This is in very sharp contrast with what happens, for instance, in the quantum Ising chain, which does not possess a $U(1)$ symmetry, and where the argument can be safely exploited [33].

**Toy model: the XX chain**

The model is a translation-invariant chain of free fermions living on lattice sites $x \in \mathbb{Z} + \frac{1}{2}$. The Hamiltonian is diagonal in $k$-space, with a single band and a dispersion relation $\varepsilon(k)$,

$$H = \int_{-\pi}^{\pi} \frac{\mathrm{d}k}{2\pi}\, \varepsilon(k)\, c^\dagger(k) c(k)\,. \tag{4.28}$$

The fermion creation/annihilation modes obey the canonical anti-commutation relations $\{c^\dagger(k), c(k')\} = 2\pi\,\delta(k-k')$ in $k$-space, or $\{c_x^\dagger, c_{x'}\} = \delta_{x,x'}$ in real space. Our convention for Fourier transforms is $c^\dagger(k) = \sum_{x\in\mathbb{Z}+\frac{1}{2}} e^{ikx} c_x^\dagger$; notice that $c^\dagger(k+2\pi) = -c^\dagger(k)$. For simplicity, we specialize to the case of nearest-neighbor hopping only, such that the dispersion relation may be

put in the form

$$\varepsilon(k) \;=\; -\cos k\,.$$

In other words, the Hamiltonian is the one of the XX chain, after the Jordan-Wigner transformation. We have normalized $\varepsilon(k)$ such that the maximal group velocity $v(k) = \frac{d}{dk}\varepsilon(k)$ is 1 (at $k = \frac{\pi}{2}$). We focus on the evolution of the fermions from a domain-wall initial state (DWIS), see

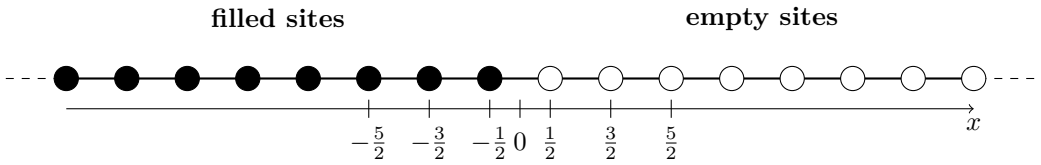


Figure 4.7: The toy-model is a chain of free fermions hopping on the lattice $x \in \mathbb{Z} + \frac{1}{2}$, evolving from the domain-wall initial state (DWIS), which is completely filled on the left, and completely empty on the right.

Fig. 5.5. The DWIS $|\Psi_0\rangle$ is completely filled on the left (density equal to one), and completely empty on the right (density equal to zero):

$$\rho(x)|\Psi_0\rangle \;=\; c_x^\dagger c_x|\Psi_0\rangle \;=\; \Theta(-x)|\Psi_0\rangle\,. \tag{4.29}$$

$\Theta$ is the Heaviside step function: $\Theta(-x) = 1$ if $x < 0$ and $\Theta(-x) = 0$ if $x > 0$. On top of this, $|\Psi_0\rangle$ is normalized: $\langle\Psi_0\,|\Psi_0\rangle = 1$. This completely determines $|\Psi_0\rangle$, up to an irrelevant phase factor. The main originality of the model, compared to previous work on the DWIS and the XX chain, is that we focus on imaginary-time evolution. We want to compute correlators $\langle\mathcal{O}_1(x_1, y_1)\ldots\mathcal{O}_n(x_1, y_1)\rangle$

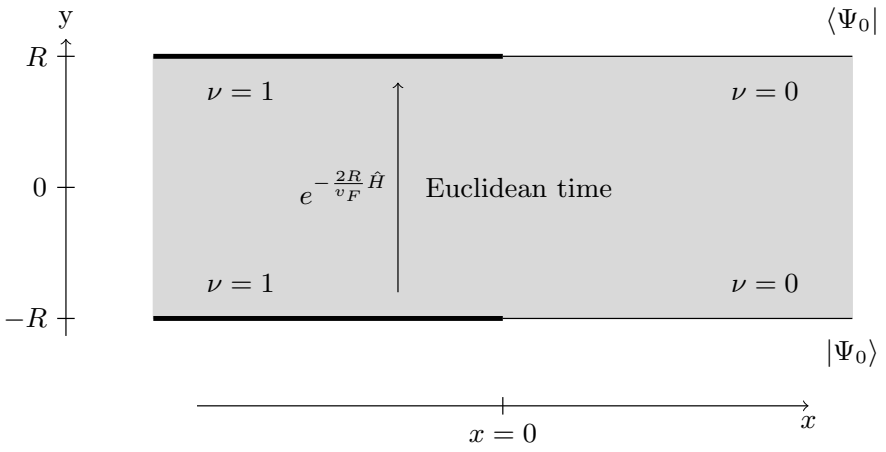


Figure 4.8: Imaginary time evolution of the initial state: one expects two frozen regions on the far left $\nu = 1$ and far right $\nu = 0$ of the system, because particles should have a finite velocity. There can be fluctuations only in the region around the origin, where some of the particles have hopped from left to right.

of local observables $\mathcal{O}(x,y)$, defined as the (imaginary-)time-ordered expectation values

$$\frac{\langle\Psi_0|\mathrm{e}^{-2R\,H}\,\mathcal{T}\left[\left(\mathrm{e}^{(R+y_1)H}\mathcal{O}_1(x_1)\mathrm{e}^{-(R+y_1)H}\right)\ldots\left(\mathrm{e}^{(R+y_n)H}\mathcal{O}_n(x_n)\mathrm{e}^{-(R+y_n)H}\right)\right]|\Psi_0\rangle}{Z},$$

where $\mathcal{T}\,[.]$ stands for time-ordering [4] and $Z$ is the partition function of the model

$$Z\;=\;\langle\Psi_0|\mathrm{e}^{-2R\,H}|\Psi_0\rangle\,,$$

such that $\langle 1\rangle = 1$. The constant $R>0$ is a parameter that sets the effective size of the system. Indeed, although the chain is infinite in the $x$-direction, it has a width $2R$ in the (imaginary-time) $y-$direction. We have the following cartoon in mind (see Fig. 5.6). One starts from the initial state $|\Psi_0\rangle$ at imaginary time $y=-R$ and one lets the system evolve freely up to imaginary time $y=+R$, where it is conditioned to come back to the initial state $|\Psi_0\rangle$. At imaginary time $y=-R$ the degrees of freedom are frozen for any $x$, because all the sites are occupied on the left and empty on the right, so all correlations are trivial. Then the particles are released and can hop between left and right. So, as soon as $y>-R$, a small region around $x=0$ must appear, where the average density is between 0 and 1. In that region, there are density fluctuations, with non-trivial correlations. At $y=+R$, the system is conditioned to come back to its initial state, so we expect the fluctuating region to shrink back to a point as $y$ increases and approaches $+R$. In fact, it is easy to see that the model is symmetric under $y\to -y$, so the fluctuating region is reflection-invariant across the horizontal axis. Our model possesses the same phenomenology as the *arctic circle* problem in its original formulation for dimer models [113]. The connection with dimers, and with other models, will be developed further in the next pages. As can be seen in Fig. 5.7, in

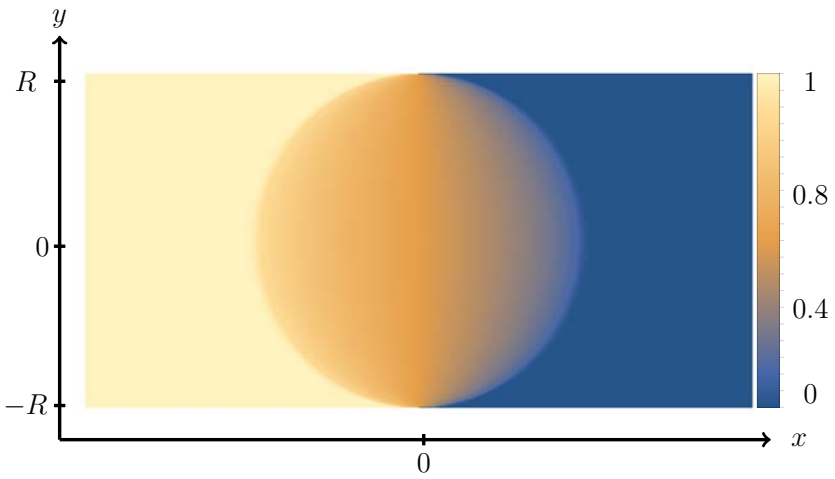


Figure 4.9: Numerical simulation of the density $\rho$ of the toy-model for $2R=512$: one sees two frozen regions on the far left with $\rho=1$ and far right of the system with $\rho=0$, because particles should have a finite velocity. There can be fluctuations only in the region around the origin, where some of the particles have hopped from left to right. In that case the arctic region is a circle of radius $R$.

[4] the factors must appear from left to right with decreasing values of $y$

the scaling limit $R \to \infty$, the exact shape of the fluctuating region is a disc of radius $R$ centered at the origin. Let us be more precise about what we mean by *scaling limit* here and in the rest of the paper. We are interested in expectation values and correlation of observables of the form $\langle \mathcal{O}_1(x_1, y_1) \dots \mathcal{O}_n(x_n, y_n) \rangle$ in the *scaling limit*

$$x_j/R \quad \text{and} \quad y_j/R \quad \text{fixed for any } j\,, \qquad \text{and} \quad R \to \infty\,. \tag{4.30}$$

In this limit, the density inside the arctic circle takes a very simple form, interpolating from $\langle \rho \rangle = 1$ on the left to $\langle \rho \rangle = 0$ on the right

$$(x^2 + y^2 < R^2) \qquad \langle \rho(x, y) \rangle \;=\; \frac{1}{\pi} \arccos \frac{x}{\sqrt{R^2 - y^2}}\,.$$

This formula for the density was already know for the real-time evolution [10], we will give a demonstration of this result using a different approach later on.

**Dirac field theory hypothesis**

The main focus of this work, however, is neither on the shape of the critically fluctuating region, nor on the density profile inside it. As we said before, the main question here is the form of field theory inside the critical region where the correlation are massless. Such correlations must be describable by a euclidean quantum field theory with a local action. The theory inside the disc, on the contrary, is non-trivial in the scaling limit; our goal is to find out what it is. In fact, it is rather easy to guess what the field theory should be. Since we are dealing with a quadratic Hamiltonian for fermionic particles, we are looking for a free fermion theory. Moreover, a key aspect of the model is particle conservation, meaning that it is invariant under $U(1)$ transformations $c^\dagger \to e^{i\varphi} c^\dagger$, $c \to e^{-i\varphi} c$. The field theory must inherit this symmetry from the lattice model. So, there is not much choice. It has to be a massless Dirac theory in two dimensions. The basic object in any such theory is the two-component Dirac spinor,

$$\Psi = \begin{pmatrix} \psi \\ \overline{\psi} \end{pmatrix} \tag{4.31}$$

$$\Psi^\dagger = \begin{pmatrix} \psi^\dagger & \overline{\psi}^\dagger \end{pmatrix}. \tag{4.32}$$

We pick our conventions for the euclidean gamma matrices as $\gamma^1 = -\sigma^2$ and $\gamma^2 = \sigma^1$ [5], such that $\gamma^5 = i\gamma^2\gamma^1 = \sigma^3$ is diagonal; we refer to $\psi$ and $\overline{\psi}$ as the chiral and anti-chiral components.

[5] the $\sigma^j$'s are the Pauli matrices

**Box 12** (Spinors in $d = 2$ curved space)**.**

For the fermionic case (the Dirac action), it is a little bit more complicated because of the Dirac matrices which satisfy $\{\gamma^\mu, \gamma^\nu\} = 2g^{\mu\nu} = 2\mathrm{e}^{2\sigma(x)}\eta_{\mu\nu}$, which is not the conventional Clifford algebra. We shall see later that this complication can be dealt with using tetrads defined as $g^{\mu\nu} = e^\mu_a e^\nu_b \eta^{ab}$ will help express everything in the Euclidian metric $\eta_{ab}$. The action for the Dirac field with no gauge field is

$$\mathcal{S}_0 = \frac{1}{2\pi}\int \sqrt{g}\,\mathrm{d}^2x\gamma^a e^\mu_a \overline{\Psi}\left(\partial_\mu + \frac{1}{2}i\omega^{bc}_\mu \sigma_{bc}\right)\Psi\,. \tag{4.33}$$

where the *Dirac adjoint* $\overline{\Psi}$ is $\Psi^\dagger\gamma^2$. The convention for the euclidean gamma matrices is $\gamma^1 = -\sigma^2$ and $\gamma^2 = \sigma^1$, such that $\gamma^5 = i\gamma^2\gamma^1 = \sigma^3$ is diagonal. The spin connection is given by

$$\omega^{ab}_\mu = e^\nu_a \partial_\mu e^{\nu b} + e^\mu_a \Gamma^\nu_{\mu\rho} e^{\rho b}, \tag{4.34}$$

where $\Gamma^\nu_{\mu\rho}$ is the affine connection

$$\Gamma^l_{jk} = \frac{1}{2}g^{lr}\big(\partial_k g_{rj} + \partial_j g_{rk} - \partial_r g_{jk}\big), \tag{4.35}$$

and $\sigma_{ab} = \frac{i}{4}[\gamma_a, \gamma_b]$ are the spinor representation of the Lorentz group. One subtlety of the curved Dirac field is the necessity to make the lagrangian hermitian [a]. In order to do that, we follow [157] and put the action in the following form (adding the hermitian conjugate to the lagrangian)

$$\mathcal{S}_0 = \frac{1}{2\pi}\int \sqrt{g}\,\mathrm{d}^2x e^\mu_a \overline{\Psi}\left(\gamma^a \overleftrightarrow{\partial_\mu} + \frac{1}{2}i\omega^{bc}_\mu\{\gamma^a, \sigma_{bc}\}\right)\Psi\,. \tag{4.36}$$

In $2d$ the only generator is $\sigma_{12} = \gamma_1\gamma_2$ which commutes with the two Dirac matrices, then $\{\gamma^a, \sigma_{bc}\} = 0$, which means that the spin connection drops out from the Dirac action and the most general form is

$$\mathcal{S}_0 = \frac{1}{2\pi}\int \sqrt{g}\,\mathrm{d}^2x e^\mu_a \overline{\Psi}\left(\gamma^a \overleftrightarrow{\partial_\mu}\Psi\right)\,. \tag{4.37}$$

In the main text, we shall use this Dirac action with the addition of gauge fields coming from the invariance of the action under the chiral group $U_V(1) \times U_A(1)$, which will be encoded in a covariant derivative $\partial_\mu \to \mathcal{D}_\mu$.

[a] which is always the case in a flat background up to a total derivative.

The latter are the local fields in the continuous theory. At a given point, one must be able to express the lattice degrees of freedom in terms of the continuous fields. Such relations hold in the sense that lattice correlators are equal, in the scaling limit, to field theory correlators of carefully chosen fields at the same point. There is always some freedom in the choice of the relation between

the lattice and the continuous degrees of freedom, because local perturbations may be absorbed either in this relation, or in the action, in the form of perturbations by irrelevant operators. Here, what we want to do is to fix this relation once and for all, and then work out the action of the theory. The lattice mode $c_x^\dagger(y)$ must be a linear combination of $\psi^\dagger$ and $\overline{\psi}^\dagger$, so let us fix

$$\begin{cases} c_x^\dagger(y) &= \dfrac{1}{\sqrt{2\pi}}\,\psi^\dagger(x,y) \,+\, \dfrac{1}{\sqrt{2\pi}}\,\overline{\psi}^\dagger(x,y) \\ c_x(y) &= \dfrac{1}{\sqrt{2\pi}}\,\psi(x,y) \,+\, \dfrac{1}{\sqrt{2\pi}}\,\overline{\psi}(x,y)\,. \end{cases} \tag{4.38}$$

The normalization factors $1/\sqrt{2\pi}$ are introduced for later convenience; global phase factors may always be absorbed in the definition of the continuous fields. The point is that we chose the expression of the lattice degree of freedom in terms of the continuous fields such that it is the same everywhere, there are no position-dependent phase or scale factors. The question is now: what is the action? The system is clearly not homogeneous so there is no reason for the field theory to be homogeneous. Therefore, we are looking for some massless Dirac action in which the parameters vary with position. As we said before in the context of the height field, we assume that the parameter which control this non-homogeneity is the metric. After all, it makes sense that the metric of a field theory describing a non-homogeneous system could vary (see the **box 12** for some details on Dirac in curved space). Also, there might be some background gauge potentials, indeed the Dirac lagrangian is invariant under the chiral group $U_V(1) \times U_A(1)$

$$\Psi' = \mathrm{e}^{i\alpha_V}\,\Psi \tag{4.39}$$

$$\Psi' = \mathrm{e}^{i\alpha_A\gamma^5}\,\Psi, \tag{4.40}$$

where $\alpha_A, \alpha_V \in \mathbb{R}$. Thus, we are led to contemplate the Dirac action in fully covariant form, allowing the possibility of both vector (v) and axial (a) background gauge fields

$$\boxed{\mathcal{S}_0 \,=\, \frac{1}{2\pi}\int \sqrt{g}\,\mathrm{d}^2x\, e_a^\mu \frac{1}{2}\left[\overline{\Psi}\overset{\leftrightarrow}{\mathcal{D}}_\mu\gamma^a\Psi\right]} \tag{4.41}$$

where the covariant derivative is defined as

$$\overset{\leftrightarrow}{\mathcal{D}}_\mu = \overset{\leftrightarrow}{\partial}_\mu + 2i(A_\mu^{(\mathrm{v})} + A_\mu^{(\mathrm{a})}\gamma^5). \tag{4.42}$$

Here, the *Dirac adjoint* $\overline{\Psi}$ is $\Psi^\dagger\gamma^2$, $e_a^\mu(x)$ is the tetrad, and $\mathrm{d}^2x\sqrt{g} = \mathrm{d}^2x|e|^{-1}$ is the volume element. This action (5.23) is *a priori* the most general [6] possibility for the field theory describing the long-range correlations inside the critically fluctuating region. The goal is now to properly identify the tetrads and the background gauge potentials in our toy-model. Before we proceed to this identification, let us stress the important difference between the vector and the axial potentials: the $U(1)$-symmetry of the lattice model (*i.e.* particle number conservation) is a genuine symmetry. These $U(1)$ gauge transformations act on the vector part, not the axial one. Physical observables must be gauge-invariant. In fact, as we will see, both the vector and axial parts are pure gauge:

$$\begin{aligned} A_\mu^{(\mathrm{v})} &= \partial_\mu f \\ A_\mu^{(\mathrm{a})} &= \partial_\mu g, \end{aligned}$$

[6] The spin connection drops out of the two-dimensional Dirac action as seen in **box 12**

for some functions $f$ and $g$, so the vector part can simply be gauged away, and $A_\mu^{(\mathrm{v})}$ can really be dropped. It can never appear in physical observables. The situation is different for the axial part, as *it does not correspond to a symmetry of the model*. There is no axial symmetry on the lattice; it happens to be a symmetry of the continuous Dirac Lagrangian, but it is well-known that the symmetry is anomal ( *i.e.* not preserved by quantification). Physical observables must not depend on $A_\mu^{(\mathrm{v})}$, but they can depend on $A_\mu^{(\mathrm{a})}$. The Dirac lagrangian we are looking for is then fully determine by three functions

- the conformal factor $\sigma(x, y)$ such that $g_{\mu\nu} = \mathrm{e}^{2\sigma}\eta_{\mu\nu}$,
- the gauge fields $A_\mu^{(\mathrm{v})}$ and $A_\mu^{(\mathrm{a})}$.

In the next section we proposed a general formalism to compute the explicit form of these three functions in the particular case of the XX chain. The same analysis can also performed for more complicated models as the 6-vertex model and dimer models.

## 4.3 Arctic field theory

We are interested in the propagator inside the slab. The first step is to compute this propagator in momentum space for the $x$ coordinate and real space for the $y$ coordinate (see again the Fig. 5.6 for the definition of the coordinates $x$ and $y$). However, we are not able to compute directly this propagator for a real position $y$, and we start with a position $y = -R$. After having express correlations exactly on the lattice we shall compute asymptotics in the particular scaling limit $x/R,\ y/R,\ x'/R,\ y'/R$ fixed and $a/R \to 0$, the aim will be to found construct the continuum field theory starting from the knowledge of the asymptotic correlations.

### 4.3.1 Exact correlation functions

In this part, we compute exactly the propagator inside the strip. The result involves the Hilbert transform of the dispersion relation $\varepsilon(k)$, which comes from the DWIS. Indeed, the DWIS acts as a projector onto the negative real axis in real-space, which, when Fourier transformed, gives the Hilbert transform. We derive this key formula in full details in the case of a single band. Not surprisingly, the main technical tool in this section is Wick's theorem; we use it in a relatively non-standard bosonized form though, which considerably simplifies the calculations. This bosonization trick will not be needed in the rest of the paper, only the results are, and the latter will be recalled when needed. This subsection is devoted to the calculation of the propagator in $k$-space for the one-band Hamiltonian (5.17). Let us recall that this propagator is defined as

$$\left\langle c^\dagger(k,y)c(k',y')\right\rangle \equiv \begin{cases} \dfrac{\langle\Psi_0|\mathrm{e}^{-(R-y)H}c^\dagger(k)\mathrm{e}^{-(y-y')H}c(k')\mathrm{e}^{-(R+y')H}|\Psi_0\rangle}{\langle\Psi_0|e^{-2R\,H}|\Psi_0\rangle} & \text{if } (y>y') \\ -\dfrac{\langle\Psi_0|\mathrm{e}^{-(R-y')\,H}c(k)\mathrm{e}^{-(y'-y)H}c^\dagger(k')\mathrm{e}^{-(R+y)\,H}|\Psi_0\rangle}{\langle\Psi_0|\mathrm{e}^{-2R\,H}|\Psi_0\rangle} & \text{if } (y<y')\,. \end{cases}$$

We are going to show that

$$\boxed{\left\langle c^\dagger(k,y)c(k',y')\right\rangle \;=\; \frac{\mathrm{e}^{y\varepsilon(k)-iR\tilde{\varepsilon}(k)}\mathrm{e}^{-y'\varepsilon(k')+iR\tilde{\varepsilon}(k')}}{2i\sin\left(\frac{k-k'}{2}-i0\right)}} \tag{4.43}$$

where $\tilde{\varepsilon}(k)$ is the Hilbert transform (see **Box 13**) of the dispersion relation $\varepsilon(k)$. The formula (4.43) is quite remarkable, and it completely solves the toy-model, as we explained in the introduction. It also solves the dimer model on the honeycomb lattice as we defined it in the past section.

**Box 13** (Some properties of the circular Hibert transfom)**.**

The circular Hilbert transform $\tilde{f}(k)$ of a $2\pi$-periodic function $f(k)$ is defined by the convolution of $f(k)$ with the Hilbert kernel $\cot\left(\frac{k-k'}{2}\right)$

$$\tilde{f}(k) \;=\; \text{p.v.}\int_{-\pi}^{\pi}\frac{\mathrm{d}k'}{2\pi}f(k')\,\cot\left(\frac{k-k'}{2}\right). \tag{4.44}$$

A nice property that will be used in the study of the XX chain, is that the Hilbert transform of $\sin(k)$ is $-\cos(k)$ and the Hilbert transform of $\cos(k)$ is $\sin(k)$.

To prove this formula, we proceed as follows. First, we note that, since

$$\begin{cases} c^\dagger(k,y) &=& \mathrm{e}^{yH}c^\dagger(k)\mathrm{e}^{-yH} &=& \mathrm{e}^{y\varepsilon(k)}c^\dagger(k) \\ c(k',y') &=& \mathrm{e}^{y'H}c(k')\mathrm{e}^{-y'H} &=& \mathrm{e}^{-y'\varepsilon(k)}c(k')\,, \end{cases}$$

the $y$- and $y'$-dependence of (4.43) is trivial. Instead, what we really need to show is

$$\left\langle c^\dagger(k,0)c(k',0)\right\rangle \;=\; \frac{\mathrm{e}^{-iR\left[\tilde{\varepsilon}(k)-\tilde{\varepsilon}(k')\right]}}{2i\sin\left(\frac{k-k'}{2}-i0\right)}\,. \tag{4.45}$$

We introduce the normal order $:\,.\,:$ adapted to our initial state $|\Psi_0\rangle$, namely

$$:c_x^\dagger c_x: \;\equiv\; \begin{cases} c_x^\dagger c_x & \text{if} \quad x>0 \\ -c_x c_x^\dagger & \text{if} \quad x<0\,, \end{cases}$$

such that

$$\begin{aligned} :c^\dagger(k)c(k'): \;&= c^\dagger(k)c(k') - \langle\Psi_0|c^\dagger(k)c(k')|\Psi_0\rangle \\ &= c^\dagger(k)c(k') - \frac{1}{2i\sin\left(\frac{k-k'}{2}-i0\right)}. \end{aligned} \tag{4.46}$$

It is probably possible to get to formula (4.43) using Wick's theorem for fermions directly, but we haven't been able to do so. So, instead, we chose to use standard bosonization formulas that make the various computational steps much lighter. For this purpose, we introduce a (real) free

bosonic field $\varphi(k)$, and we bosonize the fermion creation/annihilation operators, as well as the Hamiltonian, according to the rules

$$\text{(bosonization)} \qquad \begin{cases} c^\dagger(k) & \to & :\mathrm{e}^{i\varphi(k)}: \\ c(k) & \to & :\mathrm{e}^{-i\varphi(k)}: \\ \int \frac{\mathrm{d}k}{2\pi}\varepsilon(k)\, c^\dagger(k)c(k) & \to & \int \frac{\mathrm{d}k}{2\pi}\varepsilon(k)\,\partial\varphi(k)\,. \end{cases} \tag{4.47}$$

The propagator of the bosonic field is chosen as

$$\langle\Psi_0|\varphi(k-i\epsilon)\varphi(k')|\Psi_0\rangle \;=\; -\log\left[2i\sin\left(\frac{k-i\epsilon-k'}{2}\right)\right]. \tag{4.48}$$

such that $\langle\Psi_0|:\mathrm{e}^{i\varphi(k-i\epsilon)}::\mathrm{e}^{-i\varphi(k')}:|\Psi_0\rangle \;=\; \langle\Psi_0|c^\dagger(k)c(k')|\Psi_0\rangle$ when $\epsilon\to 0^+$. When computing correlators or commutators, one needs to carefully regularize the bosonic expressions. This is done by adding some small imaginary part to the argument $k$, which is larger, or smaller, depending on the order of appearance of the operators in the different expressions.

**Box 14** (Example using bosonization)**.**

An instructive example consists in recovering the commutator $\big[H, c^\dagger(k)\big] \;=\; \varepsilon(k)\, c^\dagger(k)$ in bosonized form:

$$\begin{aligned}
\big[H, c^\dagger(k)\big] \;&\to\; \lim_{\epsilon\to 0^+}\int\frac{\mathrm{d}q}{2\pi}\varepsilon(q)\Big(\partial\varphi(q-i\epsilon)\;:\mathrm{e}^{i\varphi(k)}:\;-\;:\mathrm{e}^{i\varphi(k)}:\;\partial\varphi(q+i\epsilon)\Big) \\
&=\; \lim_{\epsilon\to 0^+}\int\frac{\mathrm{d}q}{2\pi}i\varepsilon(q)\partial_q\left(\langle\Psi_0|\varphi(q-i\epsilon)\varphi(k)|\Psi_0\rangle - \langle\Psi_0|\varphi(k)\varphi(q+i\epsilon)|\Psi_0\rangle\right):\mathrm{e}^{i\varphi(k)}: \\
&=\; \lim_{\epsilon\to 0^+}\int\frac{\mathrm{d}q}{2\pi}\varepsilon(q)\left(-\frac{i}{2}\cot\left(\frac{q-i\epsilon-k}{2}\right)\;+\;\frac{i}{2}\cot\left(\frac{q+i\epsilon-k}{2}\right)\right):\mathrm{e}^{i\varphi(k)}: \\
&=\; \int\frac{\mathrm{d}q}{2\pi}\varepsilon(q)\,2\pi\delta(q-k)\;:\mathrm{e}^{i\varphi(k)}:\;=\;\varepsilon(k)\;:\mathrm{e}^{i\varphi(k)}:,
\end{aligned}$$

which is the expected result. In the first line, we used the bosonization formulas (4.47), introducing the regulator $\varepsilon>0$ according to the respective position of the two operators; in the second line we applied Wick's theorem; in the third line we used the bosonic propagator (4.48); in the last line we used

$$\lim_{\epsilon\to 0^+}\cot\left(\frac{k-k'\pm i\epsilon}{2}\right) \;=\; \mp i2\pi\,\delta(k-k') \;+\; \text{p.v.}\left[\cot\left(\frac{k-k'}{2}\right)\right]. \tag{4.49}$$

With these bosonization tricks at hand, it is a relatively pleasant exercise to prove formula (4.45). Indeed, the quantity that we need to evaluate becomes

$$\begin{aligned}
&\frac{\langle\Psi_0|\mathrm{e}^{-RH}c^\dagger(k)c(k')\mathrm{e}^{-RH}|\Psi_0\rangle}{\langle\Psi_0|\mathrm{e}^{-2RH}|\Psi_0\rangle} \\
&\to\; \frac{\langle\Psi_0|:\mathrm{e}^{-R\int\frac{\mathrm{d}q}{2\pi}\varepsilon(q)\,\partial\varphi(q-2i\epsilon)}::e^{i\varphi(k-i\epsilon)}::\mathrm{e}^{-i\varphi(k')}::e^{-R\int\frac{\mathrm{d}q'}{2\pi}\varepsilon(q')\,\partial\varphi(q'+i\epsilon)}:|\Psi_0\rangle}{\langle\Psi_0|:\mathrm{e}^{-R\int\frac{\mathrm{d}q}{2\pi}\varepsilon(q)\,\partial\varphi(q)}::\mathrm{e}^{-R\int\frac{\mathrm{d}q'}{2\pi}\varepsilon(q')\,\partial\varphi(q')}:|\Psi_0\rangle},
\end{aligned} \tag{4.50}$$

and we may compute this by applying the fusion formula for vertex operators

$$:\mathrm{e}^{\alpha\varphi(k)}::\mathrm{e}^{\beta\varphi(k')}:\;=\;\mathrm{e}^{\alpha\beta\langle\Psi_0|\varphi(k)\varphi(k')|\Psi_0\rangle}\;:\mathrm{e}^{\alpha\varphi(k)+\beta\varphi(k')}:$$

which follows from Wick's theorem. In (4.50), we start by fusing the two central vertex operators that come from $c^\dagger(k)$ and $c(k')$. This gives

$$\langle\Psi_0|c^\dagger(k)c(k')|\Psi_0\rangle\;\times\;\frac{\langle\Psi_0|:\mathrm{e}^{-R\int\frac{\mathrm{d}q}{2\pi}\varepsilon(q)\,\partial\varphi(q-2i\epsilon)}::\mathrm{e}^{i\varphi(k-i\epsilon)-i\varphi(k')}::\mathrm{e}^{-R\int\frac{\mathrm{d}q'}{2\pi}\varepsilon(q')\,\partial\varphi(q'+i\epsilon)}:|\Psi_0\rangle}{\langle\Psi_0|:\mathrm{e}^{-R\int\frac{\mathrm{d}q}{2\pi}\varepsilon(q)\,\partial\varphi(q)}::\mathrm{e}^{-R\int\frac{\mathrm{d}q'}{2\pi}\varepsilon(q')\,\partial\varphi(q')}:|\Psi_0\rangle}.$$

Next, we fuse the vertex operator involving the integral over $q$ with the one involving the integral over $q'$, both in the numerator and in the denominator. Clearly, the scalar factor that comes out of the fusion is the same in both cases, so it cancels when we take the ratio, and we do not need to evaluate it. The denominator is then the expectation value of a single normal-ordered exponential, which is one by definition. Thus, we are left with

$$\langle\Psi_0|c^\dagger(k)c(k')|\Psi_0\rangle\;\times\;\langle\Psi_0|:\mathrm{e}^{-R\int\frac{\mathrm{d}q}{2\pi}\varepsilon(q)\,\partial\varphi(q-2i\epsilon)-R\int\frac{\mathrm{d}q'}{2\pi}\varepsilon(q')\,\partial\varphi(q'+i\epsilon)}::\mathrm{e}^{i\varphi(k-i\epsilon)-i\varphi(k')}:|\Psi_0\rangle.$$

We use the fusion formula one last time to get

$$\begin{aligned}\langle\Psi_0|c^\dagger(k)c(k')|\Psi_0\rangle\;\times\;\mathrm{e}^{-R\int\frac{\mathrm{d}q}{2\pi}\varepsilon(q)\,i\partial_q\langle\Psi_0|\varphi(q-2i\epsilon)\varphi(k-i\epsilon)|\Psi_0\rangle-R\int\frac{\mathrm{d}q'}{2\pi}\varepsilon(q')\,i\partial_{q'}\langle\Psi_0|\varphi(q'+i\epsilon)\varphi(k-i\epsilon)|\Psi_0\rangle}\\ \times\mathrm{e}^{R\int\frac{\mathrm{d}q}{2\pi}\varepsilon(q)i\partial_q\langle\Psi_0|\varphi(q-2i\epsilon)\varphi(k')|\Psi_0\rangle+R\int\frac{\mathrm{d}q'}{2\pi}\varepsilon(q')\,i\partial_{q'}\langle\Psi_0|\varphi(q'+i\epsilon)\varphi(k')|\Psi_0\rangle}.\end{aligned}$$

Finally, we plug in the explicit form of the bosonic propagator (4.48),

$$\begin{aligned}\langle\Psi_0|c^\dagger(k)c(k')|\Psi_0\rangle\;\times\;\mathrm{e}^{iR\int\frac{\mathrm{d}q}{2\pi}\varepsilon(q)\left(\frac{1}{2}\cot\left(\frac{q-k-i\epsilon}{2}\right)+\frac{1}{2}\cot\left(\frac{q-k+2i\epsilon}{2}\right)\right)}\\ \times\,\mathrm{e}^{-iR\int\frac{\mathrm{d}q}{2\pi}\varepsilon(q)\left(\frac{1}{2}\cot\left(\frac{q-k'-2i\epsilon}{2}\right)+\frac{1}{2}\cot\left(\frac{q-k'+i\epsilon}{2}\right)\right)},\end{aligned}$$

and we take the limit $\epsilon\to0^+$, using (4.49). The integrals in the exponentials become the principal value that appears in the definition of the Hilbert transform (see **Box 13**). We arrive at

$$\frac{\langle\Psi_0|\mathrm{e}^{-RH}c^\dagger(k)c(k')\mathrm{e}^{-RH}|\Psi_0\rangle}{\langle\Psi_0|\mathrm{e}^{-2RH}|\Psi_0\rangle}\;=\;\mathrm{e}^{-iR\left[\tilde\varepsilon(k)-\tilde\varepsilon(k')\right]}\;\langle\Psi_0|c^\dagger(k)c(k')|\Psi_0\rangle.$$

as claimed above. This formula will be used in the next section to extract asymptotic behavior of fermion correlators inside the arctic circle in order to give us informations about the field theory governing the large scale fluctuations. The formula Eq. (4.43) can also be helpful to study correlations near the boundaries, and the results discussed in the beginning of the chapter can be recover.

### 4.3.2 Long-range correlations

The parameters in the action would be easily obtained if we knew the long-range behavior of fermionic correlators $\left\langle c^\dagger_{x_1}(y_1)\dots c^\dagger_{x_n}(y_n)c_{x'_1}(y'_1)\dots c_{x'_n}(y'_n)\right\rangle$ in the strip of width $2R$. As we show

in the previous section, these correlators can be computed exactly. They turn out to be directly related to the correlators in the DWIS, through a rather simple linear transformation,

$$\begin{aligned}\left\langle c^\dagger_{x_1}(y_1)\dots c^\dagger_{x_n}(y_n)c_{x'_1}(y'_1)\dots c_{x'_n}(y'_n)\right\rangle \;=\; & \int\prod_j \frac{\mathrm{d}k_j}{2\pi}\mathrm{e}^{-ik_jx_j+y_j\varepsilon(k_j)-iR\tilde\varepsilon(k_j)} \\ & \times\int\prod_p \frac{\mathrm{d}k'_p}{2\pi}\mathrm{e}^{ik'_px'_p-y'_p\varepsilon(k'_p)+iR\tilde\varepsilon(k'_p)} \qquad (4.52)\\ & \times\langle\Psi_0|c^\dagger(k_1)\dots c^\dagger(k_n)c(k'_1)\dots c(k'_n)|\Psi_0\rangle\,. \qquad (4.53)\end{aligned}$$

Here $\tilde\varepsilon(k)$ is the *Hilbert transform* of the dispersion relation $\varepsilon(k)$. For $\varepsilon(k)=-\cos k$, this is simply $\tilde\varepsilon(k)=-\sin k$. Of course, since we are dealing with a free fermion model, Eq. (4.52) requires a proof only for $n=1$. For later purposes, notice that the propagator in the DWIS appearing in the r.h.s is

$$\langle\Psi_0|c^\dagger(k)c(k')|\Psi_0\rangle \;=\; \sum_{x\in\mathbb{Z}+\frac12}\mathrm{e}^{i(k-k')x}\Theta(-x) \;=\; \frac{1}{2i\sin\left(\frac{k-k'}{2}-i0\right)}\,. \qquad (4.54)$$

The formula (4.52) and the role played by $\tilde\varepsilon(k)$ are a key aspect of this work. Let us notice that the same kind of formula can be obtained for dimers and 6-vertex model. First we introduce some useful piece of notation

$$\begin{cases} c^\dagger_x(y) \;\doteq\; \displaystyle\int_{-\pi}^{\pi}\frac{\mathrm{d}k}{2\pi}\mathrm{e}^{-ikx+y\varepsilon(k)-iR\tilde\varepsilon(k)}c^\dagger(k) \\[2ex] c_x(y) \;\doteq\; \displaystyle\int_{-\pi}^{\pi}\frac{\mathrm{d}k}{2\pi}\mathrm{e}^{ikx-y\varepsilon(k)+iR\tilde\varepsilon(k)}c(k), \end{cases} \qquad (4.55)$$

where we use the symbol $\doteq$ to emphasize that the relation must be understood in the sense of Eq. (4.52). It is *not an equality between operators*. Instead, it holds inside correlators, the l.h.s being inserted inside the bracket $\langle.\rangle$, and the r.h.s between $\langle\Psi_0|$ and $|\Psi_0\rangle$. Eq. (4.55) is really nothing more than the equality (4.52), but it is written in a more compact way. Next, we observe that the scaling limit (5.19) of the correlators may be obtained with the steepest descent method. In the relations (4.55), the contour of integration over $k$ may be deformed such that it passes through the points where the phase is stationary; these are the solutions of

$$\frac{x}{R}+i\frac{y}{R}\frac{\mathrm{d}\varepsilon(k)}{\mathrm{d}k}+\frac{\mathrm{d}\tilde\varepsilon(k)}{\mathrm{d}k} \;=\; \frac1R\frac{\mathrm{d}}{\mathrm{d}k}\left[kx+iy\varepsilon(k)-R\tilde\varepsilon(k)\right] \;=\; 0\,.$$

For $\varepsilon(k)=-\cos k$ and $\tilde\varepsilon(k)=-\sin k$, this is a quadratic equation in $e^{ik}$, which is solved straightforwardly. As long as $x^2+y^2<R^2$, there are two simple roots: $k=z(x,y)$ and $k=-z^*(x,y)$, where $z^*$ is the complex conjugate of $z$, with

$$z \;=\; z(x,y) \;\equiv\; \arccos\frac{x}{\sqrt{R^2-y^2}} \;-\; i\,\mathrm{arcth}\,\frac{y}{R}\,.$$

The integral over $k$ is then evaluated by the stationary phase approximation around these points: we approximate the argument of the exponential by

$$\begin{cases} \mathrm{e}^{-ikx+y\varepsilon(k)-iR\tilde\varepsilon(k)} \;\simeq\; \mathrm{e}^{-i\varphi-\frac{i}{2}(k-z)^2\,\mathrm{e}^{\sigma}} & \text{around}\quad k=z \\ \mathrm{e}^{-ikx+y\varepsilon(k)-iR\tilde\varepsilon(k)} \;\simeq\; \mathrm{e}^{i\varphi^*+\frac{i}{2}(k+z^*)^2\,\mathrm{e}^{\sigma}} & \text{around}\quad k=-z^*\,, \end{cases}$$

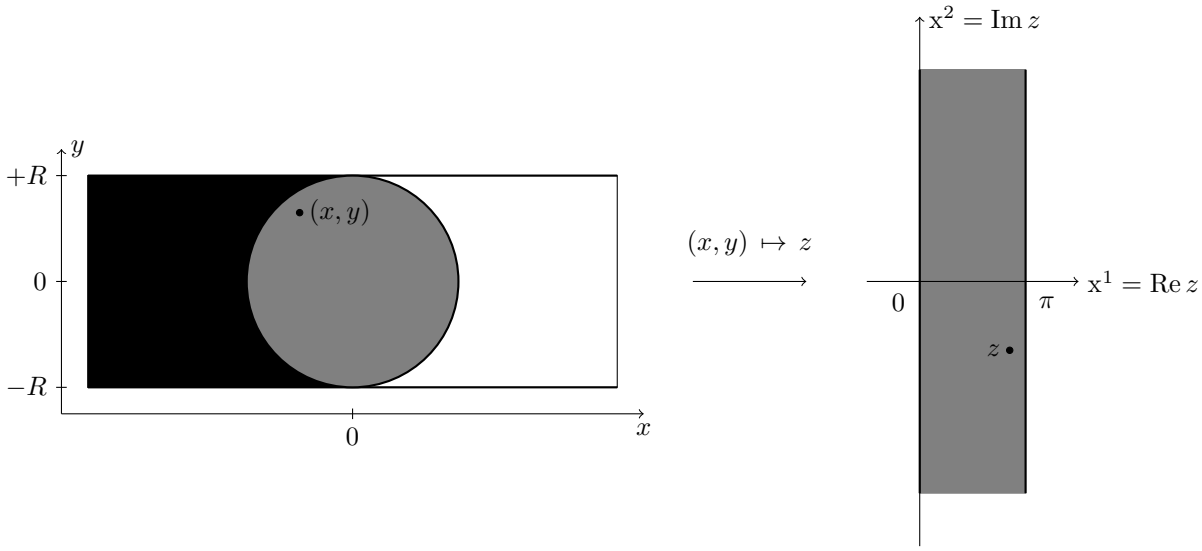


Figure 4.10: The critically fluctuating region $x^2 + y^2 < R^2$ is mapped to an infinite strip of width $\pi$ by $z(x, y)$. The boundary of the circle is mapped into the two edges of the strip, the left edge corresponds to $x > 0$ and the right edge to $x < 0$. The north and south poles are mapped at infinity.

where we have defined

$$\varphi = \varphi(x,y) \equiv z(x,y)x + iy\varepsilon(z(x,y)) + R\tilde{\varepsilon}(z(x,y)) = z(x,y)x - \sqrt{R^2 - x^2 - y^2}, \tag{4.56}$$

$$e^{\sigma} = e^{\sigma(x,y)} \equiv iy\frac{\mathrm{d}^2\varepsilon}{\mathrm{d}k^2}(z(x,y)) + R\frac{\mathrm{d}^2\tilde{\varepsilon}}{\mathrm{d}k^2}(z(x,y)) = \sqrt{R^2 - x^2 - y^2}. \tag{4.57}$$

Finally, one performs the integral in (4.55), which is now gaussian; it yields the asymptotic formulas

$$\begin{cases} c_x^\dagger(y) \underset{R\to\infty}{\doteq} \dfrac{\mathrm{e}^{-i\varphi(x,y)-i\frac{\pi}{4}}}{\sqrt{2\pi}}\mathrm{e}^{-\frac{1}{2}\sigma(x,y)}c^\dagger(z) + \dfrac{\mathrm{e}^{i\varphi^*(x,y)+i\frac{\pi}{4}}}{\sqrt{2\pi}}\mathrm{e}^{-\frac{1}{2}\sigma(x,y)}c^\dagger(-z^*) \\ c_x(y) \underset{R\to\infty}{\doteq} \dfrac{\mathrm{e}^{i\varphi(x,y)+i\frac{\pi}{4}}}{\sqrt{2\pi}}\mathrm{e}^{-\frac{1}{2}\sigma(x,y)}c(z) + \dfrac{\mathrm{e}^{-i\varphi^*(x,y)-i\frac{\pi}{4}}}{\sqrt{2\pi}}\mathrm{e}^{-\frac{1}{2}\sigma(x,y)}c(-z^*)\,. \end{cases} \tag{4.58}$$

What exactly do we mean by $c^\dagger(z)$, $c(z)$ here, when $z \notin \mathbb{R}$? Again, these relations must be understood in the sense of Eqs. (4.52)-(4.55): the correlator of fermions in the l.h.s of (4.58) are equal to expressions that involve $\langle\Psi_0|c^\dagger(z)c(z')|\Psi_0\rangle = 1/(2i\sin\frac{z-z'}{2})$, the analytic continuation of (4.54).

### 4.3.3 Dirac field theory in curved space

Now let us come back to Eqs. (5.20)-(5.23) and to the discussion around them. The resemblance with Eq. (4.58) is striking, and clearly suggests that the continuous field $\psi^\dagger$ is, roughly speaking,

nothing but $e^{-i\varphi - i\frac{\pi}{4}} e^{-\frac{1}{2}\sigma} c^\dagger$ (and similar relations for $\psi$, $\overline{\psi}^\dagger$ and $\overline{\psi}$). It is then very easy to extract the parameters of the Dirac action in the toy-model. One simple way of doing this is to match the local behaviors of the lattice and continuous propagators. The behavior of the lattice propagator follows from Eqs. (4.58), which give its scaling limit in the form of a sum of four terms. When $(x', y')$ approaches $(x, y)$, it is dominated by only two of the terms, that diverge as

$$\left\langle c_x^\dagger(y) c_{x'}(y') \right\rangle \simeq \frac{\mathrm{e}^{-\frac{\sigma+\sigma'}{2}}}{2\pi i} \left( \frac{\mathrm{e}^{-i(\varphi-\varphi')}}{z-z'} - \frac{\mathrm{e}^{i(\varphi^*-\varphi'^*)}}{z^*-z'^*} \right). \tag{4.59}$$

Looking back at Eq. (5.20), one sees that the propagator of the continuous fields must have the local behavior

$$\left\langle \psi^\dagger(x,y)\psi(x',y') \right\rangle \simeq \mathrm{e}^{-\frac{\sigma+\sigma'}{2}} \frac{\mathrm{e}^{-i(\varphi-\varphi')}}{i(z-z')} \qquad \left\langle \overline{\psi}^\dagger(x,y)\overline{\psi}(x',y') \right\rangle \simeq \mathrm{e}^{-\frac{\sigma+\sigma'}{2}} \frac{\mathrm{e}^{i(\varphi^*-\varphi'^*)}}{-i(z^*-z'^*)},$$

implying that they are Green's functions for the following operators,

$$\begin{aligned} \mathrm{e}^{\sigma} \left( i\partial_{\bar{z}} + \frac{i}{2}(\partial_{\bar{z}}\sigma) - (\partial_{\bar{z}}\varphi) \right) \left\langle \psi^\dagger(z,\bar{z})\psi(z',\bar{z}') \right\rangle &= \pi\, \delta^{(2)}(z-z') \\ \mathrm{e}^{\sigma} \left( -i\partial_{z} - \frac{i}{2}(\partial_{z}\sigma) - (\partial_{z}\varphi^*) \right) \left\langle \overline{\psi}^\dagger(z,\bar{z})\overline{\psi}(z,\bar{z}') \right\rangle &= \pi\, \delta^{(2)}(z-z'). \end{aligned}$$

We view the latter as arising from the action

$$\mathcal{S}_0 = \frac{1}{\pi} \int \mathrm{d}^2 z\ \mathrm{e}^{\sigma} \Psi^\dagger \hat{G} \Psi, \tag{4.60}$$

where

$$\hat{G} = \begin{pmatrix} -\frac{i}{2} \overset{\leftrightarrow}{\partial}_{\bar{z}} - (\partial_{\bar{z}}\varphi) & 0 \\ 0 & \frac{i}{2} \overset{\leftrightarrow}{\partial}_{z} - (\partial_{z}\varphi^*) \end{pmatrix}. \tag{4.61}$$

This, as anticipated in the discussion above, is a particular case of the generic Dirac action (5.23). To match the two expressions, one needs to write (5.23) in the coordinate system provided by the map $(x, y) \mapsto z(x, y)$,

$$\begin{cases} \mathrm{x}^1 + i\,\mathrm{x}^2 &= z(x,y) \\ \mathrm{x}^1 - i\,\mathrm{x}^2 &= z^*(x,y), \end{cases}$$

where $0 < \mathrm{x}^1 < \pi$ and $\mathrm{x}^2 \in \mathbb{R}$ (Fig. 4.10). The tetrad in (5.23) must be taken as the diagonal matrix

$$e^{\mu}{}_{a} = \mathrm{e}^{-\sigma} \delta^{\mu}{}_{a}, \tag{4.62}$$

so the corresponding metric is

$$\mathrm{d}s^2 = \mathrm{e}^{2\sigma}[(\mathrm{dx}^1)^2 + (\mathrm{dx}^2)^2]. \tag{4.63}$$

In other words, what the map $(x, y) \mapsto z(x, y)$ does for us is that it provides isothermal coordinates, for free. In the isothermal coordinate system above, $\sigma = \log(R \sin(\mathrm{x}^1)/\cosh(\mathrm{x}^2))$, which gives the following scalar curvature

$$\mathcal{R} = -\mathrm{e}^{2\sigma}\partial_\mu^2\sigma = \frac{\sin^2(\mathrm{x}^1) + \cosh^2(\mathrm{x}^2)}{R^2 \sin^4(\mathrm{x}^1)}. \tag{4.64}$$

The background gauge potentials are readily identified as

$$A_\mu^{(\mathrm{v})} \;=\; -i\partial_\mu \mathrm{Im}\varphi \qquad\qquad A_\mu^{(\mathrm{a})} \;=\; -\partial_\mu \mathrm{Re}\varphi\,. \tag{4.65}$$

They are both pure gauge. It may look problematic that $A_\mu^{(\mathrm{v})}$ is imaginary, but again, it can never appear in physical observables, which must be gauge invariant. The axial potential, on the other hand, does appear in physical quantities. One example is the density: it may be obtained from Eq. (4.59) by taking $y' = y$ first, and then $x' \to x$:

$$\langle \rho(x,y)\rangle \;=\; -\frac{\mathrm{e}^{-\sigma}}{\pi}\frac{\partial_x \mathrm{Re}\varphi}{\partial_x z} \;=\; \frac{1}{\pi}\frac{A_x^{(\mathrm{a})}}{\mathrm{e}^{\sigma}\partial_x z}\,.$$

Plugging the formulas for $z$, $\varphi$ and $\sigma$, one finds $\langle\rho\rangle = \frac{1}{\pi}\arccos\frac{x}{\sqrt{R^2-y^2}}$ as claimed above. The details of the boundary conditions for the field theory are not discussed here and can be found in [6].

**Summary**

We defined a two-dimensional toy-model that displays an *arctic circle*, it is discrete in one direction (space coordinate $x$) and continuous in the other direction (imaginary-time coordinate $y$). It was argued, on general grounds, that the long-range correlations inside the fluctuating region should be described by a massless Dirac theory.

- Independently of these field theory considerations, we exhibited an exact formula for the lattice fermion propagator $\left\langle c_x^\dagger(y) c_{x'}(y')\right\rangle$.
- The *scaling limit* of this propagator was analyzed with the stationary phase approximation. We found that the stationary points are the solution of a quadratic equation. If one solution is called $z$, the other is $-z^*$. The mapping $(x,y) \mapsto z$ is a diffeomorphism that sends the interior of the 'arctic circle' to a certain subset of $\mathbb{C}$ (here, an infinite strip), so it can be used as a coordinate system. Moreover, in the analysis of the stationary points, two other functions $\sigma$ and $\varphi$ show up naturally.
- Trying to match the local asymptotic behavior of the lattice fermion propagator with the one coming from the generic Dirac action (5.23), we were able to fix the free parameters in this action, namely the tetrad and the background gauge potentials. It turns out that the coordinate system provided by $(x,y) \mapsto z$ is isothermal, with a conformal factor given by $e^\sigma$, and that the gauge potentials are given by the real- and imaginary-part of $\partial_\mu\varphi$.

The point we wish to emphasize in this summary is that, if one is willing to describe the fluctuating region by a field theory, then the theory must be *inhomogeneous*, in the sense that, once a constant relation between the lattice and the continuous degrees of freedom is fixed (such as Eq. (5.20) above), then the parameters in the action vary with position. Since the components of the metric themselves are such parameters, it is natural that one ends up with a theory in curved euclidean space. The same picture remains valid for the honeycomb dimer model without no additional complication and for the square lattice dimer model and 6-vertex where the formalism has to be slightly modified to take into account the "two-bands" effects that we discussed in the previous section. The details of these models could be found in [6].

## 4.4 Conclusions

In conclusions, we have shown that the conjecture announced in the beginning of the chapter can be actually checked out for free-fermionic case where the exact calculations of correlation functions on the lattice can be done explicitly. The phenomenon known as arctic circle for the dimer model seems very general and the transfer matrix formalism ables us to tackle a large class of statistical or quantum systems where these phenomena show up. In all the cases discussed here, the final result of the scaling limit of the underlying action lead to an Dirac action with a non-flat metric. The details of the explicit form metric will depend on the specific parameters of the model, *i.e.* the dispersion relation. We have not discussed in details the case of model with two-bands like 6-vertex and dimer models but the picture is essentially the same (see [6] for details). A lot of perspectives can be imagine, but probably the most interesting question would be to figure out if this non-flat action appears in interacting model like the XXZ chain as well. There, the natural conjecture is that the continuous theory is a gaussian free field, but this time with a stiffness that depends on position as well. The reason is that, as is well-known, the density fluctuations of one-dimensional quantum systems with conserved particle number can always be described by a scalar field theory which is gaussian up to irrelevant perturbations. These systems are known as Luttinger liquids, and they are all described by a free boson action, with (at least) two free parameters: the velocity $v$ of the low-energy excitations, and the Luttinger parameter $K$, related to the stiffness of the gaussian free field. The variation of the velocity with position in space-time is, in the language of this paper, equivalent to the variation of the metric: $\mathrm{d}s^2 \sim v(x,t)^2\,\mathrm{d}t^2 - \mathrm{d}x^2$. We also believe that some of the ideas exposed here will be useful to tackle other problems involving inhomogeneous systems, including inhomogeneous quantum quenches, particles trapped by inhomogeneous potentials as well as closely related random matrix questions. Another possible extension of the present work, not quite as ambitious as trading the XX chain for the XXZ one, is to look at free fermion models with more bands and with energy gaps. This is achieved by increasing the size of the unit cell in the model, namely by breaking the symmetry group of translations $\mathbb{Z}$ to a subgroup $n\mathbb{Z}$. This is a particularly simple realization of a situation with three phases, a phenomenon already studied by [160, 129], and also revisited recently in [40, 57]. This phenomenon appears to be quite generic when one starts from a quantum $1d$ system that is gapped; this is the case for free fermion cases, as the previous references illustrate, but also when the gap is due to interactions [9] rather than to broken translation symmetry.

CHAPTER 5

# Résumé en français de la partie I

## Propriétés critiques des modèles de dimères

Suite à la solution de Onsager du modèle d'Ising à deux dimensions dans les années quarantes, l'introduction de l'Ansatz de Bethe et l'étude systématique des matrices de transferts, le domaine des solutions exactes de modèles bidimensionnels de physique statistique a explosé conduisant à la naissance d'un nouveau champs de la physique théorique et mathématique connu sous le nom de modèles exactement solubles. La rencontre de ce nouveau domaine avec la théorie des champs conformes initiée par Belavin, Polyakov et Zamolodchikov eu un impact énorme en physique théorique, des hautes énergies à la matière condensée. Dans les prochaines pages, un résumé de quelques résultats de la première partie de cette thèse sont détaillées .

### Le modèle de dimères

Dans ce paragraphe, nous allons commencer par définir le modele de dimères sur un graphe arbitraire. Un graphe $\mathcal{G}$ est définit par par un ensemble de noeuds $V$ et liens $E$. On définit la matrice adjacente $A = (A_{ij})$, où l'entrée $ij$ est associée une paire de noeuds, $(v_i, v_i)$, alors $A_{ij} = 1$ si $v_i$ et $v_j$ sont liés par un lien et 0 sinon. Le nombre d'appariement parfait est le nombre de configuration

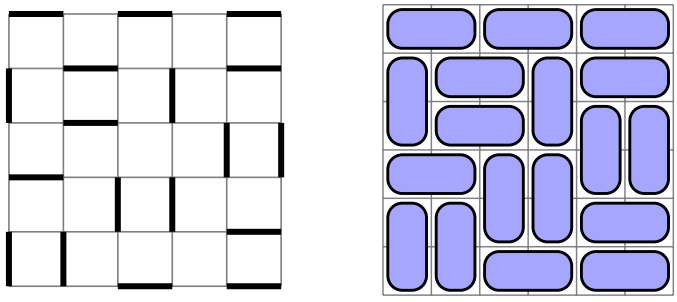

$(a)$ $(b)$

Figure 5.1: $(a)$ "Perfect matching" sur le réseau carrée, et $(b)$ sa représentation en terme de "domino".

avec la propriété que chaque site du réseau est lié avec exactement un de ses voisins [151].

### La fonction de partition

La fonction de partition du modèle de dimères a $2d$ sur le réseau carré a été résolu [120, 71, 201] pour plusieurs conditions aux limites. Le théorème de Kasteleyn est une recette pour trouver une matrice $K$ tel que $\mathrm{hf}A = \mathrm{pf}K$, où les élements de matrices sont $K_{ij} = \pm 1$. Le théorème de Kasteleyn postule que le nombre d'appariement parfait d'un graphe planaire $\mathcal{G}$ est donné par

$$\text{perfect } \mathcal{G} = \mathrm{hf}A = \mathrm{pf}K. \tag{5.1}$$

Pour le réseau carré, nous pouvons choisir des poids de Boltzmann $t_x$ et $t_y$ pour les dimères horizontaux et verticaux, le pfaffien peut être calculé par transformée de Fourier et l'on trouve pour des conditions aux limites libres

$$Q_0[t_x, t_y] = \prod_{p=1}^{M/2} \prod_{q=1}^{N/2} \left[ 4t_x^2 \cos^2 \frac{\pi p}{M+1} + 4t_y^2 \cos^2 \frac{\pi q}{N+1} \right]. \tag{5.2}$$

La forme asymptotique $L \to \infty$ de la fonction de partition (pour $M = N = L$) peut facilement être dérivée aisément

$$Q_0 \sim \exp \frac{GL^2}{\pi}, \tag{5.3}$$

où $G$ est la constante de Catalan. Le facteur $G/\pi$ correspond à l'entropie par site du modèle.

### Methode de Plechko

L'approche introduire ici a été développée par Plechko dans une série de papiers [171, 172]. Le hamiltonien du modèle de dimères sur un graphe générique peut être écrit comme

$$Q_0 = \int \mathcal{D}[\eta] \exp\Big( -\frac{t}{2} \sum_{ij} \eta_i A_{ij} \eta_j \Big), \tag{5.4}$$

dans le cas particulier du réseau carré de taille $L \times L$ avec $L$, on a

$$Q_0 = \int \mathcal{D}[\eta] \prod_{m,n}^{L} (1 + t_x \eta_{mn} \eta_{m+1n})(1 + t_y \eta_{mn} \eta_{mn+1}), \tag{5.5}$$

où $\eta_{mn}$ sont des variables nilpotentes et commutantes en chaque site du réseau. Les intégrales peuvent être effectuées en introduisant des variables de Grassmann $(a_{mn}, \bar{a}_{mn}, b_{mn}, \bar{b}_{mn})$, tel que

$$\begin{aligned}
(1 + t_x \eta_{mn} \eta_{m+1n}) &= \int \mathcal{D}[\bar{a}]\, \mathcal{D}[a] e^{a_{mn}\bar{a}_{mn}} (1 + a_{mn}\eta_{mn})(1 + t_x \bar{a}_{mn} \eta_{m+1n}), \\
(1 + t_y \eta_{mn} \eta_{mn+1}) &= \int \mathcal{D}[\bar{b}]\, \mathcal{D}[b] e^{b_{mn}\bar{b}_{mn}} (1 + b_{mn}\eta_{mn})(1 + t_y \bar{b}_{mn} \eta_{mn+1}).
\end{aligned} \tag{5.6}$$

Cette décomposition permet d'intégrer les variables $\eta_{mn}$, après réarrangement $A_{mn} := 1 + a_{mn}\eta_{mn}$, $\bar{A}_{m+1n} := 1 + t_x \bar{a}_{mn} \eta_{m+1n}$, $B_{mn} := 1 + b_{mn}\eta_{mn}$ et $\bar{B}_{mn+1} := 1 + t_y \bar{b}_{mn} \eta_{mn+1}$. Ensuite, la fonction de partition devient

$$Q_0 = \mathrm{Tr}_{\{a,\bar{a},b,\bar{b},\eta\}} \prod_{n=1}^{\overrightarrow{L}} \Big( \prod_{m=1}^{\overleftarrow{L}} \bar{B}_{mn} \prod_{m=1}^{\overrightarrow{L}} \bar{A}_{mn} B_{mn} A_{mn} \Big). \tag{5.7}$$

L'intégration sur les variables $\eta_{mn}$ est effectuée de manière récursive de $m = 1$ à $m = L$ pour chaque $n$. Enfin on obtient simplement le résultat bien connu

$$Q_0 = \prod_{p,q=1}^{L/2} \left[ 4t_x^2 \cos^2 \frac{\pi p}{L+1} + 4t_y^2 \cos^2 \frac{\pi q}{L+1} \right]. \tag{5.8}$$

**Fonction de partition avec $2n$ monomères**

Prenons maintenant le cas où un nombre pair de monomères sont présents sur le réseau à des positions différentes $\mathbf{r}_i = (m_i, n_i)$ avec $i = 1, \cdots, 2n$. La fonction de partition $Q_{2n}(\{\mathbf{r}_i\})$ est le nombre

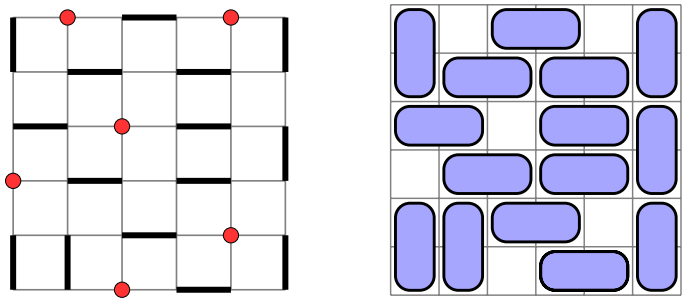

(a) (b)

Figure 5.2: Configuration typique pour un système de taille $6 \times 6$ avec 6 monomère.

de configurations possibles avec la contrainte imposée par les monomères fixes. Cette quantité peut être évaluée par insertion de variables nilpotentes $\eta_{m_i n_i}$ dans la fonction de partition, ce qui empêche les dimères d'occuper les sites $\mathbf{r}_i$. Il peut être utile d'introduire des variables de Grassmann $h_i$ tel que $\eta_{m_i n_i} = \int \mathrm{d}h_i \exp(h_i \eta_{m_i n_i})$. La fonction de partition peut être exprimée comme une intégrale gaussienne, avec une somme de termes correspondant à l'insertion de monomères,

$$Q_{2n}(\{\mathbf{r}_i\}) = \int \mathcal{D}[c]\, \mathcal{D}[h] \exp \left[ S_0 + \sum_{\mathbf{r}_i} c_{m_i n_i} h_i + 2t_y \sum_{\mathbf{r}_i, m=m_i+1}^{L} (-1)^{m+1} c_{mn_i-1} c_{mn_i} \right]. \tag{5.9}$$

La présence de monomères est équivalent à l'insertion d'un champ magnétique $h_i$ aux points $\mathbf{r}_i$, ainsi qu'une somme de termes quadratiques $c_{mn_i-1} c_{mn_i}$ allant de la position du monomère à la frontière droite du système. Enfin, nous avons trouvé l'expression suivante pour la fonction de partition

$$Q_{2n}(\{\mathbf{r}_i\}) = \mathrm{pf}(W)\mathrm{pf}(C), \tag{5.10}$$

où $C$ est une matrice réelle antisymétrique $(2n \times 2n)$ avec éléments $C_{ij} = \Lambda^{\mu}_{i,\alpha} (W^{-1})^{\mu\nu}_{\alpha\beta} \Lambda^{\nu}_{j,\beta}$.

**Champ de hauteur et théorie conforme**

Pour toute configuration de dimères, on peut associer un champ de hauteur sur les plaquettes, qui est défini dans le texte principal [217, 148, 97, 95]. un exemple en est donné sur la figure ci-dessous.

Une action effective $\mathcal{S}$ peut être dérivée pour les fluctuation du champ de hauteur $\phi(\vec{r})$,

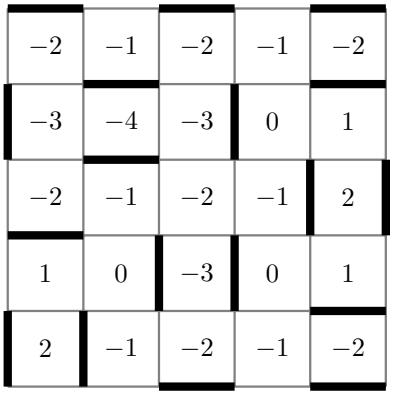


Figure 5.3: Le champ de hauteur du modèle avec des conditions aux limites libres

$$\mathcal{S}[\phi] = \frac{g}{2}\int \mathrm{d}x\,\mathrm{d}y\,\left(\nabla\phi\right)^2. \tag{5.11}$$

Ici $g$ une constante qui commande la rigidité du modèle de hauteur. Les charges magnétiques $m$ correspondent à une dislocation du champ de hauteur et correspondent à des opérateurs de vertex

$$\begin{aligned} V_e(z) &= :\mathrm{e}^{ie\phi}: \\ V_m(z) &= :\mathrm{e}^{im\psi}: \end{aligned} \tag{5.12}$$

où $\psi$ est le champ dual de $\phi$. Ces opérateurs sont des opérateurs primaires de la CFT. La dimension d'échelle associée à l'insertion d'une particule de charge électromagnétique $(e, m)$ est donnée par

$$x_g(e,m) = \frac{e^2}{4\pi g} + \pi g m^2. \tag{5.13}$$

Par exemple, deux monomères sur des sous-réseaux opposés correspondent à deux charges $m = 1$ et $m = -1$. Il est bien connu [71, 72] que l'exposant des corrélations monomère-monomère est $1/2$, cela fixe $g_{\text{libre}} = 1/4\pi$ pour la constante de rigidité de la théorie des champ décrivant le modèle de dimères libre. Nous avons vu précédemment que l'exposant dimère-dimère est 2. Par conséquent, les dimensions de monomères et dimères défini par $x_b^{(m)} := x_{\frac{1}{4\pi}}(0,1)$et $x_b^{(d)} := x_{\frac{1}{4\pi}}(1,0)$ sont

$$\text{free dimer}: \;\; g_{\text{free}} = \frac{1}{4\pi} \to \begin{cases} x_b^{(d)} := x_{\frac{1}{4\pi}}(1,0) = 1 \\ x_b^{(m)} := x_{\frac{1}{4\pi}}(1,0) = 1/4. \end{cases} \tag{5.14}$$

Ici, nous allons analyser des fonctions de corrélation monomère-monomère en utilisant notre solution exacte ainsi que l'interprétation en terme de gaz de Coulomb du modèle de dimères. Comme nous le détaillé dans corps du texte, le modèle de dimères dans une géométrie rectangulaire comporte des opérateurs de changement de conditions aux bords aux quatre coins, et ils doivent être

pris en compte pour l'analyse des dimensions des opérateurs de la théorie, en particulier pour analyser le comportement près des coins. Les résultats suivant sont trouvés

$$\text{monomer correlations} \rightarrow \begin{cases} \text{bulk-bulk behavior} \rightarrow C(L) \sim L^{-2x_b^{(m)}} \sim L^{-1/2} \\ \text{surface-surface behavior} \rightarrow C(L) \sim L^{-2x_s^{(m)}} \sim L^{-1} \\ \text{bulk-surface behavior} \rightarrow C(L) \sim L^{-x_s^{(m)}-x_b^{(m)}} \sim L^{-3/4}. \end{cases} \tag{5.15}$$

### Cercle arctique

Le cercle arctique est le nom donné par Jockush, Propp & Shor à un phénomène qu'ils ont découvert en 1995 [113] en étudiant les pavages de dimères sur le diamant Azteque [63, 65]. Le phénomène consiste en l'apparition, dans la limite thermodynamique, d'une courbe qui sépare deux domaines macroscopiques, une dans laquelle les dimères apparaissent gelés et un autre domaine où les dimères fluctuent. Cette géométrie est appelé le diamant aztèque et peut être considérée comme un réseau carré régulier où les quatre coins sont enlevés. Puis l'on considère l'ensemble des pavages aléatoires de dimères du diamant aztèque avec un poids uniforme. Le nombre de configuration de dimères

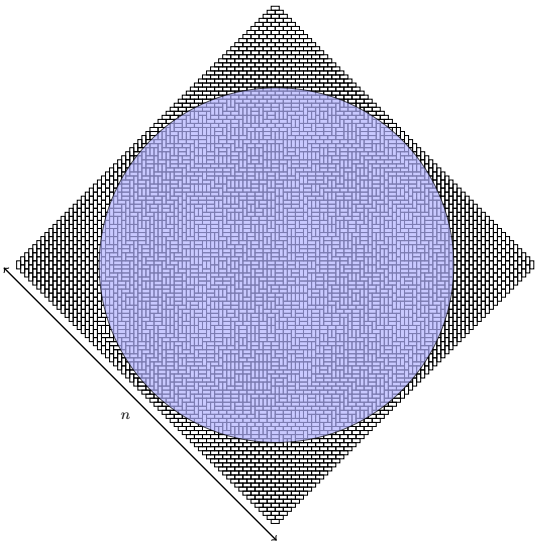


Figure 5.4: Phénomène de cercle arctique apparaissant dans le modele de dimères sur le réseau Azteque

AD($n$) sur le réseau Aztec de taille $n$ a été calculé [64, 65] et un résultat particulièrement simple apparait

$$\boxed{\text{AD}(n) = 2^{\frac{n(n+1)}{2}}.} \tag{5.16}$$

Pour grand $n$ le diamant Azteque se divise en cinq régions délimitées par le cercle arctique. L'intérieur du cercle arctique est une région désordonnée avec des correlations critiques. En dehors de cette limite le pavage forme un motif tout à fait régulier.

### Modèle simple

Notre motivation pour revisiter problème vient de la physique des trempes dans les chaînes de spins quantiques, et notamment leur description en terme de CFT. La correspondance classique/quantique nous indique que, l'évolution en temps imaginaire d'un modèle quantique unidimensionnel est équivalent à un modèle statistique classique à deux dimensions. Dans cette formulation, l'état initial du système quantique devient une condition aux limites dans le modèle classique. Ensuite, il convient de choisir le système quantique et l'état initial tel

- Les fluctuations en volume soient décrites par une théorie des champs sans masse
- L'état de bord $|\Psi_0\rangle$ renormalise vers une condition de bord conforme

Le modèle que nous considérons ici est une chaine de fermions libres vivant sur les sites $x \in \mathbb{Z} + \frac{1}{2}$. Le Hamiltonien est diagonal dans l'espace de Fourier avec une relation dispersion $\varepsilon(k)$,

$$H \;=\; \int_{-\pi}^{\pi} \frac{\mathrm{d}k}{2\pi}\, \varepsilon(k)\, c^\dagger(k) c(k)\,. \tag{5.17}$$

Pour plus de simplicité, nous considérons le cas de saut entre plus proche voisins, de telle sorte que la relation de dispersion peut être mise sous la forme

$$\varepsilon(k) \;=\; -\cos k\,.$$

l'état initial $|\Psi_0\rangle$ du modele, complètement rempli à gauche et vide à droite,

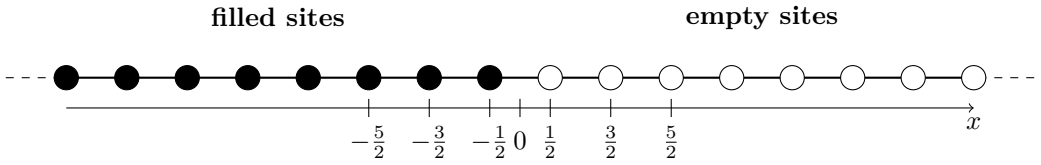


Figure 5.5: Représentation de l'état initial du modèle, complètement rempli à gauche et vide à droite

$$\rho(x)|\Psi_0\rangle \;=\; c_x^\dagger c_x |\Psi_0\rangle \;=\; \Theta(-x)|\Psi_0\rangle\,. \tag{5.18}$$

$\Theta$ est la distribution de Heaviside $\Theta(-x) = 1$ si $x < 0$ et $\Theta(-x) = 0$ si $x > 0$. On souhaite calculer des correlateurs de la forme $\langle \mathcal{O}_1(x_1, y_1) \dots \mathcal{O}_n(x_1, y_1)\rangle$ d'observables locales $\mathcal{O}(x, y)$

$$\frac{\langle \Psi_0 | \mathrm{e}^{-2R\,H}\, \mathcal{T}\left[\left(\mathrm{e}^{(R+y_1)H}\mathcal{O}_1(x_1)\mathrm{e}^{-(R+y_1)H}\right)\dots\left(\mathrm{e}^{(R+y_n)H}\mathcal{O}_n(x_n)\mathrm{e}^{-(R+y_n)H}\right)\right]|\Psi_0\rangle}{Z},$$

où $\mathcal{T}[.]$ est la prescription d'ordre temporel et $Z$ est la fonction de partition du modèle

$$Z \;=\; \langle \Psi_0 | \mathrm{e}^{-2R\,H} | \Psi_0 \rangle\,,$$

tel que $\langle 1 \rangle = 1$. On commence avec l'état initial $|\Psi_0\rangle$ au temps $y = -R$ et on laisse évoluer le système jusqu'au temps $y = +R$, où l'on projette de nouveau sur $|\Psi_0\rangle$. Notre modèle possède

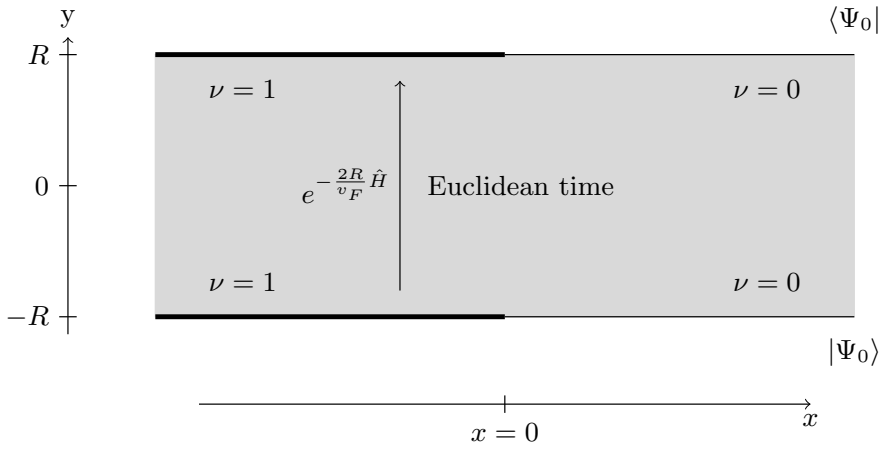


Figure 5.6: Evolution en temps imaginaire de l'état initial, on attend deux régions gelés à gauche $\nu = 1$ et à droite $\nu = 0$ du système

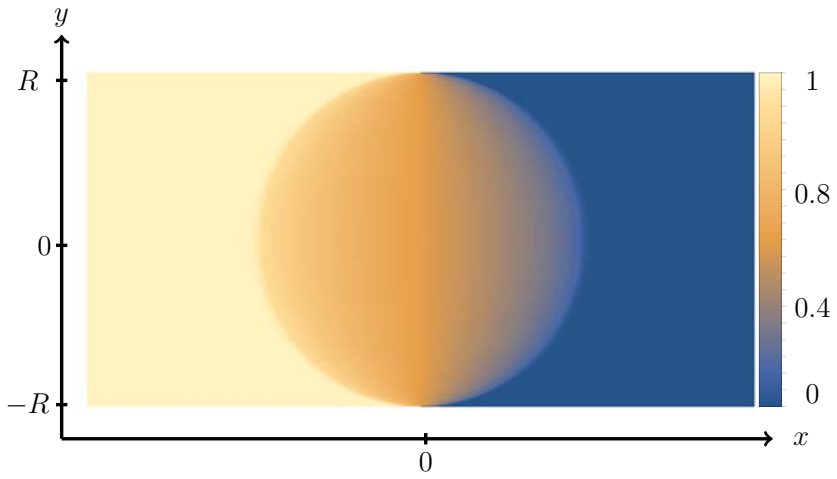


Figure 5.7: Simulation numérique de notre modèle, le phénomène de cercle arctique est apparent

la même phénoménologie de cercle arctique observée sur le diamant Azteque. Maintenant on s'interresse au comportement de correlateurs $\langle \mathcal{O}_1(x_1, y_1) \dots \mathcal{O}_n(x_n, y_n) \rangle$ dans la limite

$$x_j/R \quad \text{et} \quad y_j/R \quad \text{fixé pour tout } j\,, \qquad \text{et} \quad R \to \infty\,. \tag{5.19}$$

Dans celle limite, la densité à l'intérieur du cercle prend une forme très simple interpolant entre $\langle \rho \rangle = 1$ et $\langle \rho \rangle = 0$

$$(x^2 + y^2 < R^2) \qquad \langle \rho(x, y) \rangle \;=\; \frac{1}{\pi} \arccos \frac{x}{\sqrt{R^2 - y^2}}\,.$$

**Théorie de Dirac**

Ces corrélations doivent être décrites par une théorie quantique des champs euclidienne avec une action locale. Puisque nous traitons un hamiltonien quadratique pour des particules fermioniques, nous sommes à la recherche d'une théorie de fermion libre. En outre, un aspect clé du modèle est la conservation du nombre de particules, ce qui signifie l'invariance par le groupe $U(1)$, $c^\dagger \to e^{i\varphi}c^\dagger$, $c \to e^{-i\varphi}c$. À un point donné, l'on doit pouvoir exprimer les degrés de libertés sur le réseau en termes des champs continus $\psi^\dagger$ et $\overline{\psi}^\dagger$. Fixons cette relation

$$\begin{cases} c_x^\dagger(y) &= \dfrac{1}{\sqrt{2\pi}}\,\psi^\dagger(x,y) \,+\, \dfrac{1}{\sqrt{2\pi}}\,\overline{\psi}^\dagger(x,y) \\ c_x(y) &= \dfrac{1}{\sqrt{2\pi}}\,\psi(x,y) \,+\, \dfrac{1}{\sqrt{2\pi}}\,\overline{\psi}(x,y)\,. \end{cases} \tag{5.20}$$

Le système est clairement inhomogène donc il n'y a aucune raison pour que la théorie des champ soit homogène. Par conséquent, nous sommes à la recherche d'une action de Dirac sans masse où les paramètres varient avec la position. Nous supposons que le paramètre qui contrôle cette inhomogénéité est la métrique. En outre, il pourrait y avoir avoir aussi des champs de jauge, en effet le lagrangien de Dirac est invariant par le groupe chiral $U_V(1) \times U_A(1)$

$$\Psi' = \mathrm{e}^{i\alpha_V}\,\Psi \tag{5.21}$$

$$\Psi' = \mathrm{e}^{i\alpha_A\gamma^5}\Psi, \tag{5.22}$$

où $\alpha_A, \alpha_V \in \mathbb{R}$. L'action de Dirac s'écrit alors

$$\boxed{\mathcal{S}_0 \;=\; \frac{1}{2\pi}\int \sqrt{g}\,\mathrm{d}^2x\, e_a^\mu \frac{1}{2}\left[\overline{\Psi}\overset{\leftrightarrow}{\mathcal{D}_\mu}\gamma^a\Psi\right]} \tag{5.23}$$

Ici,l'*adjoint de Dirac* $\overline{\Psi}$ est $\Psi^\dagger\gamma^2$, $e_a^\mu(x)$ est la tétrade, $\mathrm{d}^2x\sqrt{g} = \mathrm{d}^2x|e|^{-1}$ est l'élément de volume et $\mathcal{D}_\mu$ est la dérivée covariante. L'action (5.23) est *a priori* l'action la plus générale décrivant les fluctuations à l'intérieur du cercle arctique. Nous verrons dans le texte principal quelle est la forme explicite des champs de jauges vecteur $A_\mu^{(\mathrm{v})}$ et axial $A_\mu^{(\mathrm{a})}$. Le lagrangien que nous recherchons est déterminé entièrement par

- le facteur conforme $\sigma(x,y)$ such that $g_{\mu\nu} = \mathrm{e}^{2\sigma}\eta_{\mu\nu}$,
- les champs de jauges $A_\mu^{(\mathrm{v})}$ and $A_\mu^{(\mathrm{a})}$.

La même analyse reste correcte pour le modèle à 6-vertex et pour les modèles de dimères comme nous l'avons vu dans le texte principal.

# PART II

# Critical properties of interface growth models

CHAPTER 6

# Introduction to interface: Markov processes and scaling behavior

## Contents

In this chapter, we are interesting in deriving continuous models of growing interface starting from a microscopic process on a lattice. In the following on considers only the $1d$ situation even tough the generalization is strait forward. The simplest microscopic process on can consider is just simple random deposition of particles on a one-dimensional substrate (see Fig. 6.1), and the question is how the interface created by this deposition will look like at large scale and how can we describe this system as a statistical system of a continuous field. The strategy that we shall follow consist to consider the process as a Markov process and to derive the master equation for probabilities in this process and goes to a continuum description through Fokker-Planck and Langevin equations. This formalism will lead us to the derivation of continuum equations for the

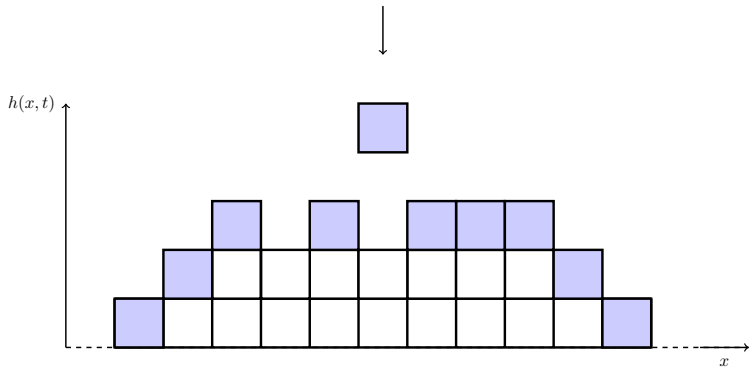


Figure 6.1: Random deposition process. The interface of the deposition is indicated by the blue particles.

height of the interface, and we will present two different cases known as the Edwards-Wilkinson equation and Kardar-Parisi-Zhang equation starting from some microscopic deposition on a $1d$ substrate. We will conclude this chapter mentioning some critical properties of these equations, which lead us to two different universality classes for interface growth processes.

## 6.1 Markov formalism

### 6.1.1 Interface as a stochastic process

As we said earlier, one considers a deposition of particles on a substrate with some rates which can be more or less complicated. We start by writing down a very general master equation describing the stochastic evolution of a random interface in any dimension. Let us note $\{h\} = \{h_0, h_1...\}$ the height of every discrete site $h_i \in \mathbb{N}$ on the lattice with periodic boundary conditions $h_1 = h_{N+1}$. In the following we shall work on the $1d$ lattice of length $N$. For any discrete time step, one allows for the deposition of one particle of the substrate according to specific rules. One defines $\{s\} = \{s_0, s_1...\}$, the set of jumps after this time interval, more precisely if we depose a particle at site $k$, then $\{s\} = \{0, 0..., s_k = a, ..., 0, 0\}$, where $a$ is a constant.

### 6.1.2 From a master equation to a Fokker-Planck equation

The derivation here follows [207, 168, 41] and we report the reader to these references for more detailed calculation and references. We define $\mathbb{P}(\{h\},t)$ the joint probability that, at time $t$, the surface is in the state $\{h\}$ et we define transition rates between two states as $\mathbb{W}(\{h\} \to \{h'\})$ in such way that we can write formally a master equation as

$$\mathbb{P}(\{h\},t+\delta t)-\mathbb{P}(\{h\},t) = \sum_{\{s\}} \mathbb{W}(\{h-s\} \to \{h\})\, \mathbb{P}(\{h-s\},t)-\mathbb{W}(\{h\} \to \{h+s\})\, \mathbb{P}(\{h\},t). \quad (6.1)$$

We make the assumption here that the process is markovian, *i.e.* the state of the surface at time $t+\delta t$ depends only of the state at time $t$, there is no memory effects and the transition rates follow a Chapman Kolmogorov equation. Our goal is to find a proper continuum limit of this kind of process, when the size of the jump goes to zero. The standard way to proceed is through a Kramers-Moyal expansion of the master equation in order to find a partial differential equation for the probability distribution $\mathbb{P}(\{h\},t)$. The full calculation is not very insightful (see [207] for details), and gives at second-order expansion the so-called Fokker-Planck equation for the probability distribution

$$\frac{\partial \mathbb{P}}{\partial t'} = -\sum_i \partial_{h_i}(M_i^{(1)}\mathbb{P}) + \frac{1}{2}\sum_{i,j} \partial_{h_i h_j}(M_{ij}^{(2)}\mathbb{P}), \quad (6.2)$$

where

$$M_i^{(1)} = \int \prod_{k=1}^{N} \mathrm{d}s_{i_k}\ s_i\ \mathbb{W}(\{h\} \to \{h+s\}), \quad (6.3)$$

$$M_{i,j}^{(2)} = \int \prod_{k=1}^{N} \mathrm{d}s_{i_k}\ s_i s_j\ \mathbb{W}(\{h\} \to \{h+s\}). \quad (6.4)$$

### 6.1.3 Langevin equation

For any Fokker-Planck equation, we can write a partial differential equation for the stochastic variables directly, here for the height $h_i$ of the interface on every site

$$\frac{\partial h_i}{\partial t'} = M_i^{(1)} + \eta_i, \quad (6.5)$$

with

$$\langle \eta_i \rangle = 0, \quad (6.6)$$

$$\langle \eta_i(t')\eta_j(t'+\tau)\rangle = M_{ij}^{(2)}\delta_\tau. \quad (6.7)$$

The Fokker-Planck equation and the Langevin equation are formally equivalent, but some features are more tractable with one or the other equation. In the following we will be interested computing quantities like the average or the fluctuation of the interface which can be simply done using the Langevin equation.

**Random deposition processes**

In a purely randomly process (see Fig. 6.1), the deposition is completely independent from site to site, then when a particle is placed at site $i$, only this site is affected. The transition rates can be written as

$$\mathbb{W}(\{h\} \to \{h'\}) = \Gamma \sum_{i=0}^{L} \delta_{s_i,1} \prod_{j \neq i} \delta_{s_j,0}, \tag{6.8}$$

then we can compute the two first moment of this process to get the corresponding Langevin equation

$$M_i^{(1)} = \int \mathrm{d}s_1 \, \mathrm{d}s_2 ... \, \mathrm{d}s_L \; s_i \; \Gamma \sum_{i=0}^{L} \delta_{s_i,1} \prod_{j \neq i} \delta_{s_j,0} = \Gamma a, \tag{6.9}$$

$$M_{i,j}^{(2)} = \int \mathrm{d}s_1 \, \mathrm{d}s_2 ... \, \mathrm{d}s_L \; s_i s_j \; \Gamma \sum_{i=0}^{L} \delta_{s_i,1} \prod_{j \neq i} \delta_{s_j,0} = \Gamma a^2 \delta_{ij}. \tag{6.10}$$

Finally the Langevin equation is just the equation of $N$ uncoupled brownian motions

$$\frac{\mathrm{d}h_i}{\mathrm{d}t'} = \Gamma a + \xi_i \tag{6.11}$$

with $\xi_i$ are uncorrelated centered white noises

$$\langle \xi_i \rangle = 0, \tag{6.12}$$

$$\langle \xi_i(t') \xi_j(t' + \tau) \rangle = \Gamma a^2 \delta_{ij} \delta_\tau. \tag{6.13}$$

The solution is simply

$$h(x,t) = \Gamma t' + \int_0^{t'} \mathrm{d}u \; \xi(x,u). \tag{6.14}$$

Therefor, the interface grows linearly and the fluctuations are given by brownian motion.

## 6.2 Interface growth process with diffusion

### 6.2.1 Deposition-relaxation processes

The first step in the description of a more realistic model of interface than the brownian interface is to add diffusion in the process. The simplest diffusion process is to allowed particles to jump of one site to the left or to the right with a fixed probability once they are on the interface (see Fig. 6.2). This process is know as the Family process [67]. The transition rates can be written as

$$\mathbb{W}(\{h\} \to \{h'\}) = \Gamma \sum_{i=0}^{N} \{\omega_i^0 \delta_{s_i,1} \prod_{j \neq i} \delta_{s_j,0} + \omega_i^d \delta_{s_{i+1},1} \prod_{j \neq i+1} \delta_{s_j,0} + \omega_i^g \delta_{s_{i-1},1} \prod_{j \neq i-1} \delta_{s_j,0}\}. \tag{6.15}$$

More precisely, when a particle drops at site $i$, it stays at this location if the heights of the right

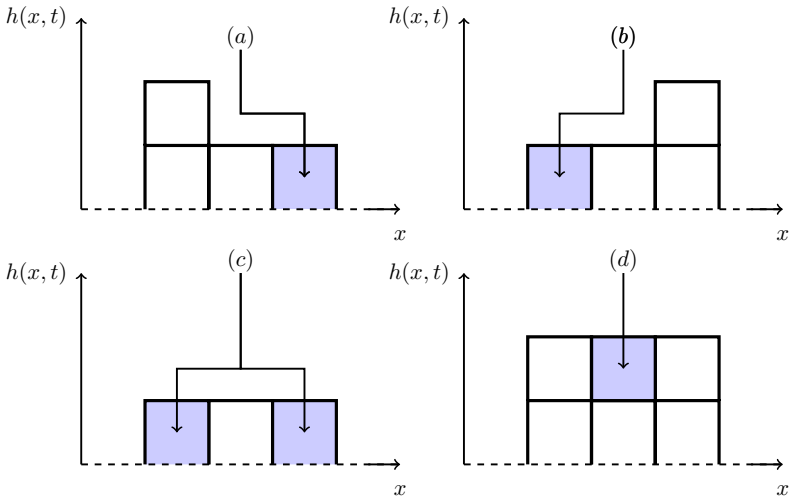


Figure 6.2: Four types of deposition are allowed in our process according the height of the two nearest neighbors. If the particle falls into a hole (or a flat zone ($d$) because we take $\theta(0) = 1$) in $i$, then it stays in $i$ ($\theta_{i+1,i}\theta_{i-1,i}$). If the particles falls on a peak ($c$) then it moves of one site to the right or the left with probability $p = 1/2$ ($\frac{1}{2}\hat{\theta}_{i-1,i}\hat{\theta}_{i+1,i}+\frac{1}{2}\hat{\theta}_{i+1,i}\hat{\theta}_{i-1,i}$). If the interface configuration is given by ($a$) then the particle moves to the right ($\theta_{i+1,i}\hat{\theta}_{i-1,i}$), and if the configuration is given by (b) then the particle moves to the left ($\theta_{i-1,i}\hat{\theta}_{i+1,i}$).

and left neighbor are bigger ($\omega_i^0$), or relax to the site $i$ś1 ($\omega_i^{d,g}$)[1] if one of the neighbor have a smaller height. We have to make sure that the process is properly normalized

$$\sum_{\{0,g,d\}} \omega_i^{0,g,d} = 1. \tag{6.16}$$

The rates are

$$\omega_i^0 = \theta_{i+1,i}\theta_{i-1,i} \tag{6.17}$$

$$\omega_i^g = \theta_{i+1,i}\hat{\theta}_{i-1,i} + \frac{1}{2}\hat{\theta}_{i-1,i}\hat{\theta}_{i+1,i} \tag{6.18}$$

$$\omega_i^d = \theta_{i-1,i}\hat{\theta}_{i+1,i} + \frac{1}{2}\hat{\theta}_{i+1,i}\hat{\theta}_{i-1,i} \tag{6.19}$$

with $\hat{\theta} = 1-\theta$ and $\theta_{i+1,i} = \theta(h_{i+1} - h_i)$ the Heaviside function, we can check that $\omega_i^0 + \omega_i^g + \omega_i^d = 1$ for any $i = 1...N$. The computation of the first moment gives

$$\begin{aligned} M_i^{(1)} &= \Gamma a \int \prod_k \mathrm{d}s_{i_k}\ s_i \ \sum_{i=0}^{N} \{\omega_i^0 \delta_{s_i,1} \prod_{j\neq i} \delta_{s_j,0} + \omega_i^d \delta_{s_{i+1},1} \prod_{j\neq i+1} \delta_{s_j,0} + \omega_i^g \delta_{s_{i-1},1} \prod_{j\neq i-1} \delta_{s_j,0}\} \\ &= \Gamma a(\omega_{i+1}^g + \omega_i^0 + \omega_{i-1}^d), \end{aligned} \tag{6.20}$$

[1] $d$ and $g$ stand for droite (right) ant gauche (left)

then the second moment

$$M_{ij}^{(2)} = \Gamma a^2 \int \prod_k \mathrm{d}s_{i_k}\ s_i s_j \sum_{i=0}^{N} \{\omega_i^0 \delta_{s_i,1} \prod_{j\neq i} \delta_{s_j,0} + \omega_i^d \delta_{s_{i+1},1} \prod_{j\neq i+1} \delta_{s_j,0} + \omega_i^g \delta_{s_{i-1},1} \prod_{j\neq i-1} \delta_{s_j,0}\}$$
$$= \Gamma a^2 \delta_{ij}(\omega_{i+1}^g + \omega_i^0 + \omega_{i-1}^d). \tag{6.21}$$

Now that we have express the quantities $M_i^{(1)}$ and $M_{ij}^{(2)}$ as function of the microscopic rates of deposition of particles on the lattice, we can formally expand the difference of height between two neighboring site as

$$h_{i\pm1} - h_i = \sum_k \frac{(\pm a)^k}{k!} \frac{\partial^k h(x)}{\partial x^k}\Big|_{(x=ia)}, \tag{6.22}$$

Now we can use a formal regularization of the Heaviside distribution

$$\theta(x) = \lim_{a\to 0} \theta_a(x), \tag{6.23}$$

where $\theta_a(x)$ is a differentiable function. Using the expansion of the function

$$\theta_a(x) = 1 + \sum c_k x^k. \tag{6.24}$$

Now we use this expansion on the discrete Langevin equation to get

$$\Gamma a\ (\omega_{i+1}^g + \omega_i^0 + \omega_{i-1}^d) \to \mathrm{cst} + \nu \nabla_i^2 h_i + \mathcal{O}(a^3) \tag{6.25}$$

Then on can write

$$\partial_t h = v + \nu \partial_x^2 h + \xi(x,t), \tag{6.26}$$

where $\nu = \Gamma a^2$. This method does not seem very mathematically well defined because of this expansion of the Heaviside function. Nevertheless it gives a fairly good result at the end. The only annoying problem is that the macroscopic parameters are not uniquely define in terms of the microscopic parameters because of the choice of the function $\theta_a(x)$, in this case the constant $v$ will depend on that. We will come back to that later in the case of KPZ equation. This equation is called the Edwards Wilkinson [62], it is nothing but a diffusion equation for the height variable with a gaussian noise, and can be easily solved by means of Fourier transform in any dimension.

### 6.2.2 Restricted solid on solid processes

Now we choose other types of depositions which can be think as constrained random depositions, known as restricted solid-on solid models. The simplest one is the Kim-Kosterlitz process [131] that we shall detailed in the following. The RSOS processes, are not standard processes of deposition of particles on a substrate because any diffusion processes are forbidden. A particle is dropped on the surface only under a restricting condition between difference of height between nearest neighbors. In the following we shall study a particular case known as the Kim-Kosterlitz restriction, where the difference is always less that one unit of height *i.e.* $|h_i - h_{i\pm1}|$ša. The continuum derivation seen

on the previous chapter can be applied to this process as well. In comparison to the deposition-relaxation seen before, the rates to go left or right are zero ($\omega^d = \omega^g = 0$) and only the rate $\omega^0$ arises in the master equation

$$\mathbb{W}(\{h\} \to \{h'\}) = \Gamma \sum_{i=0}^{L} \omega_i \delta_{s_i,1} \prod_{j \neq i} \delta_{s_j,0}, \tag{6.27}$$

with $\omega_i = \theta_{i+1,i}\theta_{i-1,i}$. We can easily understand that if the interface is initially flat $h_i = 0$, then the choice of this rate will create an interface over time that will respect the Kim-Kosterlitz restriction $|h_i - h_{i\pm1}|$ša. Now we can proceed in the exact same way as for the previous model and compute the two first moments of the Kramers-Moyal expansion

$$M_i^{(1)} = \int \mathrm{d}s_1 \, \mathrm{d}s_2 ... \, \mathrm{d}s_L \; s_i \; \Gamma \sum_{i=0}^{L} \omega_i \delta_{s_i,1} \prod_{j \neq i} \delta_{s_j,0} = \Gamma a \hat{\mathrm{E}} \omega_i, \tag{6.28}$$

$$M_{i,j}^{(2)} = \int \mathrm{d}s_1 \, \mathrm{d}s_2 ... \, \mathrm{d}s_L \; s_i s_j \; \Gamma \sum_{i=0}^{L} \omega_i \delta_{s_i,1} \prod_{j \neq i} \delta_{s_j,0} = \Gamma a^2 \omega_i \delta_{ij}. \tag{6.29}$$

And then the discrete Langevin equation for the height at site $i$ follows

$$\frac{\mathrm{d}h_i}{\mathrm{d}t} = M_i^{(1)} + \eta_i \tag{6.30}$$

with with $\xi_i$ are uncorrelated centered white noises

$$\langle \eta_i \rangle = 0, \tag{6.31}$$

$$\langle \eta_i(t') \eta_j(t' + \tau) \rangle = \Gamma a^2 \delta_{ij} \delta_\tau. \tag{6.32}$$

The discrete Langevin equation can be written $\forall i$ as

$$\frac{\mathrm{d}h_i}{\mathrm{d}t} = \Gamma a \; \theta_{i+1,i}\theta_{i-1,i} + \eta_i(t) \tag{6.33}$$

where $\theta_{i+1,i} := \theta(h_{i+1} - h_i)$, $\theta(0) = 1$ and $\eta_i$ is the discrete white noise. In the RSOS process, one have $h_{i\pm1} - h_i \sim \mathcal{O}(a)$. Now we can use a formal regularization of the Heaviside distribution

$$\theta(x) = \lim_{a \to 0} \theta_a(x) \tag{6.34}$$

where $\theta_a(x)$ is a differentiable function. Using the expansion of the function

$$\theta_a(x) = 1 + \sum c_k x^k \tag{6.35}$$

Now we use this expansion on the discrete Langevin equation

$$\frac{\partial h(x,t)}{\partial t} = \Gamma a \Big[ 1 + a^2 c_1 \frac{\partial^2 h}{\partial x^2} + (2c_2 a^2 - c_1^2 a^2) \Big( \frac{\partial h}{\partial x} \Big)^2 + \mathcal{O}(a^3) \Big] + \eta \tag{6.36}$$

We define $\Gamma a^2 \to \nu$ in the thermodynamic limit, as the diffusive parameter which is always constant. Here, we notice that the factor in front of the non-linear (we call it $\lambda$) term is not wheel defined

because $\Gamma a(2c_2a^2 - c_1^2a^2)$ goes to infinity when $a \to 0$ ($\lambda \sim \mathcal{O}(\Gamma a) \to \infty$) because $c_p \sim \mathcal{O}(a^{-p})$. With this method the nonlinear coupling of the theory is diverging when the lattice unit goes to zero, so the theory is not coherent and the macroscopic quantities cannot be interpreted using microscopic parameters. One can mention that this divergence can be avoiding using the same method with small modifications in the definition of the space derivative, leading to the exact same form for the continuum equation with different explicit expression for the macroscopic parameters. Finally on can argue that this "master equation to Langevin equation" derivation gives the right answer for the form of the macroscopic equation but not the explicit relation between parameters.

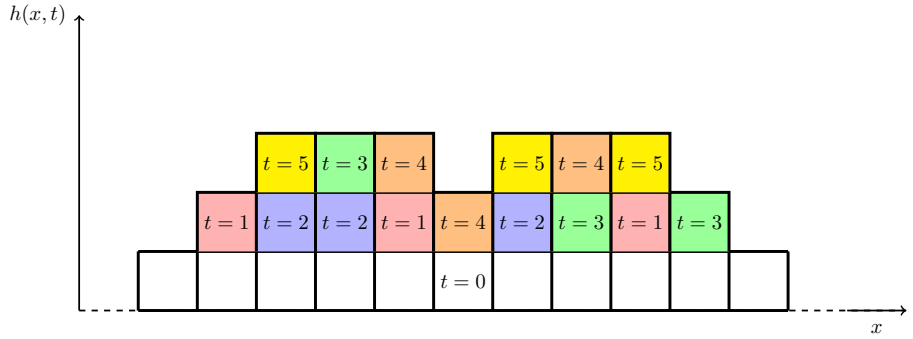


Figure 6.3: Kim-Kosterlitz process on a $1d$ substrate. The initial state at $t = 0$ is the white flat interface, then a fixed (3 in the figure) number of particles can reached the substrate if the condition $|h_{i\pm1} - h_i|$š$a$ is fulfilled, at each time ($t = 1$ red particles, $t = 2$ blue particles...).

### 6.2.3 Other processes and universality classes

There exists a lot of microscopic processes that leads to the same scaling limit of the EW and KPZ equation. But not all the processes fall into this two classes. Another class is governed by the Mullins-Herring equation

$$\partial_t h = -\kappa \partial_x^4 h + \xi(x,t), \tag{6.37}$$

where $\xi$ is a gaussian white noise. This equation is particularly useful in the context of molecular beam epitaxy (see [14] for an overview). We do not want to enter into these details but let us just stress that one microscopic process that gives this equation in the scaling limit is the so-called Wolf-Villain process described on Fig. 6.4. To include some surface relaxation, we allow the deposited particle to diffuse along the surface up to a finite distance, stopping when it finds the position with the lowest height. As we shall see later, those three equations (EW, MH and KPZ) are the main classes of non-disorder interface growth processes. They define three universality classes defined by a set of critical exponents that we shall briefly detailed in the following.

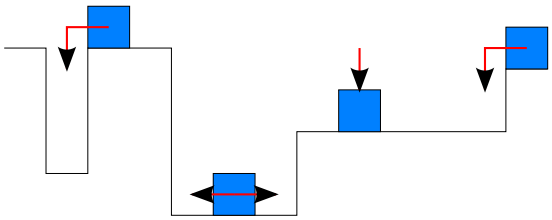

Figure 6.4: Wolf-Villain process on a one-dimensional substrate

## 6.3 Critical behavior

Interface growth processes are dynamical, out of equilibrium phenomena that can be described by Langevin equations for a "order parameter" (in that case the height $h(x,t)$). Contrary to equilibrium (or non-equilibrium) critical phenomena, there is no strict phase transition in these models but a critical behavior of fluctuations. As we said before, the concept of renormalization apply in these problems leading to different universality classes for interface growth processes. The language of usual critical phenomena is then used in a broader sense, and the notion of universality class of interface can be defined.

### 6.3.1 Langevin equation and scaling properties

In this chapter, we shall briefly recall some of the main critical features of interface growth equations. The simplest non-trivial equation describing the fluctuation of an interface due to deposition-relaxation process is, as we have seen before, the Edwards-Wilkinson equation

$$\partial_t h(x,t) = \nu \partial_x^2 h(x,t) + \eta(x,t), \tag{6.38}$$

where $\eta$ is a gaussian white noise,

$$\langle \eta(x,t) \rangle = 0 \tag{6.39}$$
$$\langle \eta(x,t)\eta(x',t') \rangle = 2D\delta(x-x')\delta(t-t'). \tag{6.40}$$

This equation is the continuum limit of a many microscopic processes and its resolution is very simple du to the linearity of the equation. The resolution leads to a set of critical exponents which characterize the EW universality class. The scaling hypothesis is a powerful tool to find critical exponents very easily, in the case of fractal interface, we rescale the height, and the space-time as follows

$$x \to x' = bx \tag{6.41}$$
$$t \to t' = b^z t \tag{6.42}$$
$$h \to h' = b^\alpha h, \tag{6.43}$$

where $\alpha, z$ are two exponents which characterize the universality class of the growth process. The statistical properties of the interface must be unchanged under this transformation. The EW

equation reads

$$\partial_t h(x,t) - \nu\nabla^2 h(x,t) = \eta(x,t). \tag{6.44}$$

After the transformation, it becomes

$$b^{\alpha-z}\partial_t h(x,t) - b^{\alpha-2}\nu\nabla^2 h(x,t) = b^{-z/2-d/2}\eta(x,t), \tag{6.45}$$

$$\partial_t h(x,t) - b^{z-2}\nu\nabla^2 h(x,t) = b^{z/2-d/2-\alpha}\eta(x,t). \tag{6.46}$$

The invariance of the equation under this transformation enforces

$$b^{z-2}\nu\nabla^2 h(x,t) + b^{z/2-d/2-\alpha}\eta(x,t) = \nu\nabla^2 h(x,t) + \eta(x,t), \tag{6.47}$$

gives us the values of $z$ and $\alpha$

$$\alpha = \frac{2-d}{2} \tag{6.48}$$

$$\beta = \frac{2-d}{4} \tag{6.49}$$

$$z = 2, \tag{6.50}$$

which leads in $1d$, to $\beta = 1/4$, $z = 2$ and $\alpha = 1/2$. Let us notice that the upper critical dimension of the EW equation is $d_c = 2$, where $\alpha = \beta = 0$. The value of $d_c$ for KPZ equation is not clear, and very controversial, opinions vary between $d_c = 2.4$ and $d_c = \infty$. In the random deposition process, each particle falls on a single site on the top of the surface and it sticks irreversibly. A a result of the relaxation process, the final interface will be smooth compared to a model without relaxation. This process generates correlations among the neighboring heights, which leads to an entire correlated interface and resulting in the saturation of the interface. Numerical simulations of a system of size $L$ with periodic boundary conditions give the following scaling behavior

$$w_L(t) = \int \mathrm{d}x \sqrt{\langle h(x,t)^2\rangle - \langle h(x,t)\rangle^2} = L^\alpha f(tL^{-z}), \tag{6.51}$$

where $f$ is a scaling function which interpolates between short times $t << L^z$

$$\lim_{u\to 0} f(u) = u^\beta, \tag{6.52}$$

and long times $t >> L^z$ with the asymptotic behavior

$$\lim_{u\to\infty} f(u) = \mathrm{cst}, \tag{6.53}$$

which means that $w(t) \sim t^\beta$ for a time smaller than the correlation time $L^z$ and reaches the saturation value for time bigger than the correlation time. This asymptotic form of the scaling function called the Family-Viczek scaling impose relation between exponents

$$z = \frac{\alpha}{\beta}. \tag{6.54}$$

This relation is valid for any equation satisfying the Family-Viczek scaling.

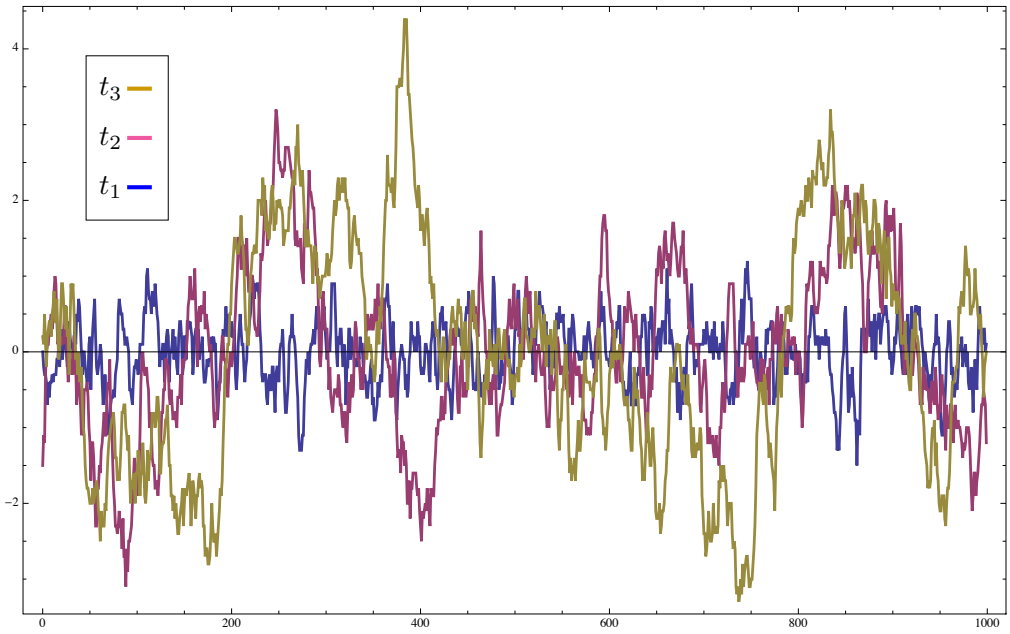


Figure 6.5: $h - \langle h \rangle$ in the Kim-Kosterlitz process for 3 different times $t_1 < t_2 < t_3$ of size $L = 1000$ with periodic boundary conditions.

### 6.3.2 Field theory formalism and ageing phenomena

The field theory describing a growth process like the Edwards-Wilkinson or the Kardar-Parisi-Zhang equation is very well known. The Janssen-De dominicis action is given by

$$\boxed{S[h,\bar{h}] = \int \mathrm{d}^d x \int \mathrm{d}t \; \bar{h} \; (\partial_t h + \frac{\delta H[h]}{\delta h}) - \nu \bar{h}^2} \tag{6.55}$$

where $-H[h]$ is the Ginsburg-Landau hamiltonian which may content all the possible derivatives and nonlinear terms and we note $x$ the $d$-dimensional spatial vector. We define the 2-point spacio-temporel correlations function by

$$C(x,y,t,s) = \langle h(x,t) h(y,s) \rangle, \tag{6.56}$$

and the 2-point spatio-temporel response function by

$$R(x,y,t,s) = \lim_{h \to 0} \frac{\delta h(x,t)}{\delta j(y,s)} = \langle h(x,t) \bar{h}(y,s) \rangle. \tag{6.57}$$

Let us point out the fact that the field $\bar{h}$ has no real physical meaning, except the property that its correlation with $h(x,t)$ gives the response function. The corresponding Langevin equation which can be derive from the action by integration over the response field $\bar{h}$ is

$$\partial_t h + \frac{\delta H[h]}{\delta h} = \eta, \tag{6.58}$$

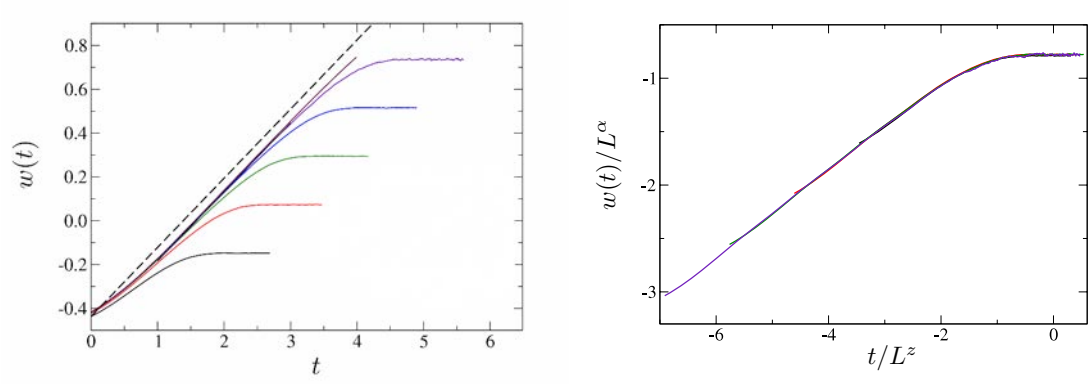


Figure 6.6: Numerical simulation of the Family process showing the Family Viczek scaling

with the following definition of the noise

$$\langle \eta(x,t) \rangle = 0 \tag{6.59}$$

$$\langle \eta(x,t)\eta(x',t') \rangle = 2D\delta(t-t')(x-x'). \tag{6.60}$$

The form of the $H[h]$ is fully determined by the symmetries of the process. The translation invariance along the growth direction ($h \to h + \delta h$) implies that the action must be constructed from combination of $\nabla h$, $\nabla^2 h$, ...$\nabla^n h$. The translation invariance under the perpendicular direction to the growth direction ($x \to x + \delta x$) excludes dependence in $x$. If we are in a periodic geometry, we must have the rotation symmetry $x \to -x$, so all the terms like $\nabla h$, $\nabla(\nabla^2 h)$ go away. And finally, the symmetry $h \to -h$ rules out terms like $(\nabla h)^{2p}$. So in order to find the correct action for our process, we have to pay attention of all the symmetries of the process and exclude all the terms which break them. This method coming from the field theory machinery is very efficient to find out what action describes a microscopic process and is significantly faster than the microscopic derivation of the corresponding Langevin equation. Nevertheless, we will see in the next chapter that this method does not give any information about what happens to an interface when one considers close (non-periodic) boundary conditions.

### 6.3.3 KPZ equation

Here we used these field theory arguments to write the correct action governing the KPZ interface. The KPZ process respects all these symmetries excepted $h \to -h$, which is related to the non-equilibrium nature of the growth, so the minimal action is

$$S[h,\bar{h}] = \int \mathrm{d}^d x \int \mathrm{d}t\ \bar{h}\big(\partial_t \phi - \nu\nabla^2 h - \frac{\mu}{2}\big(\nabla h\big)^2\big) - \nu\bar{h}^2, \tag{6.61}$$

which corresponds to the KPZ equation

$$\partial_t h = \nu\nabla^2 h + \frac{\mu}{2}\big(\nabla h\big)^2 + \eta(x,t). \tag{6.62}$$

The KPZ equation is known to describe a wide range of phenomena [86, 146, 14] and admits the exact critical exponents $z = 3/2$, $\beta = 1/3$ and $\alpha = 1/2$. These exponents in $1d$ has been found using a dynamical variation of the renormalization group [119]. Recently the $1d$ KPZ equation has been also shown to be exactly solvable (integrable in some sense) [34, 187, 186] and even more recently, an extension to a semi-infinite system has been studied [85]. In the case of the KPZ equation in any dimension, a new kind of symmetry can be found, which is

$$h \to h' = h + \epsilon x, \tag{6.63}$$

$$x \to x' = x - \frac{\mu}{2}\epsilon t, \tag{6.64}$$

$$t \to t' = t, \tag{6.65}$$

where $\epsilon$ is an infinitesimal angle. The consequence is the relation between exponents

$$\alpha + z = 2, \tag{6.66}$$

which holds in any dimensions. In the special case of $1d$, the action is also invariant under the time reversal symmetry which leads to the fluctuation-dissipation theorem. All the terms like $(\nabla\phi)^4)$ or $(\nabla\phi)^6)$ are irrelevant in the renormalization group sense. Of course, if we choose $\mu = 0$ then we recover the Edwards-Wilkinson action

$$S[h, \bar{h}] = \int \mathrm{d}^d x \int \mathrm{d}t \; \bar{h}\big(\partial_t h - \nu\nabla^2 h\big) - \nu\bar{h}^2, \tag{6.67}$$

which is invariant under the $h \to -h$ transformation, that telling us that the EW equation is a dynamical equilibrium growth process.

**Box 15** (Some relations between KPZ equation and RMT)**.**

In this small digression, let us mention that the concept of universality class in stochastic integrable systems possesses some new features that are absent from usual equilibrium universality classes. One interesting feature is that the KPZ universality class which is characterized by the set of exponents $\alpha, \beta, z$ is not enough to define the complete universality nature of the process, and several processes can have the same set of exponents but still be different. This difference lives in the full probability distribution of the field (here the height $h$ of the interface), and three different universality classes in the "exponent universality" has been defined. In the past years, a lot of results in that direction has emerged in connection with random matrix theory (see [70] for a nice introduction on relation between growth models and random matrices). Indeed, exact solutions of the KPZ equation has been found ([34, 187, 186] to cite a few), and probability distributions are now available for different geometries (*cf.* for a review from the mathematical side). Let us take the case of KPZ with flat initial condition, the rescaled distribution of the height is surprisingly asymptotically equal the distribution of the largest eigenvalue in the gaussian orthogonal ensemble (GOE) of random matrices and would be different for circular geometry (namely one found the GUE ensemble). These results are not just a funny mathematical structure, but a very profound result that has actually been verified with high precision in fascinating experiments on crystal liquids [198] and one sends the reader to the very nice review [199] covering both experimental and theoretical advances.

CHAPTER 7

# Boundary interface growth processes

## Contents

## 7.1 Interface growth near a boundary

Here we continue the analogy between usual critical phenomena and growth interface equations. We have seen that the concept of universality class (the "exponent" universality) is rather similar to the universality class in equilibrium (or non-equilibrium) critical phenomena. From this perspective, one question that we may ask is about the robustness of this universality when we are dealing with boundaries. In the case of equilibrium magnetic systems like Ising, Heisenberg or generally $\mathcal{O}(n)$ models, it is known that the critical behavior close to a boundary can drastically change, and even have consequences for the bulk critical properties leading to new phase transitions like the special and exceptional transitions. The purpose of this chapter is to try to understand how to describe an interface, like the EW or KPZ interface, not on a periodic substrate but on a finite non-periodic one. In order to find the proper equation to analyze, we will use the same microscopic derivation we have presented in the past chapter to describe the scaling limit of the height of the process. The presentation follows closely the original paper [8].

### 7.1.1 Introduction to the problem

Here, we are interested in how a boundary in the substrate may affect the properties of the interface. For a system on the half-line $x \geq 0$ with a boundary at $x = 0$, space-translation-invariance is broken and both $\langle h(t,x)\rangle$ and $w(t,x)$ depend on the distance $x$ from the boundary. Still, one expects that deep in the bulk $x \gg 1$, the width $w(t,x)$ should converge towards the bulk roughness $w^2(t,x) \sim_{x\to\infty} w^2_\infty(t) = w^2_{\exp,\infty}(t)$. For finite values of $x$, however, the precise properties of the width $w(t,x)$ will depend on the precise boundary conditions not contained in global quantities such as $w_L(t)$ and $w_{\exp,L}(t)$. These studies usually begin by prescribing some fixed boundary conditions and then proceed to analyze the position-dependent interface, often through the height profile. In this work, we start from the situation where particles are deposited on a bounded substrate and first ask how the deposition rules become modified in the vicinity of the boundary as compared to deep in the bulk. Generically, bulk models of particle-deposition select first a site on which one attempt to deposit a particle, often followed by a slight redistribution of the particle in the vicinity of the initially selected site, where the details of these rules lead to the numerous recognised universality classes [14, 86, 146]. If one conceives of the boundary as a hard wall which the particles cannot penetrate, those particles which would have to leave the system are kept on the boundary site. Restricting this study for simplicity to a semi-infinite system in $d = 1$ space dimensions, this suggests the *boundary condition* $h_0(t) \geq h_1(t)$, where $h_i(t)$ is the local height on the site $i \geq 0$ such that the boundary occurs at $i = 0$.

Another motivation of this work comes from the empirical observation that Family-Viczek scaling must be generalized in that *global* and *local* fluctuations with different values of $\beta$ are to be distinguished [181]. Furthermore, the experimentally measured values of $\beta$ [158, 153, 84, 130, 52] are larger than those expected in many simple model systems [14, 86, 146]. In certain cases, these enhanced values of $\beta$ are experimentally observed together with a grainy, *faceted morphology of the interfaces* and furthermore, a cross-over in the effective value of $\beta$ from small values at short times to larger values at longer times is seen.

We study the influence of a substrate boundary on a growing interface by analyzing the simplest case of a single boundary in a semi-infinite system, with the condition $h_0(t) \geq h_1(t)$. It is left for future work to elucidate any possible direct relevance for anomalous roughening. First, we

shall study the semi-infinite $1d$ Edwards-Wilkinson (EW) model [62], whose bulk behavior is well-understood from an exact solution. We shall write down a physically correct Langevin equation in semi-infinite space which includes this new kind of boundary contribution. Its explicit exact solution, of both the height profile as well as the site-dependent interface width, will be seen to be in agreement with a large-scale Monte Carlo (MC) simulations. It turns out that there exists a surprisingly large intermediate range of times where the model crosses over to a new fixed point, with an effective and non-trivial surface growth exponent $\beta_{1,\text{eff}} > \beta$, which is qualitatively analogous to the experiments cited above. However, at truly large times, typically above the diffusion time, the system converts back to the FV scaling, as expected from the bulk RG [150]. Second, in order to show that these observations do not come from the fact that the Langevin equation of the EW model is linear, we present numerical data for a model in the universality class of the semi-infinite $1d$ Kardar-Parisi-Zhang (KPZ) equation [119]. We find the same qualitative results as for the EW class, with modified exponents. We point out that the time scales needed to see these cross-overs are considerably larger than those studied in existing experiments.

### 7.1.2 Deposition-relaxation process with a boundary

In this section we want to generalize the deposition-relaxation process that we have presented in the periodic boundary conditions case in the previous chapter, for a non-translational invariant situation. We have in mind to build a deposition process on the semi-infinite line ($i = 1, 2...$) with some wall at the origin. There are many possibilities to this process, but we want to do the

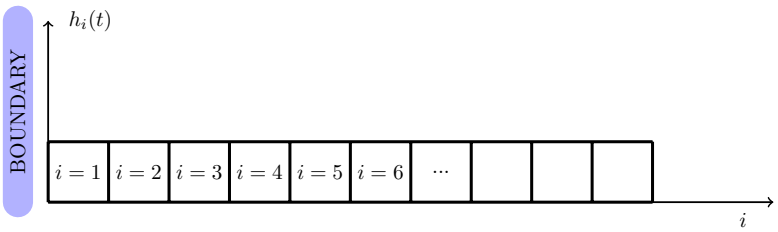


Figure 7.1: Etat initial plat d'un processus de croissance semi-infini

simplest thing possible, *i.e.* the process in the bulk has to be the same as for the periodic case, and the presence of the wall is purely geometric and do not add some other physical phenomena. To be clear, we need to express the transition rates when particles fall down close to the wall. The rules is that the wall is impenetrable, which means that a particle which deposit in $i = 1$ can stick to this site or move to $i = 2$ with some rates but not diffuse to $i = 0$. In that particular model, the only rates that will change are those in $i = 1$ and $i = 2$ and all the others will be the same, we will use the notation $\tilde{\omega}$ for rates which are different from the periodic case. With those notations the rates $\omega_1^0$ and $\omega_1^d$ in $i = 1$ and $i = 2$ will be For more generality we can assume a small transition $\epsilon$

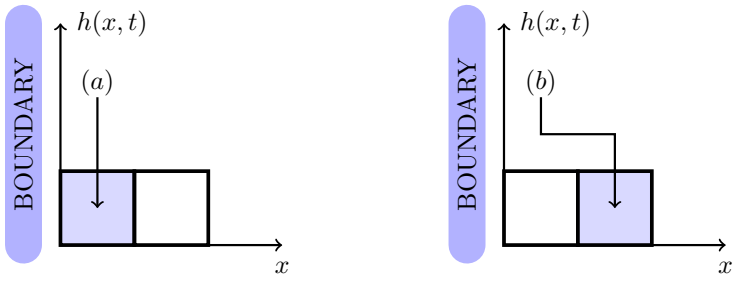


Figure 7.2: Modification of the transition rates close to the wall. Case $(a)$ corresponds to transition rate $\tilde{\omega}_1^{(0)}$ and case $(b)$ to $\tilde{\omega}_1^{(d)}$.

from $i = 1$ to $i = 0$, leading to a small flux of particles through the wall,

$$\tilde{\omega}_1^0 = \theta_{21}(1-\epsilon) \sim \mathcal{O}(1) \tag{7.1}$$

$$\tilde{\omega}_1^d = (1-\epsilon)\hat{\theta}_{21} + \frac{\epsilon}{2}\hat{\theta}_{21} \sim \mathcal{O}(1), \tag{7.2}$$

$$\tilde{\omega}_1^g = \epsilon\theta_{21} + \frac{\epsilon}{2}\hat{\theta}_{21} \sim \mathcal{O}(\epsilon), \tag{7.3}$$

$$\tilde{\omega}_0^d = \epsilon\theta_{10} + \frac{\epsilon}{2}\hat{\theta}_{10} \sim \mathcal{O}(\epsilon). \tag{7.4}$$

In the limit $\epsilon \to 0$, one recover $\tilde{\omega}_1^0 = \theta_{21}$, $\tilde{\omega}_1^d = \hat{\theta}_{21}$ for a hard-wall and $\tilde{\omega}_1^g = \tilde{\omega}_0^d = 0$. All the others transition rates remain the same

$$\omega_i^0 = \theta_{i+1,i}\theta_{i-1,i}, \tag{7.5}$$

$$\omega_i^g = \theta_{i+1,i}\hat{\theta}_{i-1,i} + \frac{1}{2}\hat{\theta}_{i-1,i}\hat{\theta}_{i+1,i}, \tag{7.6}$$

$$\omega_i^d = \theta_{i-1,i}\hat{\theta}_{i+1,i} + \frac{1}{2}\hat{\theta}_{i+1,i}\hat{\theta}_{i-1,i}, \tag{7.7}$$

with the proper normalization $\sum \omega_i = 1 \; \forall i > 1$ and $\sum \tilde{\omega}_1 = 1$. Now that all the rates are explicitly written, on can write down the Langevin equation as in the previous chapter for every site from $i = 1, 2...$

$$\frac{\mathrm{d}h_1}{\mathrm{d}t} = \Gamma a\Big[\tilde{\omega}_1^0 + \omega_2^g + \tilde{\omega}_0^d\Big] + \eta_1(t), \tag{7.8}$$

$$\frac{\mathrm{d}h_2}{\mathrm{d}t} = \Gamma a\Big[\omega_2^0 + \omega_3^g + \tilde{\omega}_1^d\Big] + \eta_2(t), \tag{7.9}$$

$$\frac{\mathrm{d}h_{i>2}}{\mathrm{d}t} = \Gamma a\Big[\omega_i^0 + \omega_{i+1}^g + \tilde{\omega}_{i-1}^d\Big] + \eta_i(t), \tag{7.10}$$

which can be put in a single equation valid for every site $i$

$$\frac{\mathrm{d}h_i}{\mathrm{d}t} = \Gamma a\Big[M_i^{(1)} + \big(\Delta\tilde{\omega}_1^{(0)} + \Delta\tilde{\omega}_0^{(d)}\big)\delta_{i,1} + \Delta\tilde{\omega}_1^{(d)}\delta_{i,2}\Big] + \eta_i(t), \tag{7.11}$$

where $\Delta\tilde{\omega} := \tilde{\omega} - \omega$, correspond to corrective terms du to the boundary. Explicitely

$$\Delta\tilde{\omega}_1^{(0)} = \tilde{\omega}_1^{(0)} - \omega_1^{(0)} = \theta_{21}(1-\epsilon) - \theta_{21}\theta_{01} = \theta_{21}(1-\epsilon-\theta_{01}), \tag{7.12}$$

$$\Delta\tilde{\omega}_1^{(d)} = \tilde{\omega}_1^{(d)} - \omega_1^{(d)} = (1-\epsilon)\hat{\theta}_{21} + \frac{\epsilon}{2}\hat{\theta}_{21} - \theta_{01}\hat{\theta}_{21} + \frac{1}{2}\hat{\theta}_{21}\hat{\theta}_{01}, \tag{7.13}$$

$$\Delta\tilde{\omega}_0^{(d)} = \tilde{\omega}_0^{(d)} - \omega_0^{(d)} = \epsilon\theta_{10} + \frac{\epsilon}{2}\hat{\theta}_{10} - \theta_{-10}\hat{\theta}_{10} + \frac{1}{2}\hat{\theta}_{10}\hat{\theta}_{-10}. \tag{7.14}$$

The term $\Delta\tilde{\omega}_0^{(d)}$ is not relevant here because it is acting on the other side of the wall and it is of order $\epsilon$ (indeed for a hard wall $\epsilon \to 0$, the probability to cross the wall is zero) while the two other terms $\Delta\tilde{\omega}_1^{(0)}$ and $\Delta\tilde{\omega}_1^{(d)}$ are of order 1. Then one can simply write

$$\begin{aligned}
\frac{\mathrm{d}h_i}{\mathrm{d}t} &= \Gamma a\Big[M_i^{(1)} + \big(\Delta\tilde{\omega}_1^{(0)} + \Delta\tilde{\omega}_0^{(d)}\big)\delta_{i,1} + \Delta\tilde{\omega}_1^{(d)}\delta_{i,2}\Big] + \eta_i(t), \\
&= \Gamma a\Big[M_i^{(1)} + \big(\Delta\tilde{\omega}_1^{(0)} + \Delta\tilde{\omega}_0^{(d)}\big)\delta_{i,1} + \Delta\tilde{\omega}_1^{(d)}\delta_{i,2} + \Delta\tilde{\omega}_1^{(d)}\delta_{i,1} - \Delta\tilde{\omega}_1^{(d)}\delta_{i,1}\Big] + \eta_i(t), \\
&= \Gamma a\Big[M_i^{(1)} + \big(\Delta\tilde{\omega}_1^{(0)} + \Delta\tilde{\omega}_0^{(d)} + \Delta\tilde{\omega}_1^{(d)}\big)\delta_{i,1} + a\Delta\tilde{\omega}_1^{(d)}\frac{\delta_{i,2}-\delta_{i,1}}{a}\Big] + \eta_i(t).
\end{aligned} \tag{7.15}$$

We put this equation is that following form in order to make transparent the fact that this equation is exactly the same as for the periodic case (the term $M_i^{(1)}$ is the same, and also the noise) up to terms that act locally on the boundary. Let us notice that, the first in $\delta_{i,1}$ act on the boundary site $i = 1$ and the second term act between $i = 1$ and $i = 2$. This last term will be absent when we will consider the same protocol for the Kim-Kosterlitz process because there are no diffusion in the definition of the rates.

### 7.1.3 Continuum Langevin equation

It is possible to analyze the scaling limit $a \to 0$ of the last equation in a general way. The idea is that, in the continuum limit where $\delta_{i,1}/a \to \delta(x)$, the equation will look like

$$\partial_t h(x,t) = v + \nu\big[\hat{M}h(x,t) + \hat{P}_0 h(0,t)\delta(x) + \hat{Q}_0 h(0,t)\delta'(x)\big] + \eta(x,t), \tag{7.16}$$

where $\hat{M}, \hat{P}_0, \hat{Q}_0$ are differential operators. The form of the 3 operators is fully determined by the symmetry of the process. The translation invariance along the growth direction ($h \to h+\delta h$) implies that the action must be constructed from combinations of $\partial h$, $\partial^2 h$, $...\partial^n h$. In a semi-infinite process, the translation invariance under the perpendicular direction to the growth direction ($x \to x + \delta x$) is broken, then dependence in $x$ is allowed. Same thing for the rotation symmetry $x \to -x$, so all the terms like $\partial h$, $\partial(\partial^2 h)$ are possible. And finally The symmetry $h \to -h$ rules out terms like $(\partial h)^{2p}$ for an equilibrium interface but are allowed for non equilibrium process. For example the KPZ process respects all this symmetries excepted $h \to -h$, which is related to the non equilibrium nature of the growth, finally

$$\begin{aligned}
\hat{M} &= \hat{M}(x, x^2...\partial_x h, \partial_x^2 h...(\partial_x h)^2, (\partial_x h)^4...) \\
\hat{P}_0 &= \hat{P}_0(x, x^2...\partial_x h_0, \partial_x^2 h_0...(\partial_x h_0)^2, (\partial_x h_0)^4...) \\
\hat{Q}_0 &= \hat{Q}_0(x, x^2...\partial_x h_0, \partial_x^2 h_0...(\partial_x h_0)^2, (\partial_x h_0)^4...).
\end{aligned} \tag{7.17}$$

In the following we will forget about the term $\hat{Q}_0$ which is of high-order and not relevant for a phenomenological discussion. One considers now the discrete Langevin equation that we obtain Eq. (7.15) and the aim is to write an continuum version of this equation for the behavior of the interface in this setup The hypothesis is to choose the interface flat behind the wall $i < 1$ *i.e.*

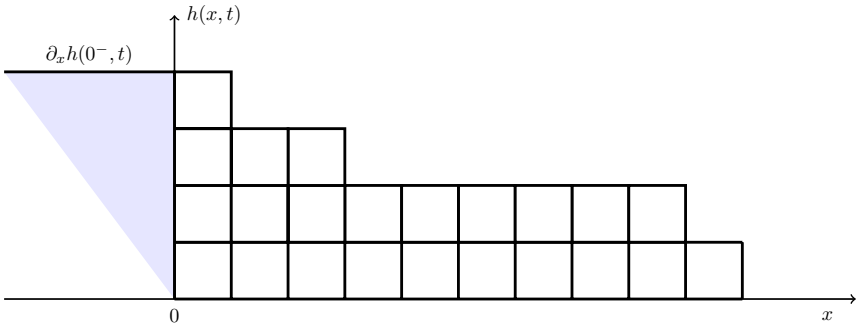


Figure 7.3: Boundary condition of the interface

$\theta_{10} = \theta_{-10} = 1$ ($h'_-(0) = 0$ in the continuum limit), one can show that, at order $a^3$ the only remaining term is $\theta_{21} \to [1 - ac_1 h'_+(0)]$, where $h'_+(0)$ is the right derivative in $x = 0$. Finally, the continuum equation for the evolution of the interface close to a wall will take the following form

$$\partial_t h(x,t) = \nu \partial_x^2 h(x,t) + \nu(\mu_1 + \mu_2 h'(0,t))\delta(x) + \eta(x,t). \tag{7.18}$$

In that case the operators of equation Eq. (7.16) are $\hat{M} = \partial_x^2$, $\hat{P}_0 = \mu_1 + \mu_2 \partial_x$ et $\hat{Q}_0 = 0$. We do not give the expressions of $\mu_1$ and $\mu_2$ in terms of microscopic parameters for the same reason that we mentioned in the previous chapter, and prefer to see this equation as a phenomenological equation that we will compare to numerical simulations.

## 7.2 Exact solution of the model and numerical comparison

In this section, the exact solution of the model is presented by mean of a spatial Laplace transform. It leads to the following form for the evolution of the height $h(x,t)$

$$\partial_t h(x,t) = \nu \partial_x^2 h(x,t) + \nu\big(\mu_1 + \mu_2 h_1(t)\big)\delta(x) + \eta(x,t), \tag{7.19}$$

where we have defined $h_1(t) = \partial_x h(x = 0, t)$ and $\eta$ is the same gaussian white noise as usual. If, however, one wishes to model thermal equilibrium interface fluctuations, one has to consider white noise with the Einstein relation $D = 2\nu k_B T$ where $T$ is the temperature and $k_B$ the Boltzmann constant. In the following, we take $\nu = k_B = 1$. In order to solve this PDE we impose the initial condition $h(x, t = 0) = 0$, meaning that we start with a flat interface at $t = 0$ and let the system evolve according to (Eq. (8.1)). The evolution equation is linear then we can solve it by an integral transformation.This holds in a co-moving frame with the average interface deep in the bulk (such that $\langle h(t,\infty)\rangle = 0$). Furthermore, $\nu$ is the diffusion constant, $\kappa_1$ can be considered as an external

source at the origin and one defines $h_1(t) := \partial_x h(t,x)|_{x=0}$. Indeed, taking the noise average of Eq. (8.1) and performing a space integration over the semi-infinite chain, we find that

$$\nu^{-1}\partial_t \int_0^\infty \mathrm{d}x h(t,x) = \kappa_1 + (\kappa_2 - 1)h_1(t). \tag{7.20}$$

We take $\kappa_2 = 1$ since this corresponds to the simplest condition of a constant boundary current $\nu\kappa_1\delta(x)$. The centered Gaussian noise has the variance $\langle \eta(t,x)\eta(t',x')\rangle = 2\nu T\delta(t-t')\delta(x-x')$, where $T$ is an effective temperature. Parameters $\nu$, $\kappa_1$, and $T$ are material-dependent constants and initially, the interface is flat $h(0,x) = 0$. With respect to the well-known description of the bulk behavior, the new properties come from the boundary terms on the r.h.s. of eq. (Eq. (8.1)). In contrast to earlier studies [210], the local slope $h_1(t)$ is not *a priori* given, but must be found self-consistently.

### 7.2.1 Laplace transform and exact solution

We define the spatial Laplace operator $\mathcal{L}_x$ as

$$\mathcal{L}_x.h(x,t) = h_p^*(t) = \int_{\mathbb{R}^+} \mathrm{d}x\ \mathrm{e}^{-px} h(x,t), \quad p \geqslant 0, \tag{7.21}$$

and the inverse Laplace transform

$$\mathcal{L}_p^{-1}.h_p^*(t) = h(x,t) = \frac{1}{2i\pi}\int_{-i\infty}^{i\infty} \mathrm{d}p\ \mathrm{e}^{px} h_p^*(t), \quad x \geqslant 0, \tag{7.22}$$

given the following moments of the noise $\eta(x,t)$ in the $p$-space

$$\begin{aligned}\langle \eta_p^*(t)\eta_q^*(s)\rangle &= \int_0^\infty \mathrm{d}p \int_0^\infty \mathrm{d}q\ \mathrm{e}^{px-qy}\ \langle \eta(x,t)\eta(y,s)\rangle \\ &= 2T\delta(t-s)\int_0^\infty \mathrm{d}p \int_0^\infty \mathrm{d}q\ \mathrm{e}^{px-qy}\ \delta(x-y) \\ &= 2T\frac{\delta(t-s)}{p+q},\end{aligned} \tag{7.23}$$

and transforming the partial differential equation into differential equation

$$\begin{aligned}\mathcal{L}_t.\partial_x^2 h(x,t) &= \int_{\mathbb{R}^+} \mathrm{d}x\ \mathrm{e}^{-px}\partial_x^2 h(x,t) \\ &= [\mathrm{e}^{-px}\partial_x h(x,t)]_0^\infty + \int_{\mathbb{R}^+} \mathrm{d}x\ p\mathrm{e}^{-px}\partial_x h(x,t) \\ &= -\partial_x h(x,t)_{x=0} + [p\mathrm{e}^{-px}h(x,t)]_0^\infty + p^2\int_{\mathbb{R}^+} \mathrm{d}x\ \mathrm{e}^{-px}h(x,t) \\ &= -h'(0,t) - ph(0,t) + p^2 h^*(p,t),\end{aligned} \tag{7.24}$$

with the assumption

$$\lim_{x\to\infty} \mathrm{e}^{-px}h(x,t) = \lim_{x\to\infty} \mathrm{e}^{-px}h'(x,t) = 0 \quad \forall t,p \in \mathbb{R}^+. \tag{7.25}$$

Now we start the resolution of (8.1) using Laplace transform, the initial condition $h(x,t)_{t=0}=0$, reduces the system to

$$\partial_t h_p^*(t) = p^2 h_p^*(t) - h'(0,t) - ph(0,t) + (\mu_1 + \mu_2 h'(0,t)) + \eta_p^*(t). \tag{7.26}$$

In order to solve this non-homogenous differential equation, we use an ansatz for the solution

$$h_p^*(t) = \mathrm{e}^{-px}\tilde{h}_p^*(t), \tag{7.27}$$

such that

$$\mathrm{e}^{-px}\partial_t\tilde{h}_p^*(t) = -ph(0,t) + \mu_1 + (\mu_2 - 1)h'(0,t) + \eta_p^*(t), \tag{7.28}$$

putting this ansatz in the evolution equation gives

$$\tilde{h}_p^*(t) = \tilde{h}_p^*(t=0) + \int_0^t \mathrm{d}\tau\ \mathrm{e}^{-p^2\tau}\{-ph(0,t) + \mu_1 + (\mu_2-1)h'(0,t) + \eta_p^*(t)\}, \tag{7.29}$$

where $\tilde{h}_p^*(t=0)=0$ because of the initial condition $h(x,t=0)=0$, then

$$\tilde{h}_p^*(t) = \int_0^t \mathrm{d}\tau\ \mathrm{e}^{-p^2\tau}\{-ph(0,t) + \mu_1 + (\mu_2-1)h'(0,t) + \eta_p^*(t)\}. \tag{7.30}$$

From now on, we will use the short hand notation $h_0 = h(0,t)$ and $h_0' = h'(0,t)$ and define

$$\zeta_p^*(t) = \int_0^t \mathrm{d}\tau\ \ \mathrm{e}^{p^2(t-\tau)}\eta_p^*(t), \tag{7.31}$$

and we can write the solution for the Laplace transform of the height as the sum of a pure noisy zero-averaged term plus a second term

$$h_p^*(t) = \zeta_p^*(t) + \int_0^t \mathrm{d}\tau\ \mathrm{e}^{-p^2(t-\tau)}\{(\mu_2-1)h_0'(\tau) - ph_0(\tau) + \mu_1\}. \tag{7.32}$$

The Inverse Laplace transform of $h_p^*(t)$ can be solved easily as function of the initial condition $h_p^*(t=0)$. Then the inverse transform of $h_p^*(t)$ is obtained by integrating over $p$ in the complex plane along the imaginary axis, leading to Gaussian integrals, and we obtain, for the general solution of $h(t,x)$

$$h(x,t) = \zeta(x,t) + \int_0^t \mathrm{d}\tau \frac{1}{\sqrt{4\pi(t-\tau)}}\big((\mu_2-1)h_0'(\tau) + \mu_1 + h_0(\tau)\frac{x}{2(t-\tau)}\big)\mathrm{e}^{\frac{-x^2}{4(t-\tau)}}. \tag{7.33}$$

We can notice that the solution is a sum of two parts, a fully noisy part, which is the same one than in the classical EW equation, plus an another contribution coming from the boundary, which contains deterministic and noisy terms. The noise $\zeta(x,t)$ is define by

$$\begin{aligned}
\zeta(x,t) &= \frac{1}{2i\pi}\int_{-i\infty}^{i\infty}\mathrm{d}p\ \mathrm{e}^{px}\ \zeta_p^*(t) \\
&= \frac{1}{2i\pi}\int_{-i\infty}^{i\infty}\mathrm{d}p\int_0^t \mathrm{d}\tau\ \ \mathrm{e}^{-p^2(t-\tau)}\mathrm{e}^{px}\ \eta_p^*(\tau) \\
&= \frac{1}{2\pi}\int_{-\infty}^{\infty}\mathrm{d}q\int_0^t \mathrm{d}\tau\ \ \mathrm{e}^{iqx-q^2(t-\tau)}\ \eta_{iq}^*(\tau),
\end{aligned} \tag{7.34}$$

or in a different form

$$\zeta(x,t) = \int_0^t \frac{\mathrm{d}\tau}{\sqrt{4\pi(t-\tau)}} \int_0^\infty \mathrm{d}u \hat{\mathrm{E}}\eta(u,\tau) \exp\frac{-(x-u)^2}{4(t-\tau)}$$
$$= \int_0^t \int_0^\infty \mathrm{d}\tau\, \mathrm{d}u\ \mathrm{K}(x-u,t-\tau)\eta(u,\tau).$$

Let's notice that the previous expression is solution of the standard Edwards-Wilkinson equation on the half-space $x \geqslant 0$. The 2-point spacio-temporal correlations function can be computed

$$\langle \zeta(t,x)\zeta(t',x')\rangle = 2T \int_0^{\min(t,t')} \mathrm{d}\tau \int_0^\infty \mathrm{d}u\ \mathrm{K}(x-u,t-\tau)\mathrm{K}(x'-u,t'-\tau) \tag{7.35}$$
$$= \frac{T}{2\sqrt{\pi}} \int_0^{\min(t,t')} \frac{\mathrm{d}\tau}{\sqrt{(t+t'-2\tau)}} \left[1 + \mathrm{erf}\left(\frac{(t-\tau)x' + (t'-\tau)x}{2\sqrt{(t-\tau)(t'-\tau)(t+t'-2\tau)}}\right)\right] \exp\left(\frac{-(x-x')^2}{4(t+t'-2\tau)}\right),$$

where we have defined the heat kernel by

$$\mathrm{K}(x,t) := \frac{\exp\left(-x^2/4t\right)}{\sqrt{4\pi t}}, \tag{7.36}$$

which is the unique Green function of the diffusion equation. Now we also define an other function $\mathrm{B}(x,t,\tau)$ which depends on the boundary condition

$$\mathrm{B}(x,t,\tau) = \big(\mu_1 + (\mu_2 - 1)h_0'(\tau) + h_0(\tau)\frac{x}{2(t-\tau)}\big), \tag{7.37}$$

in order to rewrite the solution as

$$h(x,t) = \int_0^t \mathrm{d}\tau \int_0^\infty \mathrm{d}u\ \mathrm{K}(x-u,t-\tau)[\eta(u,\tau) + \delta(u)\mathrm{B}(t,\tau)]. \tag{7.38}$$

Finally, by using space Laplace-transform on the boundary Edwards-Wilkinson equation, we were able to find the full solution. It appears that this solution is of course depending on the gaussian white noise $\eta(x,t)$ but also on two boundary conditions, the height of the interface in $x = 0$ *ie* $h_0(t)$ and its first spatial derivative $h_0'(t)$. To completely determine the solution, we have to found the values of those two quantities, this will be done in the next section, using a self-consistence method.

**Self-consistent solution**

The general solution depends on two unknown functions $h(t,0) =: h_0(t)$ and $\partial_x h(t,0) =: h_0'(t)$ which can be determined by self-consistency. Considering in the following initial conditions where $h(0,x) = 0$, $h_0(t)$ and the derivative $h_0'(t)$ can be obtained from (7.38) after analyzing carefully the limit $x \to 0$. Indeed, taking directly the derivative of (7.38) inside the integrals and putting afterwards $x = 0$ leads to divergences due to non-analicity, which can be taken care of by first a change of variable $u = (t-\tau)/x^2$ in the integrals

$$h(t,x) = \int_0^{t/x^2} \mathrm{d}u\, \frac{\mathrm{e}^{-1/(4u)}}{\sqrt{4\pi u}} \left[x\mu_1 + x(\mu_2 - 1)h_0'(t-ux^2) + \frac{1}{2u}h_0(t-ux^2)\right] + \zeta(t,x). \tag{7.39}$$

Expanding (7.39) formally in series functions $h_0'(t-ux^2)$ and $h_0(t-ux^2)$ for $x$ small, we can perform the integrations over $u$ for each term of the expansion and express them with the help of the incomplete Gamma functions. Then, using the series expansion for parameter $\lambda := x^2/(4t)$, $\Gamma(a,\lambda) \simeq \Gamma(a) - \lambda^a/a$, we can isolate terms up to order one in $x$ (the next terms of the gamma expansion are proportional to $x^2$ and can be discarded)

$$h_0(t) = 2\left(\mu_1\sqrt{\frac{t}{\pi}} + (\mu_2-1)\int_0^t \frac{\mathrm{d}\tau}{\sqrt{4\pi\tau}} h_0'(t-\tau) + \zeta(t,0)\right), \tag{7.40}$$

$$h_0'(t) = -\frac{2}{\mu_2+1}\left(\frac{\mu_1}{2} - \frac{h_0(t)}{\sqrt{4\pi t}} + \frac{1}{4\sqrt{\pi}}\int_0^t \frac{\mathrm{d}\tau}{\tau^{3/2}}\left[h_0(t-\tau)-h_0(t)\right] + \partial_x\zeta(t,0)\right).$$

We obtain a system of two integro-differential equations which has a very simple solution for the simple case $\mu_2 = 1$, for which

$$h_0(t) = 2\left(\mu_1\sqrt{\frac{t}{\pi}} + \zeta(t,0)\right), \tag{7.41}$$

$$h_0'(t) = -\mu_1 - \frac{\zeta(t,0)}{\sqrt{\pi t}} + \partial_x\zeta(t,0) + \frac{1}{2\sqrt{\pi}}\int_0^t \frac{\mathrm{d}\tau}{\tau^{3/2}}\left[\zeta(t-\tau,0)-\zeta(t,0)\right].$$

Since $\langle\zeta(x,t)\rangle = 0\ \forall x,t \geqslant 0$ we found the following scaling for the mean height and mean slope at the boundary, $\langle h_0(t)\rangle \sim \sqrt{t}$ and $\langle h_0'(t)\rangle \sim t^0$.

### 7.2.2 Mean profile of the interface

Here we are going to compute the mean profile created by the boundary condition, by computing the inverse transform of the mean solution $\langle h_p^*(x)\rangle$ for all the possible different cases. This mean field calculation will be useful in order to determine the shape of the solution close to the boundary and to inform us about the evolution of correlations in the process. We know that the interface will create some perpendicular and parallel correlations, which increase on time, $L_\perp(t) \sim t^{1/\gamma}$ and $L_\parallel(t) \sim t^{1/z_\parallel}$ where $z_\parallel = z$ is the standard dynamical exponent and $\gamma$ is the $\perp$-direction dynamical exponent, which characterize correlation length in the growing direction. An asymptotic scaling law for the mean profile can be written as

$$\langle h(x,t)\rangle \sim t^{1/\gamma}\ \Psi(x/\xi(t)), \tag{7.42}$$

where $\Psi(u)$ is a scaling function to determine, which is constant for $u=0$ and has to decrease to zero for time bigger $t^{1/z}$. The same kind of scaling function can be written for the derivative of the profile,

$$\partial_x\langle h(x,t)\rangle = \frac{t^{1/\gamma}}{\xi(t)}\partial_u\Psi(u) \sim t^\rho\ \Phi(x/\xi(t)), \tag{7.43}$$

with $L_\parallel(t)$ scale identically in the two functions $\Psi(u)$ and $\Phi(u)$, and $\rho = 1/\gamma - 1/z$, then $h_0'(t) \sim t^\rho$. Those two scaling hypothesis should be valid no matter what kind of growth process we look at, hence the mean profile of boundary MH or boundary KPZ equation takes also this scaling form, and contact angle could be found, knowing the value of $\gamma$ and $z$. Now lets try to found the form of the scaling function $\Psi(\lambda)$ using the equation (8.1) and the scaling form

$$\langle h(x,t)\rangle \sim t^{1/\gamma}\Psi\Big(\frac{x}{t^{1/z}}\Big). \tag{7.44}$$

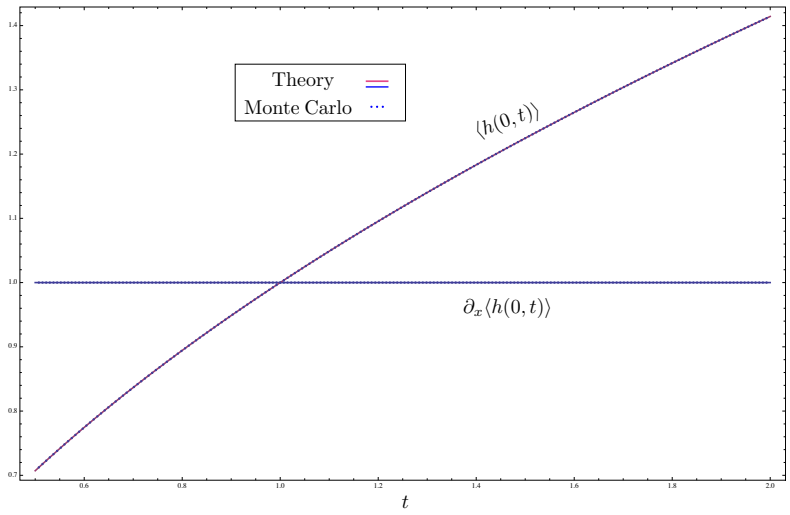


Figure 7.4: Numerical evidence for the scaling $\langle h(0,t)\rangle \sim t^{1/2}$ and $\partial_x\langle h(0,t)\rangle \sim t^0$ using the boundary deposition relaxation process

Putting this scaling ansatz in the $b$-EW equation gives

$$\frac{1}{\gamma}\Psi(\lambda) - \frac{1}{z}\lambda\Psi'(\lambda) = t^{1-2/z}\Psi''(\lambda) + t^{1-1/z-1/\gamma}\mu_1\delta(\lambda) + t^{1-2/z}\Psi'(0)\delta(\lambda), \tag{7.45}$$

where $\lambda = x^2/4t$ is the scale free diffusion parameter. The only solution to cancel all the temporal dependance is to choose $z = \gamma = 2$ to obtain

$$\langle h(x,t)\rangle \sim t^{1/2}\Psi(\lambda). \tag{7.46}$$

We shall notice that we recover the standard dynamical exponent $z = 2$, characteristic of the Edwards-Wilkinson equation meaning that the boundary does not affect it, as we expected regarding other phenomena like directed percolation or magnetic critical dynamics. In addition we found that the height at boundary scale as $\langle h_0(t)\rangle \sim \sqrt{t}$ and its derivative as $\langle h_1(t)\rangle \sim t^0$. The scaling function $\Psi(\lambda)$ is governed by the equation

$$\Psi''(\lambda^2) + \frac{\lambda^2}{2}\Psi'(\lambda^2) - \frac{1}{2}\Psi(\lambda^2) + \mu_1\delta(\lambda^2) + \Psi'(0)\delta(\lambda^2) = 0, \tag{7.47}$$

which has a simple solution

$$\Psi(\lambda) = \Psi_0(\mathrm{e}^{-\lambda} - \sqrt{\pi\lambda}\,\mathrm{erfc}\,\sqrt{\lambda}). \tag{7.48}$$

This scaling function decrease exponentially to zero and we recover the flat interface for $\lambda > 1$. The scaling hypothesis $\langle h(x,t)\rangle = \sqrt{t}\ \Psi(\lambda)$ we have found is in very good agreement with the Monte-Carlo simulations and the next step will be to show rigorously this scaling by exact computation of the mean height of the boundary EW equation.

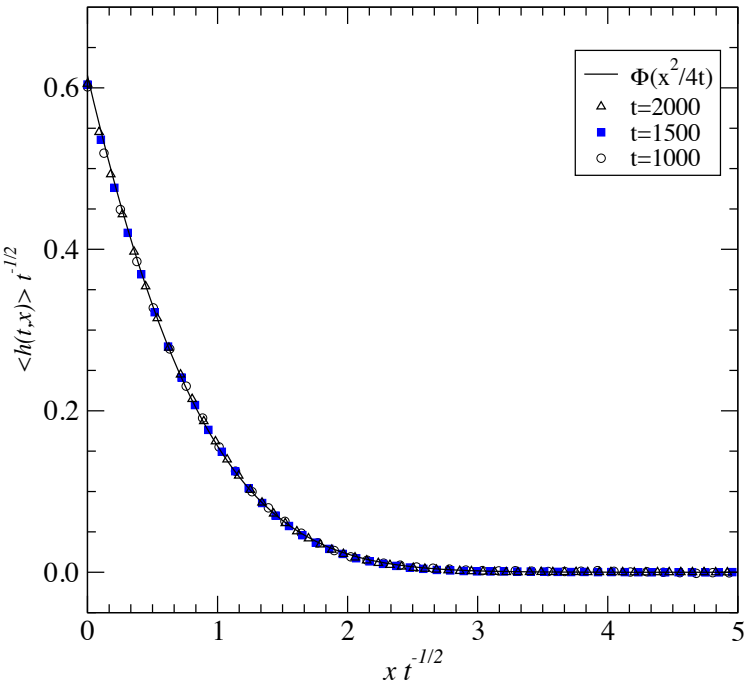


Figure 7.5: Mean profile simulated by the deposition-relaxation algorithm. The data are obtained for a system of size $L = 10^4$ and averaged over $2.10^5$ realizations.

**Exact solution**

The resolution of the boundary EW equation gives us the exact form of the height

$$h(x,t) = \int_0^t \mathrm{d}\tau \int_0^\infty \mathrm{d}u \ \mathrm{K}(x-u, t-\tau)[\eta(u,\tau) + \delta(u)\mathrm{B}(x,t,\tau)], \tag{7.49}$$

where $\langle \eta(x,t)\rangle = \langle \zeta(x,t)\rangle = 0$, then the mean solution is given by

$$\begin{aligned} \langle h(x,t)\rangle &= \int_0^t \mathrm{d}\tau \ \langle f(x,t,\tau)\rangle \int_0^\infty \mathrm{d}u \ \mathrm{K}(x-u,t-\tau)\delta(u), \\ &= 2\int_0^t \mathrm{d}\tau \ \mathrm{K}(x,t-\tau)\langle \mathrm{B}(x,t,\tau)\rangle, \end{aligned} \tag{7.50}$$

which can be written, after some variable changes

$$\begin{aligned} \langle h(x,t)\rangle = \frac{t^{1/2}}{\sqrt{4\pi}} \int_\lambda^\infty \mathrm{d}u \frac{\lambda^{1/2}}{u^{3/2}} \big((\mu_2 - 1)h_0'(t(1-\lambda u^{-1})) + \mu_1\big)\mathrm{e}^{-u}, \\ + \frac{1}{\sqrt{4\pi}} \int_\lambda^\infty \mathrm{d}u \frac{1}{u^{1/2}} h_0(t(1-\lambda u^{-1}))\mathrm{e}^{-u}. \end{aligned} \tag{7.51}$$

Using the expressions of $h_0(t)$ and averaging over the noise, we obtain the profile of height after integrating over the remaining variable

$$\langle h(x,t)\rangle = \frac{\mu_1 t^{1/2}}{\sqrt{4\pi}}\Gamma(-1/2,\lambda), \tag{7.52}$$

where $\lambda = x^2/4t$. Using the expression of the Gamma function

$$\Gamma(-1/2,\lambda) = 2\big(\frac{\mathrm{e}^{-\lambda}}{\sqrt{\lambda}} - \sqrt{\pi}\,\mathrm{erfc}\,\sqrt{\lambda}\big), \tag{7.53}$$

we obtain the final result

$$\langle h(x,t)\rangle = \frac{\mu_1}{\sqrt{\pi}} t^{1/2}\big(\mathrm{e}^{-\lambda} - \sqrt{\pi\lambda}\,\mathrm{erfc}\,\sqrt{\lambda}\big). \tag{7.54}$$

We can notice that our choice $\mu_1 = 1$ help us to recover the correct scaling of the mean height.

### 7.2.3 Fluctuation of the height of the interface

Monte-Carlo simulations suggest that fluctuations of the interface does not have the exact behavior when we studies a process with or without boundary. For a periodic boundary conditions growth process, the width $w(x,t)$ of the interface does not depend on the position $x$, and scale as $t^\beta$ before saturate at a time $t_{sat} \sim L^z$ and a value $w_{sat} \sim L^\alpha$. This regime is reach when the correlation length $\xi(t)$ of the interface becomes equal to the size $L$ of the system, after that the process becomes stationary. This scaling informations will be very useful in order to analyze what happens when we add a fix boundary in our systems. Simulations seems to confirm that exponents are the same close or far away from the boundary, but a crossover between two regimes appears on a time $t_c$ characterized by a anomal fluctuation of the interface. The new scaling is now quit different from the periodic case, because $w(x,t)$ become $x$-dependent and some corrections appears. The width of the interface changes at a time $t_c$ from a standard bulk behavior to a surface behavior when the correlation length of the systems $\xi(t) = x$ , where $x$ is the point where we measure the width. Consequently, this new regime appears at a time $t_c \sim x^z$ and at a value $w_c \sim x^\alpha$. The space-time width $w(t,x)$ is given by

$$w^2(t,x) = C(t,t,x,x) = \langle (h(t,x) - \langle h(t,x)\rangle)^2\rangle, \tag{7.55}$$

where, using the change of variable $v = 1/(4u)$ in (7.39),

$$h(t,x) - \langle h(t,x)\rangle = \frac{1}{\sqrt{\pi}}\int_\lambda^\infty \frac{\mathrm{e}^{-v}}{\sqrt{v}}\,\zeta(t-\lambda t/v,0) + \zeta(t,x). \tag{7.56}$$

$w^2(t,x)$ can be written as the sum of three terms,

$$w^2(t,x) = \sum_{i=1}^{3} w_i^2(t,x), \tag{7.57}$$

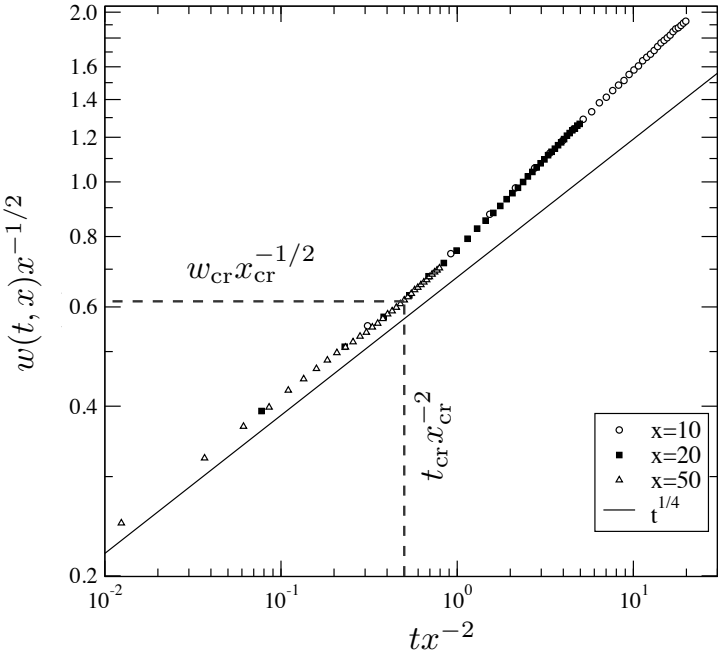


Figure 7.6: Width $w(x,t)$ simulated by the deposition-relaxation algorithm, we notice a clear variation relative to the standard scaling. The data are obtained for a system of size $L = 10^4$ and averaged over $2.10^5$ realizations.

using the expression of the two-point correlation function between the modified random noise (7.35), we found

$$\begin{aligned} w_1^2(t,x) &= \frac{1}{\pi}\int_\lambda^\infty\int_\lambda^\infty \mathrm{d}v\,\mathrm{d}v' \frac{\exp(-v-v')}{\sqrt{vv'}}\langle\zeta(t-t\lambda/v,0)\zeta(t-t\lambda/v',0)\rangle \\ &= \frac{T\sqrt{t}\lambda}{2\pi^{3/2}}\int_1^\infty \mathrm{d}v\int_1^\infty \mathrm{d}v' \frac{\exp(-\lambda v-\lambda v')}{vv'}\left\{\sqrt{2vv'-v-v'}-\sqrt{|v-v'|}\right\} \\ &= T\sqrt{t}\left[\frac{\sqrt{\lambda}}{\pi}\mathrm{Ei}(2\lambda)-(\sqrt{2}-1)\sqrt{\lambda}\,\mathrm{erfc}^2\,\lambda-\frac{1}{\sqrt{2\pi}}\mathrm{e}^{-\lambda}\,\mathrm{erfc}\,\sqrt{\lambda}\right], \end{aligned} \tag{7.58}$$

where $\mathrm{Ei}(x) = \int_{-x}^\infty \mathrm{d}u\ \ u^{-1}e^{-u}$ is the exponential integral,

$$\begin{aligned} w_2^2(t,x) &= \frac{2}{\sqrt{\pi}}\int_\lambda^\infty \mathrm{d}v\frac{\mathrm{e}^{-v}}{\sqrt{v}}\langle\zeta(t-t\lambda/v,0)\zeta(t,x)\rangle \\ &= \frac{T\sqrt{t\lambda}}{\pi}\int_1^\infty \mathrm{d}v\frac{\mathrm{e}^{-\lambda v}}{v}\int_1^v \frac{\mathrm{d}u}{\sqrt{1+u}}\left[1+\mathrm{erf}\left(\sqrt{\frac{(u-1)\lambda v}{u(1+u)}}\right)\right]\exp\left(-\frac{\lambda v}{1+u}\right), \end{aligned} \tag{7.59}$$

and

$$w_3^2(t,x) = \langle \zeta^2(t,x) \rangle = \frac{T\sqrt{t}}{\sqrt{8\pi}} \int_0^1 \frac{\mathrm{d}\tau}{\sqrt{\tau}} \left[ 1 + \mathrm{erf}\left( \sqrt{\frac{2\lambda}{\tau}} \right) \right] \tag{7.60}$$
$$= \frac{T\sqrt{t}}{\pi\sqrt{\lambda}} \{ \sqrt{\frac{\pi\lambda}{2}} - \lambda\gamma - \lambda\log(2) + 2\lambda - \lambda\log(\lambda) + \frac{2}{3}\lambda^2 \, {}_3F_3(1,1,\frac{3}{2};2,2,\frac{5}{2};-2\lambda) \}.$$

where ${}_3F_3(1,1,\frac{3}{2};2,2,\frac{5}{2};-2\lambda)$ is a generalized hypergeometric function. Then the width can be expressed in the form $w(t,x) = \sqrt{T} t^{1/4} \Phi_w(\lambda)$. The serie-expansion for $\lambda \ll 1$ gives for each term

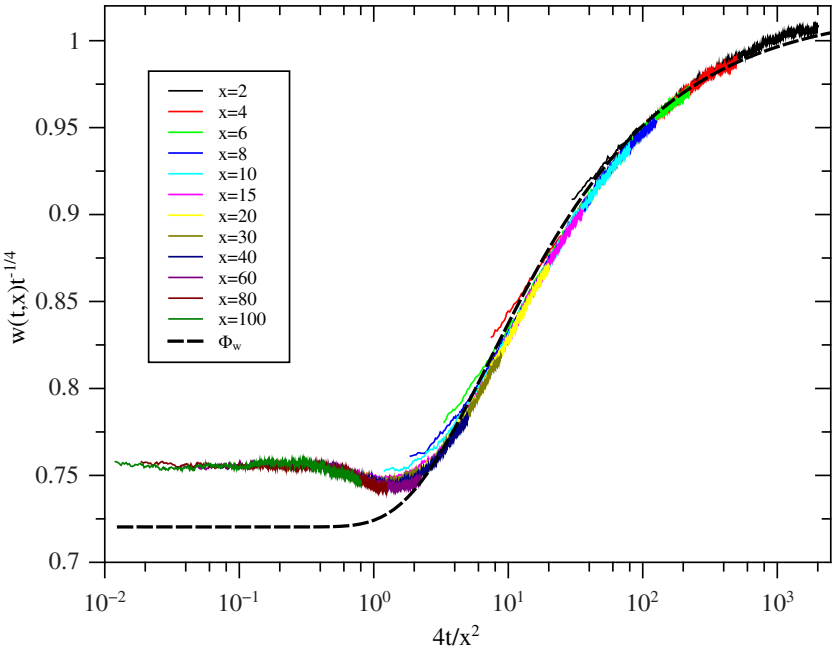


Figure 7.7: Effective correction to the exponent $\beta = 1/4$. The width scale as $w \sim t^{1/4}$ for short and long time, but a notable correction appears between the two regimes characterized by an effective exponent $\beta_{\text{eff}} \approx 0.31$.

$$w_1^2(t,x) \simeq T\sqrt{t} \left( \frac{1}{\sqrt{2\pi}} - \left[ \frac{\sqrt{2}}{\pi} + \frac{\sqrt{2}-1}{2} - \frac{1}{\pi}(\gamma + \log(2\lambda)) \right] \sqrt{\lambda} + \frac{3\sqrt{2}-4}{2\sqrt{\pi}} \lambda + O(\lambda^{3/2}) \right)$$
$$w_2^2(t,x) \simeq T\sqrt{t} \left[ \frac{2}{\sqrt{2\pi}} + \frac{\sqrt{\lambda}}{\pi} \left( \frac{\pi^2}{8} + \frac{\pi}{2} - 4\sqrt{2} + \gamma + \gamma\log(2) + \sqrt{2}\log(3+2\sqrt{2}) \right) \frac{\sqrt{\lambda}\log(\lambda)}{\pi} [1 + \log(2)] + O(\lambda) \right]$$
$$w_3^2(t,x) \simeq T\sqrt{t} \left( \frac{1}{\sqrt{2\pi}} + \frac{-\gamma + 2 - \log(2\lambda)}{\pi} \sqrt{\lambda} + O(\lambda^{3/2}) \right).$$

This sum of this three terms are compared to the numerical simulations on the Fig. 7.7 and a rather good match is found, specially out of the region of small $\lambda$.

### 2-times correlations

Two-time quantities have been shown in many circumstances to yield useful insights into the dynamical behavior of systems far from equilibrium. Of special interest are space and time dependent functions as for example the space-time response $R(t,s,x,y)$ or the height-height space-time correlation $C(t,s,x,y)$, which are both defined in the same way as for the magnetic systems considered before

$$C(t,s,x,y) = \langle h(t,x)h(s,y)\rangle - \langle h(t,x)\rangle\langle h(s,y)\rangle, \tag{7.61}$$

where the brackets indicate an average over the realization of the noise. In general, without assuming any space-time translation, $C$ can always be written as $C(t+s,t-s,x+y,x-y)$. The space-time response, defined by

$$R(t,s,x,y) = \lim_{j\to 0}\frac{\delta\langle h(t,x)\rangle}{\delta j(s,y)}, \tag{7.62}$$

measures the response of the interface at time $t$ and position $x$ to a small perturbation $j(s,y)$ at an earlier time $s$ and at a different position $y$. For reasons of causality we have $t > s$. At the level of the Langevin equation the perturbation enters through the addition of $j$ to the right hand side. In our semi-infinite model, spatial translation invariance in the direction parallel to the interface is broken, we have in general

$$\begin{aligned} C(t,s,x,y) &= C(t-s,t+s,x-y,x+y), \\ R(t,s,x,y) &= R(t-s,x-y,x+y). \end{aligned} \tag{7.63}$$

The response function depends only on $t-s$ because of causality of the response. The autocorrelation and auto-response functions are then defined by

$$\begin{aligned} C(t,s) &= C(t-s,x-y=0,x), \\ R(t,s) &= R(t-s,x-y=0,x). \end{aligned} \tag{7.64}$$

It is well known that the systems discussed here present a simple dynamical scaling behavior in the standard infinite model. For the two-time quantities one expects the same scaling behavior. For the auto-response and the autocorrelation functions we expect the scaling forms

$$\begin{aligned} C(t,s,x) &\sim s^{-b}F_C(|x|^z s^{-1}, ts^{-1}), \\ R(t,s,x) &\sim s^{-1-a}F_R(|x|^z s^{-1}, ts^{-1}). \end{aligned} \tag{7.65}$$

For the auto-response and the auto-correlation functions we expect the scaling forms which defines the non-equilibrium exponents $a$ and $b$. One ends up with the scaling relation $b = -2\alpha/z$, which relates $b$ to the known exponents $\alpha$ and $z$. In addition the scaling functions $F_C$ and $F_R$ define two additional exponents $\lambda_C$ and $\lambda_R$ by their asymptotic behavior. In the next section, we will see by exact computation if the scaling hypothesis above is correct, and how the two functions $F_R$ and $F_R$ looks like and how are they related to infinite scaling.

### Scaling of correlation functions

The 2-space time correlation function is defined as

$$C(t,s,x,y) = \big\langle (h(t,x) - \langle h(t,x)\rangle)(h(s,y) - \langle h(s,y)\rangle)\big\rangle. \tag{7.66}$$

The computation for the EW equation is rather tedious and not relevant for the understanding, we just write the solution and explore the consequences. The 2-space-time correlation function can be written as

$$C(t,s,x,y) = C(t-s,t+s)_\infty \Psi_C\Big(\frac{x-y}{\sqrt{4(t-s)}},\frac{x+y}{\sqrt{4(t+s)}},\frac{x+y}{\sqrt{4(t-s)}},\frac{x-y}{\sqrt{4(t+s)}}\Big)$$
$$\sim s^{-b} F_C\Big(\frac{t}{s}\Big)\Psi_C^{\text{asympt}}\Big(\frac{x-y}{\sqrt{s}},\frac{x+y}{\sqrt{s}}\Big). \tag{7.67}$$

The auto-correlation function then reads

$$C(t,s,0,x) := C(t,s,x) = C_\infty(t-s,t+s)\Psi_C\Big(\frac{t}{s},\frac{x}{\sqrt{4(t-s)}},\frac{x}{\sqrt{4(t+s)}}\Big) \tag{7.68}$$
$$\sim\ s^{-b} F_C\Big(\frac{t}{s}\Big)\Psi_C^{\text{asympt}}\Big(\frac{t}{s},\frac{x}{s^{1/z}}\Big),$$

where

$$C_\infty(t-s,t+s) = T(\sqrt{t+s}-\sqrt{t-s}). \tag{7.69}$$

This quantity $C_\infty(t-s,t+s)$ is the exact expression for 2-space-time correlation function in EW equation with periodic boundary conditions as we except.

**Scaling of the response function**

The space-time response, measures the response of the interface at time $t$ and position $x$ to a small perturbation $j(y,s)$ at an earlier time $s$ and at a different position $y$. For reasons of causality we have $t > s$. At the level of the Langevin equation the perturbation enters through the addition of $j$ to the right hand side. The response function, which results from a perturbation in the flux, can be viewed as the response of the system to the noise itself

$$R(x,y,t,s) = \lim_{j\to 0}\frac{\delta\langle h(x,t)\rangle}{\delta j(y,s)} = \Big\langle\frac{\delta h(x,t)}{\delta\eta(y,s)}\Big\rangle. \tag{7.70}$$

In order to compute the response of the interface to a small perturbation we add the term $j(\mathbf{x},t)$ to the right-hand side of the Langevin equation and then go to reciprocal space. In the infinite EW case the solution of the resulting equation is

$$\hat{h}(\mathbf{k},t) = \mathrm{e}^{-\nu\mathbf{k}^2 t}\int_0^t \mathrm{d}t\ \mathrm{e}^{-\nu\mathbf{k}^2 t'}(\hat{\eta}(\mathbf{k},t')+\hat{j}(\mathbf{k},t')). \tag{7.71}$$

Taking the functional derivative of and transforming back to real space yields the result

$$R(t,s,\mathbf{x}-\mathbf{y}) = \frac{(t-s)^{-d/2}}{(2\sqrt{\pi\nu})^d}\exp\frac{-(\mathbf{x}-\mathbf{y})^2}{4\nu(t-s)}.$$

In dimension $d = 1$, it gives

$$\boxed{R(t,s,x-y) = R(t-s,x-y) = \theta(t-s)\frac{(t-s)^{-1/2}}{(2\sqrt{\pi\nu})}\exp\frac{-(x-y)^2}{4\nu(t-s)}}$$

The solution of the boundary EW equation with $\nu = 1$ and $\mu_2 = 1$ is

$$h(x,t) = \zeta(x,t) + \int_0^t \mathrm{d}\tau \frac{1}{\sqrt{4\pi(t-\tau)}} \Big( (\mu_1 + h_0(\tau) \frac{x}{2(t-\tau)} \Big) \mathrm{e}^{\frac{-x^2}{4(t-\tau)}}. \tag{7.72}$$

where $\zeta(x,t)$ is a convolution of the noise $\eta(x,t)$ with the heat kernel

$$\begin{aligned} \zeta(x,t) &= \int_0^t \frac{\mathrm{d}\tau}{\sqrt{4\pi(t-\tau)}} \int_0^\infty \mathrm{d}u \hat{\mathrm{E}}\eta(u,\tau) \exp \frac{-(x-u)^2}{4(t-\tau)} \\ &= \int_0^t \int_0^\infty \mathrm{d}\tau \, \mathrm{d}u \; \mathrm{K}(x-u, t-\tau)\eta(u,\tau). \end{aligned}$$

where we have defined the heat kernel by

$$\mathrm{K}(x,t) := \frac{\exp\left(-x^2/4t\right)}{\sqrt{4\pi t}}, \tag{7.73}$$

Putting all together, we find

$$\begin{aligned} R(t,s,x,y) &= \theta(t-s)\mathrm{K}(x-y,t-s) + \theta(t-s) \int_0^{t-s} \frac{\mathrm{d}\tau}{\sqrt{4\pi(t-s-\tau)}} \frac{x}{t-s-\tau} \mathrm{e}^{-\frac{x^2}{4(t-s-\tau)} - \frac{y^2}{4\tau}} \\ &= \theta(t-s)\mathrm{K}(x-y,t-s) + \theta(t-s)\mathrm{K}(x+y,t+s) \\ &= \frac{\theta(t-s)}{\sqrt{4\pi(t-s)}} \exp \frac{-(x-y)^2}{4(t-s)} + \frac{\theta(t-s)}{\sqrt{4\pi(t-s)}} \exp \frac{-(x+y)^2}{4(t-s)}. \end{aligned} \tag{7.74}$$

Assuming $t > s$, one have

$$\begin{aligned} R(t,s,x,y) &= R(t-s, x-y, x+y) \\ &= R_\infty(t-s) \Psi_R\Big( \frac{x-y}{(t-s)^{1/z}}, \frac{x+y}{(t-s)^{1/2}} \Big) \\ &\sim s^{-1/2} F_R\Big(\frac{t}{s}\Big) \Psi_R^{\mathrm{asympt}}\Big( \frac{x-y}{s^{1/2}}, \frac{x+y}{s^{1/2}} \Big) \end{aligned} \tag{7.75}$$

We can choose $x = y$, and we obtain the auto-response function

$$\begin{aligned} R(t,s,x) &= \frac{1}{\sqrt{4\pi(t-s)}} \Big( 1 + \exp \frac{-4x^2}{4(t-s)} \Big) \\ &\sim s^{-1/2} F_R\Big(\frac{t}{s}\Big) \Psi_R^{\mathrm{asympt}}\Big( \frac{t}{s}, \frac{x}{\sqrt{s}} \Big) \\ &\sim s^{-1/2} \tilde{F}_R\Big(\frac{t}{s}\Big) \Phi_R^{\mathrm{asympt}}\Big( \frac{x}{\sqrt{s}} \Big), \end{aligned} \tag{7.76}$$

where $F_R(u) \sim u^{-\lambda_R/z}$ is the same scaling function as the infinite EW equation. Here we notice a scaling relation, since in the infinite EW case the auto-response is

$$R_\infty(t-s) = \frac{1}{\sqrt{4\pi(t-s)}} \sim s^{-a-1} F_R\Big(\frac{t}{s}\Big),$$

then the auto-response ($x = y$) function reads

$$\boxed{R(t,s,x) = R_\infty(t-s)\Psi_R\Big(\frac{x}{\sqrt{t-s}}\Big) \sim s^{-a-1}F_R\Big(\frac{t}{s}\Big)\Psi_R^{\text{asympt}}\Big(\frac{t}{s},\frac{x}{\sqrt{s}}\Big)}$$

The auto-response function does depend only on the time difference $R(t,s,x) = R(t-s,x)$ and not on $t+s$ as in the correlation case $C(t,s,x) = C(t+s,t-s,x)$, this difference comes from the causality nature of the response function. The scaling function $\Psi_R$ interpolates between the surface and the bulk and behaves as $\Psi_R(\infty) \sim \Psi_R(0) \sim$ cst.

**Summary of relations**

Generally speaking, we can write relations for quantities close to the boundary as the product of the same quantities on the bulk times scaling functions which interpolate between two regimes. We will not show here the explicit forms of the scaling functions for correlations for the sake of clarity. This scaling behaviors of the auto-response and auto-correlations seem to be similar to those of the width of the interface

$$\begin{aligned}
&t^{-1/\gamma}\langle h(t,x)\rangle = \langle h(t,x)\rangle_\infty \Psi_h\Big(\frac{x}{t^{1/z}}\Big) \sim \text{cst}\ \Psi_w^{\text{asympt}}\Big(\frac{x}{t^{1/z}}\Big) \\
&w(t,x) = w_\infty(t)\Psi_w\Big(\frac{x}{t^{1/z}}\Big) \sim t^\beta\ \Psi_w^{\text{asympt}}\Big(\frac{x}{t^{1/z}}\Big) \\
&C(t,s,x) = C_\infty(t-s,t+s)\Psi_C\Big(\frac{x}{(t+s)^{1/z}},\frac{x}{(t-s)^{1/z}}\Big) \sim s^{-b}F_C\Big(\frac{t}{s}\Big)\Psi_C^{\text{asympt}}\Big(\frac{t}{s},\frac{x}{s^{1/z}}\Big) \\
&R(t,s,x) = R_\infty(t-s)\Psi_R\Big(\frac{x}{(t-s)^{1/z}}\Big) \sim s^{-1-a}F_R\Big(\frac{t}{s}\Big)\Psi_R^{\text{asympt}}\Big(\frac{t}{s},\frac{x}{s^{1/z}}\Big)
\end{aligned} \tag{7.77}$$

to compare to the standard infinite scaling

$$\begin{aligned}
&\langle h(t,x)\rangle_\infty \sim \text{cst} \\
&w_\infty(t) \sim t^\beta \\
&C_\infty(t-s,t+s) \sim s^{-b}F_C(ts^{-1}) \\
&R_\infty(t-s) \sim s^{-1-a}F_R(ts^{-1}),
\end{aligned} \tag{7.78}$$

where $F_{C,R}(u) \sim u^{-\lambda_{C,R}/z}$ in the asymptotic limit. The infinite label refers to the scaling of the infinite equation and to the scaling limit $x/\sqrt{s} \to \infty$ as well, because we recover the standard behavior for short time or/and large distance. One define $\tilde{F}_{R,C}$ such that

$$C(t,s,x) \sim s^{-b}F_C\Big(\frac{t}{s}\Big)\Psi_C^{\text{asympt}}\Big(\frac{t}{s},\frac{x}{s^{1/z}}\Big) \sim s^{-b}\tilde{F}_C\Big(\frac{t}{s}\Big)\Phi_C^{\text{asympt}}\Big(\frac{x}{s^{1/z}}\Big) \tag{7.79}$$

$$R(t,s,x) \sim s^{-1-a}F_R\Big(\frac{t}{s}\Big)\Psi_R^{\text{asympt}}\Big(\frac{t}{s},\frac{x}{s^{1/z}}\Big) \sim s^{-1-a}\tilde{F}_R\Big(\frac{t}{s}\Big)\Phi_R^{\text{asympt}}\Big(\frac{x}{s^{1/z}}\Big). \tag{7.80}$$

## 7.3 Boundary KPZ equation

In this part, we want to continue the analysis of the growth of an interface close to a boundary in the case where the microscopic process belongs to the KPZ equation. We will use again the same machinery to derive the continuous equation for the height and study some of the properties using a combination of numerical simulations and scaling calculations.

### 7.3.1 Introduction and definition of the problem

It is very simple to add a boundary in the Kim-Kosterlitz process, we just need to take a semi-infinite lattice $i = 1, 2, 3, ...$ and just precise the rates to impose to the first site $i = 1$. In the

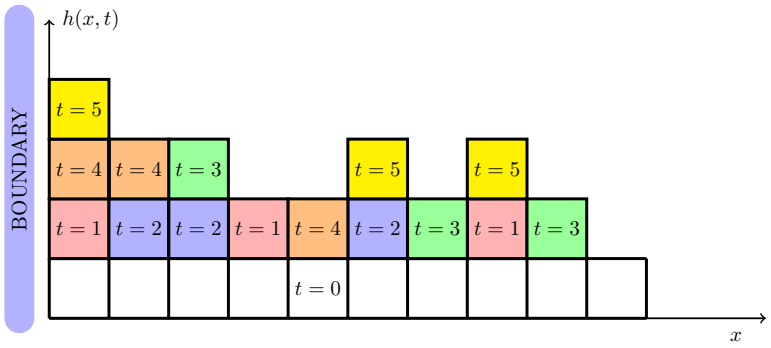


Figure 7.8: Kim-Kosterlitz algorithm with a boundary on a semi-infinite ($i = 1, 2, 3...$) substrate. The initial state at $t = 0$ is the white flat interface, then a fixed (3 in the figure) number of particles can reached the substrate if the condition $|h_{i\pm1} - h_i|$ša is fulfilled for $i > 1$ and $|h_2 - h_1|$ša for the site $i = 1$, at each time ($t = 1$ red particles, $t = 2$ blue particles...).

bulk $i \neq 1$ we use the same algorithm than in the standard periodic process, and at the origin, we just impose $h_0 > h_1$ such that we always have the condition in the left side of the wall, and a particle is dropped in $i = 1$ if the condition $|h_1 - h_2|$ša is fulfilled on the right side. In that case the boundary acts like a source of particle. In this process, we can argue that there is less restriction in the boundary than in the bulk. For all the site but $i = 1$ the equation in unchanged

$$\frac{\mathrm{d}h_{i>1}}{\mathrm{d}t} = \Gamma a\ \omega_i^{(0)} + \eta_i(t), \tag{7.81}$$

$$= \Gamma a\ \theta_{i+1,i}\theta_{i-1,i} + \eta_i(t), \tag{7.82}$$

and the modification for the site $i = 1$ is simply

$$\frac{\mathrm{d}h_1}{\mathrm{d}t} = \Gamma a\ \theta_{21}(1-\epsilon) + \eta_1(t) \tag{7.83}$$

$$= \Gamma a\ \tilde{\omega}_1^{(0)} + \eta_i(t), \tag{7.84}$$

where $\tilde{\omega}_1^{(0)}$ is the modified transition rate. Now we want to make clear the difference with the $i > 1$ case so we write the previous equation as

$$\frac{\mathrm{d}h_1}{\mathrm{d}t} = \Gamma a\big(\omega_1^{(0)} + \Delta\tilde{\omega}_1^{(0)}\big) + \eta_i(t), \tag{7.85}$$

where we define $\Delta\tilde{\omega}_1^{(0)} = \tilde{\omega}_1^{(0)} - \omega_1^{(0)}$ in such way that we can write down an equation for $i = 1, 2, 3...$ using $\delta_{ij} = 1$ if $i = j$ and 0 else

$$\frac{\mathrm{d}h_i}{\mathrm{d}t} = \Gamma a\big(\omega_i^{(0)} + \Delta\tilde{\omega}_i^{(0)}\delta_{i,1}\big) + \eta_i(t). \tag{7.86}$$

### 7.3.2 KPZ equation with a boundary

As for the EW case the equation is exactly the same for every $i > 1$ plus a correction term which acts locally on the boundary. Explicitely $\Delta\tilde{\omega}_1^{(0)} = \tilde{\omega}_1^{(0)} - \omega_1^{(0)} = \theta_{21}(1 - \epsilon - \theta_{01})$ After going to the limit $a \to 0$, we end up with the same form as for the EW case

$$\frac{\partial h}{\partial t} = \nu \frac{\partial^2 h}{\partial x^2} + \lambda \Big(\frac{\partial h}{\partial x}\Big)^2 + \nu \Big(\mu_1 + \mu_2 h_1(t)\Big)\delta(x) + \eta(x,t). \tag{7.87}$$

where $h_1(t) =: \frac{\partial h(x,t)}{\partial x}|_{x=0}$. The following result is exactly the KPZ equation plus the boundary term. As for the EW case, we will suppose $\mu_2 = 1$ and then fit the numerics with the parameters of the equation.

### 7.3.3 Scaling hypothesis and numerical results

This scaling calculation will be useful in order to have informations about the shape of the solution close to the boundary and about the evolution of correlations in the process. In the following, we shall proceed to the same analysis as we have done for the linear case. We suppose an asymptotic scaling law for the mean profile

$$\boxed{\langle h(x,t)\rangle \sim t^{1/\gamma}\Psi(x/\xi(t)}, \tag{7.88}$$

where $\Psi(u)$ is a scaling function to determine, which is constant for $u = 0$ and has to decrease to zero for time bigger $t^{1/z}$. The same kind of scaling function can be written for the derivative of the profile,

$$\partial_x \langle h(x,t)\rangle = \frac{t^{1/\gamma}}{\xi(t)} \partial_u \Psi(u) \sim t^{\rho}\ \Phi(x/\xi(t)), \tag{7.89}$$

with $\xi(t)$ scale identically in the two functions $\Psi(u)$ and $\Phi(u)$, and $\rho = 1/\gamma - 1/z$

$$\theta(t) = \partial_x \langle h(x,t)\rangle_{x=0}, \tag{7.90}$$

scale as $\theta(t) \sim t^{\rho}$. Those two scaling hypothesis should be valid no matter what kind of growth process we look at, hence the mean profile of boundary MH or EW equation (exact solution) takes also this scaling form

$$\begin{aligned} \langle h_0(t)\rangle &\sim t^{1/\gamma} \\ \langle h_1(t)\rangle &\sim t^{\rho}. \end{aligned} \tag{7.91}$$

Now let us try to determine phenomenologically the value of these two exponents. Let us start with the phenomenological boundary KPZ equation

$$\frac{\partial h}{\partial t} = \nu \frac{\partial^2 h}{\partial x^2} + \lambda \Big(\frac{\partial h}{\partial x}\Big)^2 + \nu \Big(\mu_1 + h_1(t)\Big)\delta(x) + \eta. \tag{7.92}$$

In the linear case $\lambda = 0$, the exact solution of the model gave us the following scaling law for the mean profile $\langle h(x,t)\rangle \sim t^{1/2}\Psi(xt^{-1/2})$, leading to $z = \gamma = 2$. In the KPZ case, we already know from a long time that $z = 3/2$, let us try to see if this exponent can be found with our scaling.

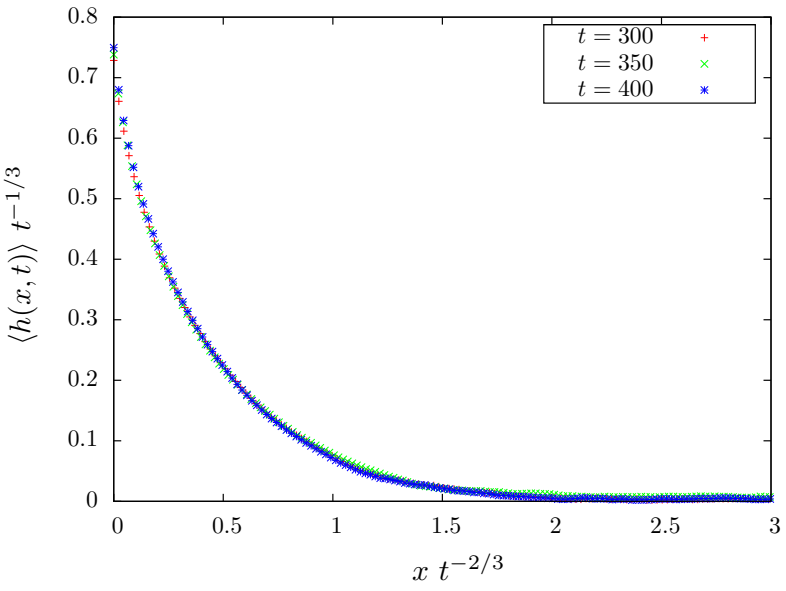


Figure 7.9: Numerical evidence for the scaling $\langle h(x,t)\rangle \sim t^{1/3}\ \Psi(xt^{-2/3})$ using the boundary RSOS process

The first thing to notice is that the mean value in the KPZ equation is not easy to take because of the non-linearity, the mean height value does not follow the noiseless KPZ equation because $\langle(\partial_x h)^2\rangle \neq (\partial_x\langle h\rangle)^2$. Let us forget this problem for a moment and consider this like a mean-field approximation and let see what we found with it. In order to find $z$ and $\gamma$, we just replace our scaling hypothesis $\langle h(x,t)\rangle \sim t^{1/\gamma}\ \Psi(xt^{-1/z})$ in the boundary KPZ equation, the result is

$$\frac{\Psi(\kappa)}{\gamma} + \kappa\Psi'(\kappa) = t^{-\frac{2}{z}+1}\Psi''(\kappa) + \frac{\lambda}{2}\Psi'(\kappa)^2 t^{\frac{1}{\gamma}-\frac{2}{z}+1} + (\mu_1 t^{-\frac{1}{z}-\frac{1}{\gamma}+1} + t^{-\frac{2}{z}+1}\Psi'(0))\delta(\kappa), \tag{7.93}$$

where $\kappa = xt^{-1/z}$ is the scaling variable and $\nu = 1$. To insure scaling invariance, naively one would expect that the last equation must be independent of time. However this procedure provides three scaling relations for two exponents. We proceed to argue that since the nonlinear part dominates over the surface tension, we can neglect the diffusion term.

$$-\frac{1}{z} - \frac{1}{\gamma} + 1 = 0 \tag{7.94}$$

$$\frac{1}{\gamma} - \frac{2}{z} + 1 = 0. \tag{7.95}$$

We thereby obtain $z = 3/2$ and $\gamma = 3$ leading to the scaling form for the mean profile of KPZ

$$\langle h(x,t)\rangle \sim t^{1/3}\ \Psi(xt^{-2/3}), \tag{7.96}$$

and $\rho = -1/3$ for the derivative of the mean profile

$$\partial_x\langle h(x,t)\rangle \sim t^{-1/3}\ \Phi(xt^{-2/3}). \tag{7.97}$$

| Model | $z$ | $\beta$ | $\alpha$ | $\gamma$ | $\rho$ |
|---|---|---|---|---|---|
| KPZ | 3/2 | 1/3 | 1/2 | 3 | $-1/3$ |
| EW | 2 | 1/4 | 1/2 | 2 | 0 |
| MH | 4 | 3/8 | 3/2 | 4/3 | 1/2 |

Table 7.1: Some exponents of several universality classes in $d = 1$ dimension.

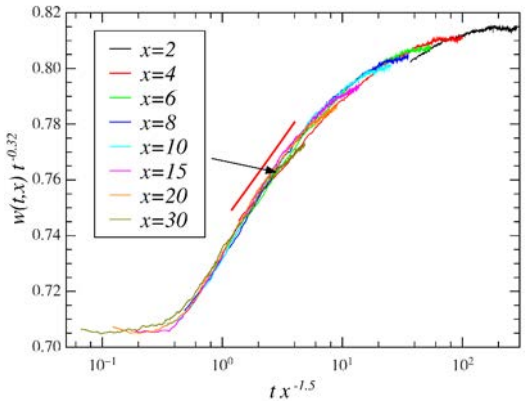


Figure 7.10: Time evolution of the local interface width $w(t, x)$, for several distances $x$ from the boundary, in the semi-infinite Kim-Kosterlitz process. The arrow indicates the location of the turning point and the slope of the straight line has the value 0.03.

We can notice that $\rho < 0$ for the KPZ equation, then $\langle h_1(t)\rangle \to 0$ meaning that the interface becomes flat for asymptotic times. The relation $1/\gamma - 1/z + 1 = 0$ is correct both for EW and KPZ to we can suppose that the relations

$$\gamma = \frac{z}{z-1} = \frac{\alpha}{\alpha - \beta}, \tag{7.98}$$

and

$$\rho = \frac{1}{\gamma} - \frac{1}{z} = \frac{\alpha - 2\beta}{\alpha}, \tag{7.99}$$

are correct for all growth processes with boundary. We can notice that the famous KPZ dynamical exponent is recover $z = 3/2$, and we can check numerically that the exponent $\gamma = 3$ is correct (see Fig. 7.9). We can test this scaling for other universality classes (see Fig. 7.1), in particular for the Mullins-Herring equation Eq. (6.37), we do not present these details here. Turning to the local width, our simulations give again a site-dependent behavior, with a crossover to an effective exponent $\beta_{\text{eff}} \approx 0.36$, larger than the bulk exponent $\beta \approx 0.32$. The scaling form $w(t, x)t^{-\beta}$ shown in Fig. 7.10 displays the same qualitative features as seen before in the EW model. This exemplifies that effective anomalous growth behavior may appear in non-linear (but non-disordered and local) growth processes.

## 7.4 Conclusions

In summary, in several semi-infinite lattice models of interface growth, the simple boundary condition $h_0(t) \geq h_1(t)$ on the heights on the two sites nearest to the boundary not only leads to non-constant and non-stationary height profiles but also to site-dependent roughness profiles. There exists a large range of times where effective growth exponents $\beta$ with values clearly larger than in deep in the bulk can be identified, in qualitative analogy with known experiments on growing interfaces [158, 130, 153, 84, 130, 52]. However, since we have concentrated on models defined in the simple geometry of a semi-infinite line with a single boundary, a quantitative comparison with the experiments, carried out on faceted growing surfaces with many interacting interfaces, may be premature. For non-disordered models with local interactions, the truly asymptotic growth exponents return to the simple bulk values, as predicted by the RG [150]. The unexpectedly complex behavior at intermediate times is only seen if appropriate boundary terms are included in the Langevin equation describing the growth process. The non-stationary height profiles are reminiscent of behavior found in systems undergoing physical ageing, which is known to occur in models describing interface growth [94]. Our results were obtained through the exact solution of the semi-infinite EW class and through extensive Monte-Carlo simulations of both profiles and widths in the EW and KPZ models. A scaling relation for the surface profile exponent $\gamma$ was proposed and is in agreement with all presently known model results.

CHAPTER 8

# Résumé en français de la partie II

## Propriétés critiques d'interfaces en croissance

Les processus de croissance d'interfaces sont des phénomènes dynamiques qui peuvent être décrits par des équations de Langevin pour un paramètre d'ordre (dans ce cas la hauteur $h(x,t)$). Contrairement aux phénomènes critiques d'équilibres, il n'y a pas de réelles transitions de phases dans ces modèles mais un comportement critique de fluctuations de l'interface.

### Dynamique d'interface et propriétés d'échelle

Un des cas le plus simple d'equation de croissance d'interface dû à un processus de deposition-relaxation, est l'équation de Edwards-Wilkinson

$$\partial_t h(x,t) = \nu \partial_x^2 h(x,t) + \eta(x,t), \tag{8.1}$$

ou $\eta$ est un bruit blanc gaussien

$$\langle \eta(x,t) \rangle = 0 \tag{8.2}$$
$$\langle \eta(x,t)\eta(x',t') \rangle = 2D\delta(x-x')\delta(t-t'). \tag{8.3}$$

Cette équation est la limite continue de nombreux processus microscopiques et sa résolution est très simple dû à la linéarité de l'équation. La résolution conduit à un ensemble d'exposants critiques qui caractérisent la classe d'universalité EW. L'hypothèse d'invariance d'échelle est un outil puissant pour trouver ces exposants très facilement. Dans le cas d'une l'interface fractale, nous redimensionnons la hauteur, et l'espace-temps comme suit

$$x \to x' = bx \tag{8.4}$$
$$t \to t' = b^z t \tag{8.5}$$
$$h \to h' = b^\alpha h, \tag{8.6}$$

où $\alpha, z$ sont deux exposants qui caractérisent la classe d'universalité du processus. Les propriétés statistiques de l'interface doivent être inchangés par cette transformation. L'équation EW s'écrit

$$\partial_t h(x,t) - \nu \nabla^2 h(x,t) = \eta(x,t). \tag{8.7}$$

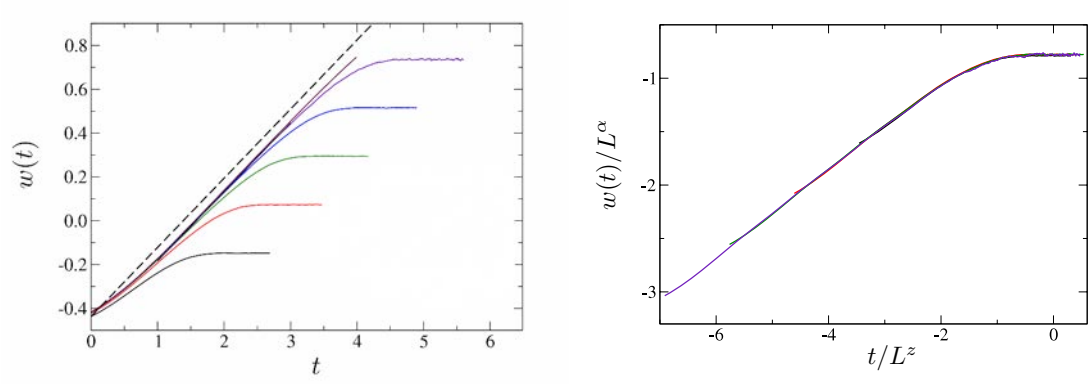


Figure 8.1: Comportement d'échelle de Family-Viczek

Après cette transformation dans l'équation ci-dessus on trouve $\beta = 1/4$, $z = 2$ and $\alpha = 1/2$. A la suite du processus de diffusion, l'interface se lisse par rapport à un modèle sans diffusion. Ce processus génère des corrélations entre les hauteurs voisines, ce qui conduit à une interface corrélée et qui entraîne une saturation de l'interface dû à la taille finie du système. Des simulations numériques d'un système de taille $L$ avec conditions périodiques montrent le comportement

$$w_L(t) = \int \mathrm{d}x \sqrt{\langle h(x,t)^2\rangle - \langle h(x,t)\rangle^2} = L^\alpha f(tL^{-z}), \tag{8.8}$$

où $f$ est une fonction qui interpole entre les temps courts $t << L^z$

$$\lim_{u\to 0} f(u) = u^\beta, \tag{8.9}$$

et les temps longs $t >> L^z$ avec le comportement asymptotique suivant

$$\lim_{u\to \infty} f(u) = \text{cst}. \tag{8.10}$$

Cette forme asymptotique de la fonction d'échelle, appelée relation de Familly-Viczek, impose la relation suivante entre les exposants

$$z = \frac{\alpha}{\beta}. \tag{8.11}$$

Cette relation est valable pour toute équation satisfaisant l'invariance d'échelle mentionnée auparavant.

### Equation de Kardar-Parisi-Zhang

L'équation KPZ s'écrit

$$\partial_t h = \nu \nabla^2 h + \frac{\mu}{2}\big(\nabla h\big)^2 + \eta(x,t). \tag{8.12}$$

Cette équation décrit un large spectre de phénomènes [86, 146, 14] et possède les exposants suivant $z = 3/2$, $\beta = 1/3$ et $\alpha = 1/2$ pour $d = 1$. Dans le cas de dimension arbitraire, une symétrie

particulière est trouvée

$$h \to h' = h + \epsilon x, \tag{8.13}$$

$$x \to x' = x - \frac{\mu}{2}\epsilon t, \tag{8.14}$$

$$t \to t' = t, \tag{8.15}$$

où $\epsilon$ est un angle infinitesimal. Une des conséquence est la relation $\alpha + z = 2$ valide en toute dimension.

### Croissance d'une interface près d'un bord

Ici nous voulons étudier le comportement d'une interface en présence d'un bord, notre modèle est décrit par l'équation suivante

$$\partial_t h(x,t) = \nu \partial_x^2 h(x,t) + \nu\big(\mu_1 + \mu_2 h_1(t)\big)\delta(x) + \eta(x,t), \tag{8.16}$$

où $h_1(t) = \partial_x h(x=0,t)$ and $\eta$ est le bruit blanc gaussien. Un ansatz d'échelle peut être postulé

$$\langle h(x,t)\rangle \sim t^{1/\gamma}\Psi\Big(\frac{x}{t^{1/z}}\Big). \tag{8.17}$$

$\Psi(u)$ est une fonction à déterminer, qui est constante pour $u = 0$ et décroit pour des temps supérieurs à $t^{1/z}$. La seule solution est de choisir $z = \gamma = 2$. La forme de la fonction $\Psi(\lambda)$ peut aussi être déduite et l'on trouve

$$\Psi(\lambda) = \Psi_0(\mathrm{e}^{-\lambda} - \sqrt{\pi\lambda}\,\mathrm{erfc}\,\sqrt{\lambda}). \tag{8.18}$$

Cette formule est en très bon accord avec les simulations et on peut montrer que cette solution est exacte. Les simulations Monte-Carlo suggèrent que les fluctuations de l'interface n'ont pas les

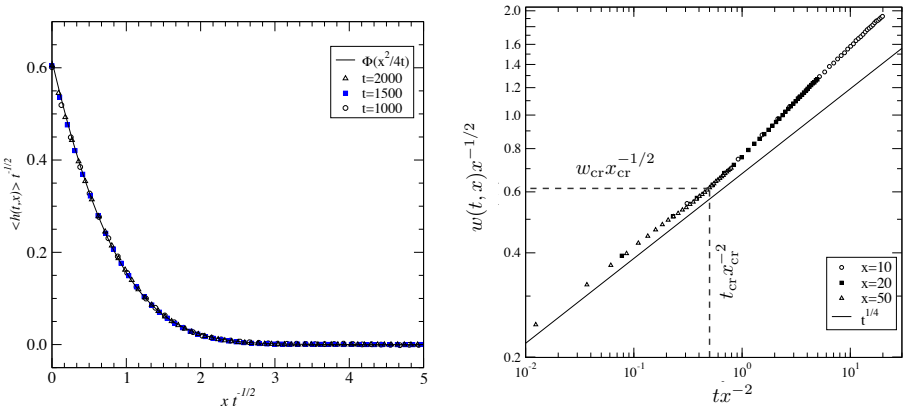


Figure 8.2: Gauche: Profil moyen de l'interface. Droite: Fluctuation $w(x,t)$, on remarque un écart significatif au comportement usuel

mêmes comportements quand on étudie le processus avec ou sans bord. Pour un processus de croissance avec conditions aux limites périodiques, la largeur $w(x,t)$ de l'interface ne dépend pas de la position $x$ et sature pour une valeur $w_{sat} \sim L^{\alpha}$. Ce régime est atteint lorsque la longueur de corrélation $\xi(t)$ de l'interface devient de l'ordre de grandeur de la taille $L$ du système. Le nouveau comportement d'échelle est maintenant assez différent du cas périodique, $w(x,t)$ devient maintenant fortement dépendant de la position. Le phénomène est explicite sur la figure ci-dessus et les détails sont exposés dans le texte principal. Le système montre un comportement de surface non standard et un calcul analytique peut être mis en oeuvre pour expliquer ce phénomène. Une étude similaire peut être faite pour l'equation KPZ et le même comportement du profil et des fluctuations de l'interface proche du bords est observé.

# Bibliography

[1] J. H. Ahrens. Paving the chessboard. *Journal of Combinatorial Theory, Series A*, 31(3):277–288, 1981.

[2] D. Alberici and P. Contucci. Solution of the Monomer-Dimer Model on Locally Tree-Like Graphs. Rigorous Results. *Communications in Mathematical Physics*, pages 1–29, 2013.

[3] F. Alet, Y. Ikhlef, J. L. Jacobsen, G. Misguich, and V. Pasquier. Classical dimers with aligning interactions on the square lattice. *Physical Review E*, 74(4):041124, 2006.

[4] F. Alet, J. L. Jacobsen, G. Misguich, V. Pasquier, F. Mila, and M. Troyer. Interacting classical dimers on the square lattice. *Physical Review Letters*, 94(23):235702, 2005.

[5] N. Allegra. Exact solution of the 2d dimer model: Corner free energy, correlation functions and combinatorics. *arXiv preprint arXiv:1410.4131*, 2014.

[6] N. Allegra, J. Dubail, J.-M. Stephan, and J. Viti. Inhomogenous field theory inside the arctic circle. *arXiv preprint arXiv:1512.02872*, 2015.

[7] N. Allegra and J.-Y. Fortin. Grassmannian representation of the two-dimensional monomer-dimer model. *Physical Review E*, 89(6):062107, 2014.

[8] N. Allegra, J.-Y. Fortin, and M. Henkel. Boundary crossover in semi-infinite non-equilibrium growth processes. *Journal of Statistical Mechanics: Theory and Experiment*, 2014(2):P02018, 2014.

[9] D. Allison and N. Reshetikhin. Numerical study of the 6-vertex model with domain wall boundary conditions. In *Annales de l'institut Fourier*, volume 55, pages 1847–1869, 2005.

[10] T. Antal, Z. Rácz, A. Rákos, and G. Schütz. Transport in the xx chain at zero temperature: Emergence of flat magnetization profiles. *Physical Review E*, 59(5):4912, 1999.

[11] C. T. Asplund and S. G. Avery. Evolution of entanglement entropy in the d1-d5 brane system. *Physical Review D*, 84(12):124053, 2011.

[12] C. T. Asplund and A. Bernamonti. Mutual information after a local quench in conformal field theory. *Physical Review D*, 89(6):066015, 2014.

[13] H. Au-Yang and J. H. H. Perk. Ising correlations at the critical temperature. *Physics Letters A*, 104(3):131–134, 1984.

[14] A.-L. Barabási and H. E. Stanley. *Fractal concepts in surface growth*. Cambridge university press, 1995.

[15] R. J. Baxter. Dimers on a rectangular lattice. *Journal of Mathematical Physics.*, 9(4):650–654, 1968.

[16] R. J. Baxter. Partition function of the eight-vertex lattice model. *Ann. Phys.*, 70(1):193–228, 1972.

[17] R. J. Baxter. *Exactly solved models in statistical mechanics*. Courier Dover Publications, 2007.

[18] A. A. Belavin, A. M. Polyakov, and A. B. Zamolodchikov. Infinite conformal symmetry in two-dimensional quantum field theory. *Nuclear Physics B*, 241(2):333–380, 1984.

[19] F. A. Berezin. *The Method of second quantization*. Academic Press, 1966.

[20] H. Bethe. Zur Theorie der Metalle. *Zeitschrift für Physik*, 71(3-4):205–226, 1931.

[21] H. Blöte, J. L. Cardy, and M. Nightingale. Conformal invariance, the central charge, and universal finite-size amplitudes at criticality. *Physical Review Letters*, 56(7):742, 1986.

[22] H. Blöte and H. Hilborst. Roughening transitions and the zero-temperature triangular ising antiferromagnet. *Journal of Physics A: Mathematical and General*, 15(11):L631, 1982.

[23] N. Bogoliubov, A. Pronko, and M. Zvonarev. Boundary correlation functions of the six-vertex model. *Journal of Physics A: Mathematical and General*, 35(27):5525, 2002.

[24] R. Bondesan, J. Dubail, J. L. Jacobsen, and H. Saleur. Conformal boundary state for the rectangular geometry. *Nuclear Physics B*, 862(2):553–575, 2012.

[25] R. Bondesan, J. L. Jacobsen, and H. Saleur. Rectangular amplitudes, conformal blocks, and applications to loop models. *Nuclear Physics B*, 867(3):913–949, 2013.

[26] C. Boutillier, J. Bouttier, G. Chapuy, S. Corteel, and S. Ramassamy. Dimers on rail yard graphs. *arXiv preprint arXiv:1504.05176*, 2015.

[27] J. Bouttier, M. Bowick, E. Guitter, and M. Jeng. Vacancy localization in the square dimer model. *Physical Review E*, 76:041140, Oct 2007.

[28] J. Bouttier, G. Chapuy, and S. Corteel. From aztec diamonds to pyramids: steep tilings. *arXiv preprint arXiv:1407.0665*, 2014.

[29] J. Brankov. Isomorphism of dimer configurations and spanning trees on finite square lattices. *Journal of Mathematical Physics*, 36(9):5071–5083, 1995.

[30] P. Calabrese and J. Cardy. Time dependence of correlation functions following a quantum quench. *Physical review letters*, 96(13):136801, 2006.

[31] P. Calabrese and J. Cardy. Entanglement and correlation functions following a local quench: a conformal field theory approach. *Journal of Statistical Mechanics: Theory and Experiment*, 2007(10):P10004, 2007.

[32] P. Calabrese and J. Cardy. Quantum quenches in extended systems. *Journal of Statistical Mechanics: Theory and Experiment*, 2007(06):P06008, 2007.

[33] P. Calabrese, C. Hagendorf, and P. Le Doussal. Time evolution of one-dimensional gapless models from a domain wall initial state: stochastic loewner evolution continued? *Journal of Statistical Mechanics: Theory and Experiment*, 2008(07):P07013, 2008.

[34] P. Calabrese and P. Le Doussal. Exact solution for the kardar-parisi-zhang equation with flat initial conditions. *Physical review letters*, 106(25):250603, 2011.

[35] S. Caracciolo, J. L. Jacobsen, H. Saleur, A. D. Sokal, and A. Sportiello. Fermionic field theory for trees and forests. *Physical Review Letters*, 93(8):080601, 2004.

[36] S. Caracciolo, A. D. Sokal, and A. Sportiello. Grassmann integral representation for spanning hyperforests. *Journal of Physics A: Mathematical and Theoretical*, 40(46):13799, 2007.

[37] J. L. Cardy. Effect of boundary conditions on the operator content of two-dimensional conformally invariant theories. *Nuclear Physics B*, 275(2):200–218, 1986.

[38] J. L. Cardy. Boundary conditions, fusion rules and the Verlinde formula. *Nuclear Physics B*, 324(3):581–596, 1989.

[39] J. L. Cardy and I. Peschel. Finite-size dependence of the free energy in two-dimensional critical systems. *Nuclear Physics B*, 300:377–392, 1988.

[40] S. Chhita and K. Johansson. Domino statistics of the two-periodic aztec diamond. *arXiv preprint arXiv:1410.2385*, 2014.

[41] A. L.-S. Chua, C. A. Haselwandter, C. Baggio, and D. D. Vvedensky. Langevin equations for fluctuating surfaces. *Physical Review E*, 72(5):051103, 2005.

[42] M. Clusel and J.-Y. Fortin. Boundary field induced first-order transition in the 2D Ising model: exact study. *J. Phys. A: Mathematical and General*, 39(5):995, 2006.

[43] M. Clusel and J.-Y. Fortin. Grassmann techniques applied to classical spin systems. *Condensed Matter Physics*, 12(3):463, 2009.

[44] M. Clusel, J.-Y. Fortin, and V. N. Plechko. Alternative description of the $2D$ Blume-Capel model using Grassmann algebra. *Journal of Physics A: Mathematical and Theoretical*, 41(40):405004, 2008.

[45] H. Cohn, N. Elkies, and J. Propp. Local statistics for random domino tilings of the aztec diamond. *arXiv preprint math/0008243*, 2000.

[46] H. Cohn, N. Elkies, J. Propp, et al. Local statistics for random domino tilings of the Aztec diamond. *Duke Mathematical Journal*, 85(1):117–166, 1996.

[47] H. Cohn, M. Larsen, and J. Propp. The shape of a typical boxed plane partition. *New York J. Math*, 4(137):165, 1998.

[48] F. Colomo and A. Pronko. On two-point boundary correlations in the six-vertex model with domain wall boundary conditions. *Journal of Statistical Mechanics: Theory and Experiment*, 2005(05):P05010, 2005.

[49] F. Colomo and A. Pronko. The arctic circle revisited. *Contemporary Mathematics*, 458:361, 2008.

[50] F. Colomo and A. Pronko. The arctic curve of the domain-wall six-vertex model. *Journal of Statistical Physics*, 138(4-5):662–700, 2010.

[51] F. Colomo, A. Pronko, and P. Zinn-Justin. The arctic curve of the domain wall six-vertex model in its antiferroelectric regime. *Journal of Statistical Mechanics: Theory and Experiment*, 2010(03):L03002, 2010.

[52] P. Córdoba-Torres, T. Mesquita, I. Bastos, and R. Nogueira. Complex dynamics during metal dissolution: From intrinsic to faceted anomalous scaling. *Physical review letters*, 102(5):055504, 2009.

[53] R. Costa-Santos and B. M. McCoy. Dimers and the critical Ising model on lattices of genus $> 1$. *Nuclear Physics B*, 623(3):439–473, 2002.

[54] L. F. Cugliandolo, G. Gonnella, and A. Pelizzola. Six vertex model with domain-wall boundary conditions in the bethe-peierls approximation. *arXiv preprint arXiv:1501.00883*, 2014.

[55] K. Damle, D. Dhar, and K. Ramola. Resonating valence bond wave functions and classical interacting dimer models. *Physical review letters*, 108(24):247216, 2012.

[56] P. Di Francesco, D. Sénéchal, and P. Mathieu. *Conformal field theory*. Springer, 1997.

[57] P. Di Francesco and R. Soto-Garrido. Arctic curves of the octahedron equation. *Journal of Physics A: Mathematical and Theoretical*, 47(28):285204, 2014.

[58] J. Dubail. *Conditions aux bords dans des théories conformes non unitaires*. PhD thesis, Université Paris 11, 2010.

[59] J. Dubail and J.-M. Stéphan. Universal behavior of a bipartite fidelity at quantum criticality. *Journal of Statistical Mechanics: Theory and Experiment*, 2011(03):L03002, 2011.

[60] B. A. Dubrovin, A. T. Fomenko, and S. P. Novikov. Modern geometryÑmethods and applications. part i, volume 93 of. *Graduate Texts in Mathematics*.

[61] B. Duplanticr and F. David. Exact partition functions and correlation functions of multiple hamiltonian walks on the manhattan lattice. *Journal of Statistical Physics*, 51(3-4):327–434, 1988.

[62] S. F. Edwards and D. Wilkinson. The surface statistics of a granular aggregate. In *Proceedings of the Royal Society of London A: Mathematical, Physical and Engineering Sciences*, volume 381, pages 17–31. The Royal Society, 1982.

[63] N. Elkies, G. Kuperberg, M. Larsen, and J. Propp. Alternating-sign matrices and domino tilings (part i). *Journal of Algebraic Combinatorics*, 1(2):111–132, 1992.

[64] N. Elkies, G. Kuperberg, M. Larsen, and J. Propp. Alternating-sign matrices and domino tilings (part i). *Journal of Algebraic Combinatorics*, 1(2):111–132, 1992.

[65] N. Elkies, G. Kuperberg, M. Larsen, and J. Propp. Alternating-sign matrices and domino tilings (part ii). *Journal of Algebraic Combinatorics*, 1(3):219–234, 1992.

[66] V. Elser. Solution of the dimer problem on a hexagonal lattice with boundary. *Journal of Physics A: Mathematical and General*, 17(7):1509, 1984.

[67] F. Family. Scaling of rough surfaces: effects of surface diffusion. *Journal of Physics A: mathematical and general*, 19(8):L441, 1986.

[68] P. Fendley, R. Moessner, and S. L. Sondhi. Classical dimers on the triangular lattice. *Physical Review B*, 66(21):214513, 2002.

[69] A. E. Ferdinand. Statistical mechanics of dimers on a quadratic lattice. *Journal of Mathematical Physics*, 8(12):2332–2339, 1967.

[70] P. L. Ferrari and H. Spohn. Random growth models. *arXiv preprint arXiv:1003.0881*, 2010.

[71] M. E. Fisher. Statistical mechanics of dimers on a plane lattice. *Physical. Review*, 124(6):1664, 1961.

[72] M. E. Fisher and J. Stephenson. Statistical mechanics of dimers on a plane lattice. II. Dimer correlations and monomers. *Physical Review*, 132(4):1411, 1963.

[73] J. Fjaerestad. Classical and quantum dimers on the star lattice. *Bulletin of the American Physical Society*, 54, 2009.

[74] J. Fjærestad. The 3-edge-colouring problem on the 4–8 and 3–12 lattices. *Journal of Statistical Mechanics: Theory and Experiment*, 2010(01):P01004, 2010.

[75] J. Fjærestad. Dimer and fermionic formulations of a class of colouring problems. *Journal of Physics A: Mathematical and Theoretical*, 45(7):075001, 2012.

[76] P. Flajolet and R. Sedgewick. *Analytic combinatorics*. Cambridge University Press, 2009.

[77] J.-Y. Fortin and M. Clusel. Second-order critical lines of spin-S Ising models in a splitting field using Grassmann techniques. *Physical Review B*, 78(17):172402, 2008.

[78] R. H. Fowler and G. S. Rushbrooke. An attempt to extend the statistical theory of perfect solutions. *Trans. Faraday Soc.*, 33:1272–1294, 1937.

[79] E. Fradkin. *Field theories of condensed matter physics*. Cambridge University Press, 2013.

[80] E. Fradkin and L. P. Kadanoff. Disorder variables and para-fermions in two-dimensional statistical mechanics. *Nuclear Physics B*, 170(1):1–15, 1980.

[81] S. Franco, A. Hanany, D. Vegh, B. Wecht, and K. D. Kennaway. Brane dimers and quiver gauge theories. *Journal of High Energy Physics*, 2006(01):096, 2006.

[82] A. Gambassi and P. Calabrese. Quantum quenches as classical critical films. *EPL (Europhysics Letters)*, 95(6):66007, 2011.

[83] A. Ghosh, D. Dhar, and J. L. Jacobsen. Random trimer tilings. *Physical Review E*, 75(1):011115, 2007.

[84] H. Gong and S. Yim. Study on anomalous scaling exponents for molecular thin film growth using surface lateral diffusion model. *Bulletin of the Korean Chemical Society*, 32(7):2237–2242, 2011.

[85] T. Gueudré and P. Le Doussal. Directed polymer near a hard wall and kpz equation in the half-space. *EPL (Europhysics Letters)*, 100(2):26006, 2012.

[86] T. Halpin-Healy and Y.-C. Zhang. Kinetic roughening phenomena, stochastic growth, directed polymers and all that. aspects of multidisciplinary statistical mechanics. *Physics reports*, 254(4):215–414, 1995.

[87] A. Hanany and K. D. Kennaway. Dimer models and toric diagrams. *arXiv preprint hep-th/0503149*, 2005.

[88] R. Hayn and V. N. Plechko. Grassmann variables and exact solutions for two-dimensional dimer models. *Physics of Atomic Nuclei*, 61:1972–1977, 1998.

[89] O. J. Heilmann and E. H. Lieb. Monomers and dimers. *Physical Review Letters*, 24:1412–1414, 1970.

[90] O. J. Heilmann and E. H. Lieb. Theory of monomer-dimer systems. *Communication in Mathematical Physics*, 25(3):190–232, 1972. reprinted in: *Statistical Mechanics*, edited by B. Nachtergaele, J. P. Solovej, and J. Yngvason, Springer (2004), pp. 45-87.

[91] H. Helfgott. *Edge effects on local statistics in lattice dimers: a study of the Aztec diamond (finite case)*. PhD thesis, Citeseer, 1998.

[92] M. Henkel. *Conformal invariance and critical phenomena*. Springer, 1999.

[93] M. Henkel. *Conformal invariance and critical phenomena*. Springer Science & Business Media, 2013.

[94] M. Henkel and M. Pleimling. Non-equilibrium phase transitions, volume 2: Ageing and dynamical scaling far from equilibrium (theoretical and mathematical physics), 2010.

[95] C. L. Henley. Relaxation time for a dimer covering with height representation. *Journal of Statistical Physics*, 89(3-4):483–507, 1997.

[96] F. Iglói, I. Peschel, and L. Turban. Inhomogeneous systems with unusual critical behaviour. *Advances in Physics*, 42(6):683–740, 1993.

[97] L. Ioffe and A. Larkin. Superconductivity in the liquid-dimer valence-bond state. *Physical Review B*, 40(10):6941, 1989.

[98] C. Itzykson and J.-M. Drouffe. *Statistical Field Theory: Volume 1, From brownian motion to renormalization and lattice gauge theory*. Cambridge University Press, 1991.

[99] C. Itzykson, H. Saleur, and J.-B. Zuber. Conformal invariance of nonunitary 2*d*-models. *EPL (Europhysics Letters)*, 2(2):91, 1986.

[100] A. G. Izergin. Partition function of the six-vertex model in a finite volume. In *Soviet Physics Doklady*, volume 32, page 878, 1987.

[101] A. G. Izergin, D. A. Coker, and V. E. Korepin. Determinant formula for the six-vertex model. *Journal of Physics A: Mathematical and General*, 25(16):4315, 1992.

[102] N. S. Izmailian and R. Kenna. Dimer model on a triangular lattice. *Physical Review E*, 84(2):021107, 2011.

[103] N. S. Izmailian, R. Kenna, W. Guo, and X. Wu. Exact finite-size corrections and corner free energies for the $c = -2$ universality class. *Nuclear Physics B*, 884:157–171, 2014.

[104] N. S. Izmailian, K. Oganesyan, and C.-K. Hu. Exact finite-size corrections of the free energy for the square lattice dimer model under different boundary conditions. *Physical Review E*, 67(6):066114, 2003.

[105] N. S. Izmailian, K. Oganesyan, M.-C. Wu, and C.-K. Hu. Finite-size corrections and scaling for the triangular lattice dimer model with periodic boundary conditions. *Physical Review E*, 73(1):016128, 2006.

[106] N. S. Izmailian, V. B. Priezzhev, P. Ruelle, and C.-K. Hu. Logarithmic conformal field theory and boundary effects in the dimer model. *Physical Review Letters*, 95:260602, Dec 2005.

[107] J. Jacobsen. AlgŔbre, intŐgralitŐ et modŔles exactement solubles (cours de m2 de physique thŐorique), 2013.

[108] J. Jacobsen and P. Zinn-Justin. Algebraic bethe ansatz for the fpl2 model. *Journal of Physics A: Mathematical and General*, 37(29):7213, 2004.

[109] J. L. Jacobsen. Bulk, surface and corner free-energy series for the chromatic polynomial on the square and triangular lattices. *Journal of Physics A: Mathematical and Theoretical*, 43(31):315002, 2010.

[110] J. L. Jacobsen and J. Kondev. Field theory of compact polymers on the square lattice. *Nuclear Physics B*, 532(3):635–688, 1998.

[111] M. Jeng, M. J. Bowick, W. Krauth, J. Schwarz, and X. Xing. Vacancy diffusion in the triangular-lattice dimer model. *Physical Review E*, 78(2):021112, 2008.

[112] M. R. Jerrum. Two-dimensional monomer-dimer systems are computationally intractable. *Journal of Statistical Physics*, 48(1-2):121–134, 1987. Erratum-ibid **59**, 1087-1088 (1990).

[113] W. Jockusch, J. Propp, and P. Shor. Random domino tilings and the arctic circle theorem. *arXiv preprint math/9801068*, 1998.

[114] K. Johansson. The arctic circle boundary and the airy process. *Annals of probability*, pages 1–30, 2005.

[115] K. Johansson. The arctic circle boundary and the airy process. *Annals of probability*, pages 1–30, 2005.

[116] K. Johansson and E. Nordenstam. Eigenvalues of gue minors. *Electron. J. Probab*, 11(50):1342–1371, 2006.

[117] P. E. John and H. Sachs. On a strange observation in the theory of the dimer problem. *Discrete Mathematics*, 216(1):211–219, 2000.

[118] L. P. Kadanoff and H. Ceva. Determination of an operator algebra for the two-dimensional Ising model. *Physical Review B*, 3(11):3918, 1971.

[119] M. Kardar, G. Parisi, and Y.-C. Zhang. Dynamic scaling of growing interfaces. *Physical Review Letters*, 56(9):889, 1986.

[120] P. W. Kasteleyn. The statistics of dimers on a lattice: I. the number of dimer arrangements on a quadratic lattice. *Physica*, 27(12):1209–1225, 1961.

[121] P. W. Kasteleyn. Dimer statistics and phase transitions. *Journal of Mathematical Physics*, 4:287, 1963.

[122] B. Kaufman. Crystal statistics. II. Partition function evaluated by spinor analysis. *Physical Review*, 76(8):1232, 1949.

[123] B. Kaufman and L. Onsager. Crystal statistics. III. Short-range order in a binary Ising lattice. *Physical Review*, 76(8):1244, 1949.

[124] D. Kennes, V. Meden, and R. Vasseur. Universal quench dynamics of interacting quantum impurity systems. *Physical Review B*, 90(11):115101, 2014.

[125] C. Kenyon, D. Randall, and A. Sinclair. Approximating the number of monomer-dimer coverings of a lattice. *Journal of Statistical Physics*, 83(3-4):637–659, 1996.

[126] R. Kenyon. Conformal invariance of domino tiling. *Annals of probability*, pages 759–795, 2000.

[127] R. Kenyon. Dominos and the gaussian free field. *Annals of probability*, pages 1128–1137, 2001.

[128] R. Kenyon. Lectures on dimers. *arXiv preprint arXiv:0910.3129*, 2009.

[129] R. Kenyon, A. Okounkov, and S. Sheffield. Dimers and amoebae. *Annals of mathematics*, pages 1019–1056, 2006.

[130] J. Kim, N. Lim, C. R. Park, and S. Yim. Growth dynamics of znpc and tiopc thin films: Effect of crystallinity on anomalous scaling behavior. *Surface Science*, 604(13):1143–1147, 2010.

[131] J. M. Kim and J. Kosterlitz. Growth in a restricted solid-on-solid model. *Physical review letters*, 62(19):2289, 1989.

[132] P. Kleban and I. Vassileva. Free energy of rectangular domains at criticality. *Journal of Physics A: Mathematical and General*, 24(14):3407, 1991.

[133] P. Kleban and I. Vassileva. Domain boundary energies in finite regions at $2d$ criticality via conformal field theory. *Journal of Physics A: Mathematical and General*, 25(22):5779, 1992.

[134] J. Kondev and C. L. Henley. Four-coloring model on the square lattice: A critical ground state. *Physical Review B*, 52(9):6628, 1995.

[135] J. Kondev and J. L. Jacobsen. Conformational entropy of compact polymers. *Physical Review Letters*, 81(14):2922, 1998.

[136] Y. Kong. Logarithmic corrections in the free energy of monomer-dimer model on plane lattices with free boundaries. *Physical Review E*, 74(1):011102, 2006.

[137] Y. Kong. Monomer-dimer model in two-dimensional rectangular lattices with fixed dimer density. *Physical Review E*, 74(6):061102, 2006.

[138] Y. Kong. Packing dimers on $(2p+1) \times (2q+1)$ lattices. *Physical Review E*, 73(1):016106, 2006.

[139] V. Korepin and P. Zinn-Justin. Thermodynamic limit of the six-vertex model with domain wall boundary conditions. *Journal of Physics A: Mathematical and General*, 33(40):7053, 2000.

[140] V. E. Korepin. Calculation of norms of bethe wave functions. *Communications in Mathematical Physics*, 86(3):391–418, 1982.

[141] V. E. Korepin. *Quantum inverse scattering method and correlation functions*. Cambridge university press, 1997.

[142] I. A. Kovács, E. M. Elçi, M. Weigel, and F. Iglói. Corner contribution to cluster numbers in the Potts model. *Physical Review B*, 89(6):064421, 2014.

[143] I. A. Kovács, F. Iglói, and J. Cardy. Corner contribution to percolation cluster numbers. *Physical Review B*, 86(21):214203, 2012.

[144] W. Krauth. *Volume 13 of Oxford master series in statistical, computational, and theoretical physics*. Oxford University Press, 2006.

[145] W. Krauth and R. Moessner. Pocket monte carlo algorithm for classical doped dimer models. *Physical Review B*, 67(6):064503, 2003.

[146] J. Krug. Origins of scale invariance in growth processes. *Advances in Physics*, 46(2):139–282, 1997.

[147] K. Kuns and D. Marolf. Non-thermal behavior in conformal boundary states. *Journal of High Energy Physics*, 2014(9):1–19, 2014.

[148] L. Levitov. Equivalence of the dimer resonating-valence-bond problem to the quantum roughening problem. *Physical Review Letters*, 64(1):92, 1990.

[149] Y. L. Loh, D.-X. Yao, and E. W. Carlson. Dimers on the triangular kagome lattice. *Physical Review B*, 78(22):224410, 2008.

[150] J. M. López, M. Castro, and R. Gallego. Scaling of local slopes, conservation laws, and anomalous roughening in surface growth. *Physical review letters*, 94(16):166103, 2005.

[151] L. Lovász and M. D. Plummer. *Matching theory*. Elsevier, 1986.

[152] S. N. Majumdar and D. Dhar. Equivalence between the Abelian sandpile model and the $q \to 0$ limit of the Potts model. *Physica A: Statistical Mechanics and its Applications*, 185(1):129–145, 1992.

[153] A. S. Mata, S. C. Ferreira Jr, I. R. Ribeiro, and S. O. Ferreira. Anomalous scaling and superroughness in the growth of cdte polycrystalline films. *Physical Review B*, 78(11):115305, 2008.

[154] B. M. McCoy and T. T. Wu. *The Two-Dimensional Ising Model*. Harvard University Press, 1973.

[155] R. Merris. Laplacian matrices of graphs: a survey. *Linear algebra and its applications*, 197:143–176, 1994.

[156] R. Moessner and K. S. Raman. Quantum dimer models. In *Introduction to Frustrated Magnetism*, pages 437–479. Springer, 2011.

[157] M. Nakahara. *Geometry, topology and physics*. CRC Press, 2003.

[158] F. S. Nascimento, S. C. Ferreira, and S. O. Ferreira. Faceted anomalous scaling in the epitaxial growth of semiconductor films. *EPL (Europhysics Letters)*, 94(6):68002, 2011.

[159] B. Nienhuis. Coulomb gas formulations of two-dimensional phase transitions. In *Phase Transitions and Critical Phenomena*, volume 11. Academic press, 1987.

[160] B. Nienhuis, H. J. Hilhorst, and H. Blöte. Triangular sos models and cubic-crystal shapes. *Journal of Physics A: Mathematical and General*, 17(18):3559, 1984.

[161] A. Nigro. Finite size corrections for dimers. *arXiv preprint arXiv:1208.2110*, 2012.

[162] A. Okounkov and N. Reshetikhin. Correlation function of schur process with application to local geometry of a random 3-dimensional young diagram. *Journal of the American Mathematical Society*, 16(3):pp. 581–603, 2003.

[163] A. Okounkov and N. Reshetikhin. The birth of a random matrix. *Mosc. Math. J*, 6(3):553–566, 2006.

[164] A. Okounkov and N. Reshetikhin. Random skew plane partitions and the pearcey process. *Communications in mathematical physics*, 269(3):571–609, 2007.

[165] L. Onsager. Crystal statistics. I. A two-dimensional model with an order-disorder transition. *Physical Review*, 65(3-4):117, 1944.

[166] K. Palamarchuk and N. Reshetikhin. The 6-vertex model with fixed boundary conditions. *arXiv preprint arXiv:1010.5011*, 2010.

[167] S. Papanikolaou, E. Luijten, and E. Fradkin. Quantum criticality, lines of fixed points, and phase separation in doped two-dimensional quantum dimer models. *Physical Review B*, 76(13):134514, 2007.

[168] K. Park and B. Kahng. Exact derivation of the kardar-parisi-zhang equation for the restricted solid-on-solid model. *Physical Review E*, 51(1):796, 1995.

[169] I. Peschel. Some more results for the Ising square lattice with a corner. *Physics Letters A*, 110(6):313–315, 1985.

[170] V. Plechko. Fermions and disorder in Ising and related models in two dimensions. *Physics of Particles and Nuclei*, 41(7):1054–1060, 2010.

[171] V. N. Plechko. Simple solution of two-dimensional Ising model on a torus in terms of Grassmann integrals. *Theoretical and Mathematical Physics*, 64(1):748–756, 1985.

[172] V. N. Plechko. Grassman path-integral solution for a class of triangular type decorated Ising models. *Physica A: Statistical and Theoretical Physics*, 152(1-2):51 – 97, 1988.

[173] V. N. Plechko. Fermionic integrals and analytic solutions for two-dimensional ising models. *Journal of Physical Studies*, 1(4):554–563, 1997.

[174] V. Poghosyan, V. Priezzhev, and P. Ruelle. Jamming probabilities for a vacancy in the dimer model. *Physical Review E*, 77(4):041130, 2008.

[175] V. S. Poghosyan, V. B. Priezzhev, and P. Ruelle. Return probability for the loop-erased random walk and mean height in the abelian sandpile model: a proof. *Journal of Statistical Mechanics: Theory and Experiment*, 2011(10):P10004, 2011.

[176] G. Pólya. Aufgabe 424. *Arch. Math. Phys*, 20(3):271, 1913.

[177] A. M. Polyakov. *Gauge fields and strings*, volume 3 in Contemporary Concepts in Physics. Harwood Academic Publishers, 1987.

[178] V. B. Priezzhev and P. Ruelle. Boundary monomers in the dimer model. *Physical Review E*, 77(6):061126, 2008.

[179] V. Privman. *Finite-size scaling theory*, volume 1. Singapore: World Scientific, 1990.

[180] J. Propp. Boundary-dependent local behavior for 2-d dimer models. *International Journal of Modern Physics B*, 11(01n02):183–187, 1997.

[181] J. J. Ramasco, J. M. López, and M. A. Rodríguez. Generic dynamic scaling in kinetic roughening. *Physical review letters*, 84(10):2199, 2000.

[182] J. Rasmussen and P. Ruelle. Refined conformal spectra in the dimer model. *Journal of Statistical Mechanics: Theory and Experiment*, 2012(10):P10002, 2012.

[183] D. S. Rokhsar and S. A. Kivelson. Superconductivity and the quantum hard-core dimer gas. *Physical Review Letters*, 61(20):2376, 1988.

[184] S. Samuel. The use of anticommuting variable integrals in statistical mechanics. I. The computation of partition functions. *Journal of Mathematical Physics.*, 21(12):2806–2814, 1980.

[185] S. Samuel. The use of anticommuting variable integrals in statistical mechanics. III. Unsolved models. *Journal of Mathematical Physics.*, 21(12):2820–2833, 1980.

[186] T. Sasamoto and H. Spohn. The crossover regime for the weakly asymmetric simple exclusion process. *Journal of Statistical Physics*, 140(2):209–231, 2010.

[187] T. Sasamoto and H. Spohn. One-dimensional kardar-parisi-zhang equation: an exact solution and its universality. *Physical review letters*, 104(23):230602, 2010.

[188] O. Schramm and S. Sheffield. Contour lines of the two-dimensional discrete gaussian free field. *Acta mathematica*, 202(1):21–137, 2009.

[189] S. Sotiriadis, P. Calabrese, and J. Cardy. Quantum quench from a thermal initial state. *EPL (Europhysics Letters)*, 87(2):20002, 2009.

[190] S. Sotiriadis and J. Cardy. Inhomogeneous quantum quenches. *Journal of Statistical Mechanics: Theory and Experiment*, 2008(11):P11003, 2008.

[191] S. Sotiriadis and J. Cardy. Quantum quench in interacting field theory: a self-consistent approximation. *Physical Review B*, 81(13):134305, 2010.

[192] J.-M. Stéphan. Emptiness formation probability, toeplitz determinants, and conformal field theory. *Journal of Statistical Mechanics: Theory and Experiment*, 2014(5):P05010, 2014.

[193] J.-M. Stéphan and J. Dubail. Local quantum quenches in critical one-dimensional systems: entanglement, the loschmidt echo, and light-cone effects. *Journal of Statistical Mechanics: Theory and Experiment*, 2011(08):P08019, 2011.

[194] J.-M. Stéphan and J. Dubail. Logarithmic corrections to the free energy from sharp corners with angle $2\pi$. *Journal of Statistical Mechanics: Theory and Experiment*, 2013(09):P09002, 2013.

[195] J.-M. Stéphan, S. Furukawa, G. Misguich, and V. Pasquier. Shannon and entanglement entropies of one-and two-dimensional critical wave functions. *Physical Review B*, 80(18):184421, 2009.

[196] J.-M. Stéphan, G. Misguich, and V. Pasquier. Phase transition in the Rényi-Shannon entropy of Luttinger liquids. *Physical Review B*, 84(19):195128, 2011.

[197] J.-M. Stéphan, G. Misguich, and V. Pasquier. Rényi entanglement entropies in quantum dimer models: from criticality to topological order. *Journal of Statistical Mechanics: Theory and Experiment*, 2012(02):P02003, 2012.

[198] K. A. Takeuchi and M. Sano. Universal fluctuations of growing interfaces: evidence in turbulent liquid crystals. *Physical review letters*, 104(23):230601, 2010.

[199] K. A. Takeuchi, M. Sano, T. Sasamoto, and H. Spohn. Growing interfaces uncover universal fluctuations behind scale invariance. *Scientific reports*, 1, 2011.

[200] H. N. V. Temperley. *Combinatorics: Proceedings of the British Combinatorial Conference 1973. 202-204*. Cambridge Univ. Press. Mathematical Reviews (MathSciNet): MR345829, 1974.

[201] H. N. V. Temperley and M. E. Fisher. Dimer problem in statistical mechanics-an exact result. *Philos. Mag.*, 6(68):1061–1063, 1961.

[202] W.-J. Tzeng and F. Y. Wu. Dimers on a simple-quartic net with a vacancy. *Journal of Statistical Physics*, 110(3-6):671–689, 2003.

[203] E. Vernier and J. L. Jacobsen. Corner free energies and boundary effects for Ising, Potts and fully packed loop models on the square and triangular lattices. *Journal of Physics A: Mathematical and Theoretical*, 45(4):045003, 2012.

[204] A. M. Vershik and S. V. Kerov. Asymptotics of plancherel measure of symmetrical group and limit form of young tables. *Doklady Akademii Nauk SSSR*, 233(6):1024–1027, 1977.

[205] D. Vukičević. Applications of perfect matchings in chemistry. In *Structural Analysis of Complex Networks*, page 463. Springer, 2010.

[206] D. Vukičević. Applications of perfect matchings in chemistry. In *Structural Analysis of Complex Networks*, pages 463–482. Springer, 2011.

[207] D. Vvedensky, A. Zangwill, C. Luse, and M. Wilby. Stochastic equations of motion for epitaxial growth. *Physical Review E*, 48(2):852, 1993.

[208] F. Wang and F. Y. Wu. Exact solution of close-packed dimers on the Kagomé lattice. *Physical Review E*, 75(4):040105, 2007.

[209] F. Wang and F. Y. Wu. Dimers on the Kagomé lattice II: Correlations and the Grassmannian approach. *Physica A: Statistical Mechanics and its Applications*, 387(16):4157–4162, 2008.

[210] D. E. Wolf and L.-H. Tang. Inhomogeneous growth processes. *Physical review letters*, 65(13):1591, 1990.

[211] F. W. Wu. Ising model with four-spin interactions. *Physical Review B*, 4(7):2312–2314, 1971.

[212] F. Y. Wu. Dimers on two-dimensional lattices. *International Journal of Modern Physics B*, 20(32):5357–5371, 2006.

[213] F. Y. Wu, W.-J. Tzeng, and N. S. Izmailian. Exact solution of a monomer-dimer problem: A single boundary monomer on a nonbipartite lattice. *Physical Review E*, 83(1):011106, 2011.

[214] F. Y. Wu and F. Wang. Dimers on the kagome lattice I: Finite lattices. *Physica A: Statistical Mechanics and its Applications*, 387(16):4148–4156, 2008.

[215] W. Yan, Y.-N. Yeh, and F. Zhang. Dimer problem on the cylinder and torus. *Physica A: Statistical Mechanics and its Applications*, 387(24):6069–6078, 2008.

[216] Z. Zhang, Y. Sheng, and Q. Jiang. Monomer–dimer model on a scale-free small-world network. *Physica A: Statistical Mechanics and its Applications*, 391(3):828–833, 2012.

[217] W. Zheng and S. Sachdev. Sine-Gordon theory of the non-Néel phase of two-dimensional quantum antiferromagnets. *Physical Review B*, 40(4):2704, 1989.

[218] P. Zinn-Justin. Six-vertex model with domain wall boundary conditions and one-matrix model. *Physical Review E*, 62(3):3411, 2000.

## Critical Properties of Dimers, Spin Chains and Interface Models

The study carried in this thesis concerns classical and quantum critical phenomena. Indeed, critical behaviors and phase transitions are fundamental topics in modern statistical physics and field theory and we propose in this thesis to study some models which exhibit such behaviors both at equilibrium and out of equilibrium. In the first part of the thesis, some properties of the two-dimensional dimer model are studied. This model has been studied extensively in the statistical physics and mathematical communities and a lot of applications in condensed matter physics exist. Here we propose to focus on exact solutions of the model and conformal invariance in order to have a deep understanding of this model in presence of monomers, and/or boundaries. The same kind of tools are then used to explore another important phenomenon appearing in dimer models and spin chains: the arctic circle. The goal was to find a proper field theoretical description of this phenomenon using exact solutions and asymptotic analysis. The second part of the thesis concerns out of equilibrium critical phenomena in the context of interface growth models. This field of research is very important nowadays, mainly because of the Kardar-Parisi-Zhang equation and its relations with random matrix ensembles. The phenomenology of these models in presence of boundaries is studied via exact solutions and numerical simulations, we show that surprising behaviors appear close to the boundaries.

**Key-words**: Critical phenomena, dimer models, Grassmann algebra, conformal invariance, spin chains, out of equilibrium statistical physics, interface growth, KPZ equation.

## Propriétés critiques des modèles de dimères, de chaînes de spin et d'interfaces

L'étude réalisée dans cette thèse porte sur les phénomènes critiques classiques et quantiques. En effet, les phénomènes critiques et les transitions de phases sont devenues des sujets fondamentaux en physique statistique moderne et en théorie des champs et nous proposons dans cette thèse d'étudier certains modèles qui présentent un comportement critique à la fois à l'équilibre et hors de l'équilibre. Dans la première partie de la thèse, certaines propriétés du modèle de dimères à deux dimensions sont étudiées. Ce modèle a été largement étudié dans les communautés de physique statistique et de mathématiques et un grand nombre d'applications en physique de la matière condensée existent. Ici, nous proposons de mettre l'accent sur des solutions exactes du modèle et d'utiliser l'invariance conforme afin d'avoir une compréhension profonde de ce modèle en présence de monomères et/ou en présence de bords. Les mêmes types d'outils sont ensuite utilisés pour explorer un autre phénomène important apparaissant dans les modèles de dimères et de chaînes de spin: le cercle arctique. Le but étant de trouver une description adéquate en terme de théorie des champs de ce phénomène en utilisant des calculs exacts ainsi que de l'analyse asymptotique. La deuxième partie de la thèse concerne les phénomènes critiques hors de l'équilibre dans le contexte des modèles de croissance d'interfaces. Ce domaine de recherche est très important de nos jours, principalement en raison de la découverte de l'équation Kardar-Parisi-Zhang et de ses relations avec les ensembles de matrices aléatoires. La phénoménologie de ces modèles en présence des bords est analysé via des solutions exactes et des simulations numériques, on montre alors que des comportements surprenants apparaissent proche des bords.

**Mots-clés**: Phénomènes critiques, modèles de dimères, algèbre de Grassmann, invariance conforme, physique statistique hors-équilibre, croissance d'interface, équation de KPZ.